Role of HMGB1 and mitochondria in organic dust induced airway inflammation

by

Sanjana Mahadev-Bhat

A dissertation submitted to the graduate faculty

in partial fulfillment of the requirements for the degree of

DOCTOR OF PHILOSOPHY

Major: Immunobiology

Program of Study Committee:
Chandrashekhar Charavaryamath, Major Professor
Michael J. Wannemuehler
Dipali G. Sashital
Jinoh Kim
Jodi L. McGill

The student author, whose presentation of the scholarship herein was approved by the program of study committee, is solely responsible for the content of this dissertation. The Graduate College will ensure this dissertation is globally accessible and will not permit alterations after a degree is conferred.

Iowa State University

Ames, Iowa

2021

DEDICATION

Dedicated to the memory of my beloved mother,

Sujatha Bhat.

TABLE OF CONTENTS

LIST OF FIGURES

Page

LIST OF TABLES

Page

ACKNOWLEDGMENTS

I would like to take this opportunity to thank the people who have, in some form, had a positive effect on my life. This acknowledgment is insufficient to demonstrate how grateful I am, but I hope it serves as a recognition for the people that made a difference.

I would like to start with Dr. Chandrashekhar Charavaryamath, my major professor, for taking me in his team and supporting my professional and career development plans from attending multiple conferences to enrolling in the Preparing Future Faculty (PFF) program, and without whom this dissertation would not have been completed. I would also like to thank the current members of the Charavaryamath lab, Nyzil Massey and Denusha Shrestha for assisting me with my research in times of need.

I would like to thank my current and former Program of Study Committee members, Dr. Michael J. Wannemuehler, Dr. Dipali G. Sashital, Dr. Jinoh Kim, Dr. Jodi L. McGill, and Dr. Jesse Hostetter. They have been instrumental in shaping my research projects and progress in my graduate studies.

I was also fortunate to have worked with Cathy Martens, a gem of the department. She was the first person I met in the department from whom I had the honor to learn from. She took great care of all of us and made me feel so welcomed, and for that, I will always be grateful.

Many other professors and colleagues were involved in supporting my efforts and offering guidance. First, I would like to thank my PFF mentor, Dr. Michael J Kimber who has been a great mentor, providing insightful feedback on my scientific and career developments. He has played an integral part in my graduate studies and I thank him for the pleasant experience in the Department of Biomedical Sciences. I owe a special thank you to Dr. Michael Lyons, who always offered kind remarks and advice, and always encouraged my love for human anatomy. I will miss our long

chats about our love for different cuisines and various other topics. Also, I thank Dr. Carly Manz for her constant support during my teaching assistantships.

I am grateful to the IMBIO interdepartmental program and the former and current DOGEs, Dr. Randy Sacco and Dr. Doug Jones. Special thanks to the former and current program coordinators of IMBIO and BMS, Katie Blair, Carla Harris, Glenn Clark, and Seth Shatto, for all the support and for answering all my questions from lab rotations, preliminary and final exams to general questions about Iowa State University (ISU). My experience at ISU has been pleasant because of their help.

My time in Ames and ISU would not have been memorable without the friends I made here. Dr. Karthik Murugan has been a long-term friend since college, confidant, a pillar of support, and has tolerated me for almost 10 years and as a roommate during graduate school. We have had many intuitive conversations and many adventures. Dr. Kritika Singh, whom I had the pleasure of meeting and befriending on my first day in Ames. From our shared love for crafts and cooking to exploring Iowa with her adopted furbaby, Astro, she has been an amazing friend. Shravanti K. Suresh and Phong T. Phan, who welcomed me into their lives and have become good friends, and made Ames so much more enjoyable. Hannah Loghry, my amazing office mate who has been by my side through the ups and downs of graduate studies, with whom I shared daily discussions ranging from protocols to our disdain for all the negativity in the world. Dr. Carmen Reynolds, who I could always depend on for advice on research and life, and being an amazing friend. Finally, Erick Hernandez-Chacon, the newest member in my life, made sure I had a life apart from research. He took me on fun adventures and made my life during the pandemic bearable and pleasant. My fur babies, Jarvis and Suki, loved me unconditionally.

All of them have been very supportive, encouraged me during the highs and lows of graduate school, and were family to me.

The most important acknowledgment that I would like to share is of my family. They have been a constant support throughout my life. I appreciate all the sacrifices and hardships my family went through to get me to where I am now. A big thank you to my mother, Sujatha Bhat, and father, Dr. H Mahadev Bhat, for giving me unconditional love and support throughout my education. I am in debt to my sister, Shishira Karanth, who has constantly been my pillar of strength, always encouraged me, and believed in me. Without her, I would be a nervous wreck. Special thanks to Nihira Karanth, my niece, who has filled me with joy since the day she was born.

This acknowledgment section is not enough to convey my gratitude to all the people who have supported me through my endeavors. I have been fortunate and humbled to have such love and support in my life. Without them, I would not have reached this stage of my life.

Finally, I thank the perseverance of all the women in science from the generations before me. Thank you for opening up a world of possibilities and opportunities. Thank you for paving the way for generations of women, a world worthy of our passion, dedication, and talent.

ABSTRACT

Due to a sharp increase in global demand for protein of animal origin, animal production systems have transformed into industrial-scale operations known as concentrated animal feeding operations (CAFOs). Due to the high animal density within CAFOs, these facilities generate and accumulate various of contaminants such as airborne dust, gases, and microbes. Organic dust (OD) from such large animal confinement facilities is a complex mixture of microbial-associated components and particulate matter known to elicit chronic respiratory diseases in exposed workers. Examination of clinical samples from exposed workers revealed the prevalence of fevers, airway hyperresponsiveness, and an increase in neutrophils, macrophages, and proinflammatory mediators including TNFα, IL-6, and IL-8 (CXCL8) in bronchoalveolar lavage (BAL) fluid. Studies have also shown the release of damage-associated molecular patterns (DAMPs) and activation of multiple overlapping signaling pathways on OD exposure.

In the following dissertation, we investigated the role of high mobility group box 1 (HMGB1), a ubiquitously present transcription factor and DAMP, in OD-mediated airway inflammation. HMGB1 has been shown to mediate the activation of innate immune responses and plays a critical role at the intersection of host inflammatory response to sterile and to infectious threats. The goal of our research was to understand the role and impact of HMGB1 in OD-mediated airway inflammation. We show that OD-mediated HMGB1 release amplifies cytokine release and tissue damage. Using experimental strategies that selectively target HMGB1, we effectively reversed activation of specific immune signaling molecules and cytokine release and significantly attenuated damage in OD exposed *in vitro* and *in vivo* models.

In addition to the myriad of immune signaling and responses, inflammation contributes to cellular structural and functional changes as well. Recently, mitochondria are emerging as

therapeutic targets in addition to their essential role in cellular respiration. Emerging evidence shows that exposure to contaminants damages mitochondrial structure and alters function. We identified that OD exposure would induce ultrastructural changes in mitochondria and transcriptional changes in genes encoding proteins related to mitochondrial structure and function. We further investigated how the pathologic (secreted) and physiologic (nuclear) roles of HMGB1 would influence OD-exposure induced mitochondrial dysfunction, and airway inflammation. By using targeted HMGB1 antagonists we identified that HMGB1 could be a critical regulator of mitochondrial structure and function. We showed that neutralization of HMGB1 rescues OD-induced mitochondrial damages at structural and transcriptomic levels. Overall, our results highlight a critical role HMGB1, and mitochondria play in the progression of OD mediated airway inflammation. Identifying a mechanistic correlation between these two factors will likely help develop effective therapeutic strategies.

CHAPTER 1. GENERAL INTRODUCTION

Dissertation Goals

This dissertation aims to mechanistically describe the role of high mobility group box 1 (HMGB1) and mitochondrial dysfunction in organic dust (OD) exposure-induced lung inflammation. Exposure-induced lung inflammation is known to drive adverse effects on the respiratory health of individuals. Here we identified high mobility group box 1 (HMGB1) protein, a prototype damage-associated molecular pattern (DAMP), and investigated its role in OD exposure-induced airway inflammation. HMGB1 is a ubiquitously present nucleosome protein and global knockdown is shown to be fatal in mouse models indicating its importance in homeostasis. However, under inflammatory or necrotic conditions, nuclear HMGB1 moves into the cytoplasm and is secreted into the extracellular milieu which exacerbates the inflammation.

Based on published data, targeting secreted HMGB1 has potential benefits in mitigating the development and propagation of OD-mediated lung inflammation. To describe the role of HMGB1 in the OD-induced airway inflammation, we used *in vitro* experiments with HMGB1 specific gene knockdown and anti-HMGB1 antibody-mediated neutralization or ethyl pyruvate (EP) mediated blocking of nucleocytoplasmic translocation. We also generated and used conditional lung club cell-specific HMGB1 knockout mouse model and administered anti-HMGB1 antibodies to mice to assess the role of intracellular and extracellular HMGB1 in OD mediated airway inflammation, respectively.

Mitochondria are essential cellular organelles with known functions in generating cellular energy (ATP), production of reactive species, and immune functions. Emerging evidence shows that mitochondrial dysfunction is central to many inflammatory diseases such as asthma, cardiovascular conditions, and neurodegenerative diseases. Therefore, we aimed to investigate the

role of mitochondrial dysfunction of airway epithelial cells and monocytes using various models. By using mitochondria-targeting antioxidants (cytoplasmic NOX-2 inhibitor, mitoapocynin), we analyzed the changes in mitochondrial dynamics, mitochondrial DNA release and signaling, as well as structural integrity, respiration, and metabolism using the *in vitro* and *in vivo* models listed. Next, we examined whether extracellular HMGB1 plays a pathologic role in exacerbating OD exposure-induced mitochondrial dysfunction. Using lung club cell-specific conditional KO mice or antibody-mediated neutralization of secreted HMGB1, we investigate the role of normal nuclear versus secreted HMGB1 in driving mitochondrial dysfunction in OD-exposure models.

Our results provide novel insights into how the host-response to OD involves secretion of HMGB1 and the potential role of HMGB1 in feeding the inflammation loop via different mediators (cytokines and reactive species) and mitochondrial dysfunction. Our results identify the potential role of novel targets (HMGB1 and mitochondria) to develop better therapeutics for OD-induced lung inflammation.

Dissertation Organization

The present dissertation is organized into chapters focused on the role and impact of HMGB1 and mitochondrial dysfunction in OD-mediated lung inflammation. Chapter 2 introduces and reviews previous and current literature on organic dust exposure, HMGB1 and mitochondrial dysfunction in airway diseases and is pertinent to understanding the background and significance of the following chapters. Chapter 3 investigates OD exposure induced release of HMGB1 and impact of translocation and signaling due to HMGB1 in human bronchial epithelial cells. Using ethyl pyruvate (blocker of HMGB1 translocation) or anti-HMGB1 neutralization antibodies, we delineated the role of HMGB1. This chapter has been published in the *Journal of Respiratory Research*. In chapter 4, we describe the effects of OD exposure on cellular mitochondria through morphological and functional changes and other possible mechanisms coming into play. The

contents of this chapter have been accepted for publication in the *Journal of Histochemistry and Cell Biology*. In chapter 5, we expand on the findings of chapter 4 and focus on the possible role of HMGB1 in OD exposure-induced mitochondrial dysfunction in primary human bronchial epithelial cells. Using this *in vitro* model, we subjected the cells to single and repeated exposure to OD and performed siRNA mediated HMGB1 knockdown or anti-HMGB1 antibody-mediated neutralization, to identify the impact of HMGB1 on the structure, respiration, and metabolism of the mitochondria. In chapters 6 and 7, we sought to further expand our understanding of the role and impact of HMGB1 in *in vivo* models of OD-exposure. In chapter 6, we used a lung club cell-specific HMGB1 knockout murine model to investigate the intracellular role of HMGB1 in the pathogenesis of OD-mediated airway inflammation. We also focused on how this loss could impact mitochondrial function by measuring the release of mitochondrial secondary messengers and markers of glycolytic activity. In chapter 7, we focus on the extracellular functions of secreted HMGB1 by systemically neutralizing secreted HMG1 using anti-HMGB1 neutralizing antibodies *in vivo*. Finally, in chapter 8 we present an overall summary, conclusion, and potential future applications of our findings including contributions towards the basic biology of HMGB1 and mitochondria in inflammation.

CHAPTER 2. LITERATURE REVIEW

Introduction

Occupational exposure to organic dust (OD) is associated with the development of negative health effects in the workers. Exposed workers report various respiratory disease symptoms including bronchitis, asthma and asthma-like symptoms, chest tightness, coughing, mucus membrane irritation, and the annual decline in lung function (Charavaryamath and Singh 2006; Sethi et al. 2017). Mechanistic studies using *in vitro* and *in vivo* models of OD exposure have unraveled details on the underlying pathophysiology. OD exposure induced generation of oxidative stress, cytokine release, and cellular dysfunction in the airway epithelial cells is known to be driving a vicious cycle of low-grade inflammation. Several recent investigations have described the role of various microbial associated molecular patterns (MAMPs), corresponding host pattern recognition receptors (PPRs), and various immune cells in orchestrating the inflammation (Poole and Romberger 2012). Due to the complex nature and composition of OD and activation of overlapping signaling pathways on exposure, there is an urgent need to characterize a common cellular target to design effective therapeutic strategies to reduce OD-induced inflammatory lung diseases (Nath Neerukonda et al. 2018). Recent findings strongly suggest an emerging role of mitochondrial dysfunction and HMGB1-induced signaling in airway inflammation and disease progression (Li et al. 2013). However, a detailed understanding of OD-induced airway inflammation, HMGB1 release and signaling, and the development of mitochondrial dysfunction largely remain unknown. This review will provide an overview and highlight the recent advances made in understanding these three factors listed.

Historical records on health effects of agricultural work

Dangers and health risks associated with working in agriculture have been documented in various historical manuscripts and art dating back to the classical Greek and Egyptian era. Early writers have also identified and documented the link between occupations and particular health disorders. For example, mining accidents and occupational diseases caused by dust inhalation in miners during the middle ages, mercury poisoning of Venetian mirror makers have been documented (Sethi et al. 2017; Nordgren and Charavaryamath 2018). The book titled *"Historia de gentibus septintrionalibus"* written in 1555 by Olaus Magnus mentions the damage to vital organs by inhaling grain dust generated by crop threshers and Bernardino Ramazzini in his book titled, *"De Morbis Artificum Diatriba"* (Felton 1997; Schenker et al. 1998). Although the incidences of many early occupational diseases have declined, there persists an innumerable number of occupational hazards warranting further investigations.

Agriculture industry in the United States

The agriculture industry employs about 23.95% of the world's population. In 2019, direct on-farm employment (2.6 million jobs in the USA) has contributed $136 billion gross domestic product (GDP) and accounts for 1.3% of the US employment. Simultaneously, a career in agriculture and food-related industries alone supported an additional 19.6 million jobs. The meat and poultry plants have employed about a third (29.3%) of the US food and beverage manufacturing employees (Hribar and Schultz). The majority of animal production is through concentrated animal feeding operations (CAFOs) in order to achieve high efficiency and meet the growing production demands.

Contaminants in livestock farming environments

An increase in global population and increasing demand for cheaper protein sources have transformed the animal production units into industrial-scale operations termed concentrated

animal feed operations (CAFOs). CAFOs are characterized by confined spaces with a high animal density resulting in a complex work environment. CAFOs are known to generate many on-site contaminants which include a large variety of gases and organic dust (OD). These contaminants are either of animal origin, animal feed components, or pesticide residues (Hribar and Schultz). To determine the cause of exposure-induced changes in the airways of exposed agricultural workers, studies have analyzed organic dust samples for the presence of quantifiable environmental agents found within the CAFOs.

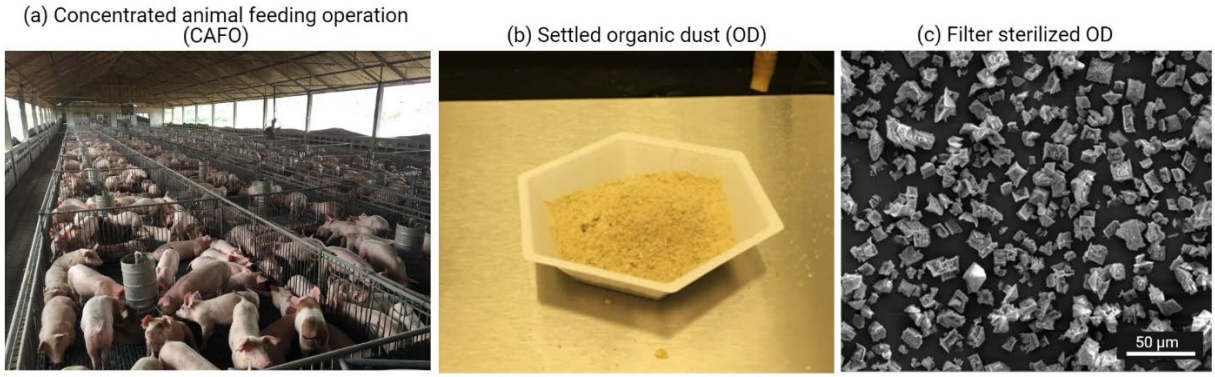

Figure 2.1 CAFOs and organic dust
Concentrated animal feeding operations (CAFOs) employ the use of large confinement buildings containing animals closely packed together (a). This results in the generation of a complex environment characterized by a large variety of gases as well as high levels of organic dust (b). Dust levels range from 1.9 to 30.0 mg/m^3 with a high percentage of particles considered to be in the respirable range (< 10 µ) (c).

Organic dust and particulate size

Airborne organic dust (OD) is one of the chief components of contaminants within occupational settings in CAFOs (Nordgren and Charavaryamath 2018). The OD is a complex mixture of a variety of substances that include particulate matter (PM) of varying sizes, microbes, and microbial products. The size of the particulate matter in OD determines their delivery and localization in the airways, which is an important factor in respiratory disease development in CAFOs (Kirychuk et al. 2010). In humans, particles of size less than 10 µm are respirable as they can be deposited anywhere in the respiratory zones of the airways, meaning from terminal

bronchioles to alveoli (Figure 2.1). In many CAFOs, as high as 50% of the total dust generated is considered to be within the respirable particle size range (≤ 10 μm) (Kilburn 1984; Kirkhorn and Garry 2000). Confinement buildings can be a dusty environment, with dust concentrations ranging from 1.9 -30 mg/m^3 of air sampled from swine and 0.16 mg/m^3 from poultry confinements. There is evidence showing that total dust levels should be kept under 2.5 mg/m^3 for a safe working environment, as high concentrations of respirable dust can lead to increased risk of respiratory diseases (DONHAM et al. 1986; Reynolds et al. 1996). The concentration of dust in CAFOs is dependent on other physical factors such as aerosolization velocity, settling velocity, and resuspension rate. Again, these factors could be influenced by facility ventilation, relative humidity, type of animal feed, methods of feeding, sources/locations of dust, animal density, general facility management, and cleanliness (May et al. 2012).

Microbial components

The chemical composition of dust particles also plays a role in their capacity to stimulate an inflammatory response. In CAFOs, the primary sources of dust are organic materials that include dried fecal matter, skin flakes, dried urine, feed materials, housing litter, mites, and spores. These organic materials promote the growth of a wide variety of microorganisms such as bacteria, viruses, and fungi.

Organic dust (OD) generated in CAFOs is rich in endotoxins with concentrations reaching 10 ng/m^3. Endotoxin concentrations in the OD samples from CAFOs are directly associated with adverse respiratory health outcomes. The term endotoxin is commonly used interchangeably for the chemically pure form of lipopolysaccharide (LPS). In humans, inhalation, or intravenous administration of LPS induces multiple clinical signs and symptoms such as fever, shivering, and coughing (Donham et al. 1995; Reynolds et al. 1996; Schenker et al. 1998; Dosman et al. 2006b). Inhaled endotoxin causes decreased lung function, low diffusion capacity, and airway obstruction.

However, the association between endotoxin levels in CAFOs and respiratory diseases is not universal because studies have reported cases of high exposure without symptoms or low exposure with a symptomatic response (Rask-Andersen et al. 1989; Senthilselvan et al. 2009).

Because of the lack of universal association between endotoxin and respiratory disease outcomes, studies demonstrated that OD samples from CAFOs treated to remove endotoxin retained the ability to induce significant inflammation. Muramic acid (the basic backbone of peptidoglycan, a component of gram-positive bacteria) is one of the key components of OD and was found to be associated with airway inflammation. High concentrations of muramic acid were reported in many CAFO facilities ranging from 5-15 ng/mL (Poole et al. 2010b). Poole et al. demonstrated that exposure to peptidoglycan alone elicited a proinflammatory response with the release of cellular mediators, leading to airway inflammation in rodents similar to that observed on exposure to organic dust extract (ODE) (Romberger et al. 2002; Poole et al. 2008). These findings underscore the importance of both gram-negative and gram-positive bacterial components in inducing respiratory inflammation in individuals exposed to OD.

Gases

CAFOs work environment contains high levels of gases primarily due to the microbial degradation of the animal manure. These gases, namely, methane (CH_4), ammonia (NH_3), hydrogen sulfide (H_2S), carbon monoxide (CO) and carbon dioxide (CO_2) together contribute and pose significant health risks for both workers and animals. Studies have linked H_2S exposure to the development of pulmonary edema and cause olfactory paralysis (Kirkhorn and Garry 2000). Studies show that exposure to ammonia can cause sinusitis and chronic obstructive pulmonary disease (COPD). In addition, dust particles absorb ammonia which allows the ammonia to travel deep into the distal airways (Von Essen and Donham 1999). Studies have also shown altered innate immune responses on prolonged exposure to CO_2 (Schneberger et al. 2017). In addition to the

gases listed above, a large number of volatile organic compounds (VOC) have been detected in the environment of CAFOs, further adding to the unpleasant odor and negative health effects (Schaeffer et al. 2017).

Airway disease manifestations

Upper airway respiratory diseases

Animal confinement workers report a variety of upper respiratory tract disease symptoms. These diseases fall along the spectrum of airway diseases associated with large animal confinement farming which include rhinitis, sinusitis, and mucous membrane inflammation syndrome with allergic and irritant rhinitis symptoms (Table 2.1) (Reynolds et al. 1996; Von Essen and Donham 1999; Kirkhorn and Garry 2000; Poole et al. 2007). Nasal lavage findings from OD exposed subjects have demonstrated increased numbers of neutrophils, and increased levels of interleukin (IL)-8 and IL-6 (Von Essen and Romberger 2003; Dosman et al. 2006a; May et al. 2012). Nasal symptoms such as congestion, rhinorrhea, and pruritus have been shown to occur in almost 50% of animal confinement workers and are associated with acute and chronic inflammation of the nasal mucous membrane (Kirkhorn and Garry 2000; Von Essen and Romberger 2003).

Lower respiratory tract inflammation

Development of chronic airway inflammation has been identified in those working for two or more hours for several years in CAFOs, where it is characterized by the presence of increased numbers of neutrophils and macrophages, but not eosinophils. Persons with pre-existing asthma may be at risk of suffering from exacerbations of asthma symptoms. However, there is little evidence of exposed individuals developing asthma. The asthma symptoms observed in adult CAFO workers are more commonly regarded as work exacerbated asthma (WEA) as opposed to occupational asthma (OA) (Eduard et al. 2009). While WEA is seen in subjects with moderate or severe asthma, OA is new-onset asthma induced by an environmental aspect of the workplace and

is mostly IgE-mediated due to the components of OD such as animal dander, storage mites, and cockroach (Tarlo and Malo 2009). There are also reports of "asthma-like syndrome" which is an airway disorder characterized by cough, chest tightness, dyspnea, and wheezing without airway obstruction on pulmonary function testing in animal confinement workers. Unlike asthma, asthma-like syndrome does not have any evidence of airway obstruction and lacks signs of persistent airway inflammation and eosinophil influx. However, symptomatic individuals with asthma-like syndrome show airway hyper-responsiveness on methacholine challenge (Table 2.1) (Dosman et al. 2006b; Von Essen et al. 2010).

Workers in CAFOs are also at an increased risk of respiratory morbidity and mortality due to the development of chronic bronchitis and chronic obstructive pulmonary disease (COPD). Multiple studies have shown that the highest prevalence of chronic bronchitis is in animal production workers as compared to non-animal agriculture workers, with some at an increased risk of developing COPD (Eduard et al. 2009). Bronchitis symptoms vary based on the duration of exposure and workers have shown intermittent symptoms suggesting the presence of acute bronchitis as well. There was also an overlap shown in the symptoms of chronic bronchitis with that of acute exacerbation and asthma-like syndrome, more common in workers who smoke cigarettes, characterized by severe airway obstruction (Viegas et al. 2018).

Studies with naïve subjects without previous exposure to organic dust have shown the development of cough, dyspnea, nasal stuffiness, headache, fever and chills, malaise, nausea, and eye irritation after a few hours of exposure, with airway hyperresponsiveness in normal and healthy subjects (Larsson et al. 1994; Cormier et al. 1997). Bronchoalveolar lavage (BAL) from these subjects revealed the presence of increased numbers of neutrophils, macrophages, eosinophils, and lymphocytes compared to unexposed reference groups. This study also identified an increase in

several inflammatory cytokines and chemokines, such as IL-6, IL-8, and IL-1β, in the lavage fluid within 24 h of exposure (Wang et al. 1997).

Organic dust toxic syndrome

Organic dust toxic syndrome (ODTS) is a disease characterized by symptoms such as fever, malaise, myalgias, chest tightness, headache, and nausea which occur 4-8 hours following exposure to large amounts of OD (Table 2.1) (Von Essen and Romberger 2003). During the acute phase of the illness, findings have shown the development of leukocytosis with a profound neutrophil influx into the lower respiratory tract, with an increased probability of it manifesting as chronic bronchitis. While ODTS was originally described after silo-unloading, it has been recently identified after a variety of exposures to OD. The prevalence of ODTS is reported to be as high as 34% in swine confinement workers (Donham et al. 1995; Von Essen and Romberger 2003).

Innate immune mechanisms

OD contains a variety of MAMPs and the biological significance of these MAMPs has been explored via the corresponding PRRs. Of the many PRRs known, OD-induced signaling via TLR2, TLR4 and NOD2 have been identified using various *in vitro* and *in vivo* models (Charavaryamath et al. 2008; Bailey et al. 2008; Poole et al. 2010a; Poole et al. 2011). In general, activation of these PRRs results in signaling through common intracellular signaling molecules and transcription factors such as myeloid differentiation factor 88 (MyD88) and nuclear factor kappa B (NFκB), respectively, to elicit the production of pro-inflammatory mediators including IL-1, IL-6, IL-8 and tumor necrosis factor (TNF)-α (Figure 2.2). Several studies have identified the activation of these signaling pathways on OD exposure (Senthilselvan et al. 2007; An et al. 2020). Protein kinase C (PKC) is a catalytic enzyme, and it is known to mediate the release of pro-inflammatory cytokines in human bronchial epithelial cells exposed to OD. Specifically, PKC isoforms, PKCα and PKCε have been shown to activate sequentially on exposure to OD

(Romberger et al. 2002). Following OD exposure of human bronchial epithelial and monocytic cell lines, a kinome analysis has revealed activation of a myriad of overlapping innate inflammatory mechanisms (Nath Neerukonda et al. 2018).

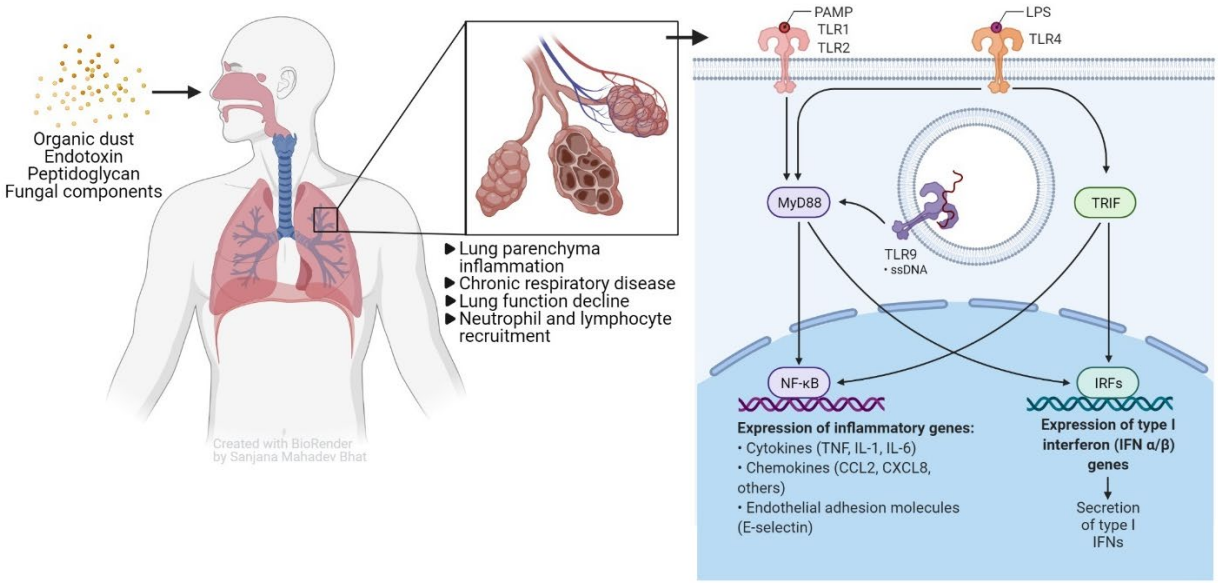

Figure 2.2 Airways diseases and inflammatory consequences on organic dust exposure Concentrated animal feeding operations (CAFOs) generate large amounts of contaminants such as organic dust (OD), containing particulate matter and microbial components (i.e. endotoxin, peptidoglycan, fungi). These contaminants of OD are recognized by several innate immune receptors resulting in a myriad of inflammatory consequences. (Adapted from Poole and Romberger 2012)

High mobility group box 1 (HMGB1): a friend or foe?

High mobility group box 1 (HMGB1) is a highly conserved (across species) non-histone chromosomal protein. This ubiquitously found nuclear protein was originally isolated and characterized in the 1970s and is a highly abundant protein with important biological activities inside as well as outside the cell (Goodwin et al. 1973). HMGB1 is also known to play multiple roles in the pathogenesis of inflammatory diseases and mediate processes that range from inflammation to repair (VanPatten and Al-Abed 2018). The biological actions of HMGB1 are diverse and it is known to bind to multiple receptors reflecting the unique biochemistry of this protein. Given that HMGB1 has potent pro-inflammatory properties, it poses a potential target for

anti-inflammatory therapy. To the best of our knowledge, there have been no reported studies performed to investigate whether it could be targeted in OD-mediated airway inflammation, hence we decided to mechanistically examine if HMGB1 is a potential therapeutic target.

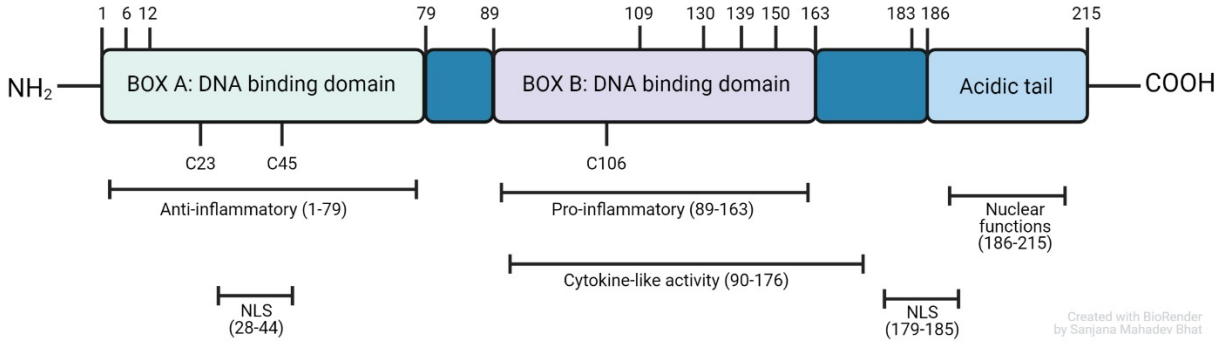

Figure 2.3 HMGB1 protein structure
Diagrammatic representation of high mobility group box 1 (HMGB1) is shown containing box A, box B, and acidic C-terminal tail. Box A and box B contain the two nuclear localization signal sequences (NLS). Both NLS contains a total of 9 conserved lysine residues which are susceptible to acetylation modification. HMGB1 also contains three cysteine residues (C23, C45, C106) which are modified into several reversible redox states. (Adapted from Yang et al. 2015; Ugrinova and Pasheva 2017a)

HMGB1: structure and modification

HMGB1 consists of 215 amino acids and is composed of three domains: A box (amino acid residues 9–79), B box (amino acid residues 95–163), and a C-terminal acidic tail (amino acid residues 186–215) (Figure 2.3) (Bianchi et al. 1992; Štros 2010). A box acts as a competitive antagonist to HMGB1 and thus inhibits HMGB1 activity as well as promotes anti-inflammatory properties *in vivo* and *in vitro*. B box has been identified as a functional domain with pro-inflammatory functions. HMGB1 also contains two nuclear localization sequences (NLS) and DNA binding domains (Box A and Box B) to recognize, bind to DNA, stabilize chromatin structure, and modulate gene transcription by bending dsDNA. HMGB1 has a bipolar charge due to the negatively charged C-terminal tail and positively charged N terminal (Bianchi et al. 1989; Bianchi et al. 1992; Li et al. 2003).

The functions of HMGB1 are defined by the posttranslational modification (PTM) it undergoes, such as acetylation, methylation, glycosylation, and phosphorylation. HMGB1 acetylation has been shown to control its translocation and secretion (Andersson et al. 2002; Andersson et al. 2014; Pisetsky 2014). Another important modification is the redox states of three of its cysteine residues, two in box A (C23 and C45) and one in box B (C106). The redox modification of HMGB1 is known to regulate its translocation, release, and activity. Fully reduced HMGB1, which expresses three cysteine thiol residues, shows chemotactic activity. Partially oxidized form of HMGB1 (C23 and C45 form a disulfide bond) exerts cytokine stimulating activity. The complete oxidation of the three cysteines to sulfonates, observed during an increase in endogenous or exogenous reactive oxygen species (ROS), promotes HMGB1 translocation and release (Tang et al. 2010; Li et al. 2013; Li et al. 2013).

HMGB1 inside the cell

Nuclear HMGB1 has been shown to act as a DNA chaperone with DNA binding and bending activities (Figure 2.4). The protein is said to interact non-specifically with DNA structures and regulate nuclear homeostasis and genome stability. HMGB1 is also involved in repair pathways such as nucleotide excision repair (NER), base excision repair, mismatch repair, and double-stranded break repair. HMGB1 binds to the nucleosome and promotes nucleosome binding, relaxing the structure allowing accessibility to the chromatin structure (Štros 2010; Ugrinova and Pasheva 2017). Recent studies have identified that HMGB1 is essential in maintaining mitochondrial quality control and autophagic surveillance (Tang et al. 2011; Zhu et al. 2015).

HMGB1 outside the cell and its receptors

Exposure to inflammatory or endogenous danger signals initiates the mobilization of nuclear HMGB1 to the cytoplasm which culminates in extracellular secretion (Figure 2.4). HMGB1 release occurs in two major ways, active secretion and passive secretion (Pisetsky 2014).

Active secretion is initiated by cell signal transduction through plasma membrane receptors resulting in the acetylation of HMGB1. HMGB1 can be actively secreted by activated macrophages, natural killer cells, dendritic cells, endothelial cells, platelets, and other immunologically competent cells on exposure to microbial associated molecular patterns (MAMPs), and endogenously derived inflammatory mediators such as TNFα, IL-1β, and IFN-γ. Passive secretion is initiated in cells undergoing necrosis where active HMGB1 diffuses out of the cells and is nearly instantaneous (Andersson and Tracey 2011; Pisetsky 2014). Thus, endogenous HMGB1 has a crucial functional role as a signaling molecule that informs other cells that damage or invasion has occurred. HMGB1 is pleiotropic in function, having multiple effects such as its involvement in inflammation and repair. Thus, it is said to play a central role in gating the magnitude of inflammatory response to clinical syndromes.

HMGB1 has distinct properties when compared to canonical pro-inflammatory cytokines where it elicits responses via unrelated receptors previously identified to transduce activation signals from exogenous and endogenous ligands. Although about 12 receptors have been identified, receptor for advanced glycation end products (RAGE), TLR2, TLR4, and TLR9 are considered to be the major receptors (Andersson and Tracey 2011; Ding et al. 2017). RAGE was the first receptor demonstrated to have a high affinity for HMGB1. RAGE is expressed in a variety of cell types and its binding to HMGB1 is said to mediate cell proliferation, growth, migration, chemotaxis, or/and differentiation (Sorci et al. 2013). TLRs are also important for the signaling mediated by HMGB1. To date, three members of the TLR family have been reported to be involved in the HMGB1 signaling pathway, namely TLR2, TLR4, and TLR9. TLR4, in particular, is more important for HMGB1 induced macrophage activation and proinflammatory cytokine release (Yang et al. 2010).

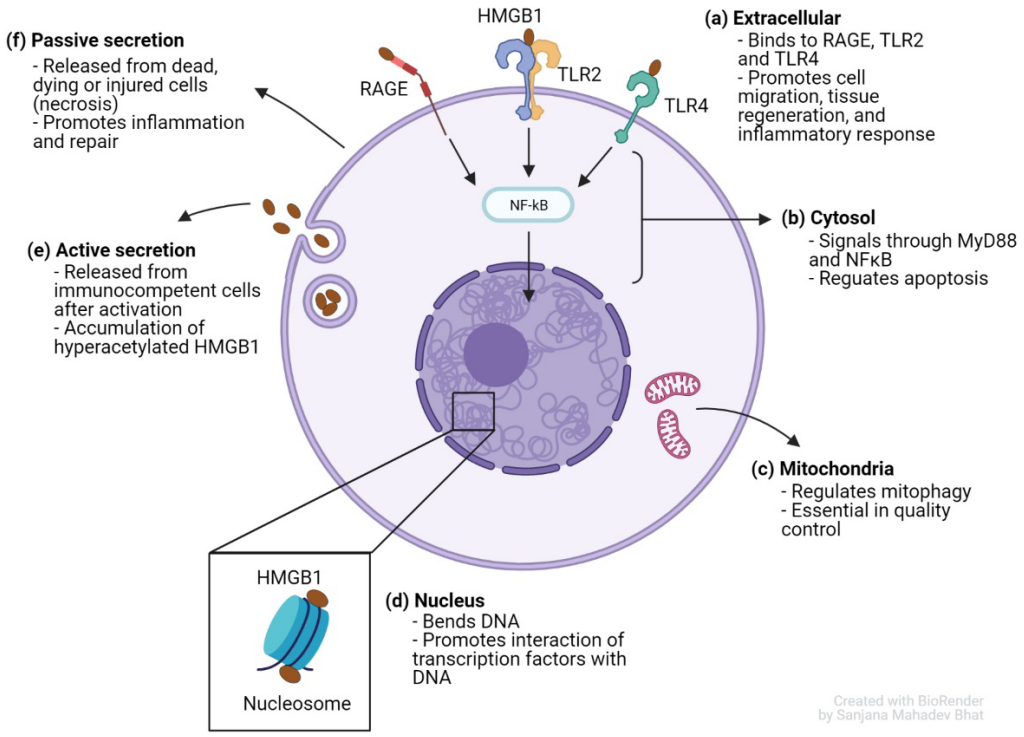

Figure 2.4 Intracellular and extracellular functions of HMGB1
High-mobility group box 1 protein (HMGB1), when secreted extracellularly, binds to and signals through RAGE (receptor for advanced glycation end products), Toll-like receptor (TLR) 2, and TLR4 (a) promoting the activation of pathways that involve MyD88, NFκB and MAP Kinase (b). Evidence suggests a role for HMGB1 in regulating apoptosis and mitochondrial quality control (c). In the nucleus, HMGB1 is transiently associated with nucleosomes and is important in controlling DNA transcription (d). HMGB1 can be secreted by immune cells after activation involving accumulation of hyperacetylated HMGB1 in secretory lysosomes, fusion with the cell membrane and release into the extracellular space (e). However, HMGB1 is passively released/leaked out during necrotic cell death (f).

HMGB1 in disease

HMGB1 has been shown to contribute to the pathogenesis of various diseases as a late mediator of sterile inflammation due to its role as a prototypic damage associated molecular pattern (DAMP). High levels of HMGB1 in tissues can cause acute damage leading to loss of function. Increasing evidence suggests that HMGB1 could serve as a therapeutic target because of its wider window for therapeutic intervention. A summary of the physiological function of HMGB1 in organ systems and disease models is described in Table 2.2.

Endotoxemia

Exposure to lethal doses of endotoxin in mammals initiates a biphasic cytokine response. Responses with a peak in levels of TNF-α or IL-1β occurring within hours of exposure constitute the early response, while the release of HMGB1 16 to 32 h after the onset of endotoxemia constitutes the late response. This late response is responsible for the complete lethal inflammatory response observed in endotoxemia. Administration of anti-HMGB1 antibodies after the early response of TNF-α conferred significant protection from endotoxemia mediated lethality (Wang et al. 1999; Abeyama et al. 2005). Based on these results, HMGB1 appears to be an attractive target to reduce tissue damage and lethality due to microbial sepsis.

Gastrointestinal inflammation

Intraperitoneal administration of LPS or cecal ligation and puncture (CLP) is known to cause an increase in HMGB1 levels which leads to the development of intestinal hyperpermeability and bacterial translocation (Sappington et al. 2002; Yang et al. 2009). Gut barrier dysfunction was shown to be restored on treatment with either anti-HMGB1 antibody or ethyl pyruvate, which blocks the extracellular release of HMGB1 (Yang et al. 2006; Davé et al. 2009). Inflammatory bowel disease models have described the positive effect of anti-HMGB1 antibody therapy in response to chemically induced colitis.

Neurological disorders

The presence of high levels of HMGB1 in animals has resulted in the development of sickness behavior. Intracerebral administration of HMGB1 induces aphagia, taste aversion, fever, IL-1β, and TNF-α production (O'Connor et al. 2003). A role for HMGB1 in mediating the activation of glial cells along the TLR4/NF-κB signaling axis in epilepsy has also been identified. In a coriaria lactone (CL)-induced epilepsy model, CL was found to increase the levels of HMGB1, TLR4, RAGE, NF-κB, and inducible nitric oxide synthases (iNOS) in human microglia (HM) cells

(Kim and Kang 2018; Paudel et al. 2019). Immunohistochemical staining suggested the nuclear to cytoplasmic translocation of HMGB1 in neurons and glial cells as well as its release into the extracellular space. In addition, HMGB1 has been shown to have a role in enhancing the toxicity of β-amyloid in Alzheimer's disease (Takata et al. 2004; Massey et al. 2019).

Respiratory disorders

Studies performed to investigate the role of HMGB1 in cigarette smoke-induced inflammation and COPD found elevated levels in BAL, sputum, and serum of COPD patients when compared to smokers without COPD and nonsmokers (Kanazawa et al. 2012). In rodent models, chronic cigarette smoke exposure was shown to induce an upregulation of HMGB1 protein expression in the lungs (Bezerra et al. 2011). HMGB1 levels are increased in the sputum of patients with cystic fibrosis and is implicated in mediating neutrophil chemotaxis which was significantly reduced on the addition of anti-HMGB1 antibodies. HMGB1 blocking therapies have been shown to ameliorate disease manifestation in cases of organic dust-induced lung inflammation, acute lung injury (ALI), pulmonary fibrosis (PF), and ventilator-induced lung injury (Abraham et al. 2000; Ogawa et al. 2006; Bhat et al. 2019).

Mitochondrial dysfunction in airway disease and pathology

Mitochondria are an indispensable organelle with an essential function in generating ATP molecules via cellular respiration. Mitochondria are shown to be involved in host response to pathogens, and a variety of diseases through a multitude of pathways such as the production of reactive species, cellular bioenergetics, secretion of mitochondrial specific DAMPs (mtDAMPs), and activation of various signaling pathways (Eisner et al. 2018). Airway epithelial cells, from the proximal airways to the terminal alveoli, act as the first line of defense against inhaled pathogens and noxious particles. Chronic exposure of lung epithelial cells to these toxicants can trigger oxidative stress, inflammation, cell death, cellular remodeling, cellular senescence, and cellular

dysfunction, all of which are key processes involved in the pathogenesis of airway inflammation. Evidence suggests abnormal mitochondrial signatures and mitochondrial dysfunction underlie the pathological mechanisms behind a plethora of lung diseases, including but not limited to chronic obstructive pulmonary disease (COPD), asthma, and lung cancer (Piantadosi and Suliman 2017; Aghapour et al. 2019). This led us to investigate the mechanistic basis of mitochondrial dysfunction in OD induced lung inflammation and how it may be promoting airway pathology.

Role of mitochondria in airways during homeostasis

The lung contains over 40 different cell types with variable mitochondrial numbers and functions (Gail and Lenfant 2015). The cell-specific distribution of mitochondria impacts the production of ATP and metabolites required for the proper functioning of cells (Figure 2.5). Mitochondria in airway cells preferentially use glucose-derived substrates for oxidative energy production. Airway epithelial cell mitochondria have a unique metabolic adaptation to aerobic oxidative phosphorylation (OXPHOS) as they possess lung-specific isoform of electron transport chain (ETC) cytochrome c oxidase (COX subunit IV-2). This isoform is oxygen-sensitive and is twofold more avid for oxygen than the COX found in other organs (Hüttemann et al. 2012). Airway bronchial epithelial cells and vascular smooth muscle cells (SMCs) require higher numbers of mitochondria for cilia to beat and allow contraction. In the alveolar region, type 2 alveolar epithelial cells (AT2) have three-fold more mitochondria per cell compared to endothelial or type 1 alveolar epithelial cells (AT1). The high mitochondrial density in AT2 cells supports synthesis, secretion, and recycling of surfactants (Massaro et al. 1975; Piantadosi and Suliman 2017).

Mitochondrial dynamics and biogenesis

The mitochondria are highly dynamic organelles that adapt to changes in homeostatic conditions such as cellular stress and damage. Mitochondria undergo membrane remodeling through cycles of fusion and fission events, creation of new mitochondria (biogenesis), or the

removal of damaged mitochondria by mitochondrial-specific autophagy (mitophagy) to control mitochondrial structure, number, and metabolism, during normal mitochondrial turnover in homeostasis and in response to cellular stress (Eisner et al. 2018). Mitochondrial fission requires the recruitment of dynamin-related protein 1 (DRP1) while mitochondrial fusion is mediated by dynamin-related GTPases mitofusin 1 and 2 (MFN1/2) on the outer mitochondrial membrane (OMM) and dynamin-related protein optic atrophy 1 (OPA1) on the inner mitochondrial membrane (IMM) (Chen et al. 2003). Mitochondrial biogenesis is regulated by PGC (PGC1α and PGC1β) along with TFAM and NRF1/2 as key downstream regulators. This has been shown to occur in distal lung cells and inflammatory cells found in the alveolar region and during conditions of high energy demand and cellular stress (Lee and Wei 2005; Agrawal and Mabalirajan 2015). Defective or damaged mitochondria are selectively removed by the formation of autophagosomes around the mitochondria resulting in their degradation, a process called mitophagy. The known regulators of mitophagy are PTEN induced kinase 1 (PINK1), the BH-3 only BCL2 protein (BNIP3), and the E3 ubiquitin ligase Parkin (Ding and Yin 2012). Mitochondrial biogenesis and mitophagy together allow cells to quickly replace metabolically dysfunctional mitochondria before energy failure (Ploumi et al. 2017). A summary of the airway diseases associated with changes in mitochondrial dynamics is listed in Table 2.3.

Mitochondrial DAMPs and inflammation

Accumulation of damaged or dysfunctional mitochondria can contribute to lung inflammation through the release of mitochondrial-derived molecules referred to as mitochondrial damage associated molecular patterns (mtDAMPs), which at normal physiological concentrations act as second messengers (Zhang et al. 2010). They are potent activators of pro-inflammatory responses due to the high level of homology they share with MAMPs. The best-studied mtDAMP is mitochondrial DNA (mtDNA), which has been shown to activate Toll-like receptor 9 (TLR9)

as well as DNA sensor cyclic GMP–AMP synthase (cGAS) (García and Chávez 2007; Motwani et al. 2019; Riley and Tait 2020). Other mitochondria specific molecules that can act as DAMPs, including ATP, TFAM, cardiolipin, carbamoyl phosphate synthetase, and cytochrome c (Cloonan and Choi 2016). mtDAMPs are involved in the pathophysiology of various diseases, however, their role in airway diseases is not well characterized. Few studies have assessed the extracellular role of mtDAMPs. Nonetheless, it has been shown that exposure of airway epithelial cell lines to cigarette smoke and organic dust induces cell death, and the release of mtDNA along with other non-mitochondrial-derived DAMPs (Prakash et al. 2017). Evidence of mtDNA release has been shown in the case of COPD and pulmonary fibrosis (PF) murine models. ATP also acts as a mtDAMP in the lungs where it can activate the proinflammatory purinergic receptors. Increased ATP levels have been observed in bronchoalveolar lavage fluid (BALF) of COPD and asthma patients as well as in murine asthma and PF (bleomycin) models, which are associated with inflammation (Aghapour et al. 2019; Cloonan et al. 2020). Together, mtDAMPs may invoke and perpetuate a cascade of inflammatory reactions as well as induce lung tissue damage (Table 2.4).

Therapeutic targeting of mitochondrial dysfunction in lung disease

Emerging mitochondria specific therapeutics have been shown to be effective in alleviating symptoms or improving pathophysiological features seen in respiratory diseases. Strategies aimed at ameliorating impaired mitochondrial bioenergetics and promoting biogenesis have shown to improve the regulation of mitochondria dynamics, and inhibition of excessive mitochondrial ROS generation. The use of small molecule antioxidants as a therapeutic target for mitochondrial dysfunction has been studied, both *in vitro* and *in vivo*. Other mitochondrial-targeted therapeutic strategies that could potentially be used to treat lung diseases include the use of metabolic modulating compounds such as dichloroacetate, histone deacetylase inhibitors, and fission inhibitors (Agrawal and Mabalirajan 2015). Stimulating adaptive mitochondrial biogenesis and

mitophagy may be a useful therapy for acute lung injury, and transfer of mitochondria from mesenchymal stromal stem cells ameliorates the imbalance in oxidative respiration, improves energy levels, and enhances mitochondrial biogenesis in damaged epithelial cells and may be beneficial in ALI, asthma, or COPD (Schumacker et al. 2014).

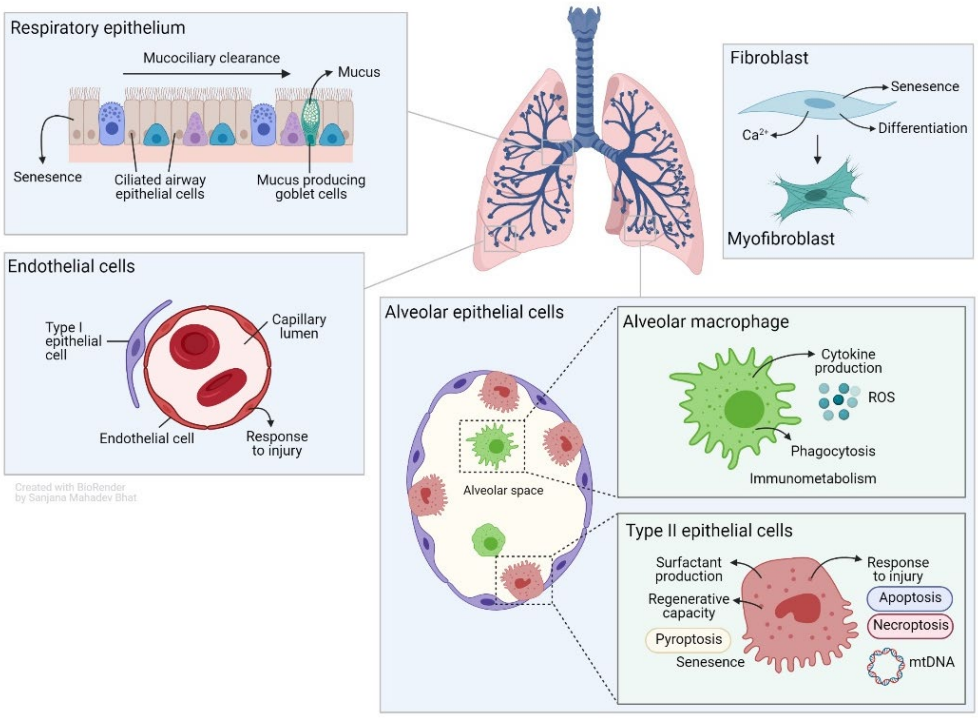

Figure 2.5 Mitochondria mediated regulation of airway homeostasis
Mitochondria are important in maintaining the proper functioning of specialized airway cells. Mitochondria regulate ciliary beat frequency in bronchial epithelial cells, mucus secretion by goblet cells, mucociliary clearance, and contraction in vascular smooth muscle cells. Functions of alveolar type II epithelial cells including surfactant production and regeneration are regulated by mitochondria. Alveolar macrophages and other immune cells respond to infections and release mitochondrial danger signals. Phagocytosis and regulation of immunometabolism is also dependent on mitochondria. Upregulation of mitochondria-specific pathways promotes differentiation of fibroblasts to myofibroblasts. (Adapted from Cloonan et al. 2020)

Conclusion

Organic dust exposure in agriculture is associated with the development of chronic respiratory diseases, but the exact etiology of the disease development remains unclear. Emerging evidence suggests that it cannot be ascribed to one or two agents alone but involves a wide range of host defense responses due to stimulation by a variety of MAMPs that likely activates a variety

of innate inflammatory pathways. Based on the evidence and importance, we have decided to focus on the role of extracellular HMGB1 and mitochondrial dysfunction on exposure to OD. Based on the information currently available, we posed the following research questions: First, what type of function does HMGB1 play in ODE-induced airway inflammation? Second, does exposure to ODE induce mitochondrial dysfunction? And third, emerging evidence suggests a correlation between HMGB1 and maintaining mitochondrial quality control. Due to this, can HMGB1 be a possible therapeutic target for ameliorating mitochondrial dysfunction due to ODE exposure? In the following chapters of this dissertation, we will attempt to address these questions mechanistically through a number of *in vitro* (cell culture models) and *in vivo* (mouse models) studies.

References

Abeyama K, Stern DM, Ito Y, Kawahara K, Yoshimoto Y, Tanaka M, Uchimura T, Ida N, Yamazaki Y, Yamada S, Yamamoto Y, Yamamoto H, Iino S, Taniguchi N, Maruyama I (2005) The N-terminal domain of thrombomodulin sequesters high-mobility group-B1 protein, a novel antiinflammatory mechanism. J Clin Invest 115(5):1267–1274. https://doi.org/10.1172/JCI200522782

Abraham E, Arcaroli J, Carmody A, Wang H, Tracey KJ (2000) Cutting Edge: HMG-1 as a Mediator of Acute Lung Inflammation. The Journal of Immunology 165(6):2950–2954. https://doi.org/10.4049/jimmunol.165.6.2950

Aghapour M, Remels AHV, Pouwels SD, Bruder D, Hiemstra PS, Cloonan SM, Heijink IH (2019) Mitochondria: at the crossroads of regulating lung epithelial cell function in chronic obstructive pulmonary disease. American Journal of Physiology-Lung Cellular and Molecular Physiology 318(1):L149–L164. https://doi.org/10.1152/ajplung.00329.2019

Agrawal A, Mabalirajan U (2015) Rejuvenating cellular respiration for optimizing respiratory function: targeting mitochondria. American Journal of Physiology-Lung Cellular and Molecular Physiology 310(2):L103–L113. https://doi.org/10.1152/ajplung.00320.2015

An J, Jr H, Aj N, Jd D, J K, Mj D, Gm T, B K, Ab S, R G, Sc G, Y T, Dj R, T K, Ja P (2020) MyD88 regulates a prolonged adaptation response to environmental dust exposure-induced lung disease. Respir Res 21(1):97–97. https://doi.org/10.1186/s12931-020-01362-8

Andersson U, Antoine DJ, Tracey KJ (2014) Expression of Concern: The functions of HMGB1 depend on molecular localization and post-translational modifications. Journal of Internal Medicine 276(5):420–424. https://doi.org/10.1111/joim.12309

Andersson U, Erlandsson-Harris H, Yang H, Tracey KJ (2002) HMGB1 as a DNA-binding cytokine. Journal of Leukocyte Biology 72(6):1084–1091. https://doi.org/10.1189/jlb.72.6.1084

Andersson U, Tracey KJ (2011) HMGB1 Is a Therapeutic Target for Sterile Inflammation and Infection. Annu Rev Immunol 29:139–162. https://doi.org/10.1146/annurev-immunol-030409-101323

Bailey KL, Poole JA, Mathisen TL, Wyatt TA, Von Essen SG, Romberger DJ (2008) Toll-like receptor 2 is upregulated by hog confinement dust in an IL-6-dependent manner in the airway epithelium. American Journal of Physiology-Lung Cellular and Molecular Physiology 294(6):L1049–L1054. https://doi.org/10.1152/ajplung.00526.2007

Bezerra FS, Valença SS, Pires KMP, Lanzetti M, Pimenta WA, Schmidt AC, Porto LC, Zin WA (2011) Long-term exposure to cigarette smoke impairs lung function and increases HMGB-1 expression in mice. Respiratory Physiology & Neurobiology 177(2):120–126. https://doi.org/10.1016/j.resp.2011.03.023

Bhat SM, Massey N, Karriker LA, Singh B, Charavaryamath C (2019) Ethyl pyruvate reduces organic dust-induced airway inflammation by targeting HMGB1-RAGE signaling. Respiratory Research 20(1):27. https://doi.org/10.1186/s12931-019-0992-3

Bianchi ME, Beltrame M, Paonessa G (1989) Specific recognition of cruciform DNA by nuclear protein HMG1. Science 243(4894):1056–1059. https://doi.org/10.1126/science.2922595

Bianchi ME, Falciola L, Ferrari S, Lilley DM (1992) The DNA binding site of HMG1 protein is composed of two similar segments (HMG boxes), both of which have counterparts in other eukaryotic regulatory proteins. EMBO J 11(3):1055–1063

Charavaryamath C, Juneau V, Suri SS, Janardhan KS, Townsend H, Singh B (2008) Role of Toll-like receptor 4 in lung inflammation following exposure to swine barn air. Exp Lung Res 34(1):19–35. https://doi.org/10.1080/01902140701807779

Charavaryamath C, Singh B (2006) Pulmonary effects of exposure to pig barn air. J Occup Med Toxicol 1:10. https://doi.org/10.1186/1745-6673-1-10

Chen H, Detmer SA, Ewald AJ, Griffin EE, Fraser SE, Chan DC (2003) Mitofusins Mfn1 and Mfn2 coordinately regulate mitochondrial fusion and are essential for embryonic development. J Cell Biol 160(2):189–200. https://doi.org/10.1083/jcb.200211046

Cloonan SM, Choi AMK (2016) Mitochondria in lung disease. J Clin Invest 126(3):809–820. https://doi.org/10.1172/JCI81113

Cloonan SM, Kim K, Esteves P, Trian T, Barnes PJ (2020) Mitochondrial dysfunction in lung ageing and disease. European Respiratory Review 29(157). https://doi.org/10.1183/16000617.0165-2020

Cormier Y, Duchaine C, Israel-Assayag E, Bedard G, Laviolette M, Dosman J (1997) Effects of repeated swine building exposures on normal naive subjects. European Respiratory Journal 10(7):1516–1522

Davé SH, Tilstra JS, Matsuoka K, Li F, DeMarco RA, Beer-Stolz D, Sepulveda AR, Fink MP, Lotze MT, Plevy SE (2009) Ethyl pyruvate decreases HMGB1 release and ameliorates murine colitis. Journal of Leukocyte Biology 86(3):633–643. https://doi.org/10.1189/jlb.1008662

Ding J, Cui X, Liu Q (2017) Emerging role of HMGB1 in lung diseases: friend or foe. J Cell Mol Med 21(6):1046–1057. https://doi.org/10.1111/jcmm.13048

Ding W-X, Yin X-M (2012) Mitophagy: mechanisms, pathophysiological roles, and analysis. Biol Chem 393(7):547–564. https://doi.org/10.1515/hsz-2012-0119

Donham KJ, Reynolds SJ, Whitten P, Merchant JA, Burmeister L, Popendorf WJ (1995) Respiratory dysfunction in swine production facility workers: dose-response relationships of environmental exposures and pulmonary function. Am J Ind Med 27(3):405–418. https://doi.org/10.1002/ajim.4700270309

DONHAM KJ, SCALLON LJ, POPENDORF W, TREUHAFT MW, ROBERTS RC (1986) Characterization of Dusts Collected from Swine Confinement Buildings. American Industrial Hygiene Association Journal 47(7):404–410. https://doi.org/10.1080/15298668691389955

Dosman JA, Fukushima Y, Senthilselvan A, Kirychuk SP, Lawson JA, Pahwa P, Cormier Y, Hurst T, Barber EM, Rhodes CS (2006a) Respiratory response to endotoxin and dust predicts evidence of inflammatory response in volunteers in a swine barn. American Journal of Industrial Medicine 49(9):761–766. https://doi.org/10.1002/ajim.20339

Dosman JA, Lawson JA, Kirychuk SP, Cormier Y, Biem J, Koehncke N (2006b) Three new cases of apparent occupational asthma in swine confinement facility employees. European Respiratory Journal 28(6):1281–1282. https://doi.org/10.1183/09031936.00096006

Eduard W, Pearce N, Douwes J (2009) Chronic Bronchitis, COPD, and Lung Function in Farmers: The Role of Biological Agents. CHEST 136(3):716–725. https://doi.org/10.1378/chest.08-2192

Eisner V, Picard M, Hajnóczky G (2018) Mitochondrial dynamics in adaptive and maladaptive cellular stress responses. Nature Cell Biology 20(7):755–765. https://doi.org/10.1038/s41556-018-0133-0

Felton JS (1997) The heritage of Bernardino Ramazzini. Occupational Medicine 47(3):167–179. https://doi.org/10.1093/occmed/47.3.167

Gail DB, Lenfant CJM (2015) Cells of the Lung: Biology and Clinical Implications1,2. American Review of Respiratory Disease

García N, Chávez E (2007) Mitochondrial DNA fragments released through the permeability transition pore correspond to specific gene size. Life Sciences 81(14):1160–1166. https://doi.org/10.1016/j.lfs.2007.08.019

Goodwin GH, Sanders C, Johns EW (1973) A New Group of Chromatin-Associated Proteins with a High Content of Acidic and Basic Amino Acids. European Journal of Biochemistry 38(1):14–19. https://doi.org/10.1111/j.1432-1033.1973.tb03026.x

Hribar C, Schultz M Understanding Concentrated Animal Feeding Operations and Their Impact on Communities. :30

Hüttemann M, Lee I, Gao X, Pecina P, Pecinova A, Liu J, Aras S, Sommer N, Sanderson TH, Tost M, Neff F, Aguilar-Pimentel JA, Becker L, Naton B, Rathkolb B, Rozman J, Favor J, Hans W, Prehn C, Puk O, Schrewe A, Sun M, Höfler H, Adamski J, Bekeredjian R, Graw J, Adler T, Busch DH, Klingenspor M, Klopstock T, Ollert M, Wolf E, Fuchs H, Gailus-Durner V, Angelis MH de, Weissmann N, Doan JW, Bassett DJP, Grossman LI (2012) Cytochrome c oxidase subunit 4 isoform 2-knockout mice show reduced enzyme activity, airway hyporeactivity, and lung pathology. The FASEB Journal 26(9):3916–3930. https://doi.org/10.1096/fj.11-203273

Kanazawa H, Tochino Y, Asai K, Ichimaru Y, Watanabe T, Hirata K (2012) Validity of HMGB1 measurement in epithelial lining fluid in patients with COPD. European Journal of Clinical Investigation 42(4):419–426. https://doi.org/10.1111/j.1365-2362.2011.02598.x

Kilburn KH (1984) Particles causing lung disease. Environ Health Perspect 55:97–109

Kim J-E, Kang T-C (2018) Differential Roles of Mitochondrial Translocation of Active Caspase-3 and HMGB1 in Neuronal Death Induced by Status Epilepticus. Front Cell Neurosci 12. https://doi.org/10.3389/fncel.2018.00301

Kirkhorn SR, Garry VF (2000) Agricultural lung diseases. Environ Health Perspect 108(Suppl 4):705–712

Kirychuk SP, Reynolds SJ, Koehncke NK, Lawson J, Willson P, Senthilselvan A, Marciniuk D, Classen HL, Crowe T, Just N, Schneberger D, Dosman JA (2010) Endotoxin and Dust at Respirable and Nonrespirable Particle Sizes are not Consistent Between Cage- and Floor-Housed Poultry Operations. The Annals of Occupational Hygiene 54(7):824–832. https://doi.org/10.1093/annhyg/meq047

Larsson KA, Eklund AG, Hansson LO, Isaksson BM, Malmberg PO (1994) Swine dust causes intense airways inflammation in healthy subjects. Am J Respir Crit Care Med 150(4):973–977. https://doi.org/10.1164/ajrccm.150.4.7921472

Lee H-C, Wei Y-H (2005) Mitochondrial biogenesis and mitochondrial DNA maintenance of mammalian cells under oxidative stress. The International Journal of Biochemistry & Cell Biology 37(4):822–834. https://doi.org/10.1016/j.biocel.2004.09.010

Li G, Tang D, Lotze MT (2013) Ménage à Trois in Stress: DAMPs, Redox and Autophagy. Semin Cancer Biol 23(5):380–390. https://doi.org/10.1016/j.semcancer.2013.08.002

Li J, Kokkola R, Tabibzadeh S, Yang R, Ochani M, Qiang X, Harris HE, Czura CJ, Wang H, Ulloa L, Wang H, Warren HS, Moldawer LL, Fink MP, Andersson U, Tracey KJ, Yang H (2003) Structural Basis for the Proinflammatory Cytokine Activity of High Mobility Group Box 1. Mol Med 9(1–2):37–45

Massaro GD, Gail DB, Massaro D (1975) Lung oxygen consumption and mitochondria of alveolar epithelial and endothelial cells. Journal of Applied Physiology 38(4):588–592. https://doi.org/10.1152/jappl.1975.38.4.588

Massey N, Puttachary S, Bhat SM, Kanthasamy AG, Charavaryamath C (2019) HMGB1-RAGE Signaling Plays a Role in Organic Dust-Induced Microglial Activation and Neuroinflammation. Toxicol Sci 169(2):579–592. https://doi.org/10.1093/toxsci/kfz071

May S, Romberger DJ, Poole JA (2012) Respiratory Health Effects of Large Animal Farming Environments. J Toxicol Environ Health B Crit Rev 15(8):524–541. https://doi.org/10.1080/10937404.2012.744288

Motwani M, Pesiridis S, Fitzgerald KA (2019) DNA sensing by the cGAS–STING pathway in health and disease. Nature Reviews Genetics 20(11):657–674. https://doi.org/10.1038/s41576-019-0151-1

Nath Neerukonda S, Mahadev-Bhat S, Aylward B, Johnson C, Charavaryamath C, Arsenault RJ (2018) Kinome analyses of inflammatory responses to swine barn dust extract in human bronchial epithelial and monocyte cell lines. Innate Immun 24(6):366–381. https://doi.org/10.1177/1753425918792070

Nordgren TM, Charavaryamath C (2018) Agriculture Occupational Exposures and Factors Affecting Health Effects. Curr Allergy Asthma Rep 18(12):65. https://doi.org/10.1007/s11882-018-0820-8

O'Connor KA, Hansen MK, Rachal Pugh C, Deak MM, Biedenkapp JC, Milligan ED, Johnson JD, Wang H, Maier SF, Tracey KJ, Watkins LR (2003) Further characterization of high mobility group box 1 (HMGB1) as a proinflammatory cytokine: central nervous system effects. Cytokine 24(6):254–265. https://doi.org/10.1016/j.cyto.2003.08.001

Ogawa EN, Ishizaka A, Tasaka S, Koh H, Ueno H, Amaya F, Ebina M, Yamada S, Funakoshi Y, Soejima J, Moriyama K, Kotani T, Hashimoto S, Morisaki H, Abraham E, Takeda J (2006) Contribution of High-Mobility Group Box-1 to the Development of Ventilator-induced Lung Injury. Am J Respir Crit Care Med 174(4):400–407. https://doi.org/10.1164/rccm.200605-699OC

Paudel YN, Semple BD, Jones NC, Othman I, Shaikh MF (2019) High mobility group box 1 (HMGB1) as a novel frontier in epileptogenesis: from pathogenesis to therapeutic approaches. Journal of Neurochemistry 151(5):542–557. https://doi.org/10.1111/jnc.14663

Piantadosi CA, Suliman HB (2017) Mitochondrial Dysfunction in Lung Pathogenesis. Annual Review of Physiology 79(1):495–515. https://doi.org/10.1146/annurev-physiol-022516-034322

Pisetsky DS (2014) The Translocation of Nuclear Molecules During Inflammation and Cell Death. Antioxid Redox Signal 20(7):1117–1125. https://doi.org/10.1089/ars.2012.5143

Ploumi C, Daskalaki I, Tavernarakis N (2017) Mitochondrial biogenesis and clearance: a balancing act. The FEBS Journal 284(2):183–195. https://doi.org/10.1111/febs.13820

Poole JA, Alexis NE, Parks C, MacInnes AK, Gentry-Nielsen MJ, Fey PD, Larsson L, Allen-Gipson D, Essen SGV, Romberger DJ (2008) Repetitive organic dust exposure in vitro impairs macrophage differentiation and function. Journal of Allergy and Clinical Immunology 122(2):375-382.e4. https://doi.org/10.1016/j.jaci.2008.05.023

Poole JA, Burrell AM, Wyatt TA, Kielian TL, Romberger DJ (2010a) NOD2 Negatively Regulates Organic Dust-Induced Inflammation in Monocytes/Macrophages. Journal of Allergy and Clinical Immunology 125(2, Supplement 1):AB118. https://doi.org/10.1016/j.jaci.2009.12.467

Poole JA, Dooley GP, Saito R, Burrell AM, Bailey KL, Romberger DJ, Mehaffy J, Reynolds SJ (2010b) Muramic Acid, Endotoxin, 3-Hydroxy Fatty Acids, and Ergosterol Content Explain Monocyte and Epithelial Cell Inflammatory Responses to Agricultural Dusts. J Toxicol Environ Health A 73(10):684–700. https://doi.org/10.1080/15287390903578539

Poole JA, Romberger DJ (2012) Immunological and Inflammatory Responses to Organic Dust in Agriculture. Curr Opin Allergy Clin Immunol 12(2):126–132. https://doi.org/10.1097/ACI.0b013e3283511d0e

Poole JA, Wyatt TA, Essen SGV, Hervert J, Parks C, Mathisen T, Romberger DJ (2007) Repeat organic dust exposure–induced monocyte inflammation is associated with protein kinase C activity. Journal of Allergy and Clinical Immunology 120(2):366–373. https://doi.org/10.1016/j.jaci.2007.04.033

Poole JA, Wyatt TA, Kielian T, Oldenburg P, Gleason AM, Bauer A, Golden G, West WW, Sisson JH, Romberger DJ (2011) Toll-like receptor 2 regulates organic dust-induced airway inflammation. Am J Respir Cell Mol Biol 45(4):711–719. https://doi.org/10.1165/rcmb.2010-0427OC

Prakash YS, Pabelick CM, Sieck GC (2017) Mitochondrial Dysfunction in Airway Disease. CHEST 152(3):618–626. https://doi.org/10.1016/j.chest.2017.03.020

Rask-Andersen A, Malmberg P, Lundholm M (1989) Endotoxin levels in farming: absence of symptoms despite high exposure levels. Br J Ind Med 46(6):412–416

Reynolds SJ, Donham KJ, Whitten P, Merchant JA, Burmeister LF, Popendorf WJ (1996) Longitudinal evaluation of dose-response relationships for environmental exposures and pulmonary function in swine production workers. Am J Ind Med 29(1):33–40. https://doi.org/10.1002/(SICI)1097-0274(199601)29:1<33::AID-AJIM5>3.0.CO;2-#

Riley JS, Tait SW (2020) Mitochondrial DNA in inflammation and immunity. EMBO Rep 21(4). https://doi.org/10.15252/embr.201949799

Romberger DJ, Bodlak V, Von Essen SG, Mathisen T, Wyatt TA (2002) Hog barn dust extract stimulates IL-8 and IL-6 release in human bronchial epithelial cells via PKC activation. Journal of Applied Physiology 93(1):289–296. https://doi.org/10.1152/japplphysiol.00815.2001

Sappington PL, Yang R, Yang H, Tracey KJ, Delude RL, Fink MP (2002) HMGB1 B box increases the permeability of Caco-2 enterocytic monolayers and impairs intestinal barrier function in mice. Gastroenterology 123(3):790–802. https://doi.org/10.1053/gast.2002.35391

Schaeffer JW, Reynolds S, Magzamen S, VanDyke A, Gottel NR, Gilbert JA, Owens SM, Hampton-Marcell JT, Volckens J (2017) Size, Composition, and Source Profiles of Inhalable Bioaerosols from Colorado Dairies. Environ Sci Technol 51(11):6430–6440. https://doi.org/10.1021/acs.est.7b00882

Schenker MB, Christiani D, Cormier Y, Dimich-Ward H, Doekes G, Dosman J, Douwes J, Dowling K, Enarson D, Green F, Heederik D, Husman K, Kennedy S, Kullman G, Lacasse Y, Lawson B, Malmberg P, May J, McCurdy S, Merchant J, Myers J, Nieuwenhuijsen M, Olenchock S, Saiki C, Schwartz D, Seiber J, Thorne P, Wagner G, White N, Xu X, Chan-Yeung M (1998) Respiratory health hazards in agriculture. American journal of respiratory and critical care medicine 158(5 II)

Schneberger D, DeVasure JM, Bailey KL, Romberger DJ, Wyatt TA (2017) Effect of low-level CO 2 on innate inflammatory protein response to organic dust from swine confinement barns. J Occup Med Toxicol 12(1):9. https://doi.org/10.1186/s12995-017-0155-8

Schumacker PT, Gillespie MN, Nakahira K, Choi AMK, Crouser ED, Piantadosi CA, Bhattacharya J (2014) Mitochondria in lung biology and pathology: more than just a powerhouse. American Journal of Physiology-Lung Cellular and Molecular Physiology 306(11):L962–L974. https://doi.org/10.1152/ajplung.00073.2014

Senthilselvan A, Chénard L, Ulmer K, Gibson-Burlinguette N, Leuschen C, Dosman JA (2007) Excess Respiratory Symptoms in Full-time Male and Female Workers in Large-Scale Swine Operations. CHEST 131(4):1197–1204. https://doi.org/10.1378/chest.06-2323

Senthilselvan A, Dosman JA, Chénard L, Burch LH, Predicala BZ, Sorowski R, Schneberger D, Hurst T, Kirychuk S, Gerdts V, Cormier Y, Rennie DC, Schwartz DA (2009) Toll-like receptor 4 variants reduce airway response in human subjects at high endotoxin levels in a swine facility. Journal of Allergy and Clinical Immunology 123(5):1034-1040.e2. https://doi.org/10.1016/j.jaci.2009.02.019

Sethi RS, Schneberger D, Charavaryamath C, Singh B (2017) Pulmonary innate inflammatory responses to agricultural occupational contaminants. Cell Tissue Res 367(3):627–642. https://doi.org/10.1007/s00441-017-2573-4

Sorci G, Riuzzi F, Giambanco I, Donato R (2013) RAGE in tissue homeostasis, repair and regeneration. Biochimica et Biophysica Acta (BBA) - Molecular Cell Research 1833(1):101–109. https://doi.org/10.1016/j.bbamcr.2012.10.021

Štros M (2010) HMGB proteins: Interactions with DNA and chromatin. Biochimica et Biophysica Acta (BBA) - Gene Regulatory Mechanisms 1799(1):101–113. https://doi.org/10.1016/j.bbagrm.2009.09.008

Takata K, Kitamura Y, Tsuchiya D, Kawasaki T, Taniguchi T, Shimohama S (2004) High mobility group box protein-1 inhibits microglial Aβ clearance and enhances Aβ neurotoxicity. Journal of Neuroscience Research 78(6):880–891. https://doi.org/10.1002/jnr.20340

Tang D, Kang R, Livesey KM, Kroemer G, Billiar TR, Van Houten B, Zeh HJ, Lotze MT (2011) High-Mobility Group Box 1 Is Essential for Mitochondrial Quality Control. Cell Metabolism 13(6):701–711. https://doi.org/10.1016/j.cmet.2011.04.008

Tang D, Kang R, Zeh HJ, Lotze MT (2010) High-Mobility Group Box 1, Oxidative Stress, and Disease. Antioxidants & Redox Signaling 14(7):1315–1335. https://doi.org/10.1089/ars.2010.3356

Tarlo SM, Malo J-L (2009) An Official ATS Proceedings: Asthma in the Workplace. Proc Am Thorac Soc 6(4):339–349. https://doi.org/10.1513/pats.200810-119ST

Ugrinova I, Pasheva E (2017) Chapter Two - HMGB1 Protein: A Therapeutic Target Inside and Outside the Cell. In: Donev R (ed) Advances in Protein Chemistry and Structural Biology. Academic Press, pp 37–76

VanPatten S, Al-Abed Y (2018) High Mobility Group Box-1 (HMGb1): Current Wisdom and Advancement as a Potential Drug Target. J Med Chem 61(12):5093–5107. https://doi.org/10.1021/acs.jmedchem.7b01136

Viegas C, Faria T, Monteiro A, Caetano LA, Carolino E, Quintal Gomes A, Viegas S (2018) A Novel Multi-Approach Protocol for the Characterization of Occupational Exposure to Organic Dust—Swine Production Case Study. Toxics 6(1):5. https://doi.org/10.3390/toxics6010005

Von Essen S, Donham K (1999) Illness and injury in animal confinement workers. Occup Med 14(2):337–350

Von Essen S, Moore G, Gibbs S, Larson KL (2010) Respiratory issues in beef and pork production: recommendations from an expert panel. J Agromedicine 15(3):216–225. https://doi.org/10.1080/1059924X.2010.486283

Von Essen S, Romberger D (2003) The respiratory inflammatory response to the swine confinement building environment: the adaptation to respiratory exposures in the chronically exposed worker. J Agric Saf Health 9(3):185–196. https://doi.org/10.13031/2013.13684

Wang H, Bloom O, Zhang M, Vishnubhakat JM, Ombrellino M, Che J, Frazier A, Yang H, Ivanova S, Borovikova L, Manogue KR, Faist E, Abraham E, Andersson J, Andersson U, Molina PE, Abumrad NN, Sama A, Tracey KJ (1999) HMG-1 as a Late Mediator of Endotoxin Lethality in Mice. Science 285(5425):248–251. https://doi.org/10.1126/science.285.5425.248

Wang Z, Larsson K, Palmberg L, Malmberg P, Larsson P, Larsson L (1997) Inhalation of swine dust induces cytokine release in the upper and lower airways. European Respiratory Journal 10(2):381–387

Yang H, Hreggvidsdottir HS, Palmblad K, Wang H, Ochani M, Li J, Lu B, Chavan S, Rosas-Ballina M, Al-Abed Y, Akira S, Bierhaus A, Erlandsson-Harris H, Andersson U, Tracey KJ (2010) A critical cysteine is required for HMGB1 binding to Toll-like receptor 4 and activation of macrophage cytokine release. PNAS 107(26):11942–11947. https://doi.org/10.1073/pnas.1003893107

Yang R, Harada T, Mollen KP, Prince JM, Levy RM, Englert JA, Gallowitsch-Puerta M, Yang L, Yang H, Tracey KJ, Harbrecht BG, Billiar TR, Fink MP (2006) Anti-HMGB1 Neutralizing Antibody Ameliorates Gut Barrier Dysfunction and Improves Survival after Hemorrhagic Shock. Mol Med 12(4–6):105–114. https://doi.org/10.2119/2006-00010.Yang

Yang R, Miki K, Oksala N, Nakao A, Lindgren L, Killeen ME, Mennander A, Fink MP, Tenhunen J (2009) Bile high-mobility group box 1 contributes to gut barrier dysfunction in experimental endotoxemia. American Journal of Physiology-Regulatory, Integrative and Comparative Physiology 297(2):R362–R369. https://doi.org/10.1152/ajpregu.00184.2009

Zhang Q, Raoof M, Chen Y, Sumi Y, Sursal T, Junger W, Brohi K, Itagaki K, Hauser CJ (2010) Circulating mitochondrial DAMPs cause inflammatory responses to injury. Nature 464(7285):104–107. https://doi.org/10.1038/nature08780

Zhu X, Messer JS, Wang Y, Lin F, Cham CM, Chang J, Billiar TR, Lotze MT, Boone DL, Chang EB (2015) Cytosolic HMGB1 controls the cellular autophagy/apoptosis checkpoint during inflammation. J Clin Invest 125(3):1098–1110. https://doi.org/10.1172/JCI76344

Appendix. Tables

Table 2.1 Respiratory diseases associated with organic dust exposure

Disease	Symptom	Pathophysiology	Source
Rhinitis	Congestion, rhinorrhea, sneezing	Neutrophil influx IL-8/CXCL8, IL-6 levels	(Dosman et al. 2006a; Poole et al. 2007)
Asthma	Wheeze, cough, chest tightness, shortness of breath	IgE-mediated eosinophilic influx	(Dosman et al. 2006b; Tarlo and Malo 2009; Eduard et al. 2009)
Asthma-like syndrome	Cough, chest tightness, dyspnea, wheezing	Normal pulmonary function testing Airway hyperresponsiveness to methacholine challenge Increased Neutrophils Absence of eosinophilic infiltrates	(Kirkhorn and Garry 2000; Dosman et al. 2006b; Von Essen et al. 2010)
Chronic Bronchitis COPD	chronic cough, sputum production, dyspnea or wheezing	Fibrosis Emphysema Mucus hypersecretion Neutrophil influx Protease release	(Eduard et al. 2009; Viegas et al. 2018)
Mucus membrane syndrome	Combination of nasal, eye and throat complaints with congestion, and rhinorrhea	Increased levels of IL-1α, IL-1β, IL-6	(Von Essen and Donham 1999; Kirkhorn and Garry 2000)
Organic dust toxic syndrome	Fever, malaise, myalgia, chest tightness, headache, nausea	Neutrophilia, Neutrophils in BALF Normal blood gases Normal lung function	(Donham et al. 1995; Von Essen and Donham 1999; Von Essen and Romberger 2003)

Table 2.2 Pathophysiological effects of HMGB1

Organ system	Response to HMGB1	Source
Central nervous	Anorexia, fever, weight loss, sickness syndrome	(Agnello et al. 2002; O'Connor et al. 2003)
Cardiovascular	Vascular leakage, suppression of cardiac output	(Liu et al. 2006b; Hagiwara et al. 2008)
Pulmonary	Inflammation, neutrophil recruitment, ARDS-like syndrome, hypoxia	(Abraham et al. 2000; Ogawa et al. 2006)
Gastrointestinal	Inflammation, bacterial translocation, loss of epithelial barrier function	(Sappington et al. 2002; Yang et al. 2006)
Renal-Hepatic	Loss of epithelial barrier function, renal tubular injury, hepatic ischemic-reperfusion injury	(Bruchfeld et al. 2008; Chung et al. 2008)

Table 2.3 Mitochondrial dynamics in airway inflammation

Name	Role in lung	Disease association
Fission/Fusion	Cells that use OXPHOS metabolism have elongated mitochondria networks	Lung cancer Pulmonary hypertension COPD
Biogenesis	Occurs in cells of distal airways, smooth muscle of small blood vessels during growth, high energy demand or stress	ALI Pneumonia Bronchial smooth muscle remodeling in asthma Lung cancer COPD *S. aureus* infection
Mitophagy	Occurs in epithelial cells, fibroblasts, and alveolar macrophages (AlvMs)	Pulmonary fibrosis COPD Cigarette smoke exposure Pulmonary vascular remodelling Pulmonary hypertension *S. aureus* infection

(Adapted from Cloonan and Choi 2016)

Table 2.4 Mitochondrial DAMPs in airway inflammation

mtDAMPs	Role in lung	Disease association
mROS	Secondary messenger Oxidative burst in AlvMs	ALI Pulmonary fibrosis COPD Asthma Pulmonary hypertension Lung cancer
ATP	Optimizes airway surface layer hydration, mucus composition, and mucociliary clearance	COPD Asthma
Calcium	Secondary messenger	Pulmonary hypertension Cystic Fibrosis
mtDNA	Encodes genes essential for OXPHOS. Activates the NLRP3. Inflammasome, neutrophils and AlvMs	IPF Pulmonary hypertension Lung cancer Asthma COPD
TFAM	Mitochondrial transcription factor Responds to cell stress	COPD *S.aureus* infection

(Adapted from Cloonan and Choi 2016)

CHAPTER 3. ETHYL PYRUVATE REDUCES ORGANIC DUST-INDUCED AIRWAY INFLAMMATION BY TARGETING HMGB1-RAGE SIGNALING

Sanjana Mahadev Bhat [1], Nyzil Massey [1], Locke A. Karriker [2], Baljit Singh [3], Chandrashekhar Charavaryamath [1*]

[1] Department of Biomedical Sciences, College of Veterinary Medicine, Iowa State University, Ames, IA., [2] Department of Veterinary Diagnostic and Production Animal Medicine, Lloyd Veterinary Medical Center, Iowa State university, Ames, IA., [3] Faculty of Veterinary Medicine, University of Calgary, Calgary, T2N 1N4, Canada

*To whom correspondence should be addressed: Chandrashekhar Charavaryamath, BVSc, MVSc, PhD., Assistant Professor, Department of Biomedical Sciences, Iowa State University, Ames, IA 50011. Telephone: (515) 294-7710; Fax: (515) 294-2315; Email: chandru@iastate.edu

Keywords: Organic Dust, HMGB1, RAGE, Lung Inflammation, Ethyl Pyruvate

Modified from a manuscript published in the *Journal of Respiratory Research* (doi: 10.1186/s12931-019-0992-3)

Author Contributions

S.M. Bhat participated in the design of experiments, performed the experiments, analyzed the data and participated in writing. N. Massey performed organic dust extraction and immunohistochemistry and scored the images, L. Karriker collected the organic dust samples and edited the manuscript, B. Singh conceptualized and designed the animal exposure studies and edited the manuscript. C. Charavaryamath conceived the study and designed the experiments, performed the animal experiments, dust extraction, participated in the interpretation of data and wrote the manuscript. All authors have read and approved the final manuscript.

Abbreviations

ASM: airway smooth muscle; BALT: bronchus associated lymphoid tissue; CAFOs: concentrated animal feeding operations; DAMPs: damage associated molecular patterns; EP: ethyl pyruvate; HMGB1: high mobility group box 1; LPS: lipopolysaccharide; NLS: nuclear

localization sites; MAMPs: microbial associated molecular patterns; PGN: peptidoglycan; OD: organic dust; ODE: organic dust extract; RAGE: receptor for advanced glycation end products

Abstract

Animal production workers are persistently exposed to organic dust and can suffer from a variety of respiratory disease symptoms and an annual decline in lung function. The role of high mobility group box-1 (HMGB1) in inflammatory airway diseases is emerging. Hence, we tested a hypothesis that organic dust exposure of airway epithelial cells induces nucleocytoplasmic translocation of HMGB1, and blocking this translocation dampens organic dust-induced lung inflammation.

Rats were exposed to either ambient air or swine barn (8 hours/day for either 1, 5, or 20 days) and lung tissues were processed for immunohistochemistry. Swine barn dust was collected, and organic dust extract (ODE) was prepared and sterilized. Human airway epithelial cell line (BEAS-2B) was exposed to either medium or organic dust extract followed by treatment with medium or ethyl pyruvate (EP) or anti-HMGB1 antibody. Immunoblotting, ELISA, and other assays were performed at 0 (control), 6, 24, and 48 hours. Data (as mean ± SEM) was analyzed using one or two-way ANOVA followed by Bonferroni's *post hoc* comparison test. A p-value of less than 0.05 was considered significant.

Compared to controls, barn exposed rats showed an increase in the expression of HMGB1 in the lungs. Compared to controls, ODE-exposed BEAS-2B cells showed nucleocytoplasmic translocation of HMGB1, co-localization of HMGB1 and RAGE, reactive species, and pro-inflammatory cytokine production. EP treatment reduced the ODE-induced nucleocytoplasmic translocation of HMGB1, HMGB1 expression in the cytoplasmic fraction, GM-CSF, and IL-1β production and augmented the production of TGF-β1 and IL-10. Anti-HMGB1 treatment reduced

ODE-induced NF-κB p65 expression, IL-6, ROS, and RNS but augmented TGF-β1 and IL-10 levels. HMGB1-RAGE signaling is an attractive target to abrogate OD-induced lung inflammation.

Introduction

Globally agriculture employs about 1.3 billion people (International Labor Organization, 2018) and in the US, about 1.8 million people work in the agriculture industry. However, agriculture is considered a dangerous profession due to significant number of deaths, injuries, and morbidities (reviewed in (Sethi, et al., 2017)). People who work in agriculture and other related industries are persistently exposed to many contaminants and suffer from respiratory diseases and other conditions (reviewed in (Sethi, Schneberger, Charavaryamath and Singh, 2017) (American Thoracic Society, 1998)). Among the occupational contaminants, persistent exposure to organic dust (OD) is central to the negative health effects of work-related exposures. OD is a complex mixture of particulate matter of varying sizes, microbes and microbial products (Wunschel and Poole, 2016). Workers from concentrated animal feeding operations (CAFOs) involved in swine, diary (Davidson, et al., 2017) and poultry production including duck hatcheries (Guillam, et al., 2017) (reviewed in (Sethi, Schneberger, Charavaryamath and Singh, 2017)) as well as other industries (sewage handlers, waste handlers and bakery workers) are persistently exposed to the OD.

In North America, more than one million men, women and children suffer from exposure to OD (AgConnections). There is a strong link between exposure to OD and development of inflammatory airway diseases and annual decline in lung function (reviewed in (Charavaryamath and Singh, 2006, Nordgren and Charavaryamath, 2018)). Individuals exposed to OD report a range of respiratory and other symptoms including bronchitis, chest tightness, nasal congestion, organic

dust toxic syndrome, occupational asthma, mucus membrane irritation, nausea, headache, mood changes, altered immunity (Iowa State University and University of Iowa, 2002, Sahlander, et al., 2012, Viegas, et al., 2013), and increased risks of lung cancer (Peters, et al., 2012). Presence of multiple microbial and non-microbial factors in OD and broad range of health effects upon exposure are a significant public health concern. Currently, there are limited therapeutic options to treat OD-induced inflammatory airway diseases.

OD exposure induced respiratory symptoms and long-term changes in lung function are a major occupational health issue in swine production workers (reviewed in (Sethi, Schneberger, Charavaryamath and Singh, 2017, Wunschel and Poole, 2016)). Previously, experimental exposure of human volunteers to swine barn environment indicated an underlying inflammatory process (Senthilselvan, et al., 1997). We employed a unique rat model mimicking human occupational exposure to swine barn environment and showed that single 8 hour exposure induces airway inflammation and reactivity. In the same model, multiple (5 and 20-day) exposures resulted in dampened airway inflammation and reactivity. Surprisingly, there was an increase in the number of mucus producing goblet cells in the airways and activation of bronchus-associated lymphoid tissue (BALT) following 20-day exposure (Charavaryamath, et al., 2005). Mechanisms leading to the development of these airway remodeling features despite dampened inflammation and airway reactivity with 20-day exposure remain elusive.

Next, using wild type or *tlr4* mutant mouse, we demonstrated that barn exposure-induced lung inflammation, but not airway reactivity, is dependent on TLR4. In the same model, we documented airway epithelial damage in a TLR4-independent manner (Charavaryamath, et al., 2008). Subsequently, the roles of TLR9 (Schneberger, et al., 2016), TLR2 (Poole, et al., 2011), NOD2 (Poole, et al., 2010), MyD88 (Bauer, et al., 2013), and protein kinase C epsilon (PKC ε) in

organic dust-induced airway inflammation have been demonstrated. OD exposure has also been linked to bone loss indicating the systemic effects of exposure (Wells, et al., 2017) (reviewed in (Carrington and Poole, 2018)). These studies and our previous work (reviewed in (Sethi, Schneberger, Charavaryamath and Singh, 2017)) demonstrate that OD is complex in composition and inhaled OD elicits host response through multiple signaling pathways. Despite increased understanding of mechanisms of OD-induced lung inflammation, therapeutic options to treat OD-induced lung diseases are limited.

Damage associated molecular patterns (DAMPs) are endogenous molecules that are released upon tissue damage (Frevert, et al., 2017). DAMPs are increasingly becoming important in chronic airway diseases (Wong, et al., 2017). High-mobility group box 1 (HMGB1) is a prototype DAMP present in almost all nucleated cells. HMGB1 is a normal nuclear protein that upon translocation to cytoplasm and secretion into extracellular milieu behaves as a DAMP with inflammatory cytokine-like properties (reviewed in (Ding, et al., 2016, Kang, et al., 2014)). Immune activation or necrosis is known to cause nucleocytoplasmic translocation and release of HMGB1 into extra-cellular space in many inflammatory airway diseases (Ding, Cui and Liu, 2016, Wong, To, Santos, Allam, Dalton, Djordjevic, Donnelly, Padula and Sukkar, 2017). HMGB1 is known to play a pathogenic role in asthma with contributions to airway smooth muscle (ASM) dysfunction and airway reactivity (Di Candia, et al., 2017). Blocking HMGB1 has been beneficial in a mouse model of allergic airway disease and sepsis (Hou, et al., 2015, Zhou, et al., 2014).

Post-translational modifications such as phosphorylation and acetylation determine the nucleocytoplasmic translocation, secretion, and pathogenic role of secreted HMGB1 (Richard, et al., 2017, Youn and Shin, 2006). Nucleocytoplasmic translocation of HMGB1 involves JAK-STAT1 mediated acetylation of lysine residues on nuclear localization sites (NLS) whereas

pyroptosis or exocytosis of secretory lysosomes leads to secretion of HMGB1 into extracellular milieu (reviewed in (Andersson, et al., 2018)). Several tools such as JAK/STAT1 inhibitor (Lu, et al., 2014), sirtuin 1 (Hwang, et al., 2015), anti-HMGB1 antibodies (Yang, et al., 2006) and ethyl pyruvate (Shin, et al., 2015) have been used to abrogate the pathological effects of HMGB1.

We tested a hypothesis that OD exposure of airway epithelial cells induces translocation of HMGB1 and blocking HMGB1 translocation dampens OD-induced lung inflammation. In the current study, using a human airway epithelial cell line (BEAS-2B) model, we demonstrate that OD-exposure induces nucleocytoplasmic translocation of HMGB1 and inflammation. Further, we show that EP or anti-HMGB1 treatment reduces OD-induced airway inflammation via blocking HMGB1 translocation and signaling through secreted HMGB1, respectively.

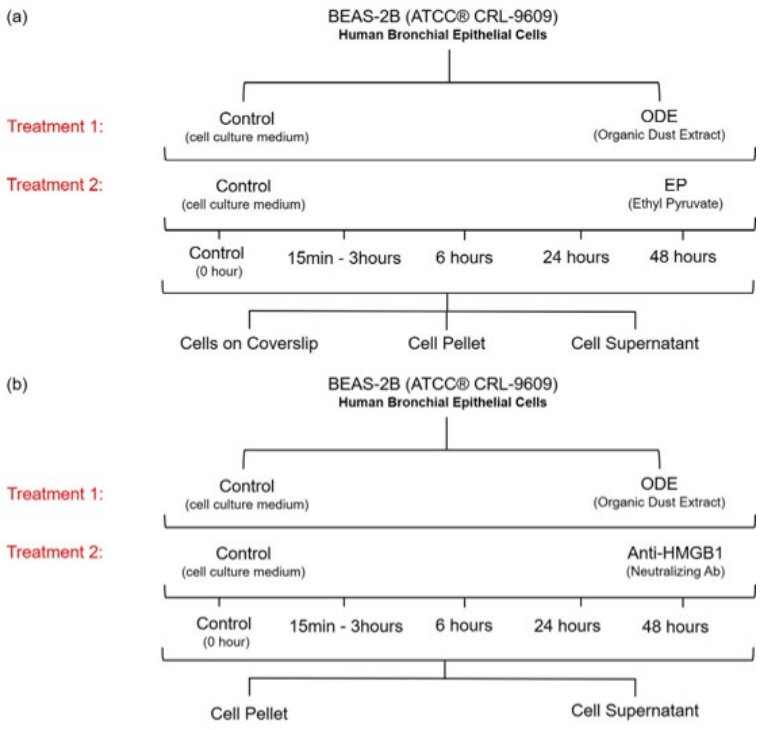

Figure 3.1 ODE exposure of BEAS-2B cells and EP or anti-HMGB1 neutralizing antibody treatment

BEAS-2B cells were treated with either medium (control) or ODE (treatment 1) followed by either medium, EP (a, treatment 2) or neutralizing HMGB1 antibody (b, treatment 2). Cells were processed for various assays at 0 (control), 6, 24 and 48 hours by collecting cells on coverslips or cell pellet or cell supernatant.

Results

Barn exposure and HMGB1 expression in the lungs

Using immunohistochemistry, we delineated cell specific semi-quantitative expression of HMGB1 in control and barn exposed rat lungs. The overall staining was assigned scores in a blinded manner by using a predetermined criterion (Table 3.2). Compared to controls, barn-exposed rat lungs showed significantly higher expression of HMGB1 in bronchiolar epithelium, alveolar septa, BALT, endothelium of blood vessels and ASM (Figure 3.2, a-g). In the bronchiolar epithelium, HMGB1 expression was at the tip of the airway epithelium. In the alveolar septa, type 2 alveolar epithelial cells showed predominant staining. Type 1 alveolar epithelial cells and alveolar macrophages were stained as well. Since these rat lungs had previously been lavaged, alveolar macrophages were not in abundance.

Endotoxin content of OD samples

Endotoxin units (EU/mL) measured in OD samples are presented (Table 3.1).

Table 3.1 Endotoxin assay to measure LPS content in the ODE samples

Sample No.	LPS (EU/mL)
1	1.140 ± 0.001
2	0.990 ± 0.0005
3	1.337 ± 0.0006
4	1.433 ± 0.02
5[a]	1.417 ± 0.002
6[b]	0.8067 ± 0.0008
7[c]	1.263 ± 0.0008

[a] pooled sample from samples 1 and 2. [b] pooled sample from samples 3 and 4. [c] pooled sample from samples 1, 2, 3 and 4.

EP treatment reduces ODE induced cytoplasmic expression of HMGB1

We used immunocytochemistry to detect expression of HMGB1. Using DAPI-stained nuclei as a reference nucleocytoplasmic translocation of HMGB1 was identified. Compared to the

medium-treated controls, ODE-treated cells (48 h) showed increased expression of HMGB1 in the cytoplasm (arrow in merged image, Figure 3.3 a). Compared to vehicle (medium), co-treatment with EP abrogated the ODE-induced increased expression of HMGB1 in the cytoplasm (arrow in merged image, Figure 3.3 b).

EP treatment reduces ODE induced HMGB1 expression in the cytoplasmic fraction

We performed western blotting to quantify the expression of HMGB1 in nuclear and cytoplasmic fractions of ODE-treated cells. Compared to controls, ODE exposure increased the HMGB1 protein levels in nuclear (6 and 48 h) and cytoplasmic (6 h) fractions (Figure 3.4, a-d). Compared to the vehicle (medium), co-treatment with EP significantly reduced the ODE-induced increase in HMGB1 protein levels in the cytoplasmic fractions at 6 h (Figure 3.4, b and d).

ODE exposure results in HMGB1 and RAGE co-localization

We performed immunocytochemistry for evaluating the expression of HMGB1 and RAGE. Following cell treatments, anti-HMGB1 and anti-RAGE stained (Cy3 and FITC, respectively) images were merged. Compared to controls (medium treated, 0 h), ODE-treatment induced an increase in the expression and co-localization of HMGB1 and RAGE in the cytoplasm (arrow, Figure 3.5a, 48 h); both changes were inhibited by co-treatment with EP. Following EP treatment, HMGB1 remained arrested in the normal nuclear location (Figure 3.5b, 48 h).

ODE induced ROS and RNS production

We quantified ROS and RNS levels in control and ODE treated cells to understand the effect of exposure to ODE in the presence or absence of HMGB1 secretion (EP treatment). Compared to the controls (medium, 0 h), ODE-treated cells produced significantly higher amounts of ROS and RNS at 6, 24, and 48 hours (Figure 3.6, a and b). Compared to vehicle (medium), co-treatment with EP significantly reduced ODE-induced ROS (Figure 3.6a) but not the RNS production (Figure 3.6b).

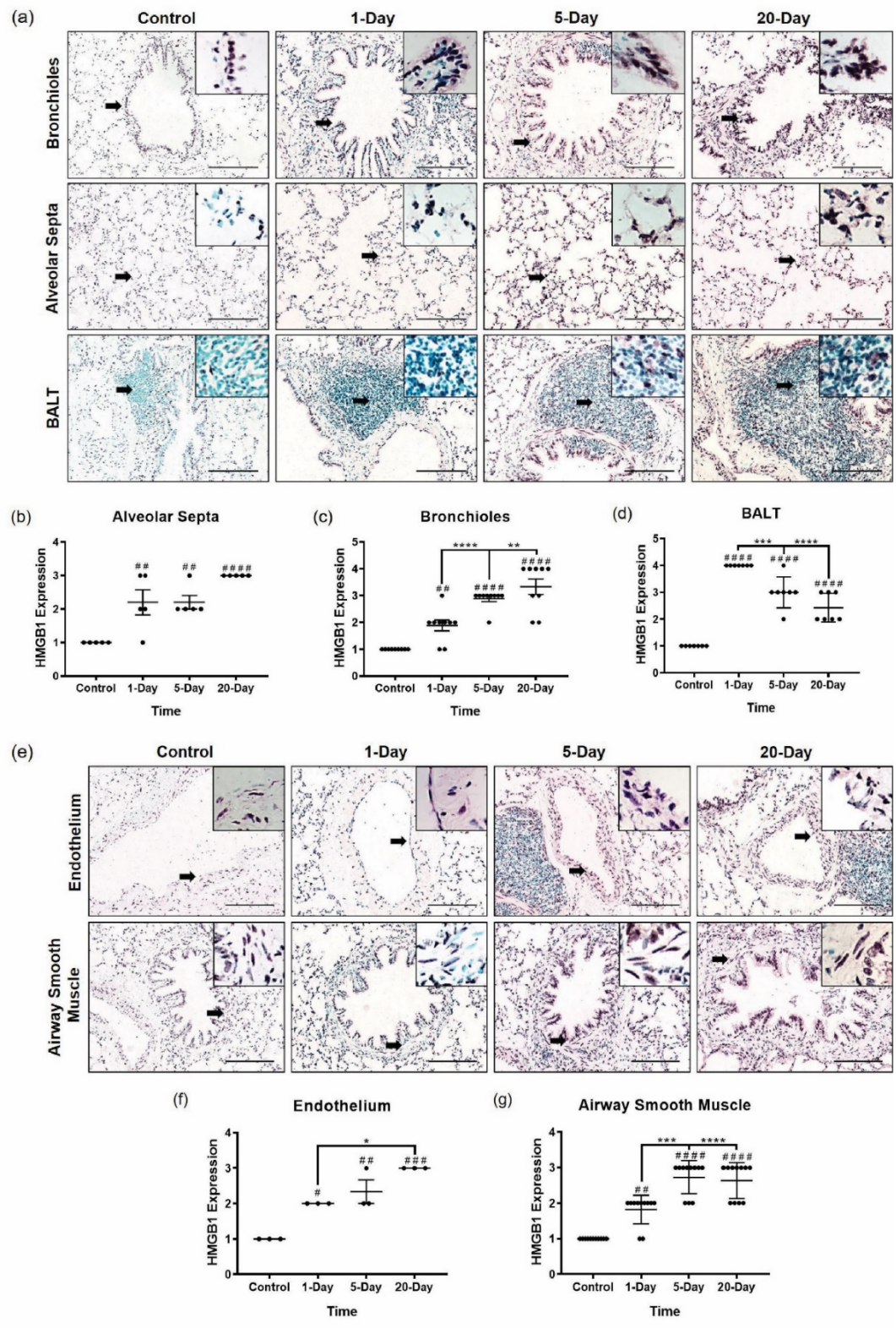

Figure 3.2 OD exposure of rats in the swine barn work environment and HMGB1 expression Immunohistochemical staining for HMGB1 expression was performed on rat lung tissues. Compared to controls, one, five and 20-day barn (organic dust) exposure of rats induced an

increase in the expression of HMGB1 in the bronchioles, alveolar septa and BALT (a) and endothelium of the blood vessels and airway smooth muscle (arrows and inset, bar = 100 µm, e), respectively. One-way ANOVA performed on immunohistochemical scores for HMGB1 expression in bronchioles (9 fields/animal), alveolar septa (5 fields/animal) and BALT (7 fields/animal) (b-d) and endothelium of blood vessels (3 fields/animal) and ASM (11 fields/animal) is presented (f and g). $^{*}p<0.05$, $^{**}p<0.005$, $^{***}p<0.0005$, $^{****}p<0.0001$.

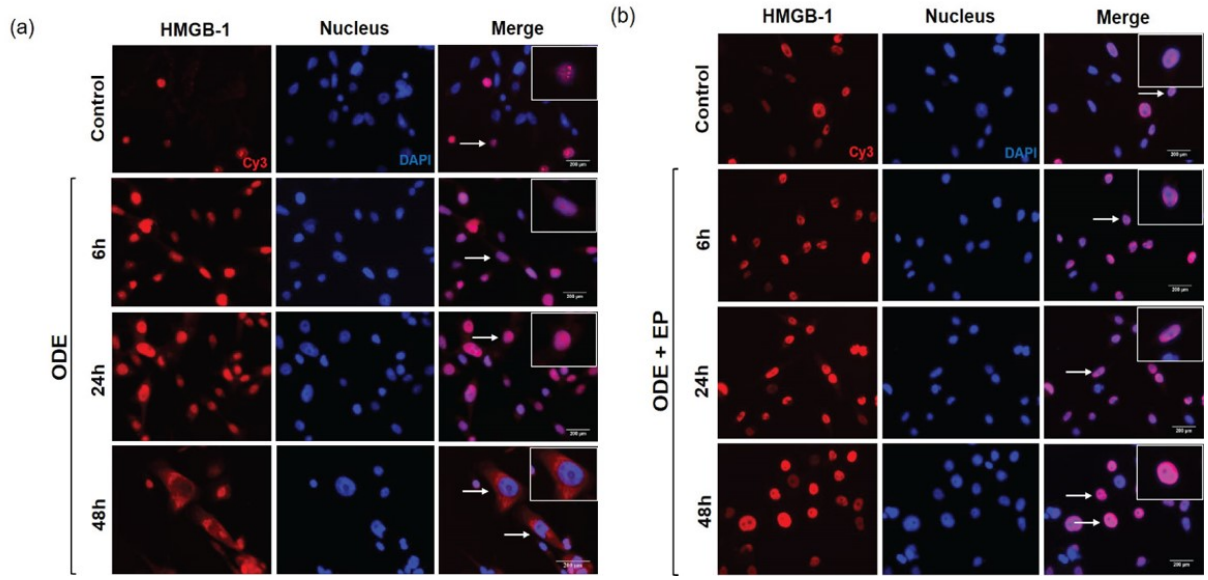

Figure 3.3 EP reduces ODE-exposure induced nucleocytoplasmic translocation of HMGB1
Medium (control, 0 h) or ODE (6, 24 and 48 h post) treated cells were stained with polyclonal anti-HMGB1 antibody and DAPI stain delineated the nuclei. Compared to controls, ODE treated cells showed nucleocytoplasmic translocation of HMGB1 (arrows and inset, bar = 200 µm, a). Compared to vehicle (medium), co-treatment with EP (2.5 µM) showed a marked decrease in ODE-induced nucleocytoplasmic translocation of HMGB-1 (arrows and inset, micrometer = 200 µm, b).

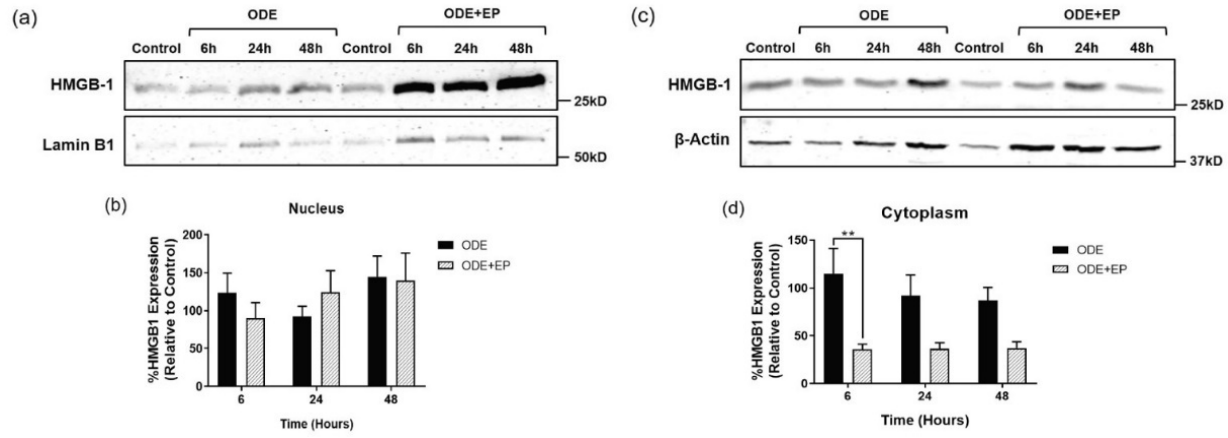

Figure 3.4 EP reduces ODE-exposure induced nucleocytoplasmic translocation of HMGB1
Medium (control, 0 h) or ODE (6, 24 and 48 h post) treated cells were processed for separation of nuclear and cytoplasmic fractions and western blotting to detect HMGB1 protein. Compared to

controls, ODE treated cells showed a temporal increase in HMGB1 expression (25 kD) in the (a) nuclear fraction at 6 and 48 h. Compared to vehicle (Ringer's solution), co-treatment with EP (2.5 μM) resulted in significantly decreased levels of HMGB1 in the cytoplasm at 6 h post-treatment indicating reduction in ODE-induced nucleocytoplasmic translocation of HMGB1 (d). HMGB1 (25kD) bands were normalized over either Lamin B1 (50kD, cytoplasmic fraction, a) or β-actin (37kD, nuclear fraction, b) and percentage intensity (n = 5/group) of treatment groups relative to control were analyzed using two-way ANOVA (c and d). $^{**}p<0.01$ (* indicates difference within the OD/barn exposure groups).

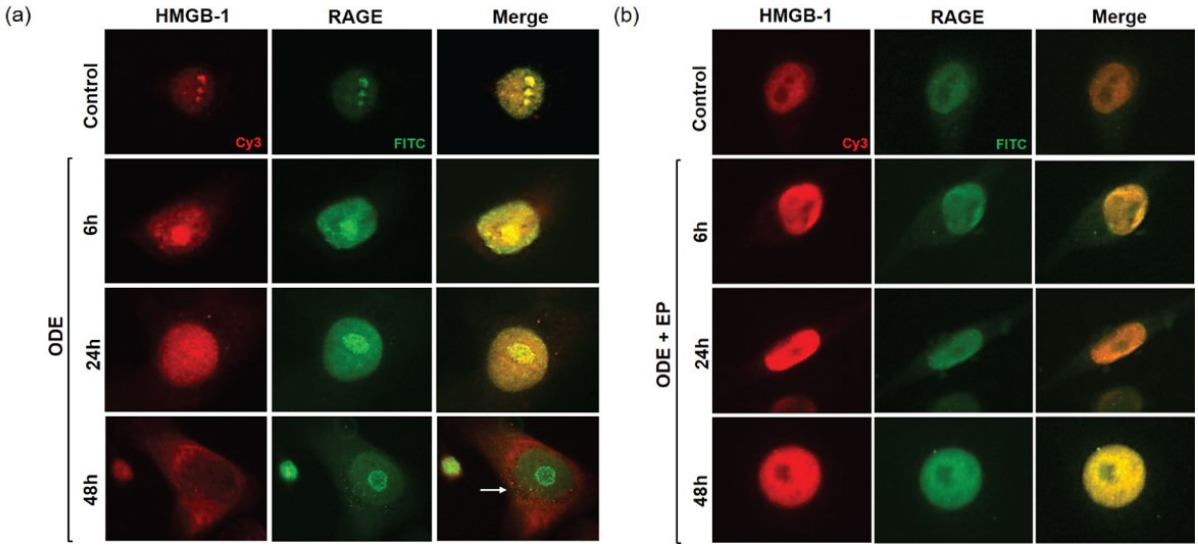

Figure 3.5 EP reduces ODE-exposure induced augmentation of RAGE expression and HMGB1-RAGE co-localization in the cytoplasm

Medium (control, 0 h) or ODE treated (6, 24 and 48 h post) treated cells were stained with polyclonal anti-HMGB1 or anti-RAGE antibodies. Compared to controls, ODE treated cells showed increased expression and nucleocytoplasmic translocation of HMGB1 (arrowhead, 48 h, a), increased expression of RAGE (48 h, a) and co-localization of HMGB1 and RAGE (white arrows, 48 h, a). Compared to vehicle (Ringer's solution), co-treatment with EP (2.5 μM) resulted in a marked decrease in ODE-induced nucleocytoplasmic translocation of HMGB-1 and co-localization of HMGB1 and expression of RAGE (arrows and inset, bar = 200μm, b).

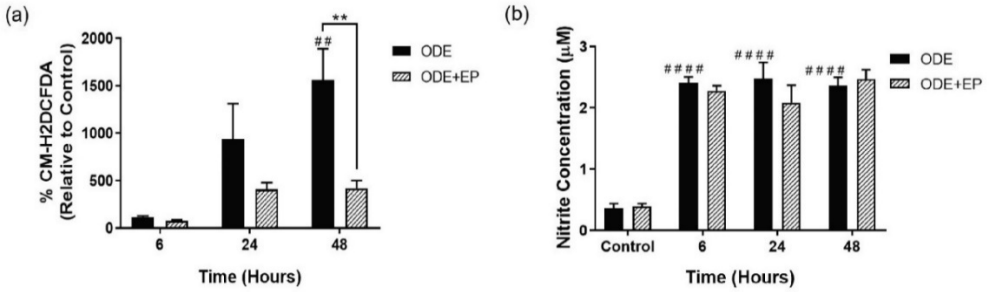

Figure 3.6 ODE exposure induces ROS and nitrite (secreted RNS) production and EP treatment reduces ODE-induced ROS production

Media alone (control, 0 h) or ODE (6, 24, and 48 h) treated cells were subjected to CM-H_2DCFDA and Griess' assay to quantify intracellular ROS production (a) and secreted nitrite concentration

(b) respectively (n=6). ODE exposure of cells resulted in significant increase in intracellular ROS and nitrite secretion (secreted RNS) into the media as early as 6 h post-treatment. Compared to vehicle treatment, cells co-treated with EP (2.5 μM) showed a significant reduction in ODE-induced ROS production at 48 h. Data analyzed with two-way ANOVA is represented (a and b). $^{\#\#}$ or $^{**}p < 0.01$ and **** or $^{\#\#\#\#}p<0.0001$. $^{\#}$ indicates significantly different from control whereas * indicates significant difference within the OD/barn exposure groups.

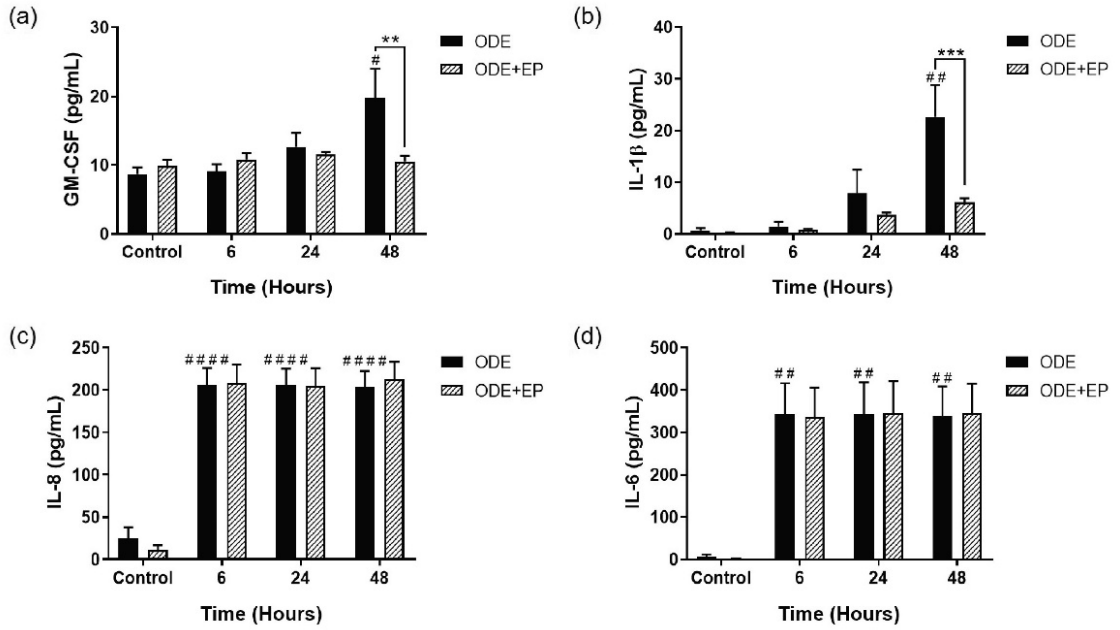

Figure 3.7 EP treatment reduces ODE exposure induced secretion of GM-CSF and IL-1β but not IL-8 and IL-6 levels

Compared to medium (controls, 0 h), ODE treated BEAS-2B cells secreted increased levels of GM-CSF, IL-1β, IL-8 and IL-6 (a-d) respectively. Compared to vehicle (Ringer's solution), co-treatment with EP (2.5 μM) significantly reduced ODE-induced GM-CSF and IL-1β levels (a and b). Data (n=6) analyzed using two-way ANOVA is represented. * or $^{\#}p<0.05$, ** or $^{\#\#}p<0.01$, *** or $^{\#\#\#}p<0.001$, **** or $^{\#\#\#\#}p<0.0001$. $^{\#}$ indicates different from control whereas * indicates difference within the OD/barn exposure groups.

ODE induced pro-inflammatory cytokines production

We quantified various cytokines in treated cell-supernatants to understand the effect of ODE in the presence or absence of HMGB1 secretion (EP treatment). Compared to controls (medium, 0 h), ODE-treated cells produced significantly higher amounts of GM-CSF, IL-1β, IL-8 and IL-6 ($p < 0.05$, Figure 3.7, a-d). Compared to vehicle (medium), co-treatment with EP significantly reduced ODE-induced increase in GM-CSF and IL-1β (Figure 3.7, a and b respectively) but not IL-8 and IL-6 levels.

EP-treatment increases ODE-induced production of TGF-β1 and IL-10

Compared to controls (medium, 0 h), ODE-treated cells produced significantly higher amounts of TGF-β1 at 6 and 24 h (Figure 3.8). Compared to vehicle (medium), co-treatment with EP significantly increased the TGF-β1 (24 and 48 h, Figure 8a) and IL-10 (6 and 48 h, Figure 8b) production.

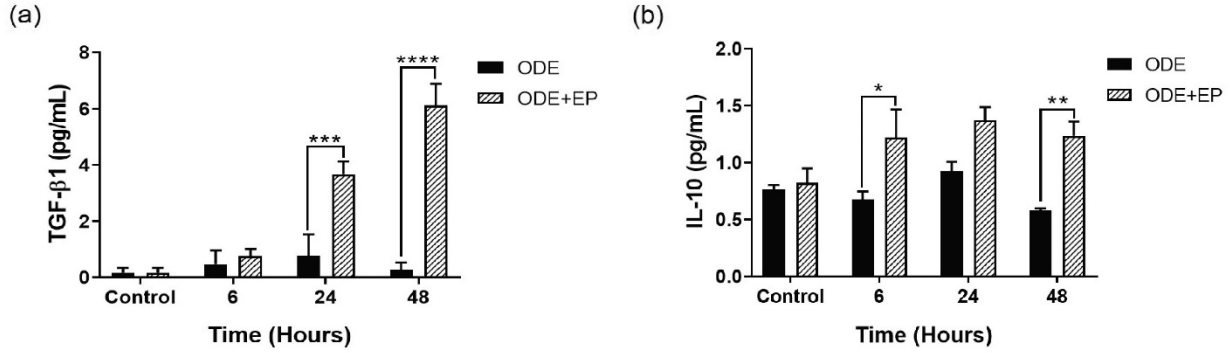

Figure 3.8 EP-treatment augments ODE-induced production of TGF-β1 and IL-10 levels in BEAS-2B cells

Compared to medium (control, 0 h), co-treatment of ODE exposed BEAS-2B cells with EP (2.5 μM) significantly increased the production of TGF- β1 (24 and 48 h) and IL-10 (6, 24 and 48 h).d Data (n=6) analyzed with two-way ANOVA is represented. * or $^{\#}p<0.05$, ** or $^{\#\#}p<0.01$, *** or $^{\#\#\#}p<0.001$, **** or $^{\#\#\#\#}p<0.0001$. $^{\#}$ indicates different from control whereas * indicates difference within the OD/barn exposure groups.

ODE exposure and NF-κB p65 levels

We measured the expression of NF-κB p65 levels in the whole cell lysates as a read-out of NF-κB activation upon ODE-exposure (both with and without EP treatment). Normalized densitometry values revealed no difference between control and ODE exposed cells with and without EP treatment at 6, 24 and 48 hours (Figure 3.9).

Neutralizing anti-HMGB1 antibody treatment reduces ODE exposure induced secretion of IL-6 but not IL-8 levels

Compared to controls, ODE exposure induced an increase in GM-CSF, IL-1β, IL-6 and IL-8 levels. Treatment with neutralizing anti-HMGB1 antibody significantly decreased IL-6 but not IL-1β or IL-8 levels (Figure 3.11, a-d).

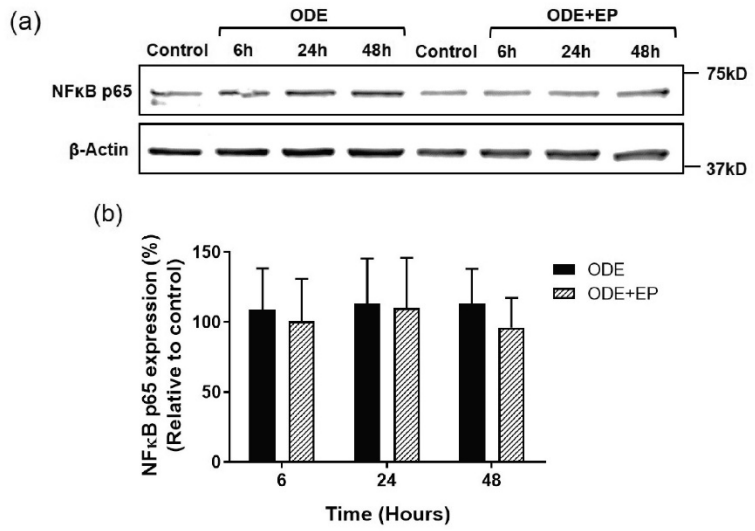

Figure 3.9 ODE exposure with or without EP-treatment does not alter NF-κB p65 levels
Medium or ODE treated (with or without co-treatment with EP) whole cell fractions were processed for western blot analysis of NF-κB p65 and β-actin proteins. Normalized intensity values (as percentage relative to controls) were compared. There was no difference between any of the treatment groups. Data (n=5) analyzed with one-way ANOVA is represented.

Treatment with EP or neutralizing anti-HMGB1 antibody reduces NF-kB p65 nuclear translocation at earlier time points

We quantified the expression of NF-κB p65 levels in both nuclear and cytoplasmic fractions to delineate the NF-κB activation upon ODE-exposure (both with and without EP or anti-HMGB1 neutralizing antibody treatment). Normalized densitometry values revealed that, compared to controls, ODE exposure increased NF-κB p65 levels in nuclear fractions at 15 and 30 minutes as well as 1, 1.5, 2 and 3 hours. Both EP and anti-HMGB1 antibody treatments significantly decreased the ODE-induced increases in NF-κB p65 nuclear levels at 15 minutes (Figure 3.10, a). Compared to controls, ODE-exposed cells showed increased levels of NF-κB p65 in the cytoplasm at all the time points. Both EP and anti-HMGB1 antibody treatment significantly decreased the levels of NF-κB p65 in the cytoplasmic fractions at 15 and 30 minutes as well as 1, 2 and 3 hours but not at 1.5 hours (Figure 3.10, b). EP treated cells at 1 and 1.5 hours still contained higher amounts of cytoplasmic NF-κB p65 than controls.

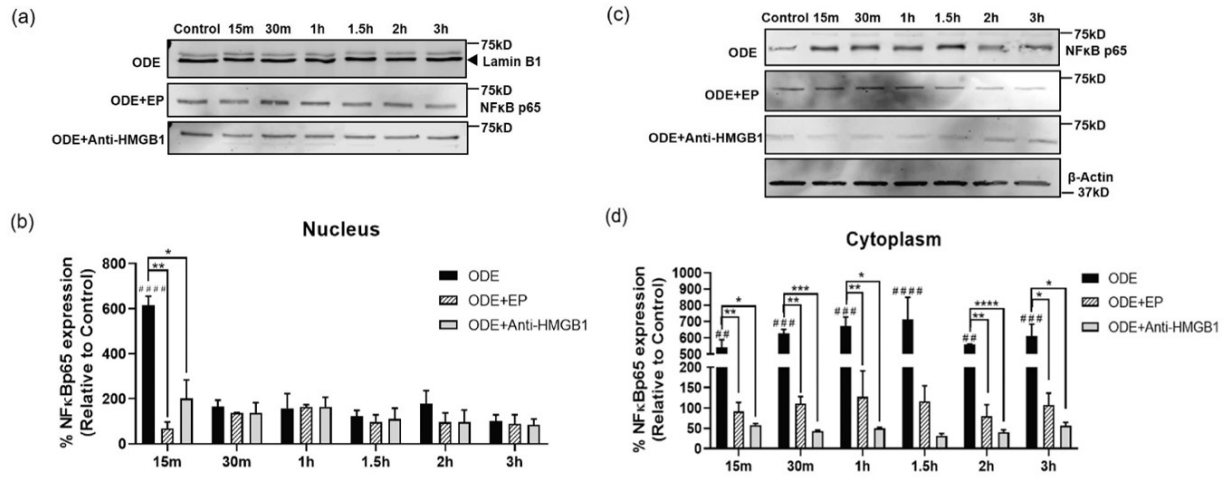

Figure 3.10 Treatment with EP or anti-HMGB1 neutralizing antibody decreases NF-κB p65 nuclear translocation

BEAS-2B cells were processed for separation of nuclear and cytoplasmic fractions and western blotting to detect NF-κBp65 protein. Compared to controls, ODE treated cells showed a temporal increase in NF-κB p65 expression (68 kDa) in the (a) nuclear fraction at 15 minutes. Compared to vehicle (medium), co-treatment with EP and anti-HMGB1 antibody (10 μM) resulted in significant decrease in the levels of NF-κB p65 in the cytoplasm at 15 minutes post-treatment indicating reduction in ODE-induced NFκB p65 activation (b and d). NF-κB p65 (68 kD) bands were normalized over either Lamin B1 (50 kD, nuclear fraction, a) or β-actin (37 kD, cytoplasmic fraction, b) and percentage intensity (n = 5/group) values of treatment groups relative to control were analyzed using two-way ANOVA (c and d). $^{*\text{ or }\#}$ $p < 0.05$, $^{**\text{ or }\#\#}$ $p < 0.01$, $^{***\text{ or }\#\#\#}$ $p < 0.001$, $^{****\text{ or }\#\#\#\#}$ $p < 0.0001$. $^{\#}$ indicates different from control whereas * indicates difference within the OD/barn exposure groups.

Neutralizing ant-HMGB1 antibody treatment augments ODE-induced production of TGF-β1 and IL-10 levels in BEAS-2B cells

Compared to controls, treatment of ODE-exposed cells with anti-HMGB1 neutralizing antibody augmented the production of TGF-β1 and IL-10 at 6, 24 and 48 hours (Figure 3.12, a and b).

Neutralizing anti-HMGB1 antibody treatment reduces ODE-induced ROS and nitrite production

Compared to controls, ODE exposure induced significant production of intracellular ROS and secreted nitrite (representing RNS). Treatment with neutralizing anti-HMGB1 antibody significantly decreased the intracellular ROS (48 hours) and secreted nitrite levels (6 and 48 hours, Figure 3.13, a and b respectively).

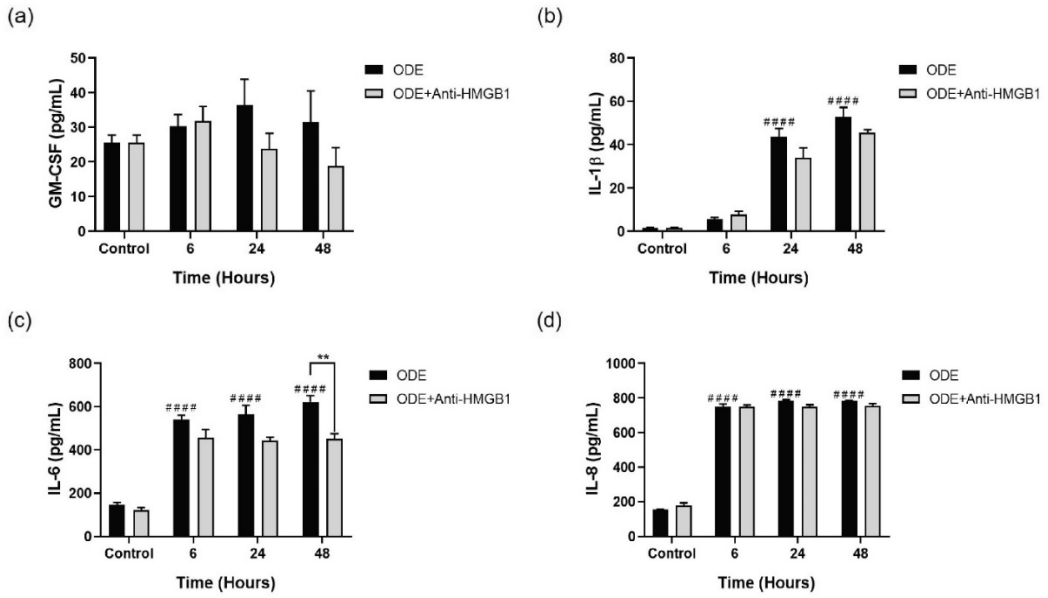

Figure 3.11 Neutralizing anti-HMGB1 antibody treatment reduces ODE exposure induced secretion of IL-6 but not IL-8 levels

Compared to controls, ODE treatment increased the production of GM-CSF (a, 24 and 48 hours), IL-1β, IL-6 and IL-8. When ODE exposed cells were treated with anti-HMGB1 antibody (10 μM), significantly reduced ODE-induced increase in IL-6 levels only (c). Data (n=6) analyzed using two-way ANOVA is represented. ** or ## $p < 0.01$ and **** or #### $p < 0.0001$. # indicates different from control whereas * indicates difference within the OD/barn exposure groups.

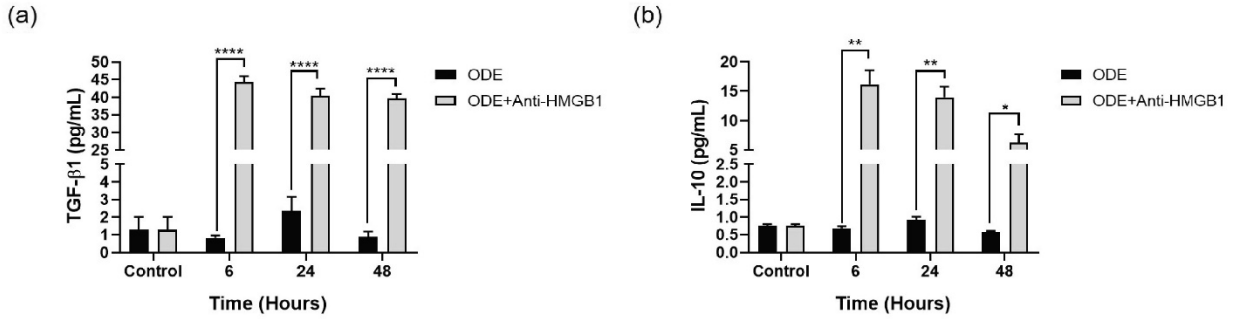

Figure 3.12 Neutralizing antibody treatment augments ODE-induced production of TGF-β1 and IL-10 levels in BEAS-2B cells

Compared to medium (control, 0 h), co-treatment of ODE exposed BEAS-2B cells with Anti-HMGB1 antibody (10 μM) significantly increased the production of TGF-β1 (6, 24 and 48 h) and IL-10 (6, 24 and 48 h). Data (n=6) analyzed with two-way ANOVA is represented. * or # $p < 0.05$, ** or ## $p < 0.01$, *** or ### $p < 0.001$, **** or #### $p < 0.0001$. # indicates different from control whereas * indicates difference within the OD/barn exposure groups.

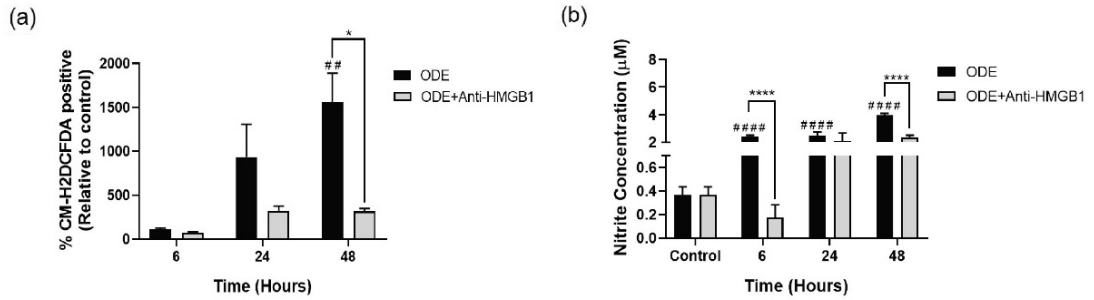

Figure 3.13 Antibody neutralization of HMGB1 reduces ODE-induced ROS and nitrite production

Cells or supernatants were subjected to CM-H_2DCFDA and Griess' assay to quantify intracellular ROS production (a) and nitrite concentration (b) respectively (n=6). Compared to ODE exposure alone, ODE exposed cells co-treated with Anti-HMGB1 antibody (10µM) showed a significant reduction in ODE-induced ROS production (48 hours) and secreted nitrite (6 and 48 hours). Data analyzed with two-way ANOVA is represented (a and b). $^{*\text{ or }\#}$ $p < 0.05$, $^{**\text{ or }\#\#}$ $p < 0.01$, $^{***\text{ or }\#\#\#}$ $p < 0.001$, $^{****\text{ or }\#\#\#\#}$ $p < 0.0001$. $^{\#}$ indicates different from control whereas * indicates difference within the OD/barn exposure groups.

ODE exposure modulates NF-κB subunit gene expression with time

Compared to controls, ODE-exposed cells showed in a significant increase in the transcripts of NF-κB subunits namely, *nfκbp65, nfκbp52 and crel* at 6, 24 and 48 hours but not *nf-κbp50* and *relb* (Figure 3.14, a-e respectively).

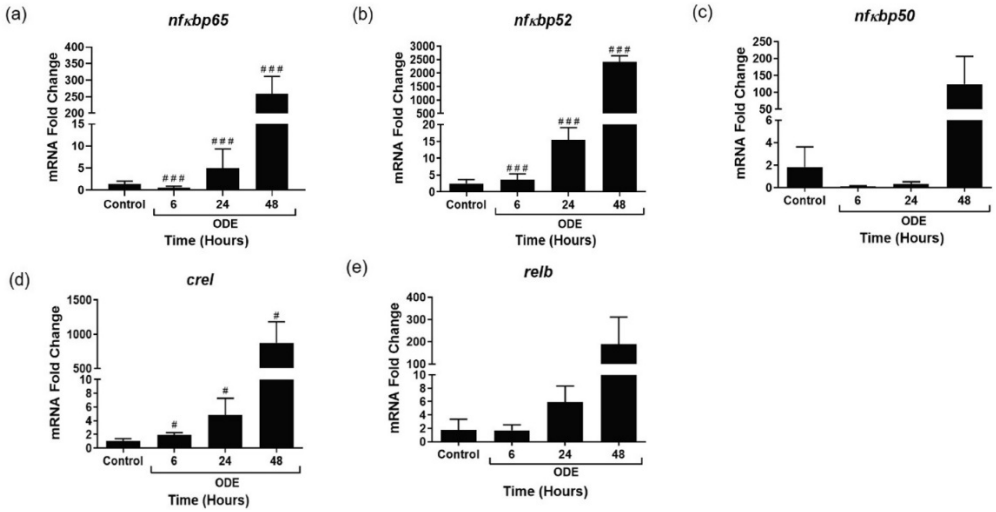

Figure 3.14 ODE exposure modulates NF-κB subunit gene expression with time

qRT-PCR analysis on NF-κB subunit genes was performed on control and ODE exposed cells at 6, 24 and 48 hours (a-e). Compared controls, ODE-exposure induced a significant increase in *nfkbp65* (a), *nfkbp52* (b) and *crel* (d) at 6, 24 and 48 hours ($^{\#}$ $p < 0.05$ and $^{\#\#\#}$ $p < 0.001$ with respect to controls). Data analyzed with one-way ANOVA is represented as fold change of mRNA expression shown relative to untreated control cells.

ODE exposure increases tlr2 and tlr4 expression

Compared to controls, ODE exposed cells showed a significant increase in the transcripts of *tlr2* and *tlr4* at 6, 24 and 48 hours (Figure 3.15, a and b).

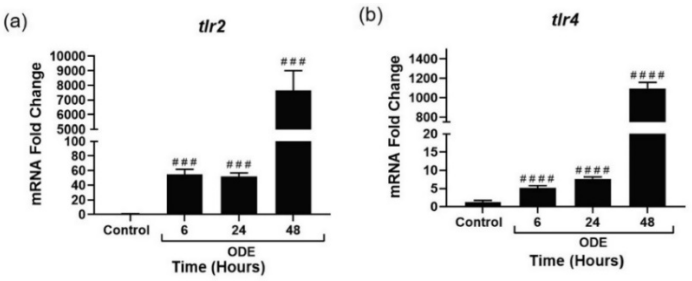

Figure 3.15 ODE exposure increases *tlr2* and *tlr4* gene expression with time
qRT-PCR analysis on *tlr2* (a) and *tlr4* (b) genes was performed on control and ODE exposed cells at 6, 24 and 48 hours. Compared to controls, ODE exposure resulted in a significant increase in fold in the expression of both tlr2 and tlr4 ($^{###}$ $p < 0.001$ and $^{####}$ $p < 0.0001$, a and b respectively). Data analyzed with one-way ANOVA is represented as fold change of mRNA expression shown relative to untreated control cells.

Discussion

Persistent exposure to OD is the hallmark of occupational respiratory diseases of agriculture production workers as well as in other industries. Early acute symptoms of airway inflammation dampen over a period of continued exposure, but long-term lung remodeling features and loss of lung function is evident (Charavaryamath and Singh, 2006, Sethi, Schneberger, Charavaryamath and Singh, 2017). Unraveling the cell and molecular basis of how low-grade inflammation drives the chronic exposure induced changes may result in better therapies. In this study, we show that OD-exposure of human airway epithelial cells induces nucleocytoplasmic translocation of HMGB1. EP or anti-HMGB1 neutralizing antibody treatment reduces OD-induced inflammation via targeting HMGB1-RAGE pathway.

First, using our well characterized rat model of OD (swine barn) exposure (Charavaryamath, Janardhan, Townsend, Willson and Singh, 2005), showed that barn exposure increases expression of HMGB1 in the lung tissue compartments upon barn exposure which

indicates a possible role in OD-induced lung inflammation and airway reactivity. Other researchers have shown that increased expression of HMGB1 in the airway epithelium leads to pulmonary fibrosis (Hamada, et al., 2008) as well as epithelial mesenchymal transition via TGF-β (reviewed in (Hamada, Maeyama, Kawaguchi, Yoshimi, Fukumoto, Yamada, Yamada, Kuwano and Nakanishi, 2008) (Chen, et al., 2016)). Next, increased expression of HMGB1 in the lung ASM observed in our study assumes importance since it is known to contribute to ASM dysfunction in a human asthma model (Di Candia, Gomez, Venereau, Chachi, Kaur, Bianchi, Challiss, Brightling and Saunders, 2017). Increased expression of HMGB1 in the blood vessels of the lung is known to cause pulmonary artery hypertension (Sadamura-Takenaka, et al., 2014) and has a role in ischemia induced blood-brain barrier disruption (Zhang, et al., 2011) . Increased expression of HMGB1 in BALT is interesting since HMGB1 is considered to be a central cytokine for all lymphoid cells (Li, et al., 2013). Increased expression of HMGB1 in the BALT partly explains our previous observation in the same rat model that a 20-day barn exposure induces activation of BALT (Charavaryamath, Janardhan, Townsend, Willson and Singh, 2005). Taken together, increased expression of HMGB1 in the lung following 1, 5, and 20-day barn exposure indicates the potential pathological role of this secreted DAMP molecule.

Using *in vitro* model of human airway exposure to OD, we now demonstrate nucleocytoplasmic translocation of HMGB1, increased expression as well as cytoplasmic co-localization of HMGB1 with RAGE in the cytoplasm. Instead of normal nuclear location, accumulation of HMGB1 in the cytoplasm indicates cellular stress and cytoplasmic HMGB1 is a chief regulator of autophagy (Zhu, et al., 2015). Secreted HMGB1 is known to potentiate inflammation in the presence of MAMPs such as LPS (Qin, et al., 2009). Our results indicate that ODE-exposure induced HMGB1 accumulation in the cytoplasm and secretion into extracellular

compartment particularly in chronic exposure to OD may drive aberrant airway inflammation and lead to lung remodeling features (Qin, Dai, Tang, Zhang, Ren, Wang and Shen, 2009). Although, our efforts to quantify secreted HMGB1 were not fully successful, we did observe higher molecular weight bands for secreted HMGB1 in the cell culture supernatant (data not shown). Posttranslational modifications such as acetylation and oxidation of HMGB1 may have contributed to this higher molecular weight HMGB1. Currently, few laboratories have expertise and established methods to measure secreted HMGB1 with post-translational modification/s.

Immunocytochemistry showed co-localization of HMGB1 and RAGE in the cytoplasm indicated possible physical interaction of HMGB1 with its main receptor RAGE. To our knowledge, this is possibly the first report of secretion of DAMP in an *in vitro* model of human airway epithelial cell exposure to OD and co-localization of HMGB1 with RAGE. It is likely that increased expression and secretion of HMGB1 (cytoplasmic and extracellular) may be driving a sustained inflammation in long-term OD-exposed individuals via HMGB1-RAGE signaling.

Next, using EP treatment we were able to abrogate ODE-induced nucleocytoplasmic translocation of HMGB1. EP treatment also decreased the expression and co-localization of HMGB1 and RAGE in the cytoplasm. EP is known to prevent phosphorylation of HMGB1 by chelating calcium and thereby prevents nucleocytoplasmic translocation of HMGB1 (Shin, Kim, Kim, Lee, Jin, Park, Kim, Suh, Kwak, Lee, Han and Lee, 2015). Other post-translational modifications such as acetylation have been shown to be important for nucleocytoplasmic translocation of HMGB1 (Kim, et al., 2016). Our study did not examine if any of the posttranslational modification were involved in OD-induced translocation of HMGB1. Our central focus was to examine if nucleocytoplasmic translocation and secretion of HMGB1 would be influencing OD-induced airway inflammation.

We have demonstrated that ODE exposure of airway epithelium results in ROS and RNS production. When we arrested nucleocytoplasmic translocation of HMGB1 using EP treatment, we observed significantly decreased levels of ROS but not RNS. It is interesting to note that, ODE exposure increased the ROS levels at 24 and 48 hours whereas RNS production was significantly higher starting from 6 h onwards. Based on our results, it is possible that ODE-induced translocation of HMGB1 has a role in potentiating ROS but not RNS levels. This is again supported by the fact that EP mediated arrest of HMGB1 translocation did not affect ODE-induced RNS levels at all the time points. Though we do not provide direct mechanistic evidence, these results pave way for further investigation.

To examine if HMGB1 translocation had any effect on inflammatory mediators, we measured the levels of GM-CSF, IL-1β and IL-6 (pro-inflammatory), TGF-β1 (pleiotropic cytokine) and IL-10 (anti-inflammatory) and IL-8 (neutrophil chemokine). ODE-exposure increased the levels of GM-CSF, IL-1β, IL-6 and IL-8. Secretion of GM-CSF by airway epithelial cells is important since it is known to sensitize the airway epithelium to allergic insults such as house dust mite or cockroach allergen (Sheih, et al., 2017). Further, GM-CSF in an inflammatory tissue milieu which acts as a link between recruited lymphocytes and monocytes and could be targeted to reduce chronic inflammation (Becher, et al., 2016). Next, our observation of increase in IL-1β production is consistent with published work on BEAS-2B cells exposed to poultry barn dust extract (Boggaram, et al., 2016). IL-1β has a variety of inflammatory effects in the lung including induction of airway hyper responsiveness (Dinarello, 2018, Fricke, et al., 2018). ODE-induced IL-6 production assumes significance since the recent work has identified IL-6 as an important link in lung-bone inflammatory axis in a mouse model of intra-nasal ODE exposure (Wells, Romberger, Thiele, Wyatt, Staab, Heires, Klassen, Duryee, Mikuls, Dusad, West, Wang

and Poole, 2017). Next, IL-8 secretion observed in our study is in line with other published evidence (Acevedo, et al., 2005, Burvall, et al., 2003). IL-8 is known to attract neutrophils to the site of inflammation and neutrophilic oxidative stress upon exposure to OD is known to drive pulmonary inflammation and airway reactivity (McGovern, et al., 2016). Using a specific antagonist against IL-8 was beneficial in an OD-induced lung inflammation model (Schneberger, et al., 2015b).

Lastly, we demonstrated that EP-treatment augments IL-10 and TGF-β production in ODE-exposed airway epithelial cells. Production of IL-10 generally results in anti-inflammatory effects (reviewed in (Behrens, et al., 2018)). Airway epithelial cell derived TGF-β is important in driving type 2 innate lymphoid cell responses to allergens and TGF-β is known to exacerbate house dust mite-induced pathology and increased expression of TGF-β is seen with viral and allergen challenge (reviewed in (Denney, et al., 2015)). Taken together, upon ODE exposure, human airway epithelial cells secrete a variety of inflammatory mediators. Since pharmacological tool blocking HMGB1 translocation and RAGE expression (EP) or genetic tool suppressing the expression of HMGB1 is able to reduce ODE-induced inflammation, HMGB1 signaling is a major driver of ODE-induced airway inflammation. Though our study has not investigated the specific downstream events in this pathway, EP or anti-HMGB1 antibody mediated targeting of HMGB1-RAGE pathway appears promising.

Our unique observation that EP treatment had no effect on the ODE-induced IL-8 and IL-6 indicates several possibilities. First, HMGB1 mediated signaling pathway as well as ODE-induced IL-8/IL-6 secretion may be independent of each other. Second, IL-8 and IL-6 production peaks from 6 h after ODE-exposure and it is likely that secreted HMGB1 acts at a later time point to potentiate the inflammation. Although we do not provide any direct evidence, there is a link

between decrease in cytoplasmic/secreted HMGB1 levels following EP treatment and decrease in ODE-induced GM-CSF and IL-1β levels. This again highlights the fact that HMGB1 is a late-player in many inflammatory events (reviewed in (VanPatten and Al-Abed, 2018)).

In order to examine mechanistically, if arrest of nucleocytoplasmic translocation of HMGB1 reduces inflammatory mediators through NF-κB, immunoblots for NF-κB p65 in control (0 h) and ODE exposure (6, 24 and 48 h) with media or EP treatments revealed no significant difference between the groups (all time points). However, when we probed the NF-κB p65 levels in the nuclear and cytoplasmic fractions at early time points, we found that ODE exposure increases both nuclear and cytoplasmic levels of NF-κB p65 as early as 15 minutes. Both EP and anti-HMGB1 antibody treatments significantly reduced NF-κB p65 levels in both nucleus and cytoplasm indicating that their anti-inflammatory action is via a reduction in the translocation of NF-κB p65.

We and others have previously shown the roles of TLR2 (Poole, Wyatt, Kielian, Oldenburg, Gleason, Bauer, Golden, West, Sisson and Romberger, 2011) and TLR4 (Charavaryamath, Juneau, Suri, Janardhan, Townsend and Singh, 2008) in OD exposure induced lung inflammation. We now show significant increase in the expression of *tlr2* and *tlr4* genes following ODE exposure. We observed translocation of NF-κB p65 into the nucleus as early as 15 minutes indicating that ODE-induced innate signaling via TLR2 and 4 results in NF-κB activation leading to cytokine secretion. However, both EP and anti-HMGB1 antibody treatments inhibited both nuclear translocation of NF-κB p65 and pro-inflammatory cytokine production to highlight the importance of targeting HMGB1.

OD exposure of human airway epithelial cell line results in the nucleocytoplasmic translocation of HMGB1, cytoplasmic co-localization of HMGB1 with RAGE as well as

production of ROS, RNS and inflammatory cytokines. EP or anti-HMGB1 antibody treatment abrogates OD exposure induced translocation of HMGB1 and expression of many inflammatory markers. Therefore, HMGB1-RAGE signaling is an attractive target to treat OD-induced occupational lung diseases.

Materials and Methods

Rats and organic dust exposure

Rat model of organic dust exposure has previously been described (Charavaryamath, Janardhan, Townsend, Willson and Singh, 2005). Rat exposure to the swine barn environment (organic dust exposure) was conducted with approved protocols from University of Saskatchewan Campus Committee on Animal Care. All the animal experiments were performed as per the Canadian Council on Animal Care Guidelines. Six-week-old, male, Sprague-Dawley rats (n=5/group, Charles River Laboratories) were exposed to either ambient air (control) or one, five or 20-days to swine barn environment (8 hours/day). At the end of the exposure period, rats were euthanized, lung tissues were collected and processed for immunohistochemistry (Charavaryamath, Janardhan, Townsend, Willson and Singh, 2005). The paraformaldehyde-fixed, paraffin-embedded tissues from these rats were used in the current study.

Immunohistochemical analysis

Immunohistochemistry on five-micron thick tissue sections (n=5 rats/group) was performed using anti-HMGB1 (1:1000, Abcam) and HRP (1:1000, ant-rabbit IgG; Abcam) and counterstained with methyl green (Vector Laboratories, Inc., Burlingame, CA). An investigator blinded to the treatment groups semi-quantified the cell specific expression of HMGB1 in bronchioles, endothelium of blood vessels, alveolar septa, ASM and bronchus associated lymphoid tissue (BALT) using predetermined scoring criteria (outlined in Table 3.2). Scored regions were photographed (Nikon Eclipse TE2000-U; Spot Advance imaging software, Michigan, USA).

Table 3.2 Semi-quantitative evaluation of HMGB1 expression and criteria for assigning scores

Score	Criteria
0	No expression
1	Minimal
2	Mild
3	Moderate
4	Intense

Organic dust extract preparation

Settled dust samples from typical swine housing facilities (representing organic dust) were collected into zip lock bags and transported on ice and stored at -80°C until processed. A sterile organic dust extract was prepared as per a published protocol (Romberger, Bodlak, Von Essen, Mathisen and Wyatt, 2002). Dust samples were weighed and for every gram of dust, 10 mL of Hanks' balanced salt solution without calcium (Gibco) was added, stirred and allowed to stand at room temperature for an hour. The mixture was centrifuged (1365 x g, 4°C) for 20 min, supernatant recovered, and pellet was discarded. Supernatant was centrifuged again with same conditions, pellet discarded and recovered supernatant was filtered using 0.22 μm filter and stored at -80°C until used. The filter sterilized organic dust extract (ODE) samples were considered 100% and diluted to 1-5% (v/v) before use in experiments.

Endotoxin estimation

The levels of endotoxin in the ODE samples was quantified using the Pyrochrome® chromogenic endotoxin assay kit (Associates of Cape Cod, Inc., East Falmouth, MA). The ODE samples were diluted in a ratio of 1:10 in endotoxin free water. The samples along with reconstituted pyrochrome lysate, were added to a 96-well plate in a sample to lysate ratio of 1:4. The standard was reconstituted as per manufacturer's recommendation and added to the plate in a sample to lysate ratio of 1:4. The microplate was incubated at 37°C with shaking and the

absorbance was read at 405 nm (every 10 minutes, three readings over a total of 30 minutes) using the Gen 5™ software in BioTek® ELx808™ spectrophotometer.

Cell culture and treatments

Immortalized human bronchial epithelial cells (BEAS-2B, ATCC CRL-9609) have previously been used to study innate inflammatory responses to ODE (Schneberger, Cloonan, DeVasure, Bailey, Romberger and Wyatt, 2015a, Wyatt, Poole, Nordgren, DeVasure, Heires, Bailey and Romberger, 2014). BEAS-2B cells were seeded onto type I bovine collagen (StemCell Technologies, Vancouver, BC, Canada) coated T-75 flasks. Cells were grown submerged in serum free LHC-9 medium (Gibco) containing 100 U/mL of Penicillin/Streptomycin (Gibco) and 2 µg/mL of Amphotericin B (Sigma) in a humidified chamber with 5% CO_2 at 37°C until approximately 80% confluence was achieved.

Ethyl pyruvate (EP, Santa Cruz Biotechnology, CA) was reconstituted in Ringer's solution (Sigma-Aldrich, St. Louis, MO, USA) and used at a final concentration of 2.5 µM in the cell culture medium (Figure 1). Neutralization of secreted HMGB1 was carried out using anti-HMGB1 antibody (BioLegend, CA) at a concentration of 10 µg/mL (Zhou, Wang, Wang, Jia, Li, Wang, Wu and Tang, 2009).

Our *in vitro* model of ODE exposure and treatments are represented (Figure 3.1 a and b). Cells were treated with either medium (control) or lipopolysaccharide (LPS, *Escherichia coli* O127:B8; Sigma) or peptidoglycan (PGN, *Staphylococcus aureus*; Sigma), or ODE (1-5% v/v) (treatment 1, Figure 3.1) followed by a co-treatment with either medium or EP (treatment 2, Figure 3.1a) or anti-HMGB1 neutralizing antibody (treatment 2, Figure 3.1b). Following treatment, 1 and 2, samples were processed at 0, 6, 24 and 48 hours for various assays. For NF-κB p65 assays, samples were collected at 15 and 30 minutes as well as 1, 1.5, 2 and 3 hours. Control samples did

not differ at various time points (6, 24 and 48 h) and hence controls samples at 0 h were included for all data analysis.

LPS and PGN were used as standard microbial associated molecular patterns (MAMPs) (data not shown). Table 3.3 summarizes the stock and working concentrations of various MAMPs used in treatment 1 (Figure 3.1) prepared by dissolving in LHC-9 medium from stock concentrations.

Table 3.3 Stock and working concentrations of cell treatments

Treatments	Stock concentration (in cell culture grade water)	Working concentration (in LHC-9)
LPS	5 mg/mL	10 µg/mL
PGN	1 mg/mL	10 µg/mL
ODE	100 %	1 - 5 %

Cell viability assay

Prior to conducting experiments, cell viability was assessed. Live/dead cell count was determined by 4% trypan blue dye (EMD Millipore, Burlington, MA) exclusion and percentage viability was calculated. Population of cells with more than 95% viability were used for the experiments.

Immunofluorescence microscopy

Cells were seeded ($1x10^6$ cells/well) in 12-well plates on Poly D-lysine hydro bromide (Sigma-Aldrich, St. Louis, MO) coated cover slips and exposed to the treatments as outlined in Figure 1. Cells were fixed with 4% paraformaldehyde in PBS for 20 minutes at room temperature and washed. Cells were blocked for an hour using a blocking buffer containing 10% normal donkey serum (EMD Millipore, Burlington, MA), 0.2% triton X 100 and PBS. Cover slips with cells were incubated with anti-HMGB1 (1:1000 dilution, rabbit polyclonal) and anti-RAGE (1:200 dilution, rabbit polyclonal) antibodies in antibody diluent solution (2.5% normal donkey serum, 0.25% sodium azide, 0.2% triton X 100, PBS) (AbCam, Cambridge, MA) with overnight at 4°C. Next,

coverslips were incubated with donkey anti-rabbit biotin conjugated secondary antibody (1:400, diluted in antibody diluent, HMGB1) and 1:500 dilutions of FITC (RAGE) (Jackson Immunoresearch, West Grove, PA) for an hour at room temperature, followed by streptavidin-Cy3 (1:300 in PBS, HMGB1). Coverslips were mounted onto slides using VECTASHIELD antifade mounting medium with 4',6-Diamidino-2-Phenylindole, Dihydrochloride (DAPI, Vector Labs, Burlingame, CA) and imaged using Axiovert 200 M Zeiss inverted fluorescence microscope (Zeiss, Deutschland, Germany) equipped with Hamamatsu camera. Images were processed using HCImage live 4 software (Hamamatsu Corporation, Sewickley, PA).

Western blot analysis

Cells were harvested followed by separation of cytoplasmic and nuclear fractions using NE-PER nuclear and cytoplasmic extraction kit supplemented with a mixture of protease and phosphatase inhibitors (Thermo Scientific, USA). For NF-κB p65 detection, whole cell lysates were used as well. Total protein levels were estimated by Bradford assay and equal amounts of protein (20 μg/sample), along with a molecular weight marker (Bio-Rad, Hercules, CA), were loaded on to 12% Tris-glycine gels (Bio-Rad, Hercules, CA) . The gels were subjected to 100V for 1-2 hours at 4°C. Next, proteins were transferred on to a nitrocellulose membrane at 23V at 4°C for 16 hours. Membranes were washed once with distilled water and non-specific binding was blocked with fluorescent western blot blocking buffer (Rockland Immunochemicals, PA, USA) in PBS at room temperature for an hour. Membranes were washed twice with 1X PBS with 0.05% tween 20 (PBST) and incubated with primary rabbit monoclonal anti-HMGB1 antibody (1:1000 dilution) or rabbit polyclonal anti-NF-κB p65 antibody (1:1000 dilution), mouse polyclonal anti-β-Actin (1:6000) and rabbit polyclonal anti-Lamin B1 (1:1000) (AbCam, Cambridge, MA) antibodies overnight at 4°C. β-actin (whole cell lysate and cytoplasmic fractions) and Lamin-B1

(nuclear fraction) were used as loading controls. Membranes were then washed and incubated with goat anti-mouse and donkey anti-rabbit IgG P680 (1:10,000 dilution) secondary antibody (Thermo-Scientific, USA). Membranes were scanned using the Odyssey® CLx IR imaging system (LI-COR Biotechnology, Lincoln, NE) and analysis was performed using ImageJ program (National Institute of Health).

Measurement of reactive oxygen species

Intracellular reactive oxygen species (ROS) production was measured using chloromethyl derivative of dichlorodihydrofluorescein diacetate (CM-H_2DCFDA) (ThermoFisher Scientific, USA). A working solution of 10 µM of DCFDA in PBS was used. BEAS-2B cells ($5x10^4$/well) were seeded in a 96 well cell culture plate and incubated in a 5% CO_2 incubator to reach confluence. The cells were incubated with H_2DCFDA working solution at 37°C for 30 min, followed by treatments as outlined in Figure 1. The fluorescence intensity of the oxidized form of H_2DCFDA was measured at excitation/emission wavelengths of 488/535 nm (SpectraMax M2 Gemini Molecular Device Microplate Reader). The results were expressed as percentage fluorescence relative to control.

Griess assay

Griess assay was performed as described (Gordon, Hogan, Neal, Anantharam, Kanthasamy and Kanthasamy, 2011). Briefly, Concentration of secreted nitric oxide was measured (representing reactive nitrogen species (RNS)) as nitrite levels in cell culture media using Griess reagent (Sigma) and sodium nitrite standard curve, prepared using a stock solution of 200 µM. The assay was performed in a 96 well-plate and absorbance was measured at 550 nm (SpectraMax M2 Gemini Molecular Device Microplate Reader). The results were expressed as µM concentration of nitrite secreted.

Cytokine analysis

GM-CSF, IL-1β, IL-8, IL-6, IL-10 and TGF-β1 levels in BEAS-2B cell culture supernatant were measured using ELISA kits (ThermoFisher Scientific, USA) in accordance with the manufacturer's recommendations.

qRT-PCR

RNA was isolated using TRIzol extraction methods (Seo, Ottesen and Singh, 2014) and RNA concentration was measured using NanoDrop spectrophotometer. Two micrograms of RNA was used to synthesize cDNA using the Superscript III first strand synthesis kit (ThermoFisher Scientific, USA) following the manufacturer's protocol. For qPCR reactions, 5 µL of SYBR Green Mastermix (ThermoFisher Scientific, USA), 1 µL of primers, 1-2 µL of water and 1–2 µL of cDNA was used. The primers for genes of interest (Table 3) were synthesized at Iowa State University's DNA Facility. The housekeeping gene 18 S rRNA (ThermoFisher Scientific, USA) was used in all qPCR reactions. No-template controls and dissociation curves were run for all reactions to exclude cross-contamination. The qRT-PCR reactions were run in a Bio-Rad CFX Connect™ detection system and the data was analyzed using $2^{-\Delta\Delta CT}$ method (Livak and Schmittgen, 2001).

Table 3.4 Primer sequences used for qRT-PCR

Gene Symbol	Primer Sequence (5'→3')	
nfκbp65	Forward	CCAGACCAACAACAACCCCT
	Reverse	TCACTCGGCAGATCTTGAGC
nfκbp50	Forward	GCAGCACTACTTCTTGACCACC
	Reverse	TCTGCTCCTGAGCATTGACGTC
nfκbp52	Forward	GGCAGACCAGTGTCATTGAGCA
	Reverse	CAGCAGAAAGCTCACCACACTC
relB	Forward	TGTGGTGAGGATCTGCTTCCAG
	Reverse	TCGGCAAATCCGCAGCTCTGAT
crel	Forward	AGTTGCGGAGACCTTCTGACCA
	Reverse	CGTGATCCTGGCACAGTTTCTG
tlr2	Forward	CTTCACTCAGGAGCAGCAAGCA
	Reverse	ACACCAGTGCTGTCCTGTGACA
tlr4	Forward	CCCTGAGGCATTTAGGCAGCTA
	Reverse	AGGTAGAGAGGTGGCTTAGGCT

Statistical analysis

Data were expressed as mean ± SEM and analyzed by one-way or two-way ANOVA followed by Bonferroni's *post hoc* comparison tests (GraphPad Prism 7.0, La Jolla, CA, USA). A p-value of < 0.05 was considered statistically significant.

Acknowledgements

Authors thank Dr. Sreekanth Puttachary (Oregon State University) and Ms. Catherine A. Martens for general help during the experiments. Authors acknowledge the help from Dr. T. Thippeswamy's laboratory (immunofluoresnce microscopy facilities), Dr. Anumantha G. Kanthasamy and Dr. Heather M. Greenlee laboratories (immunohistochemistry imaging) and Biomedical Sciences departmental core facilities for access to various instruments.

Conflict of Interest

The authors declare that they have no competing interests.

Funding

Animal experiments were performed in Dr. B. Singh's laboratory and his research was supported through Lung Association of Saskatchewan and Dr. C. Charavaryamath was a recipient of a Graduate Merit Scholarship from College of Graduate Studies and Research, Founding Chairs Graduate Fellowship from Canadian Centre for Health and Safety in Agriculture, University of Saskatchewan and a scholarship from the CIHR Strategic Training Program in Public Health and the Agricultural Rural Ecosystem and Partner Institutes including the Institute of Cancer Research, Institute of Circulatory and Respiratory Health, Institute of Infection and Immunity, Institute of Population and Public Health and the University of Saskatchewan. Current research in Dr. Charavaryamath's laboratory is supported through funding from Iowa State University and CDC-NIOSH pilot grant (5 U54 OH007548). Dr. Karriker's research is supported through funding from Iowa State University. Ms. Sanjana Mahadev Bhat is supported through teaching assistant (TA)

position through Genetics, Development and Cell biology (GNCB), Biomedical Sciences and Immunobiology graduate program at Iowa State University.

References

Acevedo F, Palmberg L, Larsson K (2005) Exposure to organic dust causes activation of human plasma complement factors C3 and B and the synthesis of factor C3 by lung epithelial cells in vitro. Inflammation 29:39-45

AgConnections Organic Dust and Respiratory Diseases in Agriculture. In: NIOSH Agricultural Research Centers Update (ed) Agricultural Safety and Health

American Thoracic Society (1998) Respiratory health hazards in agriculture. Am J Respir Crit Care Med, vol 158, pp S1-S76

Andersson U, Yang H, Harris H (2018) Extracellular HMGB1 as a therapeutic target in inflammatory diseases. Expert Opin Ther Targets 1-15

Bauer C, Kielian T, Wyatt TA, Romberger DJ, West WW, Gleason AM, Poole JA (2013) Myeloid differentiation factor 88-dependent signaling is critical for acute organic dust-induced airway inflammation in mice. Am J Respir Cell Mol Biol 48:781-789

Becher B, Tugues S, Greter M (2016) GM-CSF: From Growth Factor to Central Mediator of Tissue Inflammation. Immunity 45:963-973

Behrens G, Winzen R, Rehage N, Dorrie A, Barsch M, Hoffmann A, Hackermuller J, Tiedje C, Heissmeyer V, Holtmann H (2018) A translational silencing function of MCPIP1/Regnase-1 specified by the target site context. Nucleic Acids Res

Boggaram V, Loose DS, Gottipati KR, Natarajan K, Mitchell CT (2016) Gene expression profiling of the effects of organic dust in lung epithelial and THP-1 cells reveals inductive effects on inflammatory and immune response genes. Physiol Genomics 48:281-289

Burvall K, Palmberg L, Larsson K (2003) Effects by 8-bromo-cyclicAMP on basal and organic dust-induced release of interleukin-6 and interleukin-8 in A549 human airway epithelial cells. Respir Med 97:46-50

Carrington JM, Poole JA (2018) The Effect of Inhalant Organic Dust on Bone Health. Curr Allergy Asthma Rep 18:16

Charavaryamath C, Janardhan KS, Townsend HG, Willson P, Singh B (2005) Multiple exposures to swine barn air induce lung inflammation and airway hyper-responsiveness. Respir Res 6:50

Charavaryamath C, Juneau V, Suri SS, Janardhan KS, Townsend H, Singh B (2008) Role of Toll-like receptor 4 in lung inflammation following exposure to swine barn air. Exp Lung Res 34:19-35

Charavaryamath C, Singh B (2006) Pulmonary effects of exposure to pig barn air. J Occup Med Toxicol 1:10

Chen YC, Statt S, Wu R, Chang HT, Liao JW, Wang CN, Shyu WC, Lee CC (2016) High mobility group box 1-induced epithelial mesenchymal transition in human airway epithelial cells. Sci Rep 6:18815

Davidson ME, Schaeffer J, Clark ML, Magzamen S, Brooks EJ, Keefe TJ, Bradford M, Roman-Muniz N, Mehaffy J, Dooley G, Poole JA, Mitloehner FM, Reed S, Schenker MB, Reynolds SJ (2017) Personal exposure of dairy workers to dust, endotoxin, muramic acid, ergosterol and ammonia on large-scale dairies in the high plains western United States. J Occup Environ Hyg 0

Denney L, Byrne Adam J, Shea Thomas J, Buckley James S, Pease James E, Herledan Gaelle M, Walker Simone A, Gregory Lisa G, Lloyd Clare M (2015) Pulmonary Epithelial Cell-Derived Cytokine TGF-β1 Is a Critical Cofactor for Enhanced Innate Lymphoid Cell Function. Immunity 43:945-958

Di Candia L, Gomez E, Venereau E, Chachi L, Kaur D, Bianchi ME, Challiss RA, Brightling CE, Saunders RM (2017) HMGB1 is upregulated in the airways in asthma and potentiates airway smooth muscle contraction via TLR4. J Allergy Clin Immunol

Dinarello CA (2018) Overview of the IL-1 family in innate inflammation and acquired immunity. Immunol Rev 281:8-27

Ding J, Cui X, Liu Q (2016) Emerging role of HMGB1 in lung diseases: friend or foe. J Cell Mol Med

Frevert CW, Felgenhauer J, Wygrecka M, Nastase MV, Schaefer L (2017) Danger-Associated Molecular Patterns Derived From the Extracellular Matrix Provide Temporal Control of Innate Immunity. J Histochem Cytochem 22155417740880

Fricke K, Vieira M, Younas H, Shin M-K, Bevans-Fonti S, Berger S, Lee R, D'Alessio FR, Zhong Q, Nelson A, Loube J, Sanchez I, Hansel NN, Mitzner W, Polotsky VY (2018) High fat diet induces airway hyperresponsiveness in mice. Sci Rep 8:6404

Gordon R, Hogan CE, Neal ML, Anantharam V, Kanthasamy AG, Kanthasamy A (2011) A simple magnetic separation method for high-yield isolation of pure primary microglia. J Neurosci Methods 194:287-296

Guillam MT, Martin S, Le Guelennec M, Puterflam J, Le Bouquin S, Huneau-Salaun A (2017) Dust exposure and health of workers in duck hatcheries. Ann Agric Environ Med 24:360-365

Hamada N, Maeyama T, Kawaguchi T, Yoshimi M, Fukumoto J, Yamada M, Yamada S, Kuwano K, Nakanishi Y (2008) The role of high mobility group box1 in pulmonary fibrosis. Am J Respir Cell Mol Biol 39:440-447

Hou C, Kong J, Liang Y, Huang H, Wen H, Zheng X, Wu L, Chen Y (2015) HMGB1 contributes to allergen-induced airway remodeling in a murine model of chronic asthma by modulating airway inflammation and activating lung fibroblasts. Cell Mol Immunol 12:

Hwang JS, Choi HS, Ham SA, Yoo T, Lee WJ, Paek KS, Seo HG (2015) Deacetylation-mediated interaction of SIRT1-HMGB1 improves survival in a mouse model of endotoxemia. Sci Rep 5:15971

International Labor Organization (2018) Agriculture: a hazardous work (online). In: International Labor Organization (ed) Hazardous work, vol 2019

Iowa State University and University of Iowa (2002) IOWA CONCENTRATED ANIMAL FEEDING OPERATIONS AIR QUALITY STUDY. Final Report., vol 2018. Iowa State University and University of Iowa, Iowa

Kang R, Chen R, Zhang Q, Hou W, Wu S, Cao L, Huang J, Yu Y, Fan XG, Yan Z, Sun X, Wang H, Wang Q, Tsung A, Billiar TR, Zeh HJ, 3rd, Lotze MT, Tang D (2014) HMGB1 in health and disease. Mol Aspects Med 40:1-116

Kim YM, Park EJ, Kim JH, Park SW, Kim HJ, Chang KC (2016) Ethyl pyruvate inhibits the acetylation and release of HMGB1 via effects on SIRT1/STAT signaling in LPS-activated RAW264.7 cells and peritoneal macrophages. Int Immunopharmacol 41:98-105

Li G, Liang X, Lotze MT (2013) HMGB1: The Central Cytokine for All Lymphoid Cells. Front Immunol 4:68

Livak KJ, Schmittgen TD (2001) Analysis of relative gene expression data using real-time quantitative PCR and the 2(-Delta Delta C(T)) Method. Methods 25:402-408

Lu B, Antoine DJ, Kwan K, Lundbäck P, Wähämaa H, Schierbeck H, Robinson M, Van Zoelen MAD, Yang H, Li J, Erlandsson-Harris H, Chavan SS, Wang H, Andersson U, Tracey KJ (2014) JAK/STAT1 signaling promotes HMGB1 hyperacetylation and nuclear translocation. Proceedings of the National Academy of Sciences 111:3068-3073

McGovern TK, Chen M, Allard B, Larsson K, Martin JG, Adner M (2016) Neutrophilic oxidative stress mediates organic dust-induced pulmonary inflammation and airway hyperresponsiveness. Am J Physiol Lung Cell Mol Physiol 310:L155-165

Nordgren TM, Charavaryamath C (2018) Agriculture Occupational Exposures and Factors Affecting Health Effects. Curr Allergy Asthma Rep 18:65

Peters S, Kromhout H, Olsson AC, Wichmann HE, Bruske I, Consonni D, Landi MT, Caporaso N, Siemiatycki J, Richiardi L, Mirabelli D, Simonato L, Gustavsson P, Plato N, Jockel KH, Ahrens W, Pohlabeln H, Boffetta P, Brennan P, Zaridze D, Cassidy A, Lissowska J, Szeszenia-Dabrowska N, Rudnai P, Fabianova E, Forastiere F, Bencko V, Foretova L, Janout V, Stucker I, Dumitru RS, Benhamou S, Bueno-de-Mesquita B, Kendzia B, Pesch B, Straif K, Bruning T, Vermeulen R (2012) Occupational exposure to organic dust increases lung cancer risk in the general population. Thorax 67:111-116

Poole JA, Burrell AM, Wyatt TA, Kielian TL, Romberger DJ (2010) NOD2 Negatively Regulates Organic Dust-Induced Inflammation in Monocytes/Macrophages. J Allergy Clin Immunol 125:AB118

Poole JA, Wyatt TA, Kielian T, Oldenburg P, Gleason AM, Bauer A, Golden G, West WW, Sisson JH, Romberger DJ (2011) Toll-like receptor 2 regulates organic dust-induced airway inflammation. Am J Respir Cell Mol Biol 45:711-719

Qin YH, Dai SM, Tang GS, Zhang J, Ren D, Wang ZW, Shen Q (2009) HMGB1 enhances the proinflammatory activity of lipopolysaccharide by promoting the phosphorylation of MAPK p38 through receptor for advanced glycation end products. J Immunol 183:6244-6250

Richard SA, Jiang Y, Xiang LH, Zhou S, Wang J, Su Z, Xu H (2017) Post-translational modifications of high mobility group box 1 and cancer. Am J Transl Res 9:5181-5196

Romberger DJ, Bodlak V, Von Essen SG, Mathisen T, Wyatt TA (2002) Hog barn dust extract stimulates IL-8 and IL-6 release in human bronchial epithelial cells via PKC activation. J Appl Physiol (1985) 93:289-296

Sadamura-Takenaka Y, Ito T, Noma S, Oyama Y, Yamada S, Kawahara K-i, Inoue H, Maruyama I (2014) HMGB1 Promotes the Development of Pulmonary Arterial Hypertension in Rats. PLoS One 9:e102482

Sahlander K, Larsson K, Palmberg L (2012) Daily exposure to dust alters innate immunity. PLoS One 7:e31646

Schneberger D, Aulakh G, Channabasappa S, Singh B (2016) Toll-like receptor 9 partially regulates lung inflammation induced following exposure to chicken barn air. J Occup Med Toxicol 11:31

Schneberger D, Cloonan D, DeVasure JM, Bailey KL, Romberger DJ, Wyatt TA (2015a) Effect of elevated carbon dioxide on bronchial epithelial innate immune receptor response to organic dust from swine confinement barns. Int Immunopharmacol 27:76-84

Schneberger D, Gordon JR, DeVasure JM, Boten JA, Heires AJ, Romberger DJ, Wyatt TA (2015b) CXCR1/CXCR2 antagonist CXCL8(3-74)K11R/G31P blocks lung inflammation in swine barn dust-instilled mice. Pulm Pharmacol Ther 31:55-62

Senthilselvan A, Zhang Y, Dosman JA, Barber EM, Holfeld LE, Kirychuk SP, Cormier Y, Hurst TS, Rhodes CS (1997) Positive human health effects of dust suppression with canola oil in swine barns. Am J Respir Crit Care Med 156:410-417

Seo J, Ottesen EW, Singh RN (2014) Antisense methods to modulate pre-mRNA splicing. Methods Mol Biol 1126:271-283

Sethi RS, Schneberger D, Charavaryamath C, Singh B (2017) Pulmonary innate inflammatory responses to agricultural occupational contaminants. Cell Tissue Res 367:1-16

Sheih A, Parks WC, Ziegler SF (2017) GM-CSF produced by the airway epithelium is required for sensitization to cockroach allergen. Mucosal Immunol 10:705-715

Shin JH, Kim ID, Kim SW, Lee HK, Jin Y, Park JH, Kim TK, Suh CK, Kwak J, Lee KH, Han PL, Lee JK (2015) Ethyl pyruvate inhibits HMGB1 phosphorylation and release by chelating calcium. Mol Med 20:649-657

VanPatten S, Al-Abed Y (2018) High Mobility Group Box-1 (HMGb1): Current Wisdom and Advancement as a Potential Drug Target. J Med Chem

Viegas S, Mateus V, Almeida-Silva M, Carolino E, Viegas C (2013) Occupational Exposure to Particulate Matter and Respiratory Symptoms in Portuguese Swine Barn Workers. J Toxicol Environ Health, A 76:1007-1014

Wells A, Romberger DJ, Thiele GM, Wyatt TA, Staab E, Heires AJ, Klassen LW, Duryee MJ, Mikuls TR, Dusad A, West WW, Wang D, Poole JA (2017) Systemic IL-6 Effector Response in Mediating Systemic Bone Loss Following Inhalation of Organic Dust. J Interferon Cytokine Res 37:9-19

Wong SLI, To J, Santos J, Allam V, Dalton JP, Djordjevic SP, Donnelly S, Padula MP, Sukkar MB (2017) Proteomic analysis of extracellular HMGB1 identifies binding partners and exposes its potential role in airway epithelial cell homeostasis. J Proteome Res

Wunschel J, Poole JA (2016) Occupational agriculture organic dust exposure and its relationship to asthma and airway inflammation in adults. J Asthma 53:471-477

Wyatt TA, Poole JA, Nordgren TM, DeVasure JM, Heires AJ, Bailey KL, Romberger DJ (2014) cAMP-dependent protein kinase activation decreases cytokine release in bronchial epithelial cells. Am J Physiol Lung Cell Mol Physiol 307:L643-651

Yang R, Harada T, Mollen KP, Prince JM, Levy RM, Englert JA, Gallowitsch-Puerta M, Yang L, Yang H, Tracey KJ, Harbrecht BG, Billiar TR, Fink MP (2006) Anti-HMGB1 neutralizing antibody ameliorates gut barrier dysfunction and improves survival after hemorrhagic shock. Mol Med 12:105-114

Youn JH, Shin JS (2006) Nucleocytoplasmic shuttling of HMGB1 is regulated by phosphorylation that redirects it toward secretion. J Immunol 177:7889-7897

Zhang J, Takahashi HK, Liu K, Wake H, Liu R, Maruo T, Date I, Yoshino T, Ohtsuka A, Mori S, Nishibori M (2011) Anti-high mobility group box-1 monoclonal antibody protects the blood-brain barrier from ischemia-induced disruption in rats. Stroke 42:1420-1428

Zhou H, Ji X, Wu Y, Xuan J, Qi Z, Shen L, Lan L, Li Q, Yin Z, Li Z, Zhao Z (2014) A Dual-Role of Gu-4 in Suppressing HMGB1 Secretion and Blocking HMGB1 Pro-Inflammatory Activity during Inflammation. PLoS One 9:e89634

Zhou H, Wang Y, Wang W, Jia J, Li Y, Wang Q, Wu Y, Tang J (2009) Generation of monoclonal antibodies against highly conserved antigens. PLoS One 4:e6087

Zhu X, Messer JS, Wang Y, Lin F, Cham CM, Chang J, Billiar TR, Lotze MT, Boone DL, Chang EB (2015) Cytosolic HMGB1 controls the cellular autophagy/apoptosis checkpoint during inflammation. J Clin Invest 125:1098-1110

CHAPTER 4. ORGANIC DUST EXPOSURE INDUCES STRESS RESPONSE AND MITOCHONDRIAL DYSFUNCTION IN MONOCYTIC CELLS

Sanjana Mahadev Bhat [1], Denusha Shrestha [1], Nyzil Massey [1], Locke A. Karriker [2], Anumantha G. Kanthasamy [1], Chandrashekhar Charavaryamath [1*]

[1] Department of Biomedical Sciences, 2008 Vet Med Building, Iowa State University, Ames, IA, USA. [2] Department of Veterinary Diagnostic and Production Animal Medicine, 2203 Lloyd Veterinary Medical Center, Iowa State university, Ames, IA, USA

*To whom correspondence should be addressed: Chandrashekhar Charavaryamath, BVSc, MVSc, PhD., Assistant Professor, Department of Biomedical Sciences, Iowa State University, Ames, IA 50011. Telephone: (515) 294-7710; Fax: (515) 294-2315; Email: chandru@iastate.edu

Keywords: Organic dust, mitoapocynin, ethyl pyruvate, mitochondrial dysfunction, mitochondrial DNA

Modified from a manuscript published in the *Journal of Histochemistry and Cell Biology* (doi: https://doi.org/10.1007/s00418-021-01978-x)

Author contributions

S.M. Bhat participated in the design of experiments, performed the experiments, analyzed the data, and wrote the manuscript. D. Shrestha performed the calcium influx assay. N. Massey performed organic dust extraction. L. Karriker collected the organic dust samples and edited the manuscript. A.G. Kanthasamy provided mitoapocynin and edited the manuscript. C. Charavaryamath conceptualized the study, participated in the design of the experiments, performed dust extraction, participated in the interpretation of data and edited the manuscript. All authors have read and approved the final manuscript.

Abbreviations

OD: Organic Dust; ODE: Organic Dust Extract; EP: Ethyl Pyruvate; MA: Mitoapocynin; LPS: Lipopolysaccharide; PGN: Peptidoglycan; MAMPs: Microbial Associated Molecular Patterns; COPD: Chronic Obstructive Pulmonary Disease; AHR: Airway hyperresponsiveness; ROS: Reactive Oxygen Species; RNS: Reactive Nitrogen Species; ATP: Adenosine Triphosphate; OXPHOS: Oxidative Phosphorylation; HMGB1: High Mobility Group Box 1; STAT: Signal Transducer and Activator of Transcription; TPP: Triphenylphosphonium; MPTP: 1-Methyl-4-

Phenyl-1,2,3,6-Tetrahydropyridine; iNOS: inducible Nitric Oxide Synthase; NOX: NADPH Oxidase; MTT: 3-[4,5-dimethylthiazole-2-yl]-2,5-diphenyltetrazolium bromide; TEM: Transmission Electron Microscopy; DMSO: Dimethyl Sulfoxide; mtND1: mitochondrial NADH dehydrogenase 1; MFN: Mitofusin; OPA1: Optic Atrophy 1; DRP1: Dynamin-related protein 1; ER: Endoplasmic Reticulum; PINK1: PTEN- induced kinase 1; BNIP3: Bcl-2 Homology 3 (BH3)-only; MPT: Mitochondrial Permeability Transition; COX4i2: Cytochrome C Oxidase subunit 4 isoform 2; ETC: Electron Transport Chain; SOD2: Superoxide Dismutase 2; mtDAMPs: mitochondrial Damage Associated Molecular Patters; mtTFA: mitochondrial Transcription Factor A; OMM: Outer Mitochondrial Membrane; IMM: Inner Mitochondrial Membrane; IMS: Intermembrane Space; IL: Interleukin; cGAS: cyclic GMP-AMP synthase; TLR: Toll-like receptor; RAGE: Receptor for advanced glycation end products; VDAC: Voltage-dependent anion channel

Abstract

Exposure to airborne organic dust (OD), rich in microbial associated molecular patterns (MAMPs), is shown to induce lung inflammation. A common manifestation in lung inflammation is altered mitochondrial structure and bioenergetics that regulate mitochondrial ROS (mROS) and feed a vicious cycle of mitochondrial dysfunction. The role of mitochondrial dysfunction in other airway diseases is well known. However, whether OD exposure induces mitochondrial dysfunction remains elusive. Therefore, we tested a hypothesis that organic dust extract (ODE) exposure induces mitochondrial stress using a human monocytic cell line (THP1). We examined whether co-exposure to ethyl pyruvate (EP) or mitoapocynin (MA) could rescue ODE exposure induced mitochondrial changes. Transmission electron micrographs showed significant differences in cellular and organelle morphology upon ODE exposure. ODE exposure with and without EP co-treatment increased the mtDNA leakage into the cytosol. Next, ODE exposure increased PINK1,

Parkin, cytoplasmic cytochrome c levels, and reduced mitochondrial mass and cell viability, indicating mitophagy. MA treatment was partially protective by decreasing Parkin expression, mtDNA and cytochrome c release and increasing cell viability.

Introduction

Industrialized agriculture production systems form the backbone of farm economy in the USA with a large number of workforce and a significant contribution to the nation's GDP (Charavaryamath and Singh 2006; Sethi et al. 2017; Nordgren and Charavaryamath 2018). Despite the production efficiency and cheaper price of food, these industries have occupational hazards in the form of exposure to many on-site contaminants. Among the contaminants, airborne organic dust (OD) and gases (mainly hydrogen sulfide, methane and ammonia), viable bacteria, fungal spores and other microbial products are known to be present (Vested et al. 2019). Bacterial lipopolysaccharide (LPS) and peptidoglycan (PGN) are the major microbial associated molecular patterns (MAMPs) present in OD (May et al. 2012). Agriculture production workers who are exposed to OD report several respiratory symptoms and annual decline in the lung function (Wunschel and Poole 2016; Sethi et al. 2017; Nordgren and Charavaryamath 2018).

Persistent exposure to OD has been linked to the development of chronic inflammatory conditions, such as chronic obstructive pulmonary disease (COPD) and asthma, including lung tissue damage and decline in lung function (Charavaryamath and Singh 2006; Wunschel and Poole 2016). Despite several research groups using both in vitro and in vivo models of OD exposure, precise cellular and molecular mechanisms responsible for the development of these chronic lung diseases remain largely unknown. In order to design effective therapeutic strategies against OD-induced airway diseases, an understanding of the underlying mechanisms of airway inflammation is essential. Studies have shown that OD-mediated lung inflammation is typically characterized by airway hyperresponsiveness (AHR), tissue remodeling, and increased influx of inflammatory cells,

particularly neutrophils and macrophages (Charavaryamath et al. 2005; Sahlander et al. 2012; Sethi et al. 2017). In previous studies, we have shown that exposure of human bronchial epithelial cells to OD results in the production of reactive oxygen species (ROS), reactive nitrogen species (RNS), and a myriad of pro-inflammatory cytokines such as interleukins IL-1β, IL-6, and IL-8 (Nath Neerukonda et al. 2018; Bhat et al. 2019). Production of pro-inflammatory mediators, development of abnormal mitochondrial signatures and mitochondrial dysfunction have been shown to contribute to the pathological mechanisms underlying airway diseases (Cloonan and Choi 2016). Mitochondria are emerging as a central focal point in many inflammatory airway diseases (Su et al. 2016; Prakash et al. 2017). Collectively, these findings suggest that instead of targeting multiple pattern recognition receptors (PRRs), focusing on mitochondrial dysfunction appears to be a more promising single common target to curtail the inflammation (Charavaryamath et al. 2008; Poole et al. 2010; Poole et al. 2011).

The role of mitochondria in OXPHOS, stress responses and programmed cell death pathways have been well studied over the past decade, the role of mitochondria in the sustained lung inflammation is of great interest (Prakash et al. 2017). Studies have demonstrated the elevation of critical enzymes involved in the production of ROS and RNS due to mitochondrial impairment in various inflammatory conditions (Zhang et al. 2010; Cloonan and Choi 2012; Eisner et al. 2018). Dysfunctional mitochondria result in impaired cellular respiration, compromised cellular immune response and cell death. (Cloonan and Choi 2012; Eisner et al. 2018).

The adverse effects of inflammation on mitochondria can be abrogated by several mechanisms. These include the induction of antioxidant defenses, maintenance of mitochondrial integrity through the selective removal of dysfunctional mitochondria (mitophagy), and the generation of new organelles to replace damaged or dysfunctional mitochondria through

mitochondrial biogenesis (Eisner et al. 2018). However, the integration of these compensatory responses, and the interaction between mitochondria and host cells following OD exposure, are not well understood. Previously, we have shown that, damage-associated molecular patterns (DAMPs) such as high mobility group box 1 (HMGB1) have a role to play in OD-induced airway epithelial inflammation (Bhat et al. 2019). Further, using a microglial model of OD-exposure, we confirmed the role of HMGB1 in inducing neuroinflammation where our data indicated involvement of mitochondria in OD-induced reactive species generation and neuroinflammation (Massey et al. 2019). We also showed that using ethyl pyruvate (EP, blocks translocation of HMGB1) or anti-HMGB1 neutralizing antibodies, OD-induced inflammation could be abrogated (Bhat et al. 2019).

The protective effects of EP have been attributed to its anti-inflammatory, antioxidative and antiapoptotic actions as well as its ability to prevent phosphorylation and release of HMGB1 (Shin et al. 2014). We also demonstrated that EP downregulates OD-induced reactive oxygen species (ROS) generation and augments IL-10 production to promote anti-inflammatory effects. (Bhat et al. 2019). Similar results have been shown in LPS injected and ischemic animal models as well (Venkataraman et al. 2002; Yu et al. 2005). Other anti-inflammatory properties of EP have been attributed to the inhibition of ROS-dependent signal transducer and activator of transcription (STAT) signaling (Kim et al. 2008; Shin et al. 2014).

Another potent mitochondrial specific antioxidant we have used previously is mitoapocynin (MA) (Massey et al. 2019). Apocynin, a plant derived antioxidant, has been used as an efficient inhibitor of cytoplasmic NADPH-oxidase complex (NOX2) in many experimental models involving phagocytic and nonphagocytic cells (Stefanska and Pawliczak 2008). Mitoapocynin (MA) is a triphenylphosphonium (TPP) conjugated apocynin designed to enhance

cellular uptake of the compound and target the mitochondria. In contrast to other popular antioxidant therapies, MA has been shown to suppress production of iNOS and various pro-inflammatory cytokines in various neuroinflammatory disease models. In addition, MA was shown to inhibit cytoplasmic NOX2 activity and reduce oxidative stress (Ghosh et al. 2016; Langley et al. 2017).

In this study we used an immortalized human monocytic cell line (THP1) and tested a hypothesis that OD-exposure induces mitochondrial stress. We further examined whether induction of antioxidant defenses with either EP or MA treatment changes mitochondrial biogenesis in THP1 cells following exposure to ODE. Here we demonstrate that mitochondrial targeting apocynin (MA) that inhibits cytoplasmic NOX2 or pharmacological inhibition of HMGB1 translocation (EP), are vital to cellular recovery following exposure to OD.

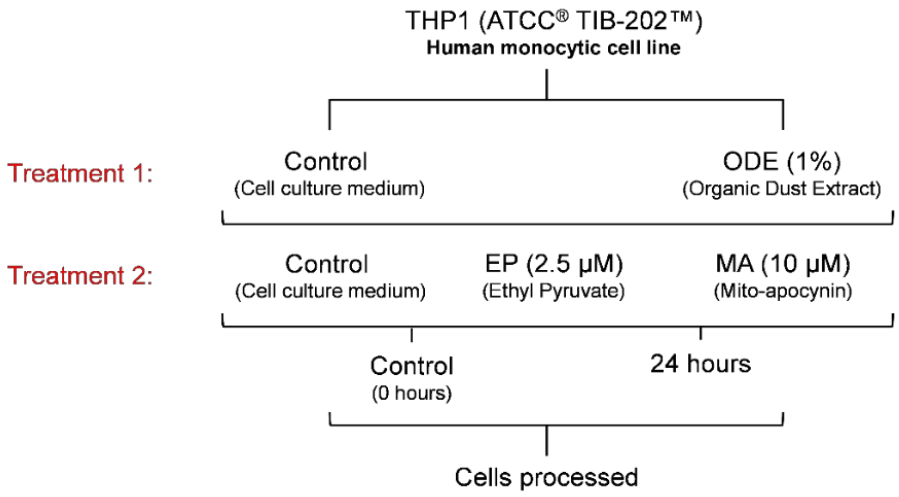

Figure 4.1 ODE exposure of THP1 cells and antioxidant treatment
THP1 cells were treated with either media (control) or ODE (treatment 1) followed by either media, EP or MA (treatment 2). Cells were processed for various assays at 0 (control), and 24 hours.

Results

Endotoxin levels in ODE samples

Endotoxin content of diluted ODE (1:10) samples was measured. From three samples collected we found that endotoxin values ranged from 0.99 ± 0.0005 to 1.433 ± 0.02 EU/mL.

Exposure to ODE impacts the cellular and mitochondrial morphology

TEM images showed that THP1 cells treated with media alone (controls) displayed normal morphology with healthy mitochondria (Figure 4.2a-d and 4.3a-d). Following ODE treatment, cytoplasmic vacuolization and pseudopod formation was observed suggesting differentiation of cells (Figure 4.2b) (Krysko et al. 2006). In addition, the mitochondria appeared larger in size and some of the mitochondria were elongated with reduced cristae numbers and/or appearance of deformed cristae (Figure 4.3b). On addition of EP, similar to ODE exposure, the mitochondria were swollen and showed disorganized cristae, along with the presence of calcium sequestration bodies in the mitochondrial matrix (Figure 4.3c). In contrast, exposure to MA seemed to restore the impact of ODE. Cells exposed to both ODE and MA showed almost no cytoplasmic vacuolization, and mitochondria showed decreased signs of damage to cristae, albeit conformed to an elongated morphology (Figure 4.2d and 4.3d). These results suggest that MA has a partial protective effect on ODE exposed macrophages.

In order to quantify ultra-structural changes observed in the TEM images, mitochondria were individually traced from the micrographs. Compared to controls, exposure to ODE significantly reduced the mitochondrial surface area (Figure 4.3e). A similar decrease was seen in the presence of MA as well, whereas EP significantly increased the surface area (mitochondrial size) comparable to that of control group (Figure 4.3e). Compared to controls, treatment with ODE and with either EP or MA decreased the mitochondrial circularity. Among these, cells co-treated with ODE with MA showed maximum decrease in mitochondrial circularity (Figure 4.3f). Other

morphological parameters such as perimeter, and Feret's diameter did not differ between any of the treatment groups (Figure 4.3g and 4.3h).

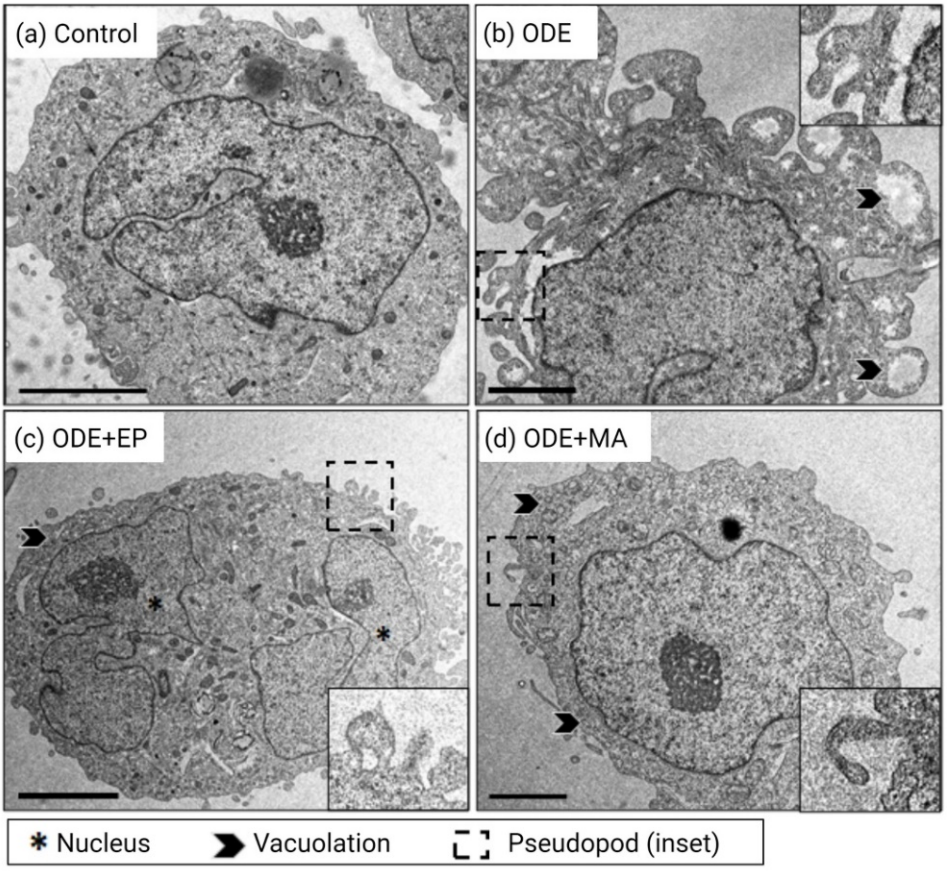

Figure 4.2 ODE exposure induces differentiation of THP1 cells with ultrastructural changes to cellular morphology
Transmission electron microscopy (TEM) of THP1 cells treated with medium or ODE (1%) followed by medium or EP (2.5 μM) or MA (10 μM) for 24 hours shows changes in cellular morphology at the ultrastructural level. Compared to controls, cells exposed to ODE differentiated into activated macrophages, with increased vacuolation and pseudopod formation (a-d, scale bar, 2-5 μm).

Targeted antioxidant therapy promotes mitochondrial fission

The mitochondrial membrane is continuously remodeled through cycles of fission and fusion events. In order to accurately interpret the impact of ODE exposure on mitochondrial morphology, expression of markers responsible for the dynamic events was measured. On ODE exposure, the expression of mitofusin 2 (MFN2) was significantly increased compared to control

(Figure 4.4a and 4.4c). In contrast, mitofusin 1 (MFN1) and optic atrophy 1 (OPA1) protein levels were not different among any of the treatment groups compared to control (Figure 4.4a, 4.4b and 4.4d). Increased expression of dynamin-related protein 1 (DRP1) was observed in cells treated with both ODE and ODE with MA (Figure 4.4e and 4.4f). Furthermore, to analyze changes in mitochondrial number, change in mitochondrial mass was measured using mitotracker green dye. There was a significant increase in the mitochondrial mass on exposure to ODE and ODE with EP, while on exposure to MA mitochondrial mass decreased comparable to controls in size (Figure 4.4g).

ODE exposure induces selective targeting of mitochondria for autophagy (mitophagy)

We investigated whether ODE exposure induces mitophagy-mediated clearance of mitochondria. The expression of the two important mediators of mitophagy, PTEN-induced kinase 1 (PINK1) and the E3 ubiquitin protein ligase Parkin, were investigated. Compared to controls, ODE exposure increased the expression of Parkin but not PINK1 (Figure 4.5a and 4.5c). Further, co-treatment with EP and MA reversed the ODE induced increase in Parkin (Figure 4.5a and 4.5b). The expression of BNIP3, a mitochondrial Bcl-2 Homology 3 (BH3)-only protein, was also observed. BNIP3 levels remained unchanged on exposure to ODE and ODE with EP (Figure 4.5a and 4.5d). While co-treatment with MA significantly decreased BNIP3 expression (Figure 4.5d).

ODE exposure impacts mitochondrial membrane permeability

Mitochondrial oxidative phosphorylation (OXPHOS) pathway is critical in determining and maintaining the immunomodulatory phenotype of activated macrophages (Kelly and O'Neill 2015). Considering this mitochondrial OXPHOS pathway was investigated. ODE exposure increased the levels of cytosolic cytochrome c, compared to that in the mitochondrial fraction indicating the release of cytochrome c from the mitochondria (Figure 4.6a-4.6c). On the other hand, MA treatment significantly decreased ODE-induced release of cytochrome c into the cytosol

(Figure 4.6a-4.6c). Following ODE exposure there was a significant decrease in the expression of lung-specific isoform of cytochrome c oxidase (COX4i2) in the mitochondrial fraction and there was no change in COX4i2 levels following treatments with either EP or MA (Figure 4.6d and 4.6f). For all treatment groups expression of SOD2 significantly increased compared to controls, while treatment with EP or MA decreased the levels when compared to cells exposed to ODE alone (Figure 4.6e and 4.6g). Presence of SOD2 is known to impart tolerance during high oxidative stress and reduce superoxide accumulation withing the mitochondria (Fukui and Zhu 2010; Ishihara et al. 2015). To identify whether this is true, mitochondrial superoxide levels were measured using MitoSOX dye. Exposure to ODE significantly decreased the mitochondrial superoxide, while treatment with MA increased the levels similar to control (Figure 4.6h). Using the Griess assay, we measured the reactive nitrite species (RNS) released into the extracellular environment. ODE exposure increased the levels of RNS in the cell culture media at 24 hours, while treatment with EP and MA significantly attenuated the RNS secretion (Figure 4.6i).

ODE induces the secretion of mitochondrial DAMPs

Mitochondrial secondary messengers can act as mitochondrial damage–associated molecular patterns (mtDAMPs) when produced excessively or secreted into other cellular locations (Cloonan and Choi 2012). Compared to controls, ODE, ODE with EP or MA treatments showed increased levels of mitochondrial transcription factor A (mtTFA) expression in both the mitochondrial and cytosolic fractions (Figure 4.7a-4.7c). On measuring the levels of mtDNA leaking into the cytosol, it was observed that exposure to ODE increased the cytosolic mtDNA levels, which was abrogated on treatment with EP or MA (Figure 4.7d). In addition, there was an increase in calcium (Ca^{2+}) influx into the mitochondria in all treatment groups, with no significant change in the presence of either MA or EP co-treatment compared to ODE (Figure 4.7e). The expression of mitochondrial HMGB1 was determined, as presence of HMGB1 in the

mitochondrial matrix is known to be critical in the regulation of mitochondrial function (Tang et al. 2011). Compared to control, expression of mitochondrial HMGB1 was significantly decreased (Figure 4.7f and 4.7g). In addition, we observed the presence of low molecular weight cleaved HMGB1 bands. However, upon quantification there were no significant differences between treatments (Data not shown). EP treatment significantly increased mitochondrial HMGB1 expression when compared to treatment with both ODE and ODE with MA (Figure 4.7f and 4.7g).

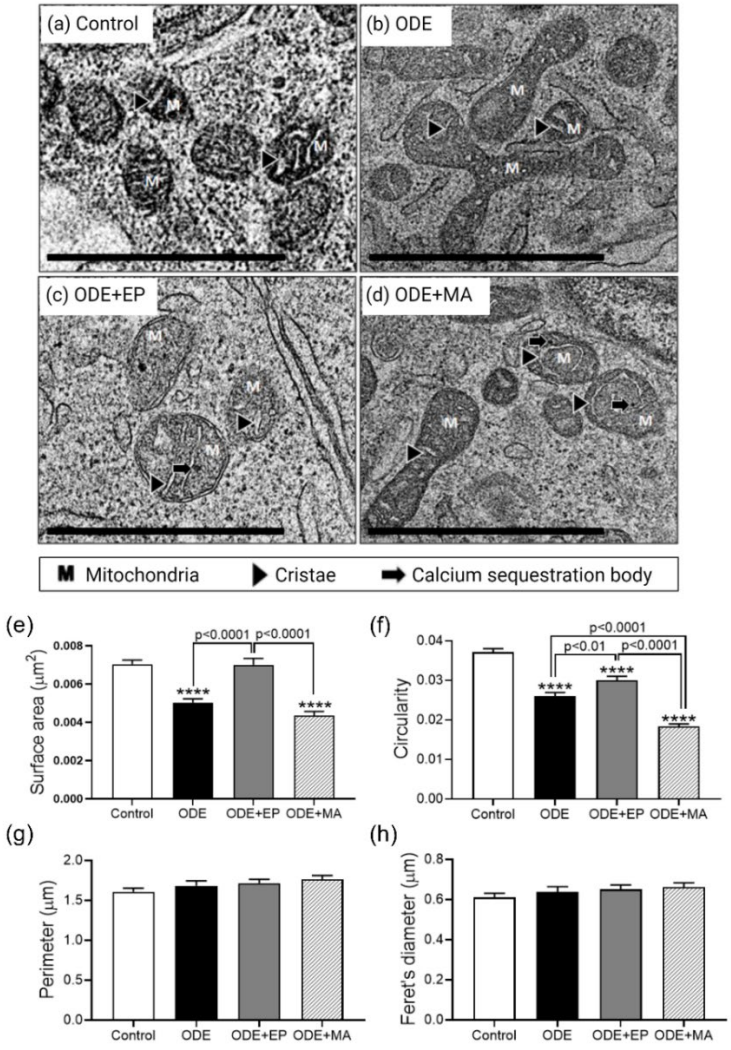

Figure 4.3 ODE exposure induces changes in mitochondrial morphological features in THP1 cells

Transmission electron microscopy (TEM) of THP1 cells treated with medium or ODE (1%) followed by medium or EP (2.5 μM) or MA (10 μM) for 24 hours show changes in the mitochondrial morphology. A number of mitochondria displayed changes in morphology

(fission/fusion) and swelling (a-d, scale bar, 2-5 µm), along with presence of calcium sequestration bodies within the mitochondrial matrix in cells co-treated with of EP (2.5 µM). Cells treated with ODE followed by MA showed noticeably healthier mitochondria with a few morphological changes (fission/fusion). Morphological parameters of mitochondria of THP1 was analyzed by ImageJ (e-f). Measurement of surface area (e), circularity (f), perimeter (g) and Feret's diameter (h) of the mitochondria were determined. Data analyzed via one-way ANOVA with Tukey's multiple comparison test (*p < 0.05, **p < 0.01, ***p < 0.001, ****p < 0.0001) and are represented as Mean ± SEM with n = 126 mitochondria/treatment (* indicates significant difference from control).

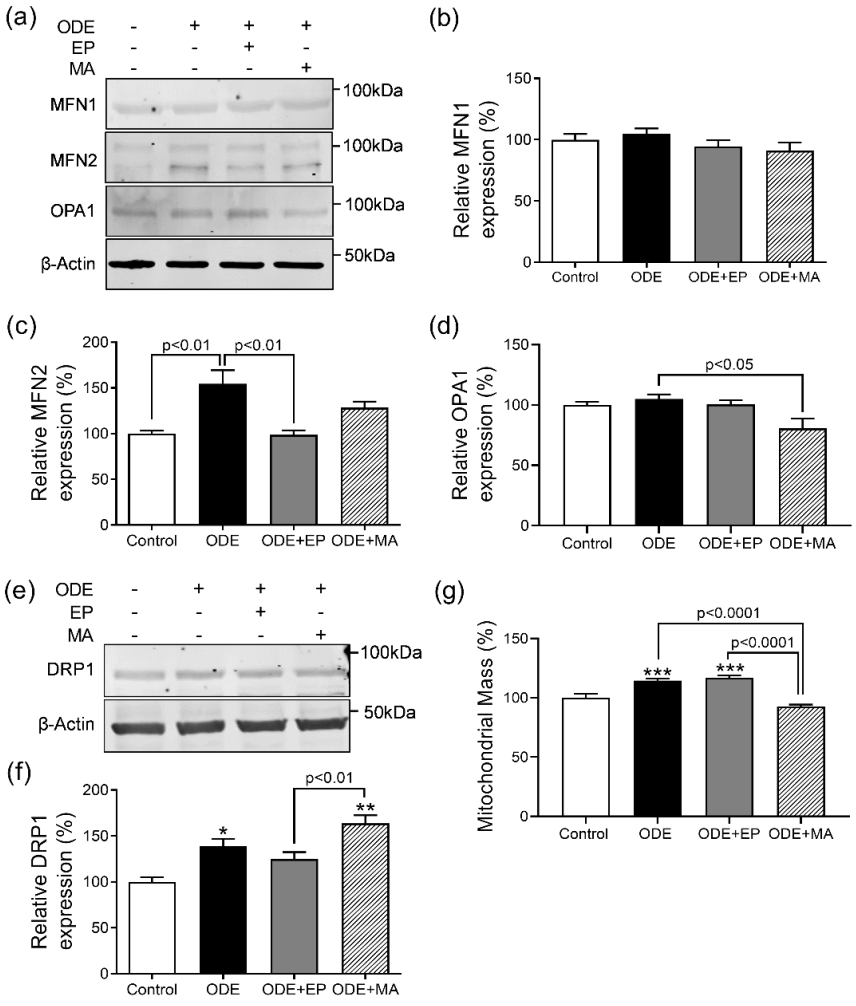

Figure 4.4 ODE exposure induces fusion of mitochondria in response to stress
Immunoblotting of whole-cell lysates of THP1 cells treated with medium or ODE (1%) followed by medium or EP (2.5 µM) or MA (10 µM) for 24 hours was performed to detect mitochondrial fusion proteins MFN1 (a,b), MFN2 (a,c) and OPA1 (a,d) and fission protein DRP1 (e,f) and compared. Mitochondrial mass was measured by staining with Mito-tracker dye (g). Samples for all assays were derived from the same experiment and were processed in parallel. All the protein bands were normalized over β-actin (37 kD) and percentage intensity relative to control was analyzed. Data was analyzed using one-way ANOVA with Tukey's multiple comparison test (*p

< 0.05, **p < 0.01, ***p < 0.001, ****p < 0.0001) and represented as mean ± SEM with n = 3-6/treatment (* indicates significant difference from control).

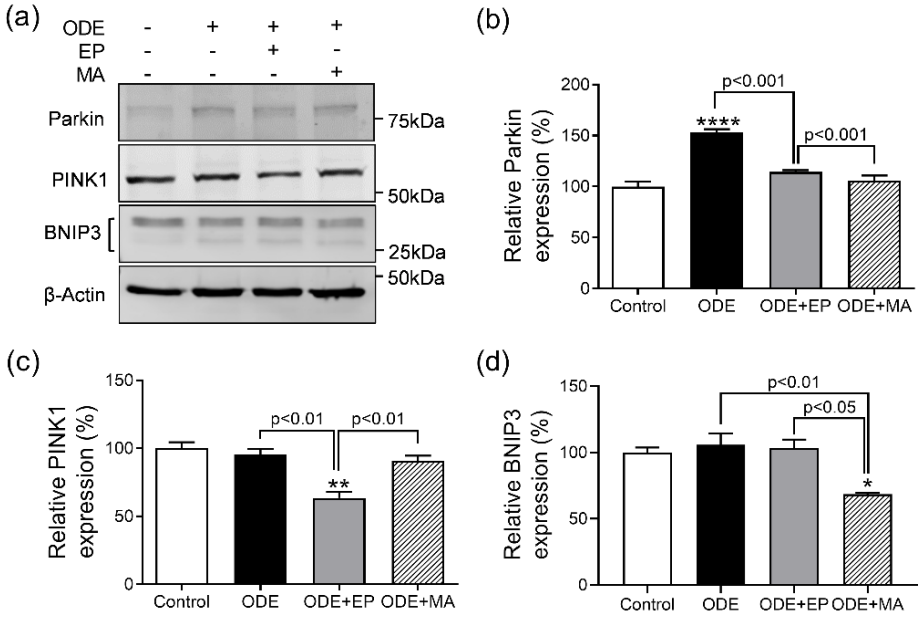

Figure 4.5 ODE exposure induces selective targeting of mitochondria for autophagy (mitophagy)
Immunoblotting of whole-cell lysates of THP1 cells, treated with medium or ODE (1%) followed by either medium or EP (2.5 μM) or MA (10 μM) for 24 hours, was performed to detect expression of mitophagy markers, Parkin (a, b) and PINK1 (a, c), and BNIP3 (a, d). For all the western blots, samples were derived from the same experiment and were processed in parallel. All the protein bands were normalized over β-actin (37 kD) and percentage intensity relative to control was analyzed. Data was analyzed using one-way ANOVA with Tukey's multiple comparison test (*p < 0.05, **p < 0.01, ***p < 0.001, ****p < 0.0001) and represented as mean ± SEM with n = 3/treatment (* indicates significant difference from control).

Mitoapocynin does not intervene in ODE mediated caspase-1 upregulation

Published work shows that the release of mtDNA and mitochondrial reactive oxygen species (mROS) activates the NLRP3 inflammasome pathway (Gong et al. 2018). Upstream of NLRP3 activation, cleavage of pro-caspase 1 to caspase 1 is seen due to increased influx of calcium induced by leaky mitochondria (Murakami et al. 2012). Based on this, changes in the expression of pro-caspase 1 and caspase 1 were measured. Compared to control, exposure to ODE, ODE and EP or MA increased the expression of pro-caspase 1. ODE with EP treatment reduced pro-caspase 1 levels significantly when compared to ODE (Figure 4.8a and 4.8b). Compared to controls, ODE

and ODE with MA exposure significantly increased the expression of cleaved caspase 1 (p10). Treatment with EP significantly decreased cleavage compared to ODE, which is consistent with the expression of pro-caspase 1. Expression of pro-caspase 3 and its cleaved product was measured in order to determine if ODE is inducing a caspase 3 mediated apoptosis. Although ODE minimally decreased the expression of pro-caspase 3 compared to control, caspase 3 expression in ODE with EP or MA treated cells remained unchanged (Figure 4.8d and 4.8e). In addition, there was absence of caspase 3 cleavage product in any of the treatment groups (Figure 4.8d).

Previously we have shown that pro-inflammatory cytokine release is induced in bronchial epithelial cells exposed to ODE. We also showed that EP has the capacity to significantly decrease the release the pro-inflammatory cytokines, particularly IL-1β and increased IL-10 production (Bhat et al. 2019). Consistent with previous studies, in this study levels of TNF-α, IL-1β and IL-6 were significantly increased in ODE exposed THP1 cells compared to controls (Figure 4.10a-4.10c). With EP or MA co-treatment, the levels were significantly reduced when compared to cells treated with ODE alone but were still higher compared to controls. Concentration of IL-10 was increase upon exposure to ODE with EP or MA, indicative of anti-inflammatory processes coming into effect. This increase was not observed in THP1 cells exposed to ODE alone (Figure 4.10d).

Mitoapocynin therapy does not inhibit ODE induced apoptosis

To identify the impact OD-induced mitochondrial dysfunction and rescue may have on cellular apoptosis, expression of Bcl-2 and Bcl-XL were measured. Decreased expression of Bcl-2 was observed among all treatment groups compared to controls with no significant impact on co-treatment with EP or MA (Figure 4.9a and 4.9b). Compared to controls, ODE, ODE with EP or MA decreased the Bcl-XL expression. However, ODE with EP or ODE with MA treatment significantly increased Bcl-XL levels compared to ODE treated cells (Figure 4.9d and 4.9e). This change in expression of Bcl-XL was corroborated by measuring cell viability by MTT colorimetric

assay. The percentage cell viability observed correlated with the expression pattern of Bcl-XL, where loss of cell viability on ODE exposure was rescued by treatment with EP or MA (Figure 4.9c).

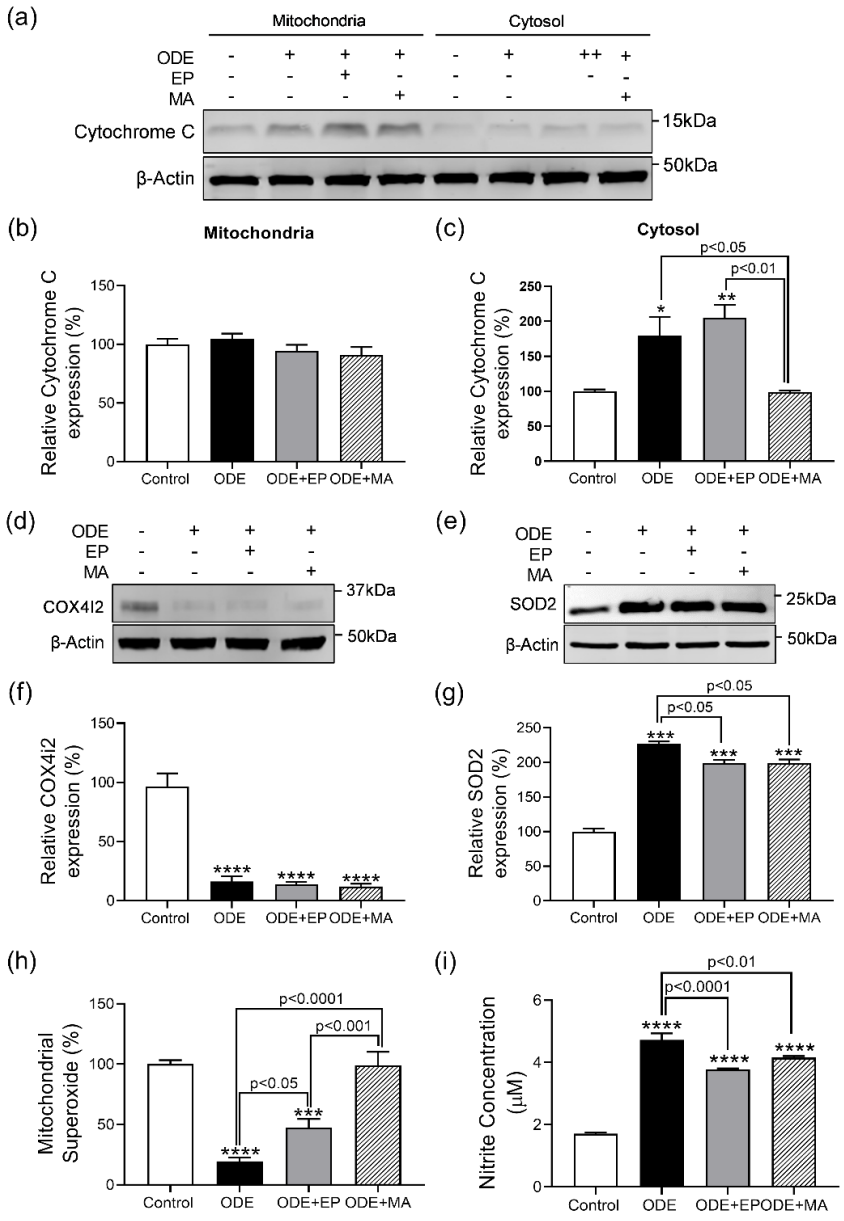

Figure 4.6 Mitoapocynin treatment decreases ODE-induced Cytochrome C release and markedly increases SOD2 expression in the cytosol

We performed the immunoblotting of mitochondrial and mitochondria-free cytosolic fractions of THP1 cells, treated with medium or ODE (1%) followed by either medium or EP (2.5 μM) or MA (10 μM) for 24 hours, to detect the presence of Cytochrome C and expression of lung-specific isoform of COX, COX4i2, and SOD2. Cytochrome C expression was compared between the

mitochondrial (a, b) and cytosolic (a, c) fractions of the cells. Measurement of expression of COX4i2 (d, f), and superoxide dismutase 2 (SOD2) (e, g) in the mitochondrial fractions of the treated cells was performed. Using the MitoSox and Griess assays, the levels of superoxide anions (SOX) (h) and secreted nitrites (i) were measured, respectively. Samples for all assays were derived from the same experiment and were processed in parallel. All the protein bands were normalized over β-actin (37 kD) and percentage intensity relative to control analyzed. Data was analyzed using one-way ANOVA with Tukey's multiple comparison test (*p < 0.05, **p < 0.01, ***p < 0.001, ****p < 0.0001) and represented as mean ± SEM with n = 3-6/treatment (* indicates significant difference from control).

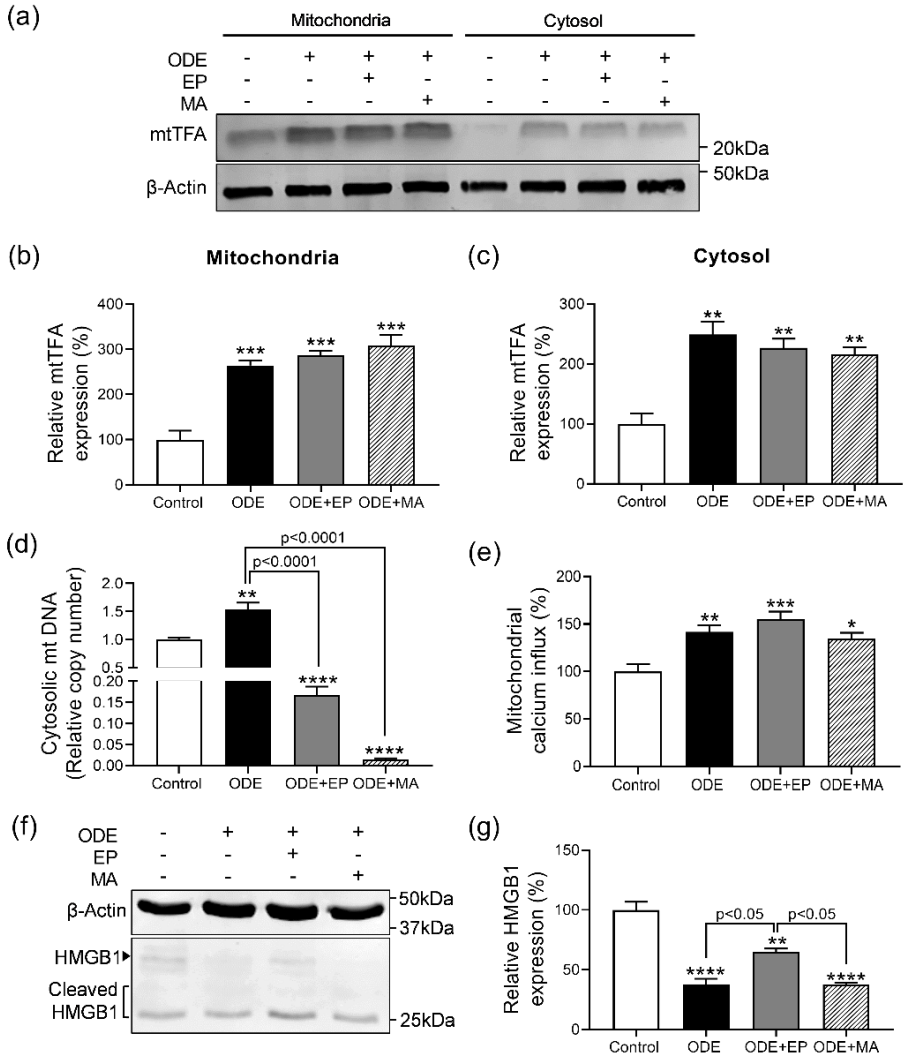

Figure 4.7 ODE exposure markedly increases secretion of mitochondrial DAMPs into the cytosol

Immunoblotting of mitochondrial and mitochondria-free cytosolic fractions of THP1 cells, treated with medium or ODE (1%) followed by either medium or EP (2.5 μM) or MA (10 μM) for 24 hours, was performed to detect expression of mitochondrial transcription factor activator (mtTFA) (a-c). mtTFA expression was compared in the mitochondrial (b) and cytosolic (c) fractions of the cells to assess leaky mitochondrial membrane. Mitochondrial DNA leakage into the cytosol was

analyzed via qPCR (d). Intra-mitochondrial calcium levels in mitochondria isolated from the treated cells was measured by Rhod 2AM staining (e). Immunoblotting of mitochondrial fraction of THP1 cells was performed to measure HMGB1 expression in mitochondria (f, g). Samples for all assays were derived from the same experiment and were processed in parallel. All protein bands were normalized over β-actin (37 kD) and percentage intensity relative to control analyzed. Data was analyzed using one-way ANOVA with Tukey's multiple comparison test (*p < 0.05, **p < 0.01, ***p < 0.001, ****p < 0.0001) and represented as mean ± SEM with n = 3-6/treatment (* indicates significant difference from control).

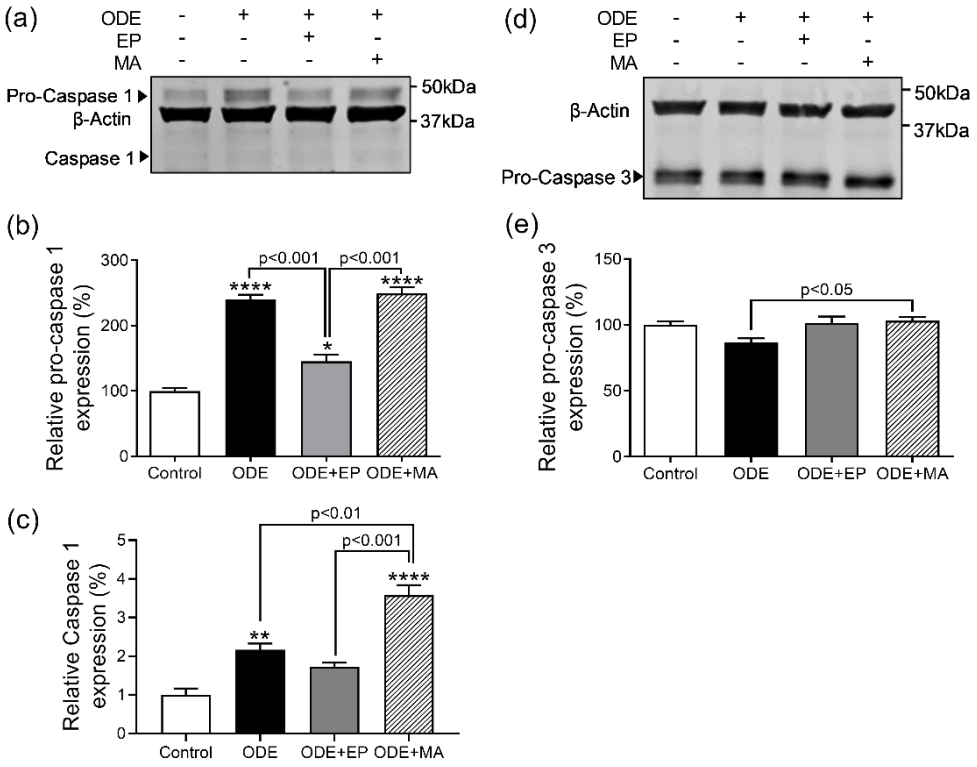

Figure 4.8 ODE exposure increases expression of Caspase 1

Immunoblotting of whole cell lysates of THP1 cells, treated with either medium or ODE (1%) followed by either medium or EP (2.5 μM) or MA (10 μM) for 24 hours was performed to detect the expression of caspase 1 and 3. Expression of pro-caspase 1 (a, b), along with the cleaved caspase 1 p10 (a, c) in treated cells was measured and compared. Expression of pro-caspase 3 in treated cells was measured (d, e). For all western blots, samples were derived from the same experiment and were processed in parallel. All protein bands were normalized over β-actin (37 kD) and percentage intensity relative to control was analyzed. Data was analyzed using one-way ANOVA with Tukey's multiple comparison test (*p < 0.05, **p < 0.01, ***p < 0.001, ****p < 0.0001) and represented as mean ± SEM with n = 3/treatment (* indicates significant difference from control).

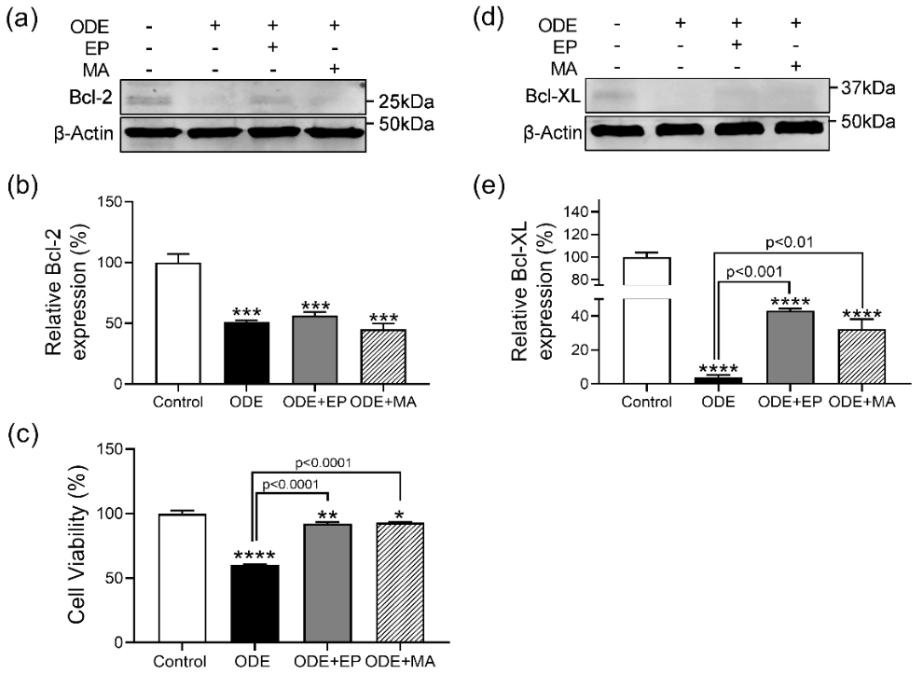

Figure 4.9 Mitochondrial targeted antioxidant treatment has no effect Bcl-2 and Bcl-XL expression

Immunoblotting of whole cell lysates of THP1 cells, treated with ODE (1%), EP (2.5 μM), or MA (10 μM) for 24 hours, was performed to observe expression of Bcl-2 (a, b) and Bcl-XL (d, e). MTT assay was performed to measure cell viability on treatment (c). Samples for all assays were derived from the same experiment and were processed in parallel. All protein bands were normalized over β-actin (37 kD) and percentage intensity relative to control analyzed. Data was analyzed using one-way ANOVA with Tukey's multiple comparison test (*$p < 0.05$, **$p < 0.01$, ***$p < 0.001$, ****$p < 0.0001$) and represented as Mean ± SEM with n = 3-6/treatment (* indicates different from control).

Discussion

Chronic exposure to OD is a key contributor to the development of respiratory symptoms and airway obstruction in exposed workers (Cole et al. 2000; Nordgren and Charavaryamath 2018). Continuous exposure to OD has been shown to alter innate immune responses in the airways (Charavaryamath and Singh 2006; Wunschel and Poole 2016; Sethi et al. 2017). These responses include recruitment of inflammatory cells, release of pro-inflammatory cytokines and reactive species (ROS/RNS) (Sahlander et al. 2012; Sethi et al. 2017; Nath Neerukonda et al. 2018; Bhat et al. 2019). Previous studies have provided a direct link between such innate immune signaling

events and mitochondrial dynamics suggesting a crucial role for mitochondria in the activation and control of airway disease progression (Cloonan and Choi 2012; Eisner et al. 2018). In this study, using THP1 cells as an *in vitro* model for alveolar macrophages, we demonstrate that OD exposure leads to significant changes in mitochondrial dynamics, integrity, and function. Next, using mitoapocynin (MA), a novel mitochondrial targeting NOX2 inhibitor, or ethyl pyruvate (EP), an inhibitor of translocation of HMGB1, we partially rescued ODE-induced mitochondrial changes and reduced the resultant inflammation.

Our TEM results demonstrate that, upon ODE exposure, there is an increased presence of cytoplasmic vacuoles and formation of pseudopods which is a characteristic feature of activated macrophages (Kim et al. 2008). Treatment with MA or EP did not prevent the ODE-induced morphological changes. To understand the impact of ODE-induced inflammation on mitochondrial biogenesis, we explored the factors involved in mitochondrial morphological changes. Mitochondria are highly dynamic organelles which continuously change their function, position, and structure to meet the metabolic demands of the cells during homeostatic conditions as well as at times of cellular stress (Wai and Langer 2016; Eisner et al. 2018). In this study, using TEM image analysis, we observed significant decrease in the mitochondrial surface area and circularity upon ODE exposure indicating that ODE-exposure could have an impact on mitochondrial dynamics and function. Similar exposure induced changes have been reported in previous studies as well (Westrate et al. 2014; Wai and Langer 2016; Eisner et al. 2018).

Exposure to toxic materials is known to alter mitochondrial morphology and biogenesis through fusion and fission (Fetterman et al. 2017). The delicate balance of these events helps in controlling mitochondrial structure and function (Wai and Langer 2016; Tilokani et al. 2018). Our results indicate that ODE exposure increased the expression of MFN2 but not MFN1 and OPA1.

Thus ODE exposure mediated increase in MFN2 could be promoting mitochondrial fusion. Further, EP treatment significantly reduced ODE induced MFN2 expression indicating that blocking nucleocytoplasmic translocation of HMGB1 could possibly reduce mitochondrial fusion. Next, our results show an increase in DRP1 as well upon exposure to ODE, which is further increased on co-treatment with MA. DRP1 dependent mitochondrial fragmentation is characterized by decreased expression of OPA1, which is observed in ODE exposed cells treated with MA (Mishra and Chan 2014; Tilokani et al. 2018). An increase in the rate of mitochondrial fragmentation is possibly a cellular response to counteract the loss of mitochondrial function and recover ATP synthesis capacity. Inhibition of DRP1-mediated mitochondrial fission has been reported to cause cellular dysfunction and replication (Qi et al. 2015). This can be corroborated by the decrease in cell viability with ODE exposure. The decreased mitochondrial mass observed with exposure to ODE and MA could be a means by which the mitochondria targeted NOX2 inhibition (antioxidant therapy) is overcoming the increase in dysfunctional mitochondria via mitochondrial biogenesis and mitophagy, thus allowing cells to quickly replace metabolically dysfunctional mitochondria.

MFN2 is known to mediate the recruitment of Parkin (an ubiquitin ligase enzyme) to damaged or dysfunctional mitochondria (Filadi et al. 2018). Binding of Parkin to MFN2 via a PINK1 dependent manner can lead to mitophagy (Narendra et al. 2008; Narendra et al. 2010; Ding and Yin 2012). Our results showing significantly higher expression of Parkin upon ODE exposure support this explanation. In our study, a balance of mitochondrial fusion, along with fission leading to mitochondrial clearance could be the most probable scenario that could be occurring aimed at compensating for the cellular stress induced by ODE (Landes et al. 2010). Albeit no significant change in BNIP3 expression was observed upon exposure to ODE or ODE followed by EP

compared to control, it was found to be significantly decreased in cells treated with ODE and MA. BNIP3, a transmembrane protein located in the OMM, imparts some pro-cell death activity and is known to regulate mitophagy (Ney 2015). Addition of BNIP3 to isolated mitochondria has resulted in cytochrome c release, depolarization, and swelling (Kim et al. 2002). This phenomenon has been linked to BNIP3-mediated permeabilization of inner and outer mitochondrial membrane involving the disruption of OPA1 complex and remodeling of the inner mitochondrial membrane leading to cell death (Landes et al. 2010). Collectively, we can assume that MA-induced decrease in BNIP3 and OPA1 expression could be having a positive impact on the mitochondria and thus improving overall cellular function. Potential mechanism by which BNIP3 is promoting cell death is through competition for binding to Bcl-2 (or a related protein) which liberates Beclin-1 from Bcl-2 complexes and activates autophagy. Taken together we document a decrease in overall cell viability with ODE exposure which is rescued by co-treatment with MA indicating that cytoplasmic NOX2 inhibition is beneficial (Langley et al. 2017).

A prominent player in cell death is cytochrome c (Cai et al. 1998; Garrido et al. 2006). Cytochrome c, a key protein of the mitochondrial inner membrane (IMM), is known to function as an electron shuttle between complex III and complex IV of the respiratory chain (Cai et al. 1998). Its activity and its release from the IMM has been implicated in caspase activation and mitochondrial outer membrane permeabilization (MOMP), leading to cell death (Garrido et al. 2006). In our findings, we observed that upon ODE exposure, there is an increase in cytosolic cytochrome c and a deficiency in the levels of COX4i2 (COX subunit 4 isoform 2), a terminal enzyme in the OXPHOS machinery. Loss of COX4i2 results in decreased COX activity and decreased ATP levels (Hüttemann et al. 2012). This loss is not reversed upon treatment with either EP or MA, albeit MA was capable of downregulating the release of cytochrome c. This is

indicative that although antioxidant therapy can decrease the cytosolic release of cytochrome c, there could be other secondary factors promoting the loss of COX4i2. NADPH oxidase is the main source of ROS that is closely linked to mitochondrial ROS production (Zorov et al. 2014). It is known that presence of ROS can promote expression of pro-inflammatory mediators (Brand et al. 2004; Bhat et al. 2019). Treatment with MA brought the mitochondrial superoxide levels to that of control, whereas with ODE and EP co-treatment, it was significantly decreased. This could be a consequence of a leaky mitochondrial membrane enabling the release of superoxide ions into the cytosol thus promoting further damage to the cell. On the other hand, the increase in the SOD2 expression observed allows us to believe that there are factors possibly promoting the attenuation of oxidative stress mediated cellular injury through compensation. This increase could be due to the presence of factors, such as interleukin 1 (IL-1), IL-4, IL-6, tumor necrosis factor α, interferon γ, and the bacterial endotoxin lipopolysaccharide, which are considered to be robust SOD2 activators (Fukui and Zhu 2010). SOD2 is also said to be regulated by RNS, where increased peroxynitrite levels can lead to its enzymatic inhibition (Redondo-Horcajo et al. 2010). These antagonistic roles that peroxynitrite and superoxide radicals have in regulating SOD2 expression and activity leads us to believe that mitochondrial antioxidant response is dysregulated.

A consequence of leaky mitochondrial membrane during mitochondrial dysfunction is the release of mtDAMPs (Nakahira et al. 2011). Mitochondrial transcription factor A (mtTFA) is an integral regulator of mtDNA integrity, which, when released from mitochondria, acts as a mtDAMP to enhance inflammatory responses (Julian et al. 2013). Release of mtTFA along with mtDNA during cell damage amplifies TNFa and type 1 interferon release, which plays a critical role in promoting sterile inflammation and autoimmune diseases (Cantaert et al. 2010; CHAUNG et al. 2012; Julian et al. 2012). This is in line with our findings where we observe an increase in

the cytosolic release of mtTFA and mtDNA upon ODE exposure. Although EP or MA therapy did not have a significant impact in reducing the release of mtTFA, it did however decrease the release of mtDNA into the cytosol. Because HMGB1 is a homolog of mtTFA (Parisi and Clayton 1991), we investigated whether it translocates from the normal nuclear location into the mitochondria in ODE exposed cells. Under pathophysiological conditions such as necrosis or inflammation, nuclear HMGB1 is immediately transported to the cytoplasm and released into the extracellular space where it acts as a signaling molecule regulating a wide range of inflammatory responses (Ugrinova and Pasheva 2017b; Bhat et al. 2019). In endothelial cells, the translocation of endogenous HMGB1 from the nucleus to the mitochondria promotes mitochondrial reorganization (Stumbo et al. 2008; Hyun et al. 2016). Therefore, it is likely that the nuclear HMGB1 export would be involved the compensatory responses for maintenance of mitochondrial functions. However, in the present study we see that treatment with MA does not revert the levels of HMGB1 within the mitochondria and match the levels observed in controls.

Mitochondria are also key regulators of calcium (Ca^{2+}) which control a diverse range of cellular processes including ROS production. Any aberrant increase in cytosolic Ca^{2+} and resultant $[Ca^{2+}]_{mito}$ overload can trigger cell death (Finkel et al. 2015). This overload has also been linked to increased permeabilization of mitochondrial membrane (Hunter et al. 1976; Finkel et al. 2015). This is corroborated by our findings where we observed increased $[Ca^{2+}]_{mito}$ levels on OD exposure. However, it could be possible that Ca^{2+} influx could possibly be occurring via the interaction of voltage-dependent anion channel (VDAC) with Mcl-1, a Bcl-2 family protein due to the decrease in Bcl-XL observed (Huang et al. 2014). Ca^{2+} signaling also plays a critical role in the activation of NLRP3 inflammasome by multiple stimuli (Murakami et al. 2012). This is corroborated by our data showing caspase-1 activation along with the increase in Ca^{2+} levels on

ODE exposure (Yu et al. 2014). This would in turn lead to IL-1β activation and release into the extracellular space. The treatment with MA does not seem to have any impact on the levels of Ca^{2+} accumulation within the mitochondria.

In conclusion, we document that co-treatment with EP and MA are partially protective as they rescue some of the ODE-exposure induced mitochondrial deficits. However, our findings may lead to new questions on how ODE exposure may be causing mitochondrial dysfunction and cell death. Although our current study is limited to using a single immortalized cell line as a model, we report preliminary data on the impact of ODE exposure on mitochondrial biogenesis and function. Future studies using functional (primary alveolar macrophages, precision-cut lung slices) and mouse models would help us to unravel further underlying mechanisms.

Materials and Methods

Chemicals and reagents

We purchased RPMI 1640, L-glutamine, penicillin-streptomycin, MitoTracker green dye, and MitoSOX Red dye from Invitrogen (ThermoFisher Scientific) and fetal bovine serum (FBS) was purchased from Atlanta Biologicals (Flowery Branch, GA, catalog # S11150H and lot # A17002). Antibodies for mitofusins (MFN1/2), DRP1, PINK1, Parkin, OPA1, BNIP3, Cytochrome C, COX4i2, Bcl-2, Bcl-XL, mtTFA, Caspase 1 and Caspase 3 was purchased from Santa Cruz Biotechnology. The anti-HMGB1 antibody, β-Actin antibody and Rhod-2AM dye were obtained from Abcam. The details of the antibodies used are listed in Table 4.2 and 4.3. MitoApocynin-C_2 (MA) was procured from Dr. Balaraman Kalyanaraman (Medical College of Wisconsin, Milwaukee, WI), stock solution (10 mM in DMSO) prepared by shaking vigorously and stored at -20°C. MA was used (10 μM) as one of the co-treatments. Ethyl pyruvate (EP, Santa Cruz Biotechnology, Dallas, TX), was reconstituted in Ringer's solution (Sigma-Aldrich) and used

at a final concentration of 2.5 μM in the cell culture medium (Ghosh et al. 2016; Langley et al. 2017).

Organic dust extract preparation

Aqueous organic dust extract (ODE) was prepared as previously described (Romberger et al. 2002; Bhat et al. 2019). Settled surface dust samples from swine production units were collected, and 1 g of the dust was placed into sterile Hank's Balanced Salt Solution (10 mL; Gibco). The solution was incubated for one hour at room temperature, centrifuged for 20 min at 1365 x g, and the final supernatant was filter-sterilized (0.22 μm), a process that removes coarse particles. Stock (100%) aliquots of ODE samples were kept frozen at −20°C until used in experiments. The filter-sterilized organic dust extract (ODE) samples were considered 100% and diluted to 1-5% (v/v) before using in the experiments. We routinely measure endotoxin concentration in our ODE samples using Pyrochrome® chromogenic endotoxin assay kit (Associates of Cape Cod, Inc., East Falmouth, MA). As per previously published study, the endotoxin concentrations found in our ODE samples were in the range of 0.8067±0.0008 to 1.433±0.02 EU/mL (Bhat et al. 2019).

Cell culture and treatments

Immortalized human monocytic cells (THP1, ATCC TIB-202™) were used in this study. The cells were characterized prior to use in experiments by confirming expression of CD14 using flow cytometry (data not shown). This cell line has previously been used by our group to study innate inflammatory responses to ODE (Nath Neerukonda et al. 2018). THP1 cells were cultured in RPMI 1640 at 37°C in a humidified chamber with 5% CO_2. The RPMI 1640 medium was supplemented with 10% (v/v) heat-inactivated FBS, 2 mM L-glutamine, 10 mM HEPES, 1.5 g/L sodium bicarbonate, 1 mM sodium pyruvate, 100 IU/ml penicillin, and 100 μg/mL streptomycin and 1 μg/mL of Amphotericin B. Cells were subcultured once a week, the morphology was observed and approximately 4 to 5-day old cultures in suspension were used for all the

experiments. Treatments were added to the cells in 1% FBS-containing medium for 24 hours and the treatment details (groups) are outlined in Figure 4.1.

The stock and working concentrations of the treatments are outlined in Table 4.1. Cells were treated with either medium (control) or ODE (1% v/v) followed by a co-treatment with either EP (2.5 μM) (Bhat et al. 2019) or MA (10 μM) (Massey et al. 2019) for 24 hours, with corresponding time matched controls. Following treatments, samples were processed at 24 hours for various assays. The concentration of DMSO used in our experiments was not toxic to cells (data now shown) and MA is well tolerated in higher doses (Anantharam et al. 2007; Cristóvão et al. 2009).

Table 4.1 Stock and working concentrations of treatments

Treatments	Stock concentration	Working concentration (in 1% FBS-containing medium)
ODE	100% in HBSS	1%
EP	5 mM in ringer's solution	2.5 μM
MA	1 mM in DMSO	10 μM

Cell viability and MTT assay

Live/dead cell numbers were enumerated by 4% trypan blue dye (EMD Millipore) exclusion and the percentage viability was calculated. Population of cells with more than 95% viability were used for the experiments. The MTT assay has been widely used in the estimation of LC_{50} and cell viability by measuring the formazan produced when mitochondrial dehydrogenase enzymes cleave the tetrazolium ring (Latchoumycandane et al. 2005). In this study, we used the MTT assay to determine the LC_{50} of ODE in THP1 cells. Cells were seeded (20,000 cells/well) in a 96-well culture plate and treated with ODE, EP, and MA for 24 hours in 1% FBS-containing RPMI medium. After treatment, the cells were washed twice with PBS and incubated with 0.5 mg/mL of MTT in 1% FBS-containing RPMI medium for 3 hours at 37°C. The supernatant was

removed, and MTT crystals were solubilized in 100 µl of DMSO. Absorbance was measured with the SpectraMax M2 Gemini Microplate Reader (Molecular Devices, San Jose, CA) at 570 nm with the reference wavelength at 630 nm.

Transmission Electron Microscopy (TEM)

Following the treatments (Figure 4.1 and Table 4.1), cells were washed twice with RPMI and fixed with 3% glutaraldehyde (w/v) and 1% paraformaldehyde (w/v) in 0.1 M cacodylate buffer, pH 7.4 for 48 hours at 4°C. Cells were pelleted and resuspended into 1% agarose. Small (1 mm) cubes containing cells were cut from the agarose and processed. Samples were rinsed three times in 0.1 M cacodylate buffer and then post-fixed in 1% osmium tetroxide in 0.1 M cacodylate buffer for 1 hour (room temperature). The samples were rinsed in deionized distilled water and *enbloc* stained with 2% aqueous uranyl acetate for 30 min., dehydrated in a graded ethanol series, cleared with ultra-pure acetone, infiltrated, and embedded using EmBed (EPON) formula epoxy resin (Electron Microscopy Sciences, Ft. Washington, PA). Resin blocks were polymerized for 48 hours at 65°C. Thick and ultrathin sections were prepared using a Leica UC6 ultramicrotome (North Central Instruments, Minneapolis, MN). Ultrathin sections were collected onto copper grids and images were captured using a JEOL 2100 scanning and transmission electron microscope (Japan Electron Optic Laboratories, Peabody, MA) with a Gatan OneView 4K camera (Gatan inc., Pleasanton, CA).

Morphological analysis

Mitochondrial shape descriptors and size measurements were obtained using ImageJ (National Institutes of Health) by manually tracing only clearly discernible outlines of mitochondria on TEM micrographs (Picard et al. 2013). Surface area (or mitochondrial size, in μm^2); perimeter (in µm), circularity [4*(surface area/perimeter^2)]; and Feret's diameter, which

represents the longest distance (μm) between any two points within a given mitochondrion, were measured. Computed values were imported into Microsoft Excel and analyzed.

Subcellular fractionation

Whole cell and subcellular (cytosol and mitochondria) protein lysate extractions were performed at 4°C using cold reagents. Subcellular fractionation of cell pellets for isolation of mitochondria was done using the Mitochondria Isolation Kit for Cultured Cells (ThermoFisher Scientific) according to the manufacturer's instructions. The whole cells, cytosolic fraction and isolated mitochondria were lysed with RIPA buffer [with protease and phosphatase inhibitors] for 30 min at 4°C and periodic sonication on ice, followed by centrifugation to collect lysate. Protein concentration of the fractions were determined by Bradford assay (Bio-Rad) and were stored at −80°C until use.

mtDNA isolation and long-range PCR

To determine mitochondrial DNA (mtDNA) leakage into cellular cytosol, mtDNA was isolated from mitochondria-free cytosolic fraction of the cells using the Genomic DNA Purification kit (ThermoFisher Scientific) as per the manufacturer's instructions. The purity and concentration of the isolated DNA was measured using NanoVue Plus Spectrophotometer (GE Healthcare). Due to low concentrations, the mtDNA was first amplified using long range PCR and the primers used were: mtDNA plasmid, sense: 5′-TGAGGCCAAATATCATTCTGAGGGGC-3' and antisense: 5′-TTTCATCATGCGGAGATGTTGGATGG-3' (Liu et al. 2015). PCR reactions were performed at 94°C for 1 min followed by 30 cycles at 98°C for 10 s, 60°C for 40 s, 68°C for 16 min and a final elongation for 10 min (Liu et al. 2015). Presence of mtDNA was confirmed by separating the PCR product by electrophoresis on a 0.8% agarose gel stained with ethidium bromide. The concentration of amplified mtDNA obtained was adjusted to ensure equal amounts of template mtDNA in each sample used for qPCR reaction.

Quantitative Real-Time PCR

Fold change in mtDNA quantity was measured by qPCR with primers specific to mitochondrial NADH dehydrogenase 1 *(mtND1).* 10 µL reaction mixtures with 500 ng of template DNA and 1 µM of forward and reverse primers in SYBR Green Mastermix (Thermo Fisher Scientific) was prepared. The primers for genes of interest were synthesized at Iowa State University's DNA Facility. The primers used were: *mtND1* gene, sense: 5'-GGCTATATACAACTACGCAAAGGC-3' and antisense: 5'-GGTAGATGTGGCGGGTTTTAGG-3'; *16s* (housekeeping gene), sense: 5'-CCGCAAGGGAAAGATGAAAGAC-3' and anti-sense: 5'-TCGTTTGGTTTCGGGGTTTC-3'. No-template and no-primer controls and dissociation curves were run for all reactions to exclude cross-contamination. The qRT-PCR reactions were run in a QuantiStudio 3 system (ThermoFisher) and the data was analyzed using $2^{-\Delta\Delta CT}$ method (Livak and Schmittgen 2001).

Western blot analysis

Lysates (whole cell, cytosol and MT) containing equal amounts of protein (20 µg/sample), along with a molecular weight marker (Bio-Rad), were run on 10–15% sodium dodecyl sulfate/polyacrylamide gel electrophoresis (SDS-PAGE) as previously described (Bhat et al. 2019). Proteins were transferred to a nitrocellulose membrane and nonspecific binding sites were blocked with Licor Odyssey blocking buffer. The membranes were then incubated with different primary antibodies, the details of which are listed in Table 4.2. Next, membranes were incubated with one of the following secondary antibodies: Alexa Fluor 680 goat anti-mouse, Alexa Fluor 680 donkey anti-rabbit (1:10,000; Invitrogen) or IRDye® 800CW donkey anti-rabbit (1:10,000; LI-COR) (Table 2). To confirm equal protein loading, blots were probed with a β-actin antibody (AbCam; 1:10,000 dilution). Western blot images were captured using Odyssey® CLx IR imaging

system (LI-COR Biotechnology) and analysis was performed using ImageJ (National Institutes of Health). The results were represented as a percentage expression relative to control.

Mitochondrial activity and MitoSOX assay

Cells were seeded (50,000 cells/well) in a 96-well culture plate and treated for 24 hours. After treatment, the media was removed and 100 µL of 200 nM MitoTracker green and 5 µM MitoSOX red dye diluted in 1% FBS-containing RPMI medium was added into each well and incubated at 37°C for 15 min. Next, the cells were washed with 1% FBS-containing RPMI medium and fluorescence intensity was measured by spectrophotometer reading taken at excitation/emission wavelengths of 485/520 nm and 510/580, respectively (SpectraMax M2 Gemini Microplate Reader, Molecular Devices, San Jose, CA). The results were represented as percentage mean fluorescence intensity (% MFI) relative to control.

Mitochondrial calcium influx measurement by Rhod-2AM staining

Mitochondrial calcium influx ($[Ca^{2+}]_{mito}$) in THP1 cells was measured using the rhod-2AM dye. The protein concentration of the isolated mitochondrial fraction was measured by bradford assay in order to maintain consistency in the number of mitochondria loaded into the wells of a 96-well plate. Equal amounts of protein (100 µg) were loaded into each well and10 µM Rhod-2AM (Abcam) dye diluted in 1% FBS-containing RPMI medium was added and incubated at 37°C for 30 minutes. The cells were washed with 1% FBS-containing RPMI medium and fluorescence was read at excitation/emission wavelengths of 552 nm/581 nm using a spectrophotometer reader (SpectraMax M2 Gemini Microplate Reader, Molecular Devices, San Jose, CA) and results represented as percentage calcium influx.

Griess assay

Griess assay was performed as described previously (Gordon et al. 2011). Nitric oxide secretion was measured (representing reactive nitrogen species (RNS)) in cell culture media using

Griess reagent (Sigma-Aldrich) along with sodium nitrite standard curve, prepared using a stock solution of 200 μM. The assay was performed in a 96 well-plate and absorbance was measured at 550 nm (SpectraMax M2 Gemini Microplate Reader, Molecular Devices, San Jose, CA). The results were represented as μM concentration of nitrite secreted.

Cytokine analysis

Levels of IL-1β, IL-6, TNF-α and IL-10 levels in THP1 cell culture supernatant were measured using commercially available ELISA kits (ThermoFisher Scientific, USA) as per the manufacturer's instructions. 96-well high binding plates (Nunc MaxiSorp, ThermoFisher Scientifc) were coated with the provided capture antibody (100 μL/well) and incubated at 4 °C overnight. All wells were blocked with the blocking buffer (200 μL/well) for an hour at room temperature followed by washing with PBS-T and then, incubated with recombinant standards and samples (cell culture supernatants) for 2 h at room temperature. Plates were then washed with PBST and incubated with the specific detection antibody (100 μL/well) for 1 h at room temperature. Following a wash, the plates were then incubated with 3,3′,5,5′-tetramethylbenzidine (TMB) solution (100 μL/well) for 15 min and the reaction (color development) was stopped by adding 50 μL/well of stop solution (2 N H_2SO_4). The absorbance was read at 450 nm (SpectraMax M2 Gemini Microplate Reader, Molecular Devices, San Jose, CA) and the results were represented as pg/mL concentration of cytokine secreted.

Statistical analysis

Data analysis and graphical representation was performed using GraphPad Prism 8.0 software (GraphPad Prism 8.0, La Jolla, CA, USA). Data was analyzed with one-way ANOVA with Tukey's multiple comparison test and a p-value of < 0.05 was considered to be statistically significant.

Acknowledgments

We would like to thank Tracey Stewart at Iowa State University's Roy J. Carver High Resolution Microscopy Facility for assistance with transmission electron microscopy.

Potential Conflicts of Interest

AGK has an equity interest in PK Biosciences Corporation located in Ames, IA. The terms of this arrangement have been reviewed and approved by Iowa State University per its conflict of interest policies. All other authors have declared no potential conflicts of interest.

Funding

C.C. laboratory is funded through startup grant through Iowa State University and a pilot grant (5 U54 OH007548) from CDC-NIOSH (Centers for Disease Control and Prevention-The National Institute for Occupational Safety and Health). A.G.K. laboratory is supported by National Institutes of Health grants (ES026892, ES027245 and NS100090).

References

Anantharam V, Kaul S, Song C, Kanthasamy A, Kanthasamy AG (2007) Pharmacological Inhibition of Neuronal NADPH Oxidase Protects against 1-Methyl-4-Phenylpyridinium (MPP+)-Induced Oxidative Stress and Apoptosis in Mesencephalic Dopaminergic Neuronal Cells. Neurotoxicology 28(5):988–997. https://doi.org/10.1016/j.neuro.2007.08.008

Bhat SM, Massey N, Karriker LA, Singh B, Charavaryamath C (2019) Ethyl pyruvate reduces organic dust-induced airway inflammation by targeting HMGB1-RAGE signaling. Respiratory Research 20(1):27. https://doi.org/10.1186/s12931-019-0992-3

Brand MD, Affourtit C, Esteves TC, Green K, Lambert AJ, Miwa S, Pakay JL, Parker N (2004) Mitochondrial superoxide: production, biological effects, and activation of uncoupling proteins. Free Radical Biology and Medicine 37(6):755–767. https://doi.org/10.1016/j.freeradbiomed.2004.05.034

Cai J, Yang J, Jones DeanP (1998) Mitochondrial control of apoptosis: the role of cytochrome c. Biochimica et Biophysica Acta (BBA) - Bioenergetics 1366(1):139–149. https://doi.org/10.1016/S0005-2728(98)00109-1

Cantaert T, Baeten D, Tak PP, van Baarsen LG (2010) Type I IFN and TNFα cross-regulation in immune-mediated inflammatory disease: basic concepts and clinical relevance. Arthritis Research & Therapy 12(5):219. https://doi.org/10.1186/ar3150

Charavaryamath C, Janardhan KS, Townsend HG, Willson P, Singh B (2005) Multiple exposures to swine barn air induce lung inflammation and airway hyper-responsiveness. Respiratory Research 6(1):50. https://doi.org/10.1186/1465-9921-6-50

Charavaryamath C, Juneau V, Suri SS, Janardhan KS, Townsend H, Singh B (2008) Role of Toll-like receptor 4 in lung inflammation following exposure to swine barn air. Exp Lung Res 34(1):19–35. https://doi.org/10.1080/01902140701807779

Charavaryamath C, Singh B (2006) Pulmonary effects of exposure to pig barn air. J Occup Med Toxicol 1:10. https://doi.org/10.1186/1745-6673-1-10

CHAUNG WW, WU R, JI Y, DONG W, WANG P (2012) Mitochondrial transcription factor A is a proinflammatory mediator in hemorrhagic shock. Int J Mol Med 30(1):199–203. https://doi.org/10.3892/ijmm.2012.959

Cloonan SM, Choi AM (2012) Mitochondria: commanders of innate immunity and disease? Current Opinion in Immunology 24(1):32–40. https://doi.org/10.1016/j.coi.2011.11.001

Cloonan SM, Choi AMK (2016) Mitochondria in lung disease. J Clin Invest 126(3):809–820. https://doi.org/10.1172/JCI81113

Cole D, Todd L, Wing S (2000) Concentrated swine feeding operations and public health: a review of occupational and community health effects. Environ Health Perspect 108(8):685–699

Cristóvão AC, Choi D-H, Baltazar G, Beal MF, Kim Y-S (2009) The Role of NADPH Oxidase 1–Derived Reactive Oxygen Species in Paraquat-Mediated Dopaminergic Cell Death. Antioxid Redox Signal 11(9):2105–2118. https://doi.org/10.1089/ars.2009.2459

Ding W-X, Yin X-M (2012) Mitophagy: mechanisms, pathophysiological roles, and analysis. Biol Chem 393(7):547–564. https://doi.org/10.1515/hsz-2012-0119

Eisner V, Picard M, Hajnóczky G (2018) Mitochondrial dynamics in adaptive and maladaptive cellular stress responses. Nature Cell Biology 20(7):755–765. https://doi.org/10.1038/s41556-018-0133-0

Fetterman JL, Sammy MJ, Ballinger SW (2017) Mitochondrial Toxicity of Tobacco Smoke and Air Pollution. Toxicology 391:18–33. https://doi.org/10.1016/j.tox.2017.08.002

Filadi R, Pendin D, Pizzo P (2018) Mitofusin 2: from functions to disease. Cell Death Dis 9(3):330. https://doi.org/10.1038/s41419-017-0023-6

Finkel T, Menazza S, Holmström KM, Parks RJ, Liu J, Sun J, Liu J, Pan X, Murphy E (2015) The Ins and Outs of Mitochondrial Calcium. Circ Res 116(11):1810–1819. https://doi.org/10.1161/CIRCRESAHA.116.305484

Fukui M, Zhu BT (2010) Mitochondrial Superoxide Dismutase SOD2, but not Cytosolic SOD1, Plays a Critical Role in Protection against Glutamate-Induced Oxidative Stress and Cell Death in HT22 Neuronal Cells. Free Radic Biol Med 48(6):821–830. https://doi.org/10.1016/j.freeradbiomed.2009.12.024

Garrido C, Galluzzi L, Brunet M, Puig PE, Didelot C, Kroemer G (2006) Mechanisms of cytochrome c release from mitochondria. Cell Death & Differentiation 13(9):1423–1433. https://doi.org/10.1038/sj.cdd.4401950

Ghosh A, Langley MR, Harischandra DS, Neal ML, Jin H, Anantharam V, Joseph J, Brenza T, Narasimhan B, Kanthasamy A, Kalyanaraman B, Kanthasamy AG (2016) Mitoapocynin Treatment Protects Against Neuroinflammation and Dopaminergic Neurodegeneration in a Preclinical Animal Model of Parkinson's Disease. J Neuroimmune Pharmacol 11(2):259–278. https://doi.org/10.1007/s11481-016-9650-4

Gong Z, Pan J, Shen Q, Li M, Peng Y (2018) Mitochondrial dysfunction induces NLRP3 inflammasome activation during cerebral ischemia/reperfusion injury. Journal of Neuroinflammation 15(1):242. https://doi.org/10.1186/s12974-018-1282-6

Gordon R, Hogan CE, Neal ML, Anantharam V, Kanthasamy AG, Kanthasamy A (2011) A simple magnetic separation method for high-yield isolation of pure primary microglia. J Neurosci Methods 194(2):287–296. https://doi.org/10.1016/j.jneumeth.2010.11.001

Huang H, Shah K, Bradbury NA, Li C, White C (2014) Mcl-1 promotes lung cancer cell migration by directly interacting with VDAC to increase mitochondrial Ca 2+ uptake and reactive oxygen species generation. Cell Death & Disease 5(10):e1482–e1482. https://doi.org/10.1038/cddis.2014.419

Hunter DR, Haworth RA, Southard JH (1976) Relationship between configuration, function, and permeability in calcium-treated mitochondria. J Biol Chem 251(16):5069–5077

Hüttemann M, Lee I, Gao X, Pecina P, Pecinova A, Liu J, Aras S, Sommer N, Sanderson TH, Tost M, Neff F, Aguilar-Pimentel JA, Becker L, Naton B, Rathkolb B, Rozman J, Favor J, Hans W, Prehn C, Puk O, Schrewe A, Sun M, Höfler H, Adamski J, Bekeredjian R, Graw J, Adler T, Busch DH, Klingenspor M, Klopstock T, Ollert M, Wolf E, Fuchs H, Gailus-Durner V, Angelis MH de, Weissmann N, Doan JW, Bassett DJP, Grossman LI (2012) Cytochrome c oxidase subunit 4 isoform 2-knockout mice show reduced enzyme activity, airway hyporeactivity, and lung pathology. The FASEB Journal 26(9):3916–3930. https://doi.org/10.1096/fj.11-203273

Hyun H-W, Ko A-R, Kang T-C (2016) Mitochondrial Translocation of High Mobility Group Box 1 Facilitates LIM Kinase 2-Mediated Programmed Necrotic Neuronal Death. Front Cell Neurosci 10. https://doi.org/10.3389/fncel.2016.00099

Ishihara Y, Takemoto T, Itoh K, Ishida A, Yamazaki T (2015) Dual Role of Superoxide Dismutase 2 Induced in Activated Microglia OXIDATIVE STRESS TOLERANCE AND CONVERGENCE OF INFLAMMATORY RESPONSES. J Biol Chem 290(37):22805–22817. https://doi.org/10.1074/jbc.M115.659151

Julian MW, Shao G, Bao S, Knoell DL, Papenfuss TL, VanGundy ZC, Crouser ED (2012) Mitochondrial Transcription Factor A Serves as a Danger Signal by Augmenting Plasmacytoid Dendritic Cell Responses to DNA. The Journal of Immunology 189(1):433–443. https://doi.org/10.4049/jimmunol.1101375

Julian MW, Shao G, Vangundy ZC, Papenfuss TL, Crouser ED (2013) Mitochondrial transcription factor A, an endogenous danger signal, promotes TNFα release via RAGE- and TLR9-responsive plasmacytoid dendritic cells. PLoS ONE 8(8):e72354. https://doi.org/10.1371/journal.pone.0072354

Kelly B, O'Neill LA (2015) Metabolic reprogramming in macrophages and dendritic cells in innate immunity. Cell Research 25(7):771–784. https://doi.org/10.1038/cr.2015.68

Kim HS, Cho IH, Kim JE, Shin YJ, Jeon J-H, Kim Y, Yang YM, Lee K-H, Lee JW, Lee W-J, Ye S-K, Chung M-H (2008) Ethyl pyruvate has an anti-inflammatory effect by inhibiting ROS-dependent STAT signaling in activated microglia. Free Radic Biol Med 45(7):950–963. https://doi.org/10.1016/j.freeradbiomed.2008.06.009

Kim J-Y, Cho J-J, Ha J, Park J-H (2002) The Carboxy Terminal C-Tail of BNip3 Is Crucial in Induction of Mitochondrial Permeability Transition in Isolated Mitochondria. Archives of Biochemistry and Biophysics 398(2):147–152. https://doi.org/10.1006/abbi.2001.2673

Krysko DV, Denecker G, Festjens N, Gabriels S, Parthoens E, D'Herde K, Vandenabeele P (2006) Macrophages use different internalization mechanisms to clear apoptotic and necrotic cells. Cell Death & Differentiation 13(12):2011–2022. https://doi.org/10.1038/sj.cdd.4401900

Landes T, Emorine LJ, Courilleau D, Rojo M, Belenguer P, Arnauné-Pelloquin L (2010) The BH3-only Bnip3 binds to the dynamin Opa1 to promote mitochondrial fragmentation and apoptosis by distinct mechanisms. EMBO reports 11(6):459–465. https://doi.org/10.1038/embor.2010.50

Langley M, Ghosh A, Charli A, Sarkar S, Ay M, Luo J, Zielonka J, Brenza T, Bennett B, Jin H, Ghaisas S, Schlichtmann B, Kim D, Anantharam V, Kanthasamy A, Narasimhan B, Kalyanaraman B, Kanthasamy AG (2017) Mito-Apocynin Prevents Mitochondrial Dysfunction, Microglial Activation, Oxidative Damage, and Progressive Neurodegeneration in MitoPark Transgenic Mice. Antioxidants & Redox Signaling 27(14):1048–1066. https://doi.org/10.1089/ars.2016.6905

Latchoumycandane C, Anantharam V, Kitazawa M, Yang Y, Kanthasamy A, Kanthasamy AG (2005) Protein kinase Cdelta is a key downstream mediator of manganese-induced apoptosis in dopaminergic neuronal cells. J Pharmacol Exp Ther 313(1):46–55. https://doi.org/10.1124/jpet.104.078469

Liu J, Fang H, Chi Z, Wu Z, Wei D, Mo D, Niu K, Balajee AS, Hei TK, Nie L, Zhao Y (2015) XPD localizes in mitochondria and protects the mitochondrial genome from oxidative DNA damage. Nucleic Acids Res 43(11):5476–5488. https://doi.org/10.1093/nar/gkv472

Livak KJ, Schmittgen TD (2001) Analysis of Relative Gene Expression Data Using Real-Time Quantitative PCR and the 2−ΔΔCT Method. Methods 25(4):402–408. https://doi.org/10.1006/meth.2001.1262

Massey N, Puttachary S, Bhat SM, Kanthasamy AG, Charavaryamath C (2019) HMGB1-RAGE Signaling Plays a Role in Organic Dust-Induced Microglial Activation and Neuroinflammation. Toxicol Sci 169(2):579–592. https://doi.org/10.1093/toxsci/kfz071

May S, Romberger DJ, Poole JA (2012) Respiratory Health Effects of Large Animal Farming Environments. J Toxicol Environ Health B Crit Rev 15(8):524–541. https://doi.org/10.1080/10937404.2012.744288

Mishra P, Chan DC (2014) Mitochondrial dynamics and inheritance during cell division, development and disease. Nature Reviews Molecular Cell Biology 15(10):634–646. https://doi.org/10.1038/nrm3877

Murakami T, Ockinger J, Yu J, Byles V, McColl A, Hofer AM, Horng T (2012) Critical role for calcium mobilization in activation of the NLRP3 inflammasome. Proc Natl Acad Sci USA 109(28):11282–11287. https://doi.org/10.1073/pnas.1117765109

Nakahira K, Haspel JA, Rathinam VAK, Lee S-J, Dolinay T, Lam HC, Englert JA, Rabinovitch M, Cernadas M, Kim HP, Fitzgerald KA, Ryter SW, Choi AMK (2011) Autophagy proteins regulate innate immune responses by inhibiting the release of mitochondrial DNA mediated by the NALP3 inflammasome. Nature Immunology 12(3):222–230. https://doi.org/10.1038/ni.1980

Narendra D, Tanaka A, Suen D-F, Youle RJ (2008) Parkin is recruited selectively to impaired mitochondria and promotes their autophagy. J Cell Biol 183(5):795–803. https://doi.org/10.1083/jcb.200809125

Narendra DP, Jin SM, Tanaka A, Suen D-F, Gautier CA, Shen J, Cookson MR, Youle RJ (2010) PINK1 Is Selectively Stabilized on Impaired Mitochondria to Activate Parkin. PLOS Biology 8(1):e1000298. https://doi.org/10.1371/journal.pbio.1000298

Nath Neerukonda S, Mahadev-Bhat S, Aylward B, Johnson C, Charavaryamath C, Arsenault RJ (2018) Kinome analyses of inflammatory responses to swine barn dust extract in human bronchial epithelial and monocyte cell lines. Innate Immun 24(6):366–381. https://doi.org/10.1177/1753425918792070

Ney PA (2015) Mitochondrial autophagy: Origins, significance, and role of BNIP3 and NIX. Biochimica et Biophysica Acta (BBA) - Molecular Cell Research 1853(10, Part B):2775–2783. https://doi.org/10.1016/j.bbamcr.2015.02.022

Nordgren TM, Charavaryamath C (2018) Agriculture Occupational Exposures and Factors Affecting Health Effects. Curr Allergy Asthma Rep 18(12):65. https://doi.org/10.1007/s11882-018-0820-8

Parisi MA, Clayton DA (1991) Similarity of human mitochondrial transcription factor 1 to high mobility group proteins. Science 252(5008):965–969. https://doi.org/10.1126/science.2035027

Picard M, White K, Turnbull DM (2013) Mitochondrial morphology, topology, and membrane interactions in skeletal muscle: a quantitative three-dimensional electron microscopy study. J Appl Physiol (1985) 114(2):161–171. https://doi.org/10.1152/japplphysiol.01096.2012

Poole JA, Burrell AM, Wyatt TA, Kielian TL, Romberger DJ (2010) NOD2 Negatively Regulates Organic Dust-Induced Inflammation in Monocytes/Macrophages. Journal of Allergy and Clinical Immunology 125(2, Supplement 1):AB118. https://doi.org/10.1016/j.jaci.2009.12.467

Poole JA, Wyatt TA, Kielian T, Oldenburg P, Gleason AM, Bauer A, Golden G, West WW, Sisson JH, Romberger DJ (2011) Toll-like receptor 2 regulates organic dust-induced airway inflammation. Am J Respir Cell Mol Biol 45(4):711–719. https://doi.org/10.1165/rcmb.2010-0427OC

Prakash YS, Pabelick CM, Sieck GC (2017) Mitochondrial Dysfunction in Airway Disease. CHEST 152(3):618–626. https://doi.org/10.1016/j.chest.2017.03.020

Qi L, Sun X, Li F-E, Zhu B-S, Braun FK, Liu Z-Q, Tang J-L, Wu C, Xu F, Wang H-H, Velasquez LA, Zhao K, Lei F-R, Zhang J-G, Shen Y-T, Zou J-X, Meng H-M, An G-L, Yang L, Zhang X-D (2015) HMGB1 Promotes Mitochondrial Dysfunction–Triggered Striatal Neurodegeneration via Autophagy and Apoptosis Activation. PLoS One 10(11). https://doi.org/10.1371/journal.pone.0142901

Redondo-Horcajo M, Romero N, Martínez-Acedo P, Martínez-Ruiz A, Quijano C, Lourenço CF, Movilla N, Enríquez JA, Rodríguez-Pascual F, Rial E, Radi R, Vázquez J, Lamas S (2010) Cyclosporine A-induced nitration of tyrosine 34 MnSOD in endothelial cells: role of mitochondrial superoxide. Cardiovasc Res 87(2):356–365. https://doi.org/10.1093/cvr/cvq028

Romberger DJ, Bodlak V, Von Essen SG, Mathisen T, Wyatt TA (2002) Hog barn dust extract stimulates IL-8 and IL-6 release in human bronchial epithelial cells via PKC activation. Journal of Applied Physiology 93(1):289–296. https://doi.org/10.1152/japplphysiol.00815.2001

Sahlander K, Larsson K, Palmberg L (2012) Daily exposure to dust alters innate immunity. PLoS ONE 7(2):e31646. https://doi.org/10.1371/journal.pone.0031646

Sethi RS, Schneberger D, Charavaryamath C, Singh B (2017) Pulmonary innate inflammatory responses to agricultural occupational contaminants. Cell Tissue Res 367(3):627–642. https://doi.org/10.1007/s00441-017-2573-4

Shin J-H, Kim I-D, Kim S-W, Lee H-K, Jin Y, Park J-H, Kim T-K, Suh C-K, Kwak J, Lee K-H, Han P-L, Lee J-K (2014) Ethyl Pyruvate Inhibits HMGB1 Phosphorylation and Release by Chelating Calcium. Mol Med 20(1):649–657. https://doi.org/10.2119/molmed.2014.00039

Stefanska J, Pawliczak R (2008) Apocynin: Molecular Aptitudes. Mediators of Inflammation 2008:1–10. https://doi.org/10.1155/2008/106507

Stumbo AC, Cortez E, Rodrigues CA, Henriques M das GMO, Porto LC, Barbosa HS, Carvalho L (2008) Mitochondrial localization of non-histone protein HMGB1 during human endothelial cell–Toxoplasma gondii infection. Cell Biology International 32(2):235–238. https://doi.org/10.1016/j.cellbi.2007.08.031

Su Y, Zhu L, Yu X, Cai L, Lu Y, Zhang J, Li T, Li J, Xia J, Xu F, Hu Q (2016) Mitochondrial Transplantation Attenuates Airway Hyperresponsiveness by Inhibition of Cholinergic Hyperactivity. Theranostics 6(8):1244–1260. https://doi.org/10.7150/thno.13804

Tang D, Kang R, Livesey KM, Kroemer G, Billiar TR, Van Houten B, Zeh HJ, Lotze MT (2011) High-Mobility Group Box 1 Is Essential for Mitochondrial Quality Control. Cell Metabolism 13(6):701–711. https://doi.org/10.1016/j.cmet.2011.04.008

Tilokani L, Nagashima S, Paupe V, Prudent J (2018) Mitochondrial dynamics: overview of molecular mechanisms. Essays Biochem 62(3):341–360. https://doi.org/10.1042/EBC20170104

Ugrinova I, Pasheva E (2017) HMGB1 Protein: A Therapeutic Target Inside and Outside the Cell. Adv Protein Chem Struct Biol 107:37–76. https://doi.org/10.1016/bs.apcsb.2016.10.001

Venkataraman R, Kellum JA, Song M, Fink MP (2002) Resuscitation with Ringer's ethyl pyruvate solution prolongs survival and modulates plasma cytokine and nitrite/nitrate concentrations in a rat model of lipopolysaccharide-induced shock. Shock 18(6):507–512. https://doi.org/10.1097/00024382-200212000-00004

Vested A, Basinas I, Burdorf A, Elholm G, Heederik DJJ, Jacobsen GH, Kolstad HA, Kromhout H, Omland Ø, Sigsgaard T, Thulstrup AM, Toft G, Vestergaard JM, Wouters IM, Schlünssen V (2019) A nationwide follow-up study of occupational organic dust exposure and risk of chronic obstructive pulmonary disease (COPD). Occup Environ Med 76(2):105–113. https://doi.org/10.1136/oemed-2018-105323

Wai T, Langer T (2016) Mitochondrial Dynamics and Metabolic Regulation. Trends in Endocrinology & Metabolism 27(2):105–117. https://doi.org/10.1016/j.tem.2015.12.001

Westrate LM, Drocco JA, Martin KR, Hlavacek WS, MacKeigan JP (2014) Mitochondrial Morphological Features Are Associated with Fission and Fusion Events. PLOS ONE 9(4):e95265. https://doi.org/10.1371/journal.pone.0095265

Wunschel J, Poole JA (2016) Occupational agriculture organic dust exposure and its relationship to asthma and airway inflammation in adults. J Asthma 53(5):471–477. https://doi.org/10.3109/02770903.2015.1116089

Yu J, Nagasu H, Murakami T, Hoang H, Broderick L, Hoffman HM, Horng T (2014) Inflammasome activation leads to Caspase-1–dependent mitochondrial damage and block of mitophagy. Proc Natl Acad Sci U S A 111(43):15514–15519. https://doi.org/10.1073/pnas.1414859111

Yu Y-M, Kim J-B, Lee K-W, Kim SY, Han P-L, Lee J-K (2005) Inhibition of the cerebral ischemic injury by ethyl pyruvate with a wide therapeutic window. Stroke 36(10):2238–2243. https://doi.org/10.1161/01.STR.0000181779.83472.35

Zhang Q, Raoof M, Chen Y, Sumi Y, Sursal T, Junger W, Brohi K, Itagaki K, Hauser CJ (2010) Circulating mitochondrial DAMPs cause inflammatory responses to injury. Nature 464(7285):104–107. https://doi.org/10.1038/nature08780

Zorov DB, Juhaszova M, Sollott SJ (2014) Mitochondrial Reactive Oxygen Species (ROS) and ROS-Induced ROS Release. Physiol Rev 94(3):909–950. https://doi.org/10.1152/physrev.00026.2013

Appendix A. Supplementary figure

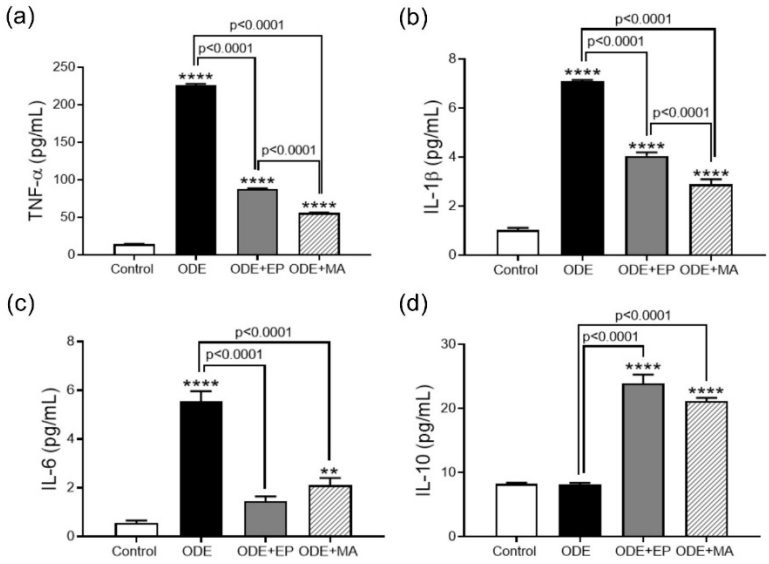

Figure 4.10 ODE increases production of proinflammatory cytokines
Cytokine levels in the supernatant of THP1 cells treated with either medium or ODE (1%) followed by either medium or EP (2.5 μM) or MA (10 μM) for 24 hours was measured. Concentration of secreted pro-inflammatory cytokines TNF-α (a), IL-1β (b), and IL-6 (c) were measured. Concentration of secreted anti-inflammatory cytokines IL-10 (d) was measured. For all assays, samples were derived from the same experiment and were processed in parallel. Data was analyzed using one-way ANOVA with Tukey's multiple comparison test (*p < 0.05, **p < 0.01, ***p < 0.001, ****p < 0.0001) and represented as mean ± SEM with n = 6/treatment (* indicates significant difference from control).

Appendix B. Supplementary tables

Table 4.2 Characteristics of primary antibodies

Epitope	Species/Clone	Dilution	Catalog #	Supplier
β-Actin	Mouse Monoclonal	1:10,000	ab6276	AbCam[a]
HMGB1	Rabbit Polyclonal	1:5000	ab79823	AbCam[a]
MFN1	Mouse Monoclonal	1:1000	sc-166644	Santa Cruz[b]
MFN2	Mouse Monoclonal	1:1000	sc-100560	Santa Cruz[b]
OPA1	Mouse Monoclonal	1:1000	sc-393296	Santa Cruz[b]
DRP1	Mouse Monoclonal	1:1000	sc-271583	Santa Cruz[b]
Parkin	Mouse Monoclonal	1:1000	sc-32282	Santa Cruz[b]
PINK1	Mouse Monoclonal	1:1000	sc-517353	Santa Cruz[b]
BNIP3	Mouse Monoclonal	1:1000	sc-56167	Santa Cruz[b]
Cytochrome C	Mouse Monoclonal	1:1000	sc-13156	Santa Cruz[b]
COX4I2	Mouse Monoclonal	1:1000	sc-100522	Santa Cruz[b]
SOD2	Mouse Monoclonal	1:1000	sc-133134	Santa Cruz[b]
MtTFA	Mouse Monoclonal	1:1000	sc-376672	Santa Cruz[b]
Caspase 1	Mouse Monoclonal	1:1000	sc-56036	Santa Cruz[b]
Caspase 3	Mouse Monoclonal	1:1000	sc-271028	Santa Cruz[b]
Bcl-2	Mouse Monoclonal	1:1000	sc-7328	Santa Cruz[b]
Bcl-XL	Mouse Monoclonal	1:1000	sc-8392	Santa Cruz[b]

[a]Cambridge, United Kingdom

[b]Dallas, Texas, USA

Table 4.3 Characteristics of secondary antibodies

Expression system	Conjugate	Species/Clone	Dilution	Catalog #	Supplier
Donkey/IgG	Alexa Fluor® 680	Rabbit Polyclonal	1:10,000	A10043	Invitrogen[c]
Rabbit/IgG	Alexa Fluor® 680	Mouse Polyclonal	1:10,000	A27031	Invitrogen[c]
Donkey/IgG	IRDye® 800CW	Rabbit Polyclonal	1:10,000	926-32213	LI-COR[d]

[c]Thermofisher Scientific, USA

[d]Nebraska, USA

CHAPTER 5. TRANSCRIPTOMIC AND ULTRASTRUCTURAL EVIDENCE INDICATE THAT ANTI-HMGB1 ANTIBODIES RESCUE ORGANIC DUST INDUCED MITOCHONDRIAL DYSFUNCTION

Sanjana Mahadev Bhat [1,2], Nyzil Massey [1], Locke A. Karriker [3], Tomislav Jelesijević [4], Chong Wang [3], Chandrashekhar Charavaryamath [1*]

[1] Department of Biomedical Sciences, Iowa State University, Ames, IA, USA. [2] Immunobiology Interdepartmental Graduate Program, Iowa State University, Ames, IA, USA. [3] Department of Veterinary Diagnostic and Production Animal Medicine, Iowa State University, Ames, IA, USA. [4] Department of Veterinary Pathology, Iowa State University, Ames, IA, USA.

[*]To whom correspondence should be addressed: Chandrashekhar Charavaryamath, BVSc, MVSc, PhD., Assistant Professor, Department of Biomedical Sciences, Iowa State University, Ames, IA 50011. Telephone: (515) 294-7710; Fax: (515) 294-2315; Email: chandru@iastate.edu

Key words: Organic dust, HMGB1, airway inflammation, Mitochondrial dysfunction, Mitochondrial DNA

Modified from a manuscript in preparation.

Author contributions

S.M. Bhat participated in the design of experiments, performed the experiments, analyzed the data, and wrote the manuscript. N. Massey performed organic dust extraction. L. Karriker collected the organic dust samples and edited the manuscript. T. Jelesijević provided the technical expertise required to perform fluorescent microscopy and participated in editing the manuscript. C. Charavaryamath conceptualized the study, participated in the design of the experiments, performed dust extraction, participated in the interpretation of data, and edited the manuscript. All authors have read and approved the final manuscript.

Abbreviations

OD: Organic Dust; ODE: Organic Dust Extract; NHBE: Normal Human Bronchial Epithelial ; BEGM: Bronchial Epithelial Growth Medium; ALI: Air Liquid Interface; HMGB1: High Mobility Group Box 1; RAGE: Receptor for advanced glycation end products; TLR: Toll-like receptor; NOD2: Nucleotide-binding Oligomerization Domain-containing 2; ATP: Adenosine

Triphosphate; OXPHOS: Oxidative Phosphorylation; ETC: Electron Transport Chain; TCA: Tricarboylic Acid; MIP1: Macrophage Inflammatory Protein 1 ; OMM: Outer Mitochondrial Membrane; IMM: Inner Mitochondrial Membrane; MPT: Mitochondrial Permeability Transition; cGAS: cyclic GMP-AMP synthase; STING: Stimulator of Interferon Genes ; MFN: Mitofusin; OPA1: Optic Atrophy 1; DRP1: Dynamin-related protein 1; PINK1: PTEN- induced kinase 1; BNIP3: Bcl-2 Homology 3 (BH3)-only; TFAM: mitochondrial Transcription Factor A; COX: Cytochrome C Oxidase; IRF3: Interferon Regulatory Factor 3; IFI16: Interferon gamma Inducible Protein 16; PGC1α: Peroxisome proliferator-activated receptor Gamma Coactivator 1-alpha; NRF2: Nuclear factor erythroid 2-related factor 2; HIF1α: Hypoxia-inducible factor 1-alpha; VHL: Von Hippel–Lindau tumor suppressor; GSTP1: Glutathione S-transferase P; HMOX1: Heme Oxygenase 1; NQO1: NAD(P)H Quinone Dehydrogenase 1; UQCR: Ubiquinol-Cytochrome C Reductase; NADUF: NADH:ubiquinone oxidoreductase; ENO1: enolase 1; SLC2A6: Solute Carrier Family 2 Member 6; FOXJ1: Forkhead box protein J1; CFAP157: Cilia And Flagella Associated Protein 157; TEM: Transmission Electron Microscopy; DMSO: Dimethyl Sulfoxide; mtND1: mitochondrial NADH dehydrogenase 1

Abstract

Exposure to organic dust (OD) in agriculture is known to cause a variety of respiratory symptoms including loss of lung function. OD exposure has been shown to activate multiple signaling pathways since it contains a variety of microbial products and particulate matter. Previously, we have shown how OD exposure leads to the secretion of HMGB1 and HMGB1-RAGE signaling, and how this can be a possible therapeutic target to reduce inflammation. Cellular mitochondria are indispensable for homeostasis and are emerging targets to curtail inflammation. Recently, we have also observed that OD exposure induces mitochondrial dysfunction characterized by loss of structural integrity and deficits in bioenergetics. However, the role of

HMGB1 in OD-induced mitochondrial dysfunction in human bronchial epithelial (NHBE) cells remains elusive. Therefore, we aimed to study whether decreased levels of intracellular HMGB1 or antibody-mediated neutralization of secreted HMGB1 would rescue mitochondrial dysfunction. Single and repeated ODE exposure showed an elongated mitochondrial network and cristolysis whereas HMGB1 neutralization or the lack thereof promotes mitochondrial biogenesis evidenced by increased mitochondrial fragmentation, increased Drp1 expression, decreased Mfn2 expression, and increased PGC1α expression. Repeated 5-day ODE exposure significantly downregulated transcripts encoding mitochondrial respiration and metabolism (ATP synthase, NADUF, and UQCR) as well as glucose uptake. This was reversed by the antibody-mediated neutralization of HMGB1. The results of this study thus support our hypothesis that in NHBE cells neutralization of ODE-induced HMGB1 secretion rescues OD-induced mitochondrial dysfunction.

Introduction

An increase in human population has led to an increased demand for protein through meat. Hence, animal production has transformed into a large-scale concentrated animal feeding operation (CAFOs). These CAFOs generate many on-site contaminants that pose a threat to workers, animals, and the environment. Agriculture workers who are exposed to the airborne contaminants are at an increased risk of developing respiratory disorders and other diseases. The on-site contaminants mainly include airborne organic dust (OD), gases, and other microbial components.

The OD is a complex mixture of various microbial associated molecular patterns (MAMPs) including endotoxin, peptidoglycans, Gram-positive bacterial components, (1→3)-β-D-glucans, and fungi which are all important pro-inflammatory mediators (Poole and Romberger 2012; Nordgren and Charavaryamath 2018; Poole et al. 2019; Kelly and Poole 2019). Recurrent inhalation of this complex OD has been implicated in respiratory disease development and

severity. Exposed workers report a variety of respiratory symptoms and suffer from asthma, chronic bronchitis, and chronic obstructive pulmonary disease (COPD) (Charavaryamath and Singh 2006; May et al. 2012; Poole and Romberger 2012; Wunschel and Poole 2016; Warren et al. 2019). Due to the complex nature of the ODs, several research studies have targeted pattern recognition receptors (PRRs) and the respective downstream regulators as a strategy to reduce the severity of OD-induced airway diseases. Several groups have targeted various PRRs and signaling molecules including TLR2, TLR4, NOD2, protein kinase C, and MyD88 (Poole et al. 2007; Bailey et al. 2008; Poole et al. 2010; Poole et al. 2011; An et al. 2020). Our recent work has examined various kinome (set of protein kinases) signaling pathways in human airway epithelial and monocytic cell lines, where we have shown that OD exposure induces several overlapping innate inflammatory signaling pathways indicating a complex host response (Nath Neerukonda et al. 2018).

Airway epithelial cells and alveolar macrophages are central to the first line of defense against the danger signals in the lungs (Whitsett and Alenghat 2015). Exposure of lung epithelial cells to OD has been shown to trigger oxidative stress, cytokine release, cellular dysfunction, and eventually cell death which are key processes involved in the pathogenesis of airway inflammation (Charavaryamath and Singh 2006; Poole and Romberger 2012; Sethi et al. 2017; Bhat et al. 2019). Mitochondria are indispensable organelles and are referred to as the powerhouse of the cells. Emerging data have identified a pivotal role of mitochondria in several inflammatory airway diseases (Prakash et al. 2017). Therefore, mitochondria represent an attractive therapeutic target in rescuing airway epithelial cells from the negative effects of chronic exposure to OD.

Alterations in mitochondrial morphology and function have been reported in airway epithelial cells in cases of COPD and asthma (Schumacker et al. 2014; Cloonan and Choi 2016;

Piantadosi and Suliman 2017; Prakash et al. 2017; Fetterman et al. 2017; Aghapour et al. 2019). This includes a decrease in oxidative phosphorylation (OXPHOS) and Krebs cycle enzymes, blunted mitochondrial respiration, and suppressed respiratory reserve, resulting in enhanced reactive oxygen species generation (ROS), which can, in turn, modulate mitochondrial morphology and function creating a vicious cycle of inflammation and exacerbate airway disease. In addition to mitochondrial dysfunction, mitochondrial damage and release of mitochondrial components either into the cytosol or extracellularly has been an emerging factor in the induction of inflammation (Cloonan and Choi 2012; Cloonan and Choi 2016; Eisner et al. 2018; Aghapour et al. 2019; Cloonan et al. 2020). Mitochondrial damage-associated molecular patterns (mtDAMPs) act as signaling molecules and activate PRRs such as TLRs and induce a myriad of inflammatory cascades (Rubartelli and Lotze 2007; Zhang et al. 2010; Cloonan and Choi 2012). In our recent study, we showed increased mitochondrial fusion and mitophagy, along with the leakage of mtDAMPs such as mitochondrial DNA (mtDNA) and mitochondrial transcription factor A (TFAM) upon exposure of THP1 cells to OD extract (ODE) (Mahadev Bhat et al., 2021). Recent studies have shown that the release of TFAM along with mtDNA amplifies TNFα and type 1 interferon release, thus promoting sterile inflammation via the cGAS-STING pathway (Cantaert et al. 2010; CHAUNG et al. 2012; Julian et al. 2013). Collectively, all these findings suggest that an understanding of the mechanism by which mitochondria promote inflammation can help in developing effective mitochondria-targeted therapies to curtail OD exposure-induced airway inflammation. To develop such therapies, an understanding of the interactions between the host airway epithelial cells and its mitochondria during OD-induced inflammation is key.

High mobility group box 1 (HMGB1) is known to be a key player in the induction of sterile inflammation. HMGB1 is an endogenous nucleoprotein that is evolutionarily conserved and

ubiquitously present and maintains nuclear homeostasis. This protein is secreted into the extracellular environment and acts as a prototypic DAMP and is important for oxidative stress response (Yang et al. 2015; Ugrinova and Pasheva 2017b). Extracellular HMGB1 is a delayed mediator of inflammation when compared to other pro-inflammatory mediators and is shown to stimulate the release of multiple pro-inflammatory cytokines including tumor necrosis factor (TNF), interleukin (IL)-1, IL-6, IL-8, and macrophage inflammatory protein (MIP)-1 (Yang et al. 2015; Bhat et al. 2019; Massey et al. 2019). The use of neutralizing monoclonal anti-HMGB1 antibodies *in vivo* has been shown to ameliorate tissue injury and reduce lethality (Zhou et al. 2009; Bhat et al. 2019). Recent studies have confirmed that siRNA-specific knockdown of HMGB1 in macrophages and dendritic cells suppressed HMGB1 release and reduced the cytokine storm (Qin et al. 2006; Ye et al. 2012). We have previously shown the pro-inflammatory effects of extracellularly secreted HMGB1 on bronchial epithelial cells on OD exposure and how its neutralization abrogates OD-induced inflammation (Nath Neerukonda et al. 2018; Bhat et al. 2019; Massey et al. 2019). Recent studies have directly correlated the alterations in mitochondrial function to the loss of HMGB1, wherein they showed a significant decrease in basal OXPHOS and glycolysis along with decreased ATP output (Qi et al. 2015). Also, a lack of HMGB1 has been shown to promote mitochondrial fragmentation and loss of mitochondrial membrane potential (Tang et al. 2011). Therefore, pertinent questions are raised as to what impact HMGB1 would have on mitochondrial morphology and function in bronchial epithelial cells on exposure to ODE.

This study examined the impact of HMGB1 on mitochondrial biogenesis and function on ODE exposure by using primary normal human bronchial epithelial (NHBE) cells. We investigated this hypothesis by using a single (acute) and repeated (chronic) OD exposure model with siRNA-mediated knockdown of HMGB1 and by neutralization of secreted HMGB1, respectively. Here

we demonstrated that ODE promotes the release of mtDAMPs and activation of cGAS-STING mediated signaling while knockdown of HMGB1 promotes mitochondrial biogenesis on single exposure to ODE. In the repeated exposure model, neutralization of extracellular HMGB1 is protective and maintains mitochondrial morphology, as well as upregulate pathways involved in mitochondrial respiration and biogenesis. Using an air-liquid interface (ALI) model, we show that neutralization of extracellular HMGB1 rescues ODE exposure-induced damages to epithelial integrity via its effect on tight junction proteins.

Results

Endotoxin levels in ODE samples

Endotoxin content of the diluted ODE samples (1:10) is listed in Table 5.1. From the seven samples, we found that endotoxin values ranged from 0.8067 ± 0.0008 to 1.433 ± 0.02 EU/mL (Table 5.3). Sample # 7 (endotoxin level 1.263 ± 0.7 EU/mL) was used for all experiments listed in this study.

Table 5.1 Endotoxin concentrations in ODE

Sample No.	Endotoxin (EU/mL)
1	1.140 ± 0.001
2	0.990 ± 0.0005
3	1.337 ± 0.0006
4	1.433 ± 0.02
5	1.417 ± 0.002
6	0.8067 ± 0.0008
7	1.263 ± 0.7

Suppression of HMGB1 expression in ODE exposed NHBE cells promotes mitochondrial fission

To assess the impact of HMGB1 on mitochondria, primary normal human bronchial epithelial (NHBE) cells were transfected with HMGB1 targeted siRNA to induce knockdown. Successful transfection was first confirmed by using a fluorescently tagged DsiRNA (DsiRNA

TYE 563; 10 nmol) that produced positive immunofluorescence in the cytoplasm of NHBE cells at 24 h post-transfection (Figure 5.12a). After establishing an optimal transfection protocol, NHBE cells were transfected with three HMGB1 targeting siRNA sequences (R1, R2, and R3; 10 nmol each) and a negative control siRNA (scrambled DsiRNA; 10 nmol) and incubated for 24 h. The knockdown was confirmed by western blot and qPCR of samples from all the groups. Quantified data showed a decrease in HMGB1 levels for all three sequences and no change in the negative control (Figure 5.12b and 5.12c). The siRNA sequence that induced the highest percentage of knockdown (siRNA.R3) was selected to perform all experiments.

NHBE cells with and without HMGB1 knockdown were exposed to either media (control) or ODE for 24 h (Table 5.2a). mRNA fold change of HMGB1 was measured and was found to increase on ODE exposure but remained low in cells with HMGB1 knockdown (Figure 5.12d). The impact of lack of HMGB1 on mitochondrial morphology was investigated. On ODE exposure, the expression of mitochondrial fusion proteins mitofusin 1 (MFN1), mitofusin 2 (MFN2), and optic atrophy 1 (OPA1) were measured. The expression of MFN1 and MFN2 decreased in NHBE cells with and without HMGB1 exposed to ODE, while OPA1 levels were significantly upregulated in NHBE cells treated with ODE alone (Figure 5.1a, 5.1b, and 5.1c). Mitochondrial fission protein, dynamin-related protein 1 (DRP1), level was significantly upregulated in the ODE exposed cells lacking in HMGB1 (Figure 5.1d). To further corroborate whether the mitochondrial morphological changes observed are associated with the number of active mitochondria, change in mitochondrial mass was measured by quantifying mitotracker green fluorescence. There was a significant decrease in the mitochondrial mass on exposure to ODE in cells with and without HMGB1 (Figure 5.1e). ODE exposed cells stained with mitotracker red dye were visualized to accurately identify the morphological changes. In NHBE cells treated with ODE alone, the

mitochondrial network appeared filamentous and branched with few fragmented or globular mitochondria (Figure 5.1f). By contrast, mitochondria appeared more fragmented or globular in ODE exposed NHBE cells lacking HMGB1 indicating mitochondrial fission.

Table 5.2 Experimental designs

(a) Acute exposure

Normal human bronchial epithelial cells			
siControl (No knockdown)		siHMGB1 (siRNA mediated HMGB1 knockdown)	
Incubate up to 24 hours			
Control (media alone)	ODE (1%)	Control (media alone)	ODE (1%)
Incubate for 24 hours			
Process cells			

(b) Chronic exposure

Normal human bronchial epithelial cells			
Control (Isotype-matched IgG)		Anti-HMGB1 antibody (10 µg/mL)	
Control (media alone)	ODE (1%)	Control (media alone)	ODE (1%)
Incubate for 8 hours/day for 5 days			
Process cells			

(c) Air-liquid interface exposure

Air-liquid interface (Apical surface)			
Control (Isotype-matched IgG)		Anti-HMGB1 antibody (10 µg/mL)	
Control (media alone)	ODE (1%)	Control (media alone)	ODE (1%)
Incubate for 1 hour/day for 5 days			
Process cells			

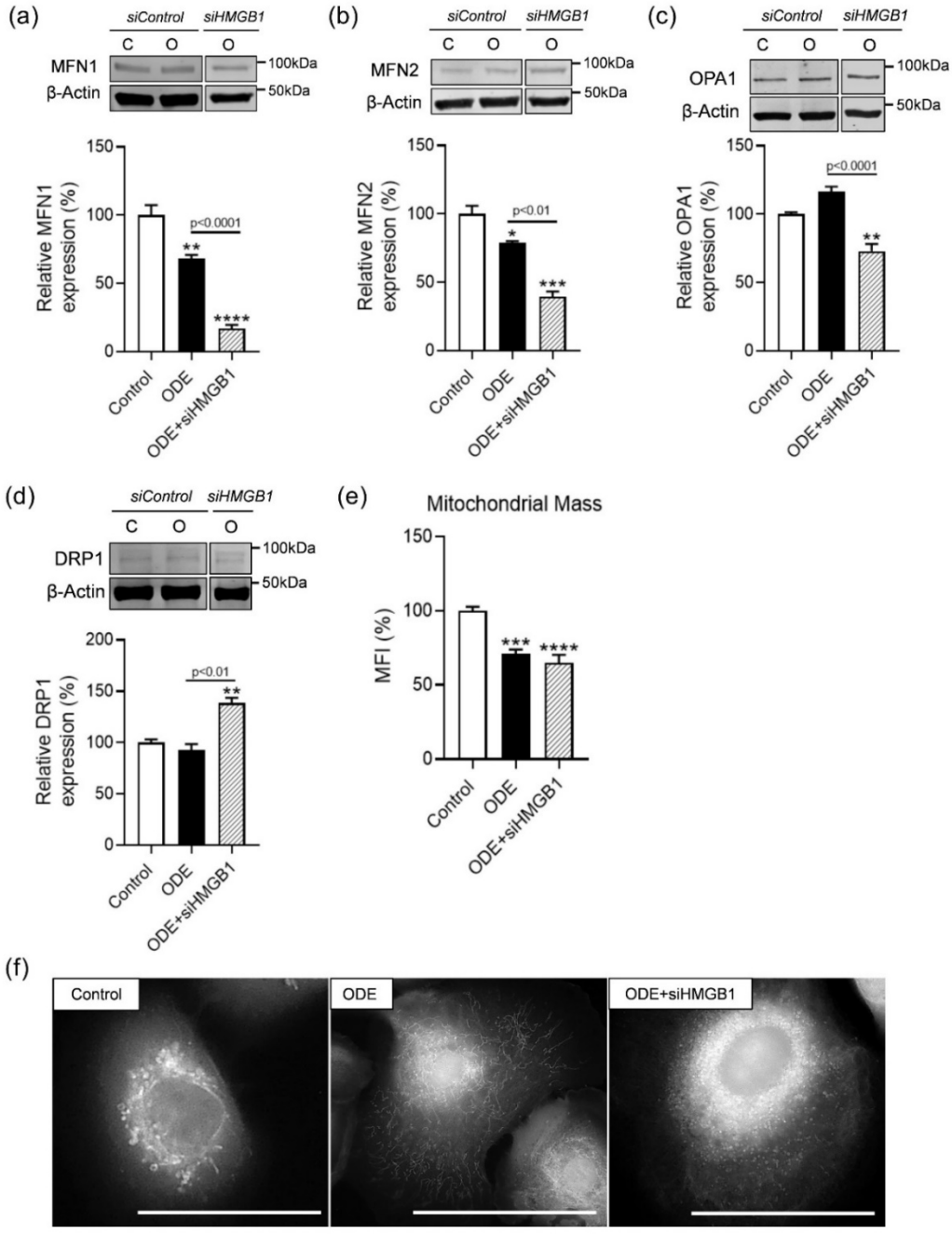

Figure 5.1 . HMGB1 knockdown promotes mitochondrial fission on OD exposure
Changes in mitochondrial morphology in NHBE cells with or without siRNA mediated HMGB1 knockdown and treated with ODE (1%) for 24 h was assessed. Immunoblotting was performed to measure the mitochondrial fusion proteins MFN1 (a), MFN2 (b) and OPA1 (c) and fission protein DRP1 (d) and compared. Mitochondrial mass was measured (e) and the morphology was visualized by staining with Mito-tracker dye (f; Scale bar = 100 μm). All the protein bands were normalized over β-actin (37 kD) and percentage intensity relative to control was analyzed. Data was analyzed using one-way ANOVA with Tukey's multiple comparison test (*$p < 0.05$, **$p < 0.01$, ***$p < 0.001$, ****$p < 0.0001$) and represented as mean ± SEM with n = 3-6/treatment (* indicates significant difference from control).

ODE exposure increases BNIP3 expression in NHBE cells

whether the lack of HMGB1 during ODE exposure impacts mitochondria-targeted autophagy called mitophagy, was investigated. The expression of the two important mediators of mitophagy, PTEN-induced kinase 1 (PINK1) and the E3 ubiquitin protein ligase Parkin, were measured. NHBE cells treated with ODE for 24 h showed no change in PINK1 but significantly decreased Parkin expression (Figure 5.2a and 5.2b). ODE-exposed NHBE cells lacking HMGB1 showed a significant decrease in both PINK1 and Parkin on exposure to ODE. The expression of BNIP3, a mitochondrial Bcl-2 Homology 3 (BH3)-only protein, known to activate mitochondrial permeability transition (MPT) was also measured (Ney 2015). BNIP3 levels were significantly increased on exposure to ODE alone, while cells treated with anti-HMGB1 siRNA showed a decrease in the expression of BNIP3 (Figure 5.2c).

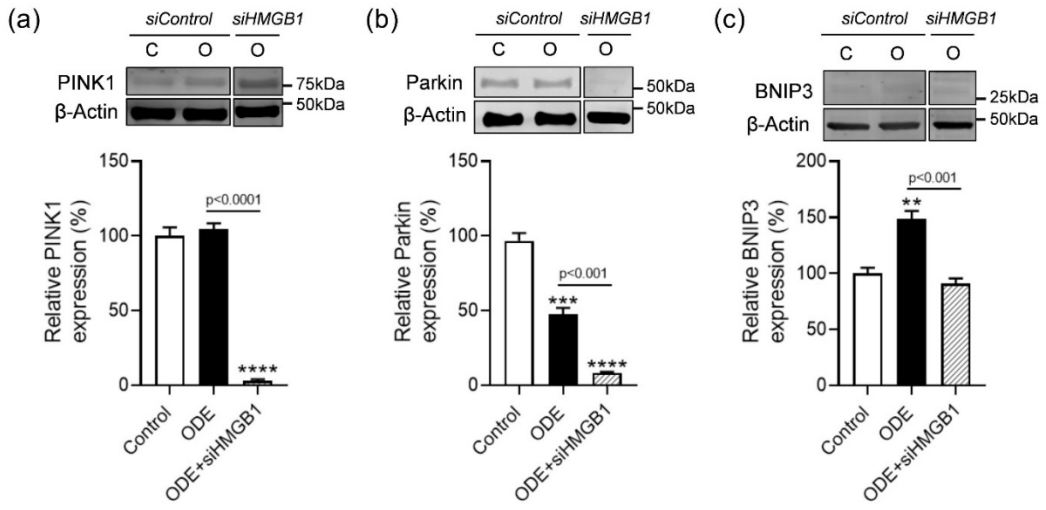

Figure 5.2 OD exposure promotes apoptosis in NHBE cells
Immunoblotting of NHBE cells, with or without siRNA mediated HMGB1 knockdown and treated with ODE (1%) for 24 h, was performed to measure expression of mitophagy markers, PINK1 (a) and Parkin (b), and BNIP3 (c). All the protein bands were normalized over β-actin (37 kD) and percentage intensity relative to control was analyzed. Data was analyzed using one-way ANOVA with Tukey's multiple comparison test (*$p < 0.05$, **$p < 0.01$, ***$p < 0.001$, ****$p < 0.0001$) and represented as mean ± SEM with n = 3/treatment (* indicates significant difference from control).

ODE exposure induces mtDNA release into extracellular fluid

Using qPCR, we measured the levels of mtDNA released into the cytosol and cell culture supernatant (extracellular spaces). NHBE cells treated with ODE for 24 h showed a significant increase in mtDNA levels both in the cytosol and supernatant, while ODE exposed cells lacking HMGB1 had decreased levels in both cytosol and supernatant (Figure 5.3a and 5.3b). In addition, ODE exposed cells showed increased expression of TLR9, a receptor that mediates cellular response to unmethylated CpG dinucleotides found in bacterial DNA to mount an innate immune response (Figure 5.3c). Next, it was assessed whether the mtDNA released from the mitochondrial matrix is activating the cGAS-STING pathway. Although no significant change in cyclic GMP-AMP synthase (cGAS) and interferon regulatory factor 3 (IRF3) expression, a significant increase in interferon gamma inducible protein 16 (IFI16) protein expression in cells treated with ODE alone was documented (Figure 5.3d, 5.3e, and 5.3f). In ODE exposed cells lacking HMGB1, the levels of these proteins were comparable to controls or significantly decreased in the case of IRF3 (Figure 5.3f). mRNA fold change of type 1 interferons, *ifna1*, *ifna4,* and *ifnb*, which are downstream targets of IFI16 and IRF3, was measured. Cells exposed to ODE for 24 h showed a significant increase in the mRNA levels of *ifna1*, *ifna4,* and *ifnb*, while the levels remained comparable to controls in cells lacking HMGB1 (Figure 5.3g, 5.3h, and 5.3i).

To investigate whether mtDNA is released during repeated exposure of ODE, NHBE cells were treated with media alone (control) or ODE (1%) followed by media (control) or HMGB1 neutralization antibody (10 μg/mL) for 8 h per day for five days (Table 5.2b). Following a 5-day exposure there was an increase in cytosolic mtDNA content in cells treated with HMGB1 neutralization antibody and an increase in extracellular mtDNA in cells treated with ODE alone (Figure 5.13a and 5.13b). There was also an increase in *ifna4* and a decrease in *ifna* and *ifnb* mRNA levels in cells treated with HMGB1 neutralization antibody (Figure 5.13c, 5.13d, and 5.13e).

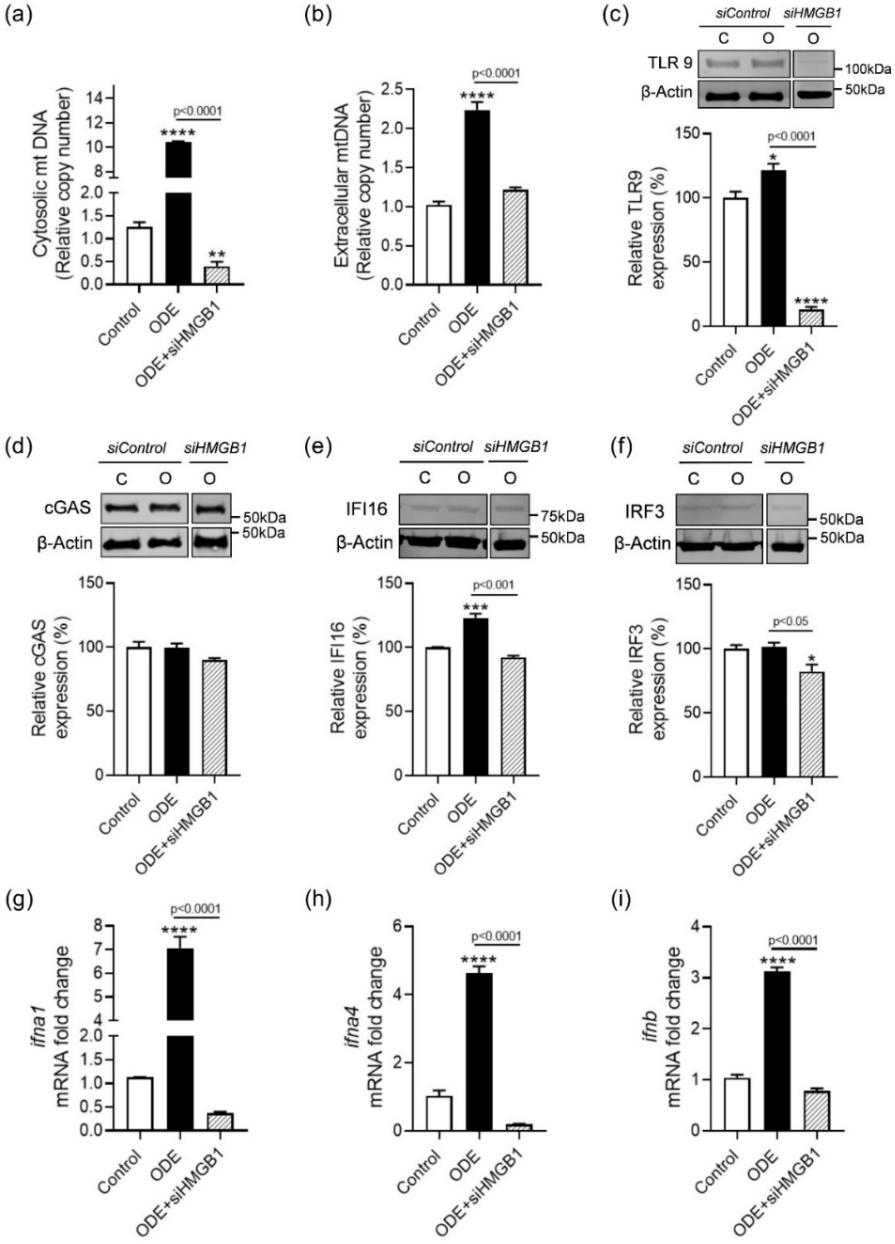

Figure 5.3 Acute OD exposure mediated release of mtDNA stimulates IFN production
Mitochondrial DNA (mtDNA) leakage into the cytosol (a) and extracellularly (b) in NHBE cells, with or without siRNA mediated HMGB1 knockdown and treated with ODE (1%) for 24 h was analyzed via qPCR. Immunoblotting was performed to measure expression of TLR9 (c), cGAS (d), IFI16 (e) and IRF3 (f). mRNA fold change of gene targets of mtDNA release, ifna1 (g), ifna4 (h), and ifnb (i), was measured by qPCR. All the protein bands were normalized over β-actin (37 kD) and percentage intensity relative to control was analyzed. Data was analyzed using one-way ANOVA with Tukey's multiple comparison test (*$p < 0.05$, **$p < 0.01$, ***$p < 0.001$, ****$p < 0.0001$) and represented as mean ± SEM with n = 3/treatment (* indicates significant difference from control).

Mitochondrial biogenesis is promoted in ODE exposed NHBE cells lacking HMGB1

Mitochondrial biogenesis in NHBE cells was assessed by measuring Peroxisome proliferator-activated receptor gamma coactivator 1-alpha (PGC1α) and Nuclear factor erythroid 2-related factor 2 (NRF2) protein expression. NHBE cells with and without HMGB1 exposed to ODE for 24 h showed a significant increase in PGC1α and NRF2 expression compared to controls (Figure 5.4a and 5.4b). Expression of TFAM, a downstream target of PGC1α and NRF2, in both the mitochondria and mitochondria-free cytosol was measured. In ODE exposed NHBE cells lacking HMGB1, we noted a small decrease in TFAM levels in the mitochondria (~10%) and an increase in the cytosolic levels (~10%) (Figure 5.4c, 5.4d, and 5.4e). We observed that the cytosolic levels of TFAM significantly decreased in cells treated with ODE alone (Figure 5.4c and 5.4e). mRNA fold change of downstream targets of NRF2, Glutathione S-transferase P *(gstp1)*, heme oxygenase 1 *(hmox1)*, and NAD(P)H Quinone Dehydrogenase 1 *(nqo1)*, was measured. In ODE exposed NHBE cells lacking HMGB1, we documented a significant decrease in *gstp1*, while we noted an increase in mRNA levels of *hmox1* and *nqo1*. In ODE treated cells, while no significant change was observed in the expression of *gstp1*, a significant increase was observed in *hmox1* and *nqo1*, when compared to control and cells lacking HMGB1 (Figure 5.4f, 5.4g, and 5.4h).

On the other hand, in the repeated long-term exposure model, we observed that ODE induced a significant decrease in mRNA fold change of *pgc1a* and *nrf2*, and HMGB1 neutralization significantly increased *pgc1a* and *nrf2* levels. However, HMGB1 neutralization did not increase the levels to that of controls. (Figure 5.14a and 5.14b). mRNA fold change of *tfam* is significantly reduced as well (Figure 5.14c). mRNA levels of *nqo1* was significantly reduced, while that of *hmox1* increased in both treatments (Figure 5.14d and 5.14e).

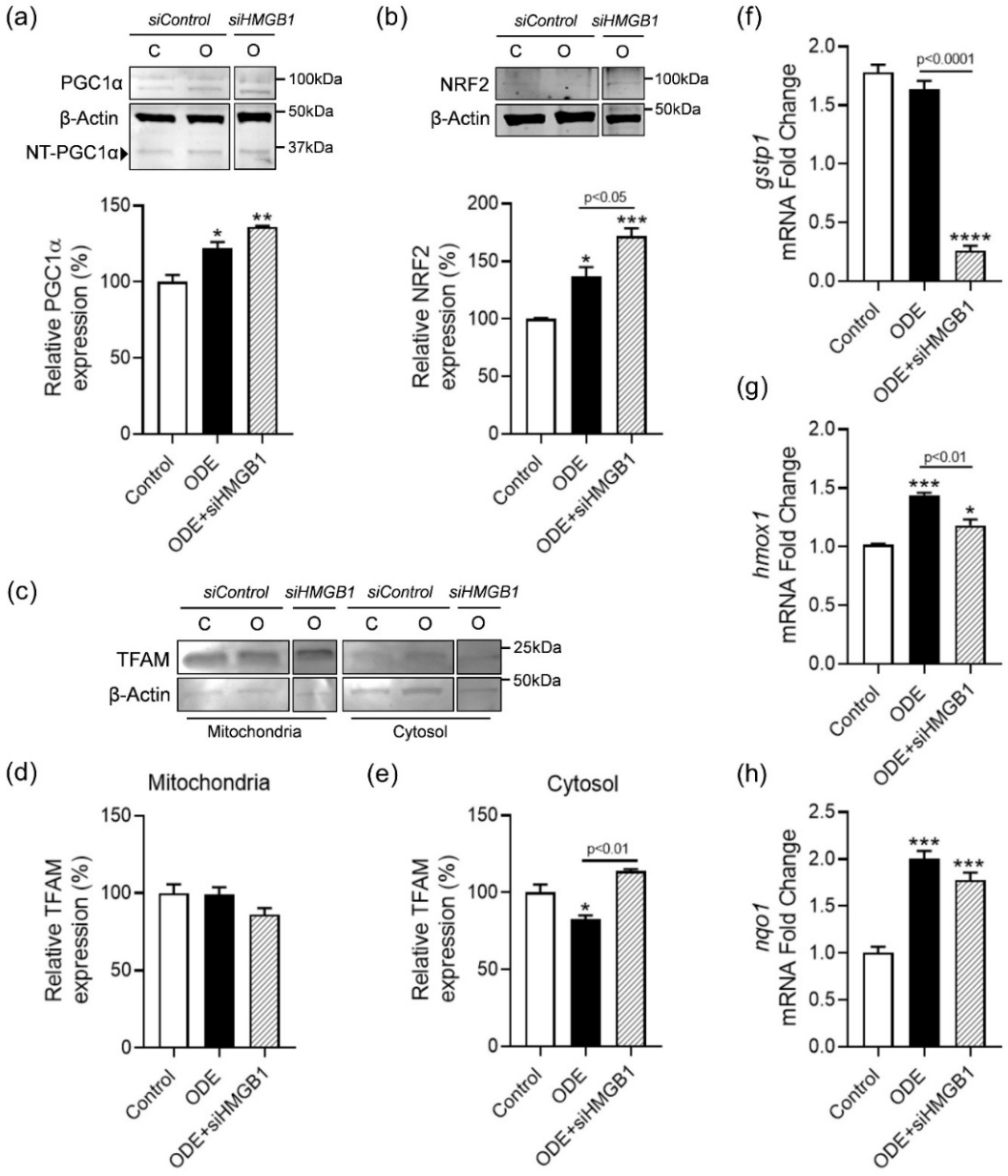

Figure 5.4 Lack of HMGB1 promotes mitochondrial biogenesis in OD exposed NHBE cells
Markers of mitochondrial biogenesis in NHBE cells with or without siRNA mediated HMGB1 knockdown and treated with ODE (1%) for 24 h was measured. Immunoblotting of whole cell lysates of NHBE cells was performed to measure PGC1α (a) and NRF2 expression (b). TFAM expression was compared in the mitochondrial (c, d) and cytosolic (c, e) fractions of the NHBE cells. mRNA fold change of gene targets downstream of NRF2, *gstp1* (f), *hmox1* (g), and *nqo1* (h), was measured by qPCR. All the protein bands were normalized over β-actin (37 kD) and percentage intensity relative to control was analyzed. Data was analyzed using one-way ANOVA with Tukey's multiple comparison test (*$p < 0.05$, **$p < 0.01$, ***$p < 0.001$, ****$p < 0.0001$) and represented as mean ± SEM with n = 3/treatment (* indicates significant difference from control).

Single ODE exposure causes cytochrome c release

To assess the impact of the increased mtDNA leakage, we measured the release of mitochondrial DAMPs (mtDAMPs) and reactive species generation. In addition to TFAM and mtDNA, another prominent mtDAMP is cytochrome c which is a key player in apoptosis (Cai et al. 1998; Ott et al. 2002). We measured the expression of cytochrome c in mitochondrial and mitochondria-free cytosolic fractions of NHBE cells. ODE exposure of NHBE cells increased the cytosolic cytochrome c levels but not the mitochondrial cytochrome c levels (Figure 5.5a, 5.5b, and 5.5c). ODE exposed cells lacking in HMGB1 showed a significant decrease in both mitochondrial and cytosolic cytochrome c protein levels. Using Griess assay we measured the levels of reactive nitrite species (RNS) secreted, where we observed an increase in RNS levels on exposure to ODE, with levels comparable to control in cells lacking HMGB1 (Figure 5.5d). To corroborate this, we measured the mRNA fold change in *nos2*, the gene coding for inducible nitric oxide synthase (iNOS) and observed an increased expression in cells treated with ODE alone while it decreased in cells lacking HMGB1 (Figure 5.5e). In addition, we saw an increase in intracellular reactive oxygen species (ROS) in ODE treated cells, which was significantly decreased in cells lacking HMGB1 (Figure 5.5f). On the other hand, the mitochondrial superoxide levels were significantly decreased in both cases compared to control (Figure 5.5g). In addition, we saw a decrease in mitochondrial calcium levels ($[Ca^{2+}]_{mito}$) in cells exposed to ODE alone and increased in cells lacking HMGB1 (Figure 5.5h and 5.5i). In the repeated ODE exposure model, ODE exposure alone decreased the ($[Ca^{2+}]_{mito}$) whereas neutralization of HMGB1 increased the ($[Ca^{2+}]_{mito}$). There was no change in the levels of mitochondrial superoxide (Figure 5.15c).

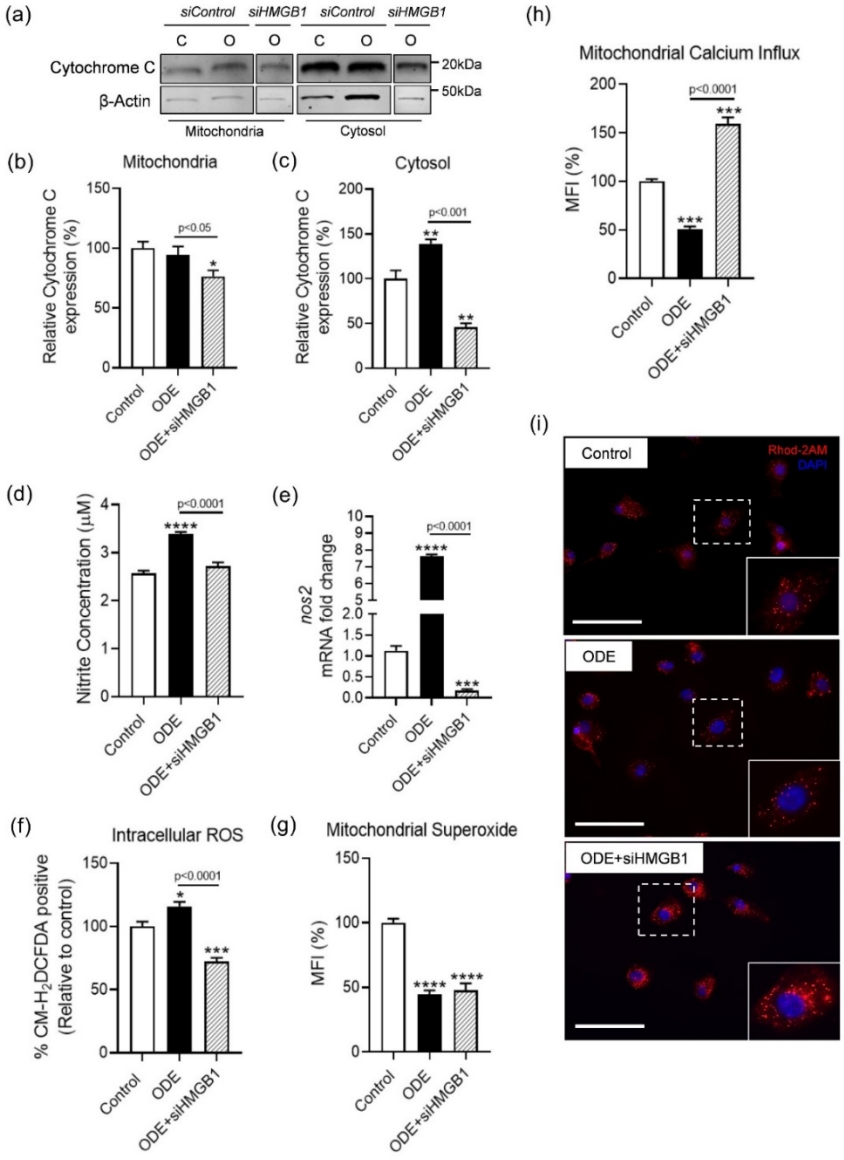

Figure 5.5 Acute OD exposure causes cytochrome c release into the cytosol
Immunoblotting of mitochondrial and mitochondria-free cytosolic fractions of NHBE cells with or without siRNA mediated HMGB1 knockdown and treated with ODE (1%) for 24 h, to detect the presence of Cytochrome C. Cytochrome C expression was compared between the mitochondrial (a, b) and cytosolic (a, c) fractions of the cells. Concentration of secreted nitrites was measured using griess assay (d) and mRNA levels of nos2 (e) was measured by qPCR. Using CM-H_2DCFDA and Mito-SOX dyes, the levels of superoxide anions (SOX) intracellularly (f) and within the mitochondria (g) was measured, respectively. Intra-mitochondrial calcium levels in mitochondria isolated from the treated cells was quantified (h) and visualized (i; Scale bar = 100 μm) by Rhod-2AM staining. For western blot, all the protein bands were normalized over β-actin (37 kD) and percentage intensity relative to control analyzed. Data was analyzed using one-way ANOVA with Tukey's multiple comparison test (*$p < 0.05$, **$p < 0.01$, ***$p < 0.001$, ****$p < 0.0001$) and represented as mean ± SEM with n = 3-6/treatment (* indicates significant difference from control).

Repeated ODE exposure promotes mitochondrial fusion

Using transmission electron microscopy (TEM), we assessed the ultrastructural changes in NHBE cells following exposure to ODE with or without HMGB1 neutralization for 8 h a day for 5 days (Table 5.2b). Compared to controls, ODE-treated NHBE cells showed change in mitochondrial morphology. Mitochondria appeared to be more elongated with cristolysis and in some cases there was mitochondrial hypertrophy (Figure 5.6a). In contrast, neutralization of HMGB1 decreased the ODE-induced cristolysis and mitochondrial shape was similar to that of control. We stained the cells with mitotracker dye to assess changes in the number of active mitochondria. Mitotracker stained cells revealed no change in mitochondrial mass among any of the treatments. However, we did observe noticeable ODE-induced changes in mitochondrial morphology. Compared to controls, ODE exposed NHBE cells showed filamentous mitochondria and mitochondria appeared to be more clustered close to the nucleus (Figure 5.6b). With HMGB1 neutralization, the mitochondria were more fragmented and globular, and were less clustered near nucleus when compared to ODE exposed cells. Using MTT assay we measured the cell viability, where HMGB1 neutralization rescued the ODE-induced decrease in cell viability (Figure 5.6c).

HMGB1 neutralization rescues mitochondrial respiration in repeated ODE exposure models

A targeted analysis of expression of genes associated with mitochondrial respiration was performed. A pre-designed gene array with 96 genes (including housekeeping genes) specific to various components involved in mitochondrial respiration was used and fold change was measured by qPCR (Table 5.6). The change in gene expression between ODE exposed NHBE cells, with or without HMGB1 neutralization for 8 h a day for 5 days, was calculated relative to control by the 2^{-DDCT} method and genes with fold change ≤10 or ≥10 were represented on a heat map (Livak and Schmittgen 2001). It was observed that neutralization of HMGB1 increased the expression of

genes of protein subunits involved in mitochondrial respiration such as various subunits of ATP synthase *(atp)*, cytochrome c oxidase *(cox)*, ubiquinol-cytochrome c reductase *(uqcr)* and NADH:ubiquinone oxidoreductase *(naduf)* when compared to ODE treated cells (Figure 5.7a). Using the Kyoto Encyclopedia of Genes and Genomes (KEGG) database, upregulated and downregulated pathways associated with mitochondria bioenergetics were analyzed (Figure 5.7b-e). Pathways related to the metabolism, respiratory electron transport, and mitochondria biogenesis which were downregulated with ODE exposure were significantly upregulated on HMGB1 neutralization (Figure 5.7c and 5.7d).

Single ODE exposure induces hypoxia response in NHBE cells lacking HMGB1

Oxygen sensing and adaptations in NHBE cells (with or without anti-HMGB1 siRNA treatment) exposed to ODE for 24 h was measured. An increase in hypoxia-inducible factor 1-alpha (HIF1α) protein expression was observed in cells lacking HMGB1 while it was significantly reduced on ODE exposure alone (Figure 5.8a). mRNA fold change of ubiquitin ligase Von Hippel-Lindau tumor suppressor *(vhl)* was significantly increased in both ODE exposed NHBE cells with or without HMGB1 (Figure 5.8b). mRNA fold change of genes involved in glucose uptake, solute carrier family 2 member 6 *(slc2a6)*, and glycolysis, enolase 1 *(eno1)*, was measured. A significant increase in *slc2a6* in both ODE exposed cells with or without HMGB1 was observed, whereas *eno1* was upregulated in cells lacking HMGB1 (Figure 5.8c and 5.8d). To corroborate this, we measured cellular glucose uptake potential and glycolytic activity in ODE exposed NHBE cells by culturing cells with the glucose analog 2-NBDG. Here a significant increase in the uptake of 2-NBDG was observed in ODE exposed cells lacking HMGB1, while exposure to ODE alone significantly decreased 2-NBDG uptake (Figure 5.8e).

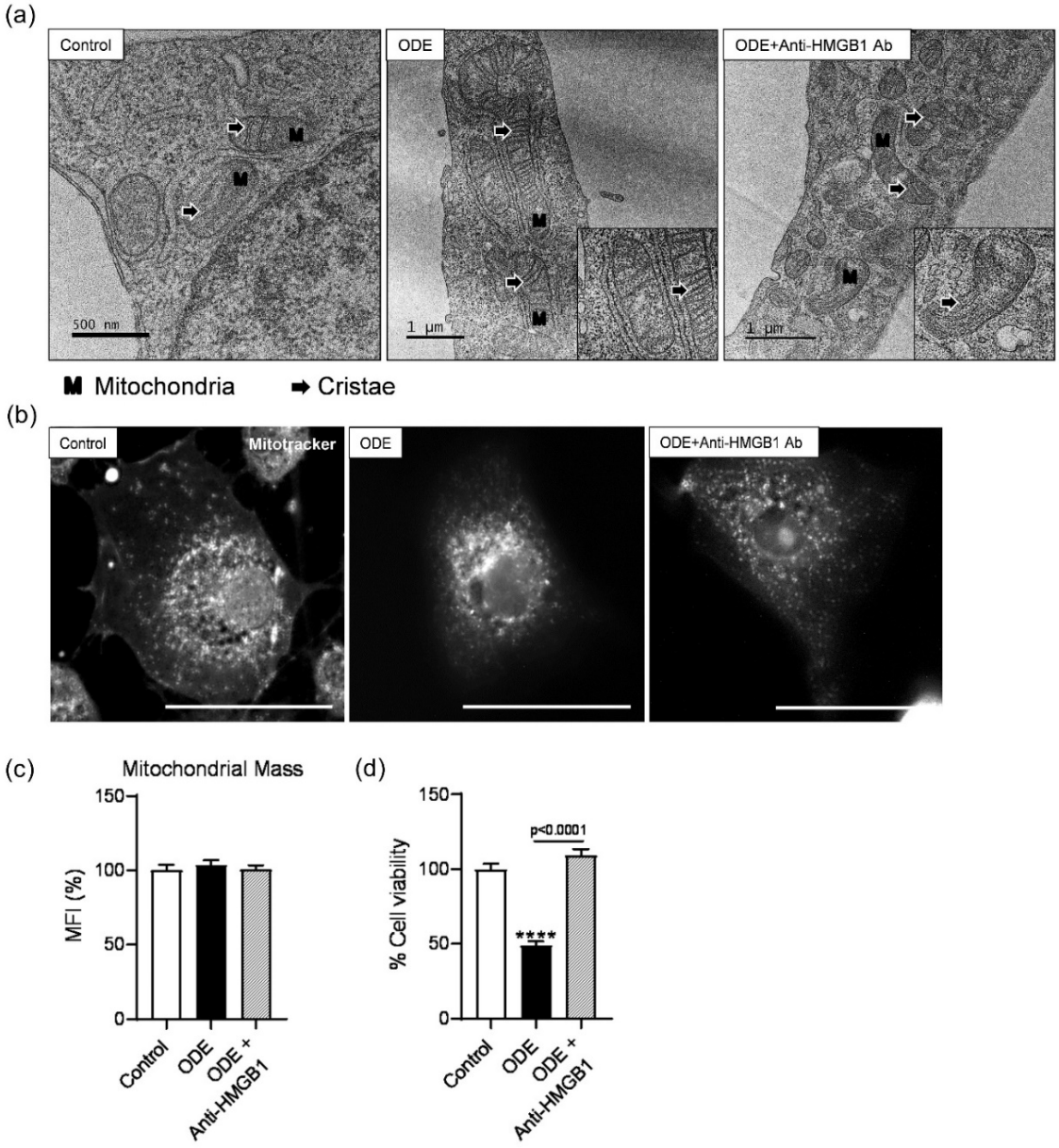

Figure 5.6 Antibody mediated neutralization of HMGB1 maintains mitochondrial morphology and cell viability

Transmission electron microscopy (TEM) of NHBE cells treated with medium or ODE (1%) followed by medium or HMGB1 neutralization antibody (10 µg/mL) for 8 h per day for 5 days show changes in the mitochondrial morphology. A number of mitochondria displayed fused and elongated mitochondrial morphology (a; scale bar, 0.5-1 µm) on treatment with ODE. Cells treated with ODE followed by HMGB1 neutralization showed noticeably healthier mitochondria with a few morphological changes. Mitochondrial mass was measured (c) and the morphology was visualized by staining with Mito-tracker dye (b; Scale bar = 100 µm). MTT assay was performed to measure cell viability on treatment (d). Data was analyzed using one-way ANOVA with Tukey's multiple comparison test (*$p < 0.05$, **$p < 0.01$, ***$p < 0.001$, ****$p < 0.0001$) and represented as mean ± SEM with n = 6/treatment (* indicates significant difference from control).

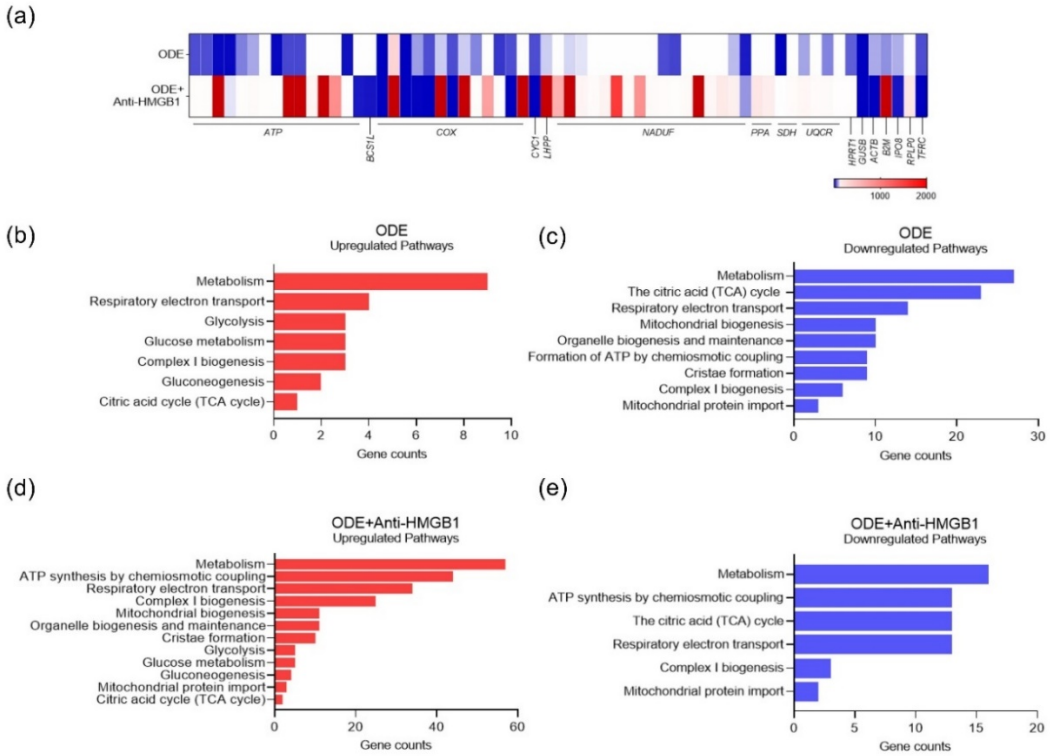

Figure 5.7 HMGB1 neutralization upregulates genes associated with mitochondrial respiration

mRNA expression profiles of genes specific to mitochondrial respiration in NHBE cells treated with medium or ODE (1%) followed by medium or HMGB1 neutralization antibody (10 µg/mL) for 8 h per day for 5 days was measured using a targeted gene array. Heatmap of mRNA transcripts of genes that had a 10-fold change in expression were selected (a). Selected upregulated (b, d) and downregulated (c, e) pathways from reactome pathway analysis of significantly altered mRNA transcripts with FDR corrected p-value cut-off <0.05 were selected and represented by gene counts. Data was analyzed using one-way ANOVA with Tukey's multiple comparison test (*p < 0.05, **p < 0.01, ***p < 0.001, ****p < 0.0001) and represented as mean ± SEM with n = 2/treatment (* indicates significant difference from control).

We compared the expression of the factors involved in hypoxia and glucose uptake in NHBE cells in the repeated ODE exposure model. mRNA fold change of *hif1a* and *vhl* was significantly decreased in ODE exposed cells but remained unchanged in cells with HMGB1 neutralization (Figure 5.9a and 5.9b). There was no significant change in the expression of *slc2a6* in any of the treatments but the expression of *eno1* was significantly downregulated in ODE exposed cells (Figure 5.9c and 5.9d). 2-NBDG uptake was decreased in ODE exposed cells and was comparable to control in cells with HMGB1 neutralization antibody (Figure 5.9e).

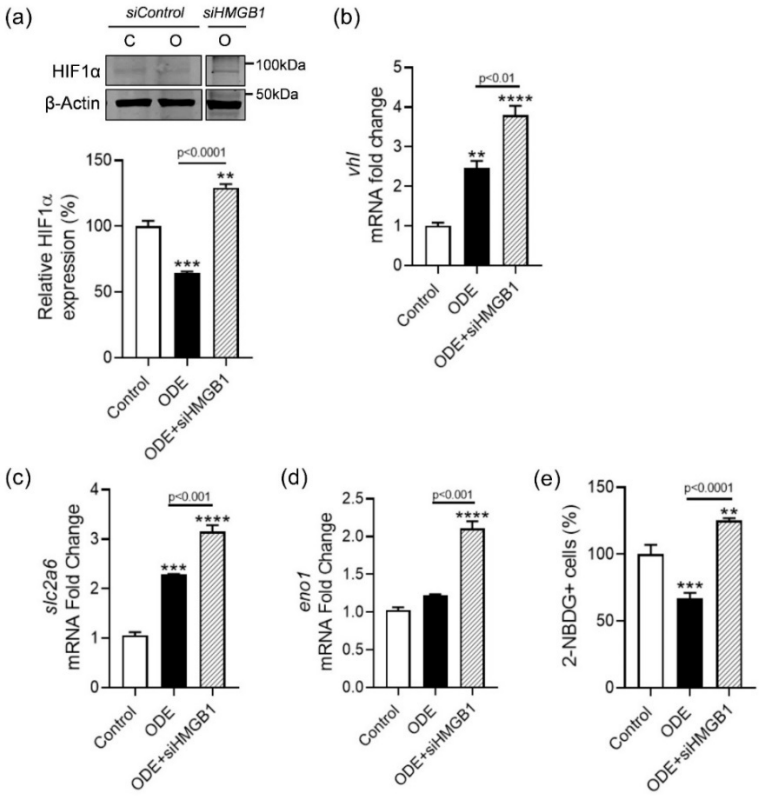

Figure 5.8 Lack of HMGB1 initiates hypoxia response on acute OD exposure
Markers of hypoxia response in NHBE cells with or without siRNA mediated HMGB1 knockdown and treated with ODE (1%) for 24 h was measured. Immunoblotting of whole-cell lysates of NHBE cells were performed to measure HIF1α (a). mRNA fold change of ubiquitin ligase, *vhl* (b), and *Slc2a6* (c) and *Eno1* (d), involved in glucose uptake and glycolysis, were measured by qPCR. 2-NBDG uptake to measure cellular glucose uptake was performed (e). For western blot, all the protein bands were normalized over β-actin (37 kD) and percentage intensity relative to control analyzed. Data was analyzed using one-way ANOVA with Tukey's multiple comparison test (*p < 0.05, **p < 0.01, ***p < 0.001, ****p < 0.0001) and represented as mean ± SEM with n = 3-6/treatment (* indicates significant difference from control).

HMGB1 neutralization increased tight junction integrity in ALI cultures of NHBE cells

NHBE cells were seeded onto a semi-permeable membrane to develop an air-liquid interface (ALI) culture model and exposed to ODE, with or without HMGB1 neutralization for 1 h per day for 5 days (Table 5.2c). mRNA fold change of forkhead box J1 *(foxj1)* and its downstream target cilia and flagella associated protein 157 *(cfap157)* was measured (Figure 5.10a and 5.10b). Exposure of cells to ODE alone showed a significant increase in fold change of both genes, while the expression was comparable to control in ODE exposed cells with HMGB1

neutralization. Tight junction integrity was determined by measuring the mRNA fold change of occludin *(ocln)* and claudin 1 *(cld1)*, and by quantifying the trans-epithelial electrical resistance (TEER). mRNA fold change of *ocln* and *cldn1* was significantly downregulated in ODE exposed cells, while on HMGB1 neutralization *ocln* levels were comparable to control and *cld1* was significantly decreased (Figure 5.10c and 5.10d). TEER measurements were performed to identify the impact of ODE on tight junction integrity. A decrease in TEER values (electrical resistance) is proportional to decreased tight junction integrity. It was observed that TEER values were significantly decreased on exposure to ODE as early as 12 h and continued to decrease with time compared to control. On the other hand, although a similar decrease was observed with the neutralization of HMGB1 at 12 h, TEER values remain steady after day 1 post-exposure and were not rescued significantly (Figure 5.10e).

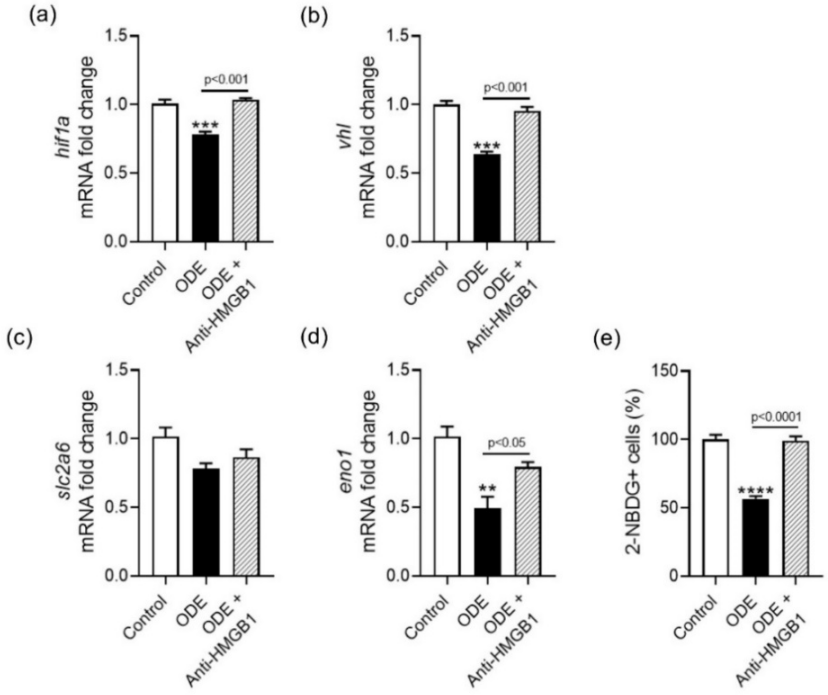

Figure 5.9 Normoxic conditions are maintained on HMGB1 neutralization during chronic OD exposure

Markers of hypoxia response in NHBE cells treated with medium or ODE (1%) followed by medium or HMGB1 neutralization antibody (10 µg/mL) for 8 h per day for 5 days was measured.

mRNA fold change of hypoxia response factor, *hif1a* (a) and ubiquitin ligase, *vhl* (b), and *Slc2a6* (c) and *Eno1* (d), involved in glucose uptake and glycolysis were measured by qPCR. 2-NBDG uptake to measure cellular glucose uptake was performed (e). Samples for all assays were derived from the same experiment and were processed in parallel. Data was analyzed using one-way ANOVA with Tukey's multiple comparison test (*p < 0.05, **p < 0.01, ***p < 0.001, ****p < 0.0001) and represented as mean ± SEM with n = 3-6/treatment (* indicates significant difference from control).

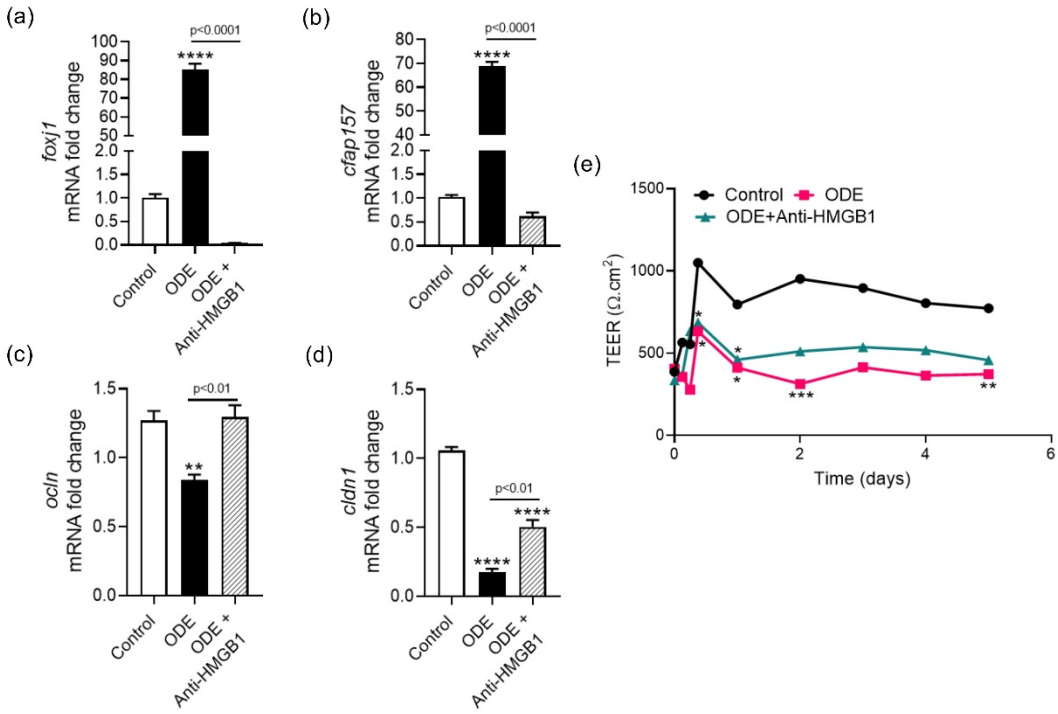

Figure 5.10 HMGB1 neutralization upregulates tight junction integrity in ALI
NHBE cells differentiated on air-liquid interface (ALI) culture treated with medium or ODE (1%) followed by medium or HMGB1 neutralization antibody (10 µg/mL) for 1 h per day for 5 days. mRNA fold change of markers of motile cilia, *foxj1* (a) and *cfap157*(b), and tight junction, *ocln* (c) and *cldn 1* (d), was measured by qPCR. Tight junction integrity was assessed by trans-epithelial electrical resistance (TEER) measurement (e). Samples for all assays were derived from the same experiment and were processed in parallel. Data was analyzed using one-way ANOVA with Tukey's multiple comparison test (*p < 0.05, **p < 0.01, ***p < 0.001, ****p < 0.0001) and represented as mean ± SEM with n = 3/treatment (* indicates significant difference from control).

Discussion

The prevalence of airway inflammatory diseases in agricultural workers is high, where the development of a myriad of respiratory symptoms has been documented (Poole and Romberger 2012). Recent studies have shown the relationship between induction of mitochondrial dysfunction

and several inflammatory airway diseases such as asthma and chronic obstructive pulmonary disease (COPD) (Schumacker et al. 2014; Prakash et al. 2017; Aghapour et al. 2019; Cloonan et al. 2020). High mobility group box 1 (HMGB1) protein, an essential protein which during inflammatory conditions has been shown to act as a DAMP in airway inflammatory conditions such as COPD, cigarette smoke exposure and acute lung injury (Rubartelli and Lotze 2007; Zhang et al. 2010; Pouwels et al. 2014; Yang et al. 2015; Ugrinova and Pasheva 2017b). Previously we showed how HMGB1 behaves as a pro-inflammatory mediator in ODE exposed cells and how antibody-mediated neutralization of secreted HMGB1 decreases the inflammatory cytokines, ROS and RNS, and had an overall protective effect 24 to 48 h post-treatment (Bhat et al. 2019; Massey et al. 2019). In the current study, we investigated the effect of secreted HMGB1 on ODE-induced mitochondrial dysfunction in primary normal human bronchial epithelial (NHBE) cell models of single and repeated five-day exposure. Overall, we demonstrated that blocking HMGB1 secretion induces mitochondrial fragmentation, mitochondrial biogenesis and increase in mitochondrial respiration. These responses were consistent across the single (acute) exposure, with siRNA knockdown of HMGB1, as well as in repeated (chronic) exposure to ODE, with antibody-mediated HMGB1 neutralization.

In the present study, we used two *in vitro* models, a 24 h ODE exposure (single, acute) with siRNA mediated knockdown of HMGB1 (Table 5.2a) and a 5-day (8 h/day) ODE exposure (repeated, chronic) with antibody-mediated HMGB1 neutralization to examine exposure-induced mitochondrial dysfunction. Mitochondrial remodeling is mediated by the balance between MFN1/2 and DRP1, which promote mitochondrial fusion and fission respectively (Song et al. 2009; Liesa et al. 2009; Palmer et al. 2011; Ranieri et al. 2013; Huang et al. 2018). Our results from single exposure showed that, ODE decreases the expression of MFN1 and MFN2 in cells

with and without HMGB1, but OPA1 expression in cells lacking HMGB1 was significantly decreased. OPA1 is a dynamin-related GTPase that has been shown to mediate inner mitochondrial membrane (IMM) fusion, while MFN1/2 mediate the fusion of the outer mitochondrial membrane (OMM) (Song et al. 2009; MacVicar and Langer 2016). OPA1 in particular has been identified as a major player in the regulation of various mitochondrial functions, including cristae morphogenesis, apoptosis, and respiratory capacity (MacVicar and Langer 2016). Loss of OPA1 has been shown to induce DRP1-dependent mitochondrial fragmentation (Lee et al. 2004). This was seen in our results where siRNA-mediated HMGB1 knockdown increased DRP1 expression in ODE exposed cells. The fusion of mitochondria is dependent on dimerization of mitofusin proteins, MFN1 and MFN2, thus the decreased MFN1/2 expression in ODE exposed cells lacking HMGB1 explains the increase in mitochondrial fragmentation as well (Chen et al. 2003; Song et al. 2009; Liesa et al. 2009; Palmer et al. 2011; Ranieri et al. 2013).

Next, we used 2D fluorescence imaging and transmission electron microscopy (TEM) to evaluate mitochondrial morphology and ultrastructural changes in both *in vitro* exposure models. First, we observed that single exposure of cells with or without HMGB1 reduced the mitochondrial mass. When visualized, cells with HMGB1 when exposed to ODE showed a filamentous and branched network of mitochondria with few fragmented and globular mitochondria. Interestingly, cells that lacked HMGB1 displayed increased fragmentation and globular mitochondria upon exposure to ODE. These results indicate that ODE exposure induced mitochondrial changes become pronounced with the loss of nuclear HMGB1 underscoring the importance of nuclear HMGB1 in maintaining the health of the cellular mitochondria (Tang et al. 2011). Our TEM images confirmed that ODE exposure induced mitochondrial elongation, cristoysis and hypertrophy, whereas HMGB1 neutralization reduced the ODE-induced cristolysis and

mitochondria appeared healthy. Further, neutralization of HMGB1 induced a globular morphology of mitochondria with elongated cristae running parallel to the longitudinal axis of the mitochondria. Overall, ODE-induced mitochondrial fusion observed in our study could be a cellular stress response aimed at compensating for the loss of important mitochondrial functions (Chen et al. 2003; Landes et al. 2010; Westrate et al. 2014; Eisner et al. 2018; Tilokani et al. 2018). Our recent work in microglial model of ODE exposure confirms that the ODE-induced cristolysis and the morphological basis of exposure induced decreases in bioenergetics (Massey et al., 2021).

One of the consequences associated with mitochondrial fragmentation is the loss of mitochondrial membrane potential and mitophagy. The PINK1-Parkin signaling pathway which is involved in mitochondrial clearance (mitophagy) was investigated. ODE exposed NHBE cells showed no significant change in PINK1 expression, while Parkin was significantly decreased and NHBE cells lacking HMGB1 had decreased levels of both PINK1 and Parkin. These results indicate that the observed fragmentation of mitochondria in cells lacking HMGB1 could be due to active mitochondrial biogenesis (Ding and Yin 2012). We also measured the expression of BNIP3, a mitochondrial transmembrane protein known to have pro-death activity and a role in activating mitochondrial permeability transition (MPT). Here we observe an increase in BNIP3 expression on ODE exposure, whereas in cells lacking HMGB1, the BNIP3 levels return to baseline (control) levels. The increase in BNIP3 expression could be promoting permeability of the inner and outer mitochondrial membranes resulting in increased ROS production, release of cytochrome c and mitochondrial depolarization, all of which together initiates cellular apoptosis (Kim et al. 2002; Ney 2015). Considering the increase in OPA1 levels in ODE exposed cells, evidence suggests that BNIP3 interacts with OPA1 inhibiting OPA1-mediated fusion, in acute conditions, or disassembly of OPA1 complexes, in chronic conditions, leading to cellular death (Landes et al. 2010). This is

further corroborated by the increase in cytosolic cytochrome C levels in 24 h ODE exposed cells. On the contrary, cytochrome C levels were decreased in cells lacking HMGB1 following exposure. The release cytochrome C in ODE exposed cells could be promoting increased ROS generation, caspase activation (caspase 3 and caspase 9), and eventually leading to apoptotic cell dismantling (Cai et al. 1998; Ott et al. 2002; Quinsay et al. 2010).

One of the major consequences of increase in MPT during cellular stress is the release of mitochondrially derived molecules referred to as mtDAMPs (García and Chávez 2007; Zhang et al. 2010; Quinsay et al. 2010; Nakahira et al. 2011). Fragmented mtDNA released from the damaged mitochondria is one of the most important mtDAMPs which regulates innate immune responses (Lee and Wei 2005; West et al. 2015; Ploumi et al. 2017). Release of mitochondrial DNA into the cytoplasm and out into the extracellular milieu activates multiple pattern recognition receptors and innate immune responses, including cGAS-STING, TLR9, and inflammasome formation leading to, among others, robust type I interferon responses (Cloonan and Choi 2012; West et al. 2015; Chen et al. 2016). The results of the present study show an increase in cytosolic and extracellular mitochondrial DNA copy number in NHBE cells exposed to ODE for 24 h, which is reduced in ODE exposed cells lacking HMGB1. Concurrently we also observed an increase in the expression of TLR9, IFI16, IRF3, and type 1 interferon, which could be leading to cell death. On the other hand, during chronic ODE exposure we see an increase in cytosolic mtDNA on HMGB1 neutralization, but not extracellularly, and an increase in only *ifna4* mRNA, which could be indicative that the neutralization of HMGB1 could be promoting mitochondrial biogenesis.

Mitochondrial reactive oxygen species (mtROS) is the most universal and well-studied mtDAMP and is a by-product of mitochondrial respiration and ATP production (Zorov et al. 2014). NHBE cells exposed to ODE for 24 h show an increase in intracellular ROS while the levels of

mtROS remain low in all the treatment groups. The ODE-mediated increase in intracellular ROS is consistent with our previous findings, where it is known to initiate the inflammatory cascade (Bhat et al. 2019; Massey et al. 2019). The lack of increase in mtROS could be another indicator of mitochondrial biogenesis in play. Thus, the observed mitochondrial fragmentation in cells lacking HMGB1 or with antibody-mediated HMGB1 neutralization may reflect an important adaptive response to protect the mitochondria from an increase in ROS production and oxidative stress on ODE exposure. In addition to this, we also document an increase in mitochondrial calcium influx in ODE treated cells lacking HMGB1 or with antibody-mediated HMGB1 neutralization. This increase could be promoting mitochondrial O_2 consumption and ATP synthesis, as well as mitochondrial metabolism (Rizzuto et al. 2000; Parekh 2003; Brookes et al. 2004; Hajnóczky et al. 2007; Finkel et al. 2015).

Mitochondrial biogenesis, along with mitophagy, allow cells to quickly replace metabolically dysfunctional mitochondria before reaching the stage of energy failure. The results of our study provide converging evidence that 24 h ODE exposure of cells with HMGB1 or cells without HMGB1 induce mitochondrial biogenesis. First, we observed an increase in PGC1α expression in cells exposed to ODE, with or without HMGB1. The role of PGC1α in regulating mitochondrial biogenesis has been well established (Wu et al. 1999; Handschin and Spiegelman 2006; Trian et al. 2007). We then measured the expression of NRF2 and observed a similar increase as that of PGC1α. NRF2 is known to regulate the expression of the electron transport chain subunits and binds to the promoter regions of genes involved in the transcription of mtDNA. NRF2 is known to be regulated by its transcriptional coactivator PGC1α, which together induces the expression of TFAM thus activating mitochondrial biogenesis. In line with this, we observe an increase in TFAM protein expression in mitochondria-free cytosolic fractions of 24 h ODE

exposed cells lacking HMGB1. However, we observed that a repeated 5-day ODE exposure resulted in significantly lower levels of the gene expression of PGC1α, NRF2, and TFAM when compared to the controls with and without HMGB1 neutralization.

The extent of mitochondrial dysfunction is determined by the level of negative impact on mitochondrial respiration and metabolism. In our study, we found that NHBE cells repeatedly exposed to ODE display a distinctive mitochondrial gene profile, where we observe a downregulation of genes associated with mitochondrial metabolism, citric acid (TCA) cycle, OXPHOS, and mitochondrial biogenesis. This is consistent with the increased levels of ROS, induction of MPT and mtDNA release on ODE exposure. With the neutralization of HMGB1, we document an increase in the fold change of genes coding protein subunits associated with mitochondrial electron transport chain (ETC), such as ATP, COX, NADUF and UQCR. In line with this, we show evidence of ODE-mediated decrease in cellular glucose uptake and glycolytic ability in both acute and chronic exposure models, while lack of or neutralization of HMGB1 increased the cellular glucose uptake and glycolytic ability. This metabolic profile in NHBE cells may have a direct impact on the maintenance of overall lung homeostasis and function on exposure to ODE *in vivo* (Wu et al. 1999; Koopman et al. 2005; Dranka et al. 2011; Agrawal and Mabalirajan 2015).

Reduced oxygen availability elicited by hypoxia and mitochondrial dysfunction leads to increased production of ROS by the electron transport chain (Baik and Jain 2020). Considering the increased intercellular ROS and downregulation of ETC, we observed the hypoxia response on ODE exposure. Interestingly, we observed a decrease in HIF1α expression in 24 h ODE exposed NHBE cells while it increases in cells lacking HMGB1, indicative of hypoxia. Cellular studies suggest that HIF1α activation could rescue the effects of ETC deficiency in mitochondrial diseases

(Jain et al. 2016). Hypoxia may be triggering a HIF-dependent transcriptional program activating key pathways promoting glycolysis, ATP production and decreased ROS generation. This would also be reducing the levels of O_2 being taken up by the cell which would, in turn, decrease the availability of substrate for free radical production and aberrant cellular signaling. We observed that, HMGB1 neutralization resulted in the normoxic conditions in the repeated ODE exposure model. Hence, we can theorize that short-term hypoxic conditions may be beneficial in reversing mitochondrial dysfunction.

In addition, using an ALI model of ODE exposure, we investigated the impact of HMGB1 on tight junction integrity. Previously we have shown the impact of 24 h ODE exposure on tight junction expression *in vivo*, but the role of HMGB1 remains to be investigated (Shrestha et al. 2021). In this study, we observe a significant decrease in transepithelial electrical resistance (TEER) with repeated ODE exposure as early as 12 hours post-exposure. Although HMGB1 neutralization does not reverse the effect of ODE on tight junction integrity, the TEER values plateau and remain unchanged 1 day post exposure. The neutralization of HMGB1 does not significantly rescue ODE-induced decrease in TEER. However, it is evident that, there is evidence of certain amount of protection of epithelial integrity. This was corroborated by the measurement of claudin-1 and occludin, indicating that ODE exposure directly affects the tight junction integrity. Although this is valid preliminary evidence on the impact of ODE on tight junction integrity, thorough *in vivo* work needs to be performed to confirm this finding.

In summary, the results of the present study indicate that targeting HMGB1 in ODE induced inflammatory process promotes mitochondrial biogenesis and metabolism by promoting hypoxic conditions and decreasing ROS production. It is likely that blocking HMGB1 release following ODE exposure leads to a coordinated adaptive response in NHBE cells involving

mitochondrial fragmentation, increased mitochondrial biogenesis, and mitochondrial metabolism. As a result, the maximum O_2 consumption and ROS production per mitochondrion are reduced, while the demand for ATP synthesis is still met. Future studies using HMGB1 airway epithelial cell-specific conditional knock-out mice or systemic neutralization of HMGB1 may unravel further mechanistic basis of targeting HMGB1 in rescuing ODE-induced mitochondrial deficits.

Materials and Methods

Chemicals and reagents

We purchased normal human bronchial epithelial cell (NHBE) – growth medium (Pneumacult-Ex media; BEGM) and differentiation media (Pneumacult-ALI media) from StemCell Technologies. MTT, CM-H_2DCFDA, 2-NBDG, MitoTracker green, and MitoSox Red dyes were purchased from Invitrogen (ThermoFisher Scientific) and Rhod-2AM dye was obtained from Abcam. Griess' reagent was purchased from Sigma-Aldrich. Antibodies used and their details have been listed in Tables 5.7 and 5.8. Primers used and their sequences are listed in Table 5.5 and were made in Iowa State University. TaqMan® Gene Expression Assay was purchased from Invitrogen (ThermoFisher Scientific). HMGB1 siRNA kit was purchased from Integrated DNA Technologies (IDT) and Anti-HMGB1 neutralizing antibody (Batch # Q2g7-47C, stock concentration 1.8 mg/mL) was a generous gift from Dr. Kevin Tracey's laboratory (Feinstein Institutes for Medical Research, Northwell Health, NY).

Organic dust extract preparation

Organic dust (OD) was collected and an aqueous extract was prepared as previously described (Romberger et al. 2002; Bhat et al. 2019). Settled surface dust samples from swine housing facilities were collected and 1 g was placed into sterile Hank's Balanced Salt Solution (10 mL; Gibco). The solution was incubated for one hour at room temperature, centrifuged for 20 min at 1365 x g to remove the larger coarse particles and microbes. The final supernatant was

filter-sterilized (0.22 μm), a process that also removes coarse particles. Stock (100%) ODE aliquots frozen at -20°C until use in experiments. The filter-sterilized organic dust extract (ODE) samples were considered 100% and diluted to 1-5% (v/v) before use in experiments.

Endotoxin estimation

The levels of endotoxin in the ODE samples were quantified using the Pyrochrome® chromogenic endotoxin assay kit (Associates of Cape Cod, Inc., East Falmouth, MA). The ODE samples were diluted in a ratio of 1:10 in endotoxin-free water. The samples along with reconstituted pyrochrome lysate were added to an endotoxin 96-well plate in a sample to lysate ratio of 1:4. The standard was reconstituted as per the manufacturer's recommendation and added to the plate in a sample to lysate ratio of 1:4. The microplate was incubated at 37°C with shaking and the absorbance was read at 405 nm (every 10 minutes, three readings over a total of 30 minutes) using the Gen 5™ software in BioTek® ELx808™ spectrophotometer.

Cell culture and treatments

The de-identified human primary airway epithelial cells were obtained from the Mayo Clinic, Rochester, MN. These cells were collected at the Mayo Clinic under an approved Institutional Review Board (IRB) protocol and tissues from those patients undergoing thoracic surgeries for focal, non-infectious causes were collected. A trained pathologist identified the normal lung areas and airway epithelial cells were isolated from the third to sixth generation human bronchi. Iowa State University's Institutional Review Board considered these de-identified cells as exempt from approval. De-identified Normal human bronchial epithelial (NHBE) cells were also received through Dr. Kristina L. Bailey (University of Nebraska Medical Center, Omaha, NE). The NHBE cells were isolated from the human donors through the Live on Nebraska, an organ and tissue donation program. All the donors were deceased and an informed consent from the relatives was obtained by the Live on Nebraska. These de-identified NHBE cells were exempt

from the Iowa State University's Institutional Review Board (IRB) approval. All the work was performed under an approved protocol from the Iowa State University's Institutional Biosafety Committee (IBC) approved protocol (IBC 19-004).

NHBE cells were seeded onto type-I bovine collagen (30 µg/mL; StemCell Technologies) coated T-75 flasks. Cells were grown submerged in BEGM (Pneumacult-EX) supplemented with 50X growth supplement (StemCell Technologies), 100 IU/mL penicillin, 100 µg/mL streptomycin (Gibco) and 1 µg/mL of Amphotericin B (Sigma-Aldrich). The cells were incubated in a humidified chamber with 5% CO_2 at 37˚C until approximately around 60-70% confluence was achieved. All groups with treatment details are outlined in Table 5.2.

The stock and working concentrations of the treatments are outlined in Table 5.3. Our *in vitro* model of ODE exposure and treatments are represented in Table 5.2a and 5.2b. Cells were treated with either medium (control) or ODE (1% v/v) after HMGB1-specific siRNA mediated knock-down or co-treatment with anti-HMGB1 antibody for 24 hours (acute exposure) or 8 hours a day for 5 days (chronic exposure), respectively, with corresponding time-matched controls. Following treatments, samples were processed for various assays.

Table 5.3 Stock and working concentrations of treatments

Treatment	Stock concentration	Working concentration (in BEGM/DPBS)
ODE	100% in HBSS	1%
Anti-HMGB1 neutralization Antibody	1.8 mg/mL	10 µg/mL

Air-Liquid Interface culture and treatment

After subculture of NHBE cells were seeded onto 10.5 mm trans-well inserts (polyester membrane inserts with 0.4 µm sized pores; Corning) coated with type-I bovine collagen (30 µg/mL; StemCell Technologies) in 12-well plates. Cells were seeded at a density of ~5 x 10^3/mm^2 in Pneumacult-EX expansion media (StemCell Technologies) onto the apical side of the insert,

with the media in the basal chamber as well. The cells were maintained in the submerged culture conditions for 2-3 days incubated in a humidified chamber with 5% CO2 at 37˚C until a confluent monolayer was developed. Fresh medium (0.5 mL in the apical chamber and 1.0 mL in the basal chamber) was added every 48 hours to replace spent media. Following attaining confluence (~80%), the expansion media in the apical and basal side was carefully removed and an ALI was developed by addition of the Pneumacult-ALI differentiation media (StemCell Technologies) in the basal chamber alone and incubated in a humidified chamber with 5% CO_2 at 37˚C. Post airlift the cells were maintained for not more than 20 days. Fresh medium (1.0 mL in the basal chamber) was replenished every 48 hours and the apical surface of the monolayer was washed with DPBS twice every 48 hours to prevent mucus build-up.

Post differentiation, the apical surface of the cells was treated with either medium (control) or ODE (1% v/v) followed by a co-treatment with either Anti-HMGB1 neutralization antibody (10 µg/mL) or isotype-matched IgG controls (corresponding time-matched control) for 1 hour per day for 5 days. Following the treatments, samples were processed after 5 days for various assays. The exposure and treatments are outlined in Table 5.2c.

siRNA mediated knockdown of HMGB1

Three (R1, R2 and R3) custom designed double-stranded anti-HMGB1 siRNAs (DsiRNA), scrambled RNA (negative control, NC), HPRT1 DsiRNA (positive control) and a fluorescent transfection control (TYE563) were purchased (Integrated DNA Technologies Inc.) to maximize the probability of achieving successful HMGB1 knockdown. Lipofectamine 2000 (ThermoFisher) was used to transfect DsiRNA into the NHBE cells. Sequences of siRNAs and NC siRNA are listed in Table 5.4.

To perform transfection with various siRNAs, NHBE cells were cultured BEGM without antibiotics. For each transfection, 1 nM of (DsiRNA) for HMGB1, scrambled RNA (negative

control), HPRT1 DsiRNA (positive control) and a fluorescent transfection control (TYE563) were diluted in Opti-MEM media and gently mixed with Lipofectamine 2000 according to the manufacturer's instructions and protocols previously published (Chang et al. 2012). Following incubation for 20 min at room temperature, the transfection mixture was added to the cells and the cells were further incubated at 37°C for 24 hours. Knockdown was confirmed by qRT-PCR and western blot analysis of the target gene and protein, respectively (Figure 5.12). Transfection was confirmed by performing immunocytochemistry (ICC) for TYE563 (fluorescent transfection control) and imaged using Nikon Eclipse TE2000-U inverted fluorescence microscope (Nikon, Tokyo, Japan). Images were processed using HCImage live 4 software (Hamamatsu Corporation, Sewickley, PA).

Cell viability assay and MTT assay

Before conducting experiments, cell viability was assessed. Live/dead cell count was determined by 4% trypan blue dye (EMD Millipore) exclusion and percentage viability was calculated. The population of cells with more than 95% viability was used for the experiments.

The MTT assay has been widely used in the estimation of LC_{50} and cell viability by measuring the formazan produced when mitochondrial dehydrogenase enzymes cleave the tetrazolium ring (Latchoumycandane et al. 2005). We used the MTT assay to determine the LC_{50} of the treatment groups in NHBE cells listed in Table 5.2a and 5.2b. Cells were seeded (20,000 cells/well) in a 96-well culture plate and treated for 24 hours and 8 hours/day for 5 days. After the treatment, the cells were washed with PBS and incubated with 200 µl of 0.25% (w/v) MTT in BEGM for 3 hours at 37°C. The supernatant was removed, and MTT crystals were solubilized in 200 µl of dimethyl sulfoxide. Mitochondrial activity was measured by quantifying fluorescence using SpectraMax spectrophotometer (Molecular Devices Corporation) at 570 nm with the reference wavelength at 630 nm.

Transmission Electron Microscopy

For transmission electron microscopy (TEM), cells were seeded ($1x10^6$ cells/well) in 12-well plates with Poly D-lysine hydrobromide (Sigma-Aldrich, St. Louis, MO) coated coverslips and chronically exposed to the treatments as outlined in Table 5.2b. Post-treatment NHBE cells were washed twice with DPBS and fixed with 3% glutaraldehyde (w/v) and 1% paraformaldehyde (w/v) in 0.1M cacodylate buffer, pH 7.4 for 48 hours at 4°C. Coverslips were rinsed 3 times in 0.1M cacodylate buffer and then post-fixed in 1% osmium tetroxide in 0.1 M cacodylate buffer for 1 hour (room temp.) The samples were rinsed in deionized distilled water and en bloc stained with 2% aqueous uranyl acetate for 30 min., dehydrated in a graded ethanol series, cleared with ultra-pure acetone, infiltrated and embedded using EmBed (EPON) formula epoxy resin (Electron Microscopy Sciences, Ft. Washington, PA) by inverting onto BEEM® capsules. Resin blocks were polymerized for 48 hours at 65°C. Coverslips were separated from the resin by using liquid nitrogen, trapping the cell monolayer in the resin. Thick and ultrathin sections were made using a Leica UC6 ultramicrotome (North Central Instruments, Minneapolis, MN). Ultrathin sections were collected onto copper grids and images were captured using a JEOL 2100 scanning and transmission electron microscope (Japan Electron Optic Laboratories, Peabody, MA) with a Gatan OneView 4K camera (Gatan inc., Pleasanton, CA).

Immunofluorescence microscopy

Cells were seeded ($1x10^6$ cells/well) in 12-well plates with Poly D-lysine hydrobromide (Sigma-Aldrich, St. Louis, MO) coated coverslips and exposed to the treatments as outlined in Table 5.2a and 5.2b. At the respective time points, the media was removed, and cells were washed with 1x PBS. Cells were fixed with 4% paraformaldehyde in PBS for 20 minutes at room temperature and washed with PBS. Cells were blocked for an hour using a blocking solution containing 10% normal donkey serum (EMD Millipore, Burlington, MA), 0.2% triton X 100 and

PBS. Coverslips with cells were incubated with anti-HMGB1 (1:1000 dilution, rabbit polyclonal) antibody in antibody diluent solution (2.5% normal donkey serum, 0.25% sodium azide, 0.2% triton X 100, PBS) (AbCam, Cambridge, MA) with overnight incubation at 4º C. Next, coverslips were incubated with donkey anti-rabbit biotin-conjugated secondary antibody (1:400, diluted in antibody diluent, HMGB1) (Jackson Immunoresearch, West Grove, PA) for an hour at room temperature. Next, 1:300 dilution of streptavidin Cy3 in PBS (HMGB1) was added. Coverslips were mounted onto slides using VECTASHIELD antifade mounting medium with 4',6-Diamidino-2-Phenylindole, Dihydrochloride (DAPI, Vector Labs, Burlingame, CA) and imaged using Nikon Eclipse TE2000-U inverted fluorescence microscope (Nikon, Tokyo, Japan). Images were processed using HCImage live 4 software (Hamamatsu Corporation, Sewickley, PA).

Subcellular fractionation

Whole-cell and subcellular protein lysate extractions (cytosol and MT) were performed at 4°C using cold reagents. For whole-cell protein lysates, cell pellets were subjected to lysis using RIPA buffer with HALT protease and phosphatase inhibitor (ThermoFisher Scientific). Subcellular fractionation of cell pellets for isolation of mitochondria was done using the Mitochondria Isolation Kit for Cultured Cells (ThermoFisher Scientific) according to the manufacturer's instructions. The cytosolic fraction and isolated mitochondria were lysed with RIPA buffer [with protease and phosphatase inhibitors] for 30 min at 4°C and periodic sonication on ice, followed by centrifugation to collect lysate. Protein concentrations of fraction were determined by Bradford assay (Bio-Rad) and were stored at −80°C until use.

mtDNA isolation and long-range PCR

To determine mitochondrial DNA (mtDNA) leakage into cellular cytosol, mtDNA was isolated from mitochondria-free cytosolic fraction of the cells using the Genomic DNA Purification kit (ThermoFisher Scientific) as per the manufacturer’s instructions. The purity and

concentration of the isolated DNA was measured using NanoVue Plus spectrophotometer (GE Healthcare, UK). Due to low concentrations, the mtDNA was first amplified using long-range PCR and the primers used are listed in Table 5.5. PCR reactions were performed at 94°C for 1 min followed by 30 cycles at 98°C for 10 s, 60°C for 40 s, 68°C for 16 min and a final elongation for 10 min (Liu et al. 2015). The presence of mtDNA was confirmed by separating the PCR product by electrophoresis on a 0.8% agarose gel stained with ethidium bromide. The concentration of amplified mtDNA obtained was adjusted to ensure equal amounts of template mtDNA in each sample used for qPCR reaction.

Real Time – qPCR

Total RNA was isolated using TRIzol extraction methods (Seo et al. 2014) and RNA concentration was measured using NanoVue Plus spectrophotometer (GE Healthcare, UK). 1 µg of RNA was used to synthesize cDNA using the High-Capacity cDNA Reverse Transcription Kit (ThermoFisher Scientific) following the manufacturer's instructions. qRT-PCR was performed using 500 ng of cDNA in a 10 µL reaction volume for each target in triplicates. The housekeeping gene 16s rRNA (for mtDNA fold change) and 18S rRNA (ThermoFisher Scientific) was used. No-template controls and dissociation curves were run for all reactions to exclude cross-contamination. The primers for genes of interest listed in Table 5.5 were synthesized at Iowa State University's DNA Facility. The qRT-PCR reactions were run in a QuantiStudio-3™ (Thermofisher Scientific) detection system and the data was analyzed using $2^{-\Delta\Delta CT}$ method (Livak and Schmittgen).

Targeted gene array

qRT-PCR using TaqMan® Gene Expression Assays (Life Technologies, Carlsbad, CA) was performed for the 96 targets specific for human mitochondrial energy metabolism listed in Table 5.6. 500 ng of cDNA in a 10 µL reaction volume was prepared for each target in duplicates.

The reaction conditions were as follows: 50°C for 2 minutes, 95°C for 2 minutes, followed by 40 cycles at 95°C for 1 second, and 60°C for 20 seconds. Data analysis was performed using the relative quantification app on ThermoFisher cloud and analyzed using $2^{-\Delta\Delta CT}$ method (Livak and Schmittgen 2001). The genes with a fold change of ≥10 and ≤10 were selected and represented on a heat map. Using the Kyoto Encyclopedia of Genes and Genomes (KEGG) database, upregulated and downregulated pathways with significantly altered mRNA transcripts with FDR corrected p-value cut-off <0.05 were selected and represented by gene counts.

Western blot analysis

Lysates (whole cell, cytosol and MT) containing equal amounts of protein (20 μg/sample), along with a molecular weight marker (Bio-Rad), were run on 10–15% sodium dodecyl sulfate/polyacrylamide gel electrophoresis (SDS-PAGE) as previously described (Bhat et al. 2019). Proteins were transferred to a nitrocellulose membrane and nonspecific binding sites were blocked with Licor Odyssey blocking buffer. The membranes were then incubated with different primary antibodies and dilutions listed in Table 5.7. Next, membranes were incubated with one of the following secondary antibodies: Alexa Fluor 680 goat anti-mouse, Alexa Fluor 680 donkey anti-rabbit, or IRDye 800CW donkey anti-rabbit (1:10,000; LI-COR). To confirm equal protein loading, blots were probed with relevant housekeeping proteins listed in Table 5.7. Western blot images were captured using Odyssey® CLx IR imaging system (LI-COR Biotechnology) and analysis was performed using ImageJ program (National Institutes of Health).

Intracellular reactive oxygen species

Intracellular reactive oxygen species (ROS) production was measured using chloromethyl derivative of dichlorodihydrofluorescein diacetate (CM-H_2DCFDA) (ThermoFisher Scientific, USA). A working solution of 10 μM of DCFDA in DPBS was used. NHBE cells (50,000 cells/well) were seeded in a 96 well plate and incubated in a 5% CO_2 incubator to reach confluence.

The cells were incubated with CM-H_2DCFDA working solution at 37°C for 30 min, following treatments as outlined in Table 5.2a. The cells were then washed and fluorescence intensity of the oxidized form of H_2DCFDA was measured at excitation/emission wavelengths of 488/535 nm using SpectraMax spectrophotometer (Molecular Devices Corporation). The results were expressed as mean fluorescence intensity relative to control.

Mitochondrial activity and mitochondrial superoxide

NHBE cells were seeded (50,000 cells/well) in a 96-well culture plate and treated as outlined in Table 5.2a and 5.2b. After treatment, the media was removed and 100 µl of 200 nM MitoTracker green and 5 µM MitoSOX red dye diluted in BEGM was added into each well and incubated at 37°C for 15 min. Following incubation, the cells were washed with DPBS and fluorescence intensity was measured by spectrophotometer reading taken at excitation/emission wavelengths of 485/520 nm and 510/580 nm, respectively, SpectraMax spectrophotometer (Molecular Devices Corporation). The results were expressed as percentage fluorescence relative to control.

NHBE cells were also seeded ($1x10^6$ cells/well) in 12-well plates with Poly D-lysine hydrobromide (Sigma-Aldrich, St. Louis, MO) coated coverslips and exposed to the treatments as outlined in Table 5.2a and 5.25.1b. At the respective time points, the media was removed, and cells were washed with DPBS. These were stained with MitoTracker Red CMXRos (200 nM) and incubated at 37°C for 15 min. The cells were washed with DPBS and fixed with 4% paraformaldehyde in PBS for 20 minutes at room temperature and washed with PBS again. Coverslips were mounted onto slides using VECTASHIELD antifade mounting medium with 4',6-Diamidino-2-Phenylindole, Dihydrochloride (DAPI, Vector Labs, Burlingame, CA) and imaged using Nikon Eclipse TE2000-U inverted fluorescence microscope (Nikon, Tokyo, Japan). Images were processed using HCImage live 4 software (Hamamatsu Corporation, Sewickley, PA).

Mitochondrial glucose uptake

Cellular glucose uptake by NHBE cells was measured using fluorescent d-glucose analog 2-[N-(7-nitrobenz-2-oxa-1,3-diazol-4-yl) amino]-2-deoxy-D-glucose (2-NBDG) (Zou et al. 2005). Cells were seeded (50,000 cells/well) in a 96-well culture plate and treated as outlined in Table 5.2a and 5.2b. After treatment, the media was removed and 100 µL of 50 µg/mL 2-FITC labeled NBDG in BEGM was added into each well and incubated at 37°C for 20 min. Following incubation, the cells were washed with DPBS and fluorescence intensity was measured by spectrophotometer reading taken at an at excitation/emission wavelengths of 465/540 nm using SpectraMax spectrophotometer (Molecular Devices Corporation). The results were expressed as percentage fluorescence relative to control.

Mitochondrial calcium influx

Mitochondrial calcium influx ($[Ca^{2+}]_{mito}$) in NHBE cells was measured using the Rhod-2AM dye. After treatment, the mitochondria were isolated using the Mitochondria Isolation Kit for Cultured Cells (ThermoFisher Scientific) was measured by Bradford assay to maintain consistency in the number of mitochondria loaded into the wells of a 96-well plate. A protein concentration of 100 µg was loaded into each well and Rhod-2AM (Abcam, 10 µM) dye was added and incubated at 37°C for 30 minutes to stain the mitochondria. The plate was later read at an excitation/emission wavelengths of 552/581 nm using SpectraMax spectrophotometer (Molecular Devices Corporation).

NHBE cells were also seeded ($1x10^6$ cells/well) in 12-well plates with Poly D-lysine hydrobromide (Sigma-Aldrich, St. Louis, MO) coated coverslips and exposed to the treatments as outlined in Table 5.2a and 5.2b. At the respective time points, the media was removed, and cells were washed with DPBS. These were stained with Rhod-2AM (Abcam, 10 µM) and incubated at 37°C for 30 min. The cells were washed with DPBS and fixed with 4% paraformaldehyde in PBS

for 20 minutes at room temperature and washed with PBS again. Coverslips were mounted onto slides using VECTASHIELD antifade mounting medium with 4',6-Diamidino-2-Phenylindole, Dihydrochloride (DAPI, Vector Labs, Burlingame, CA) and imaged using EVOS M5000 imaging system (ThermoFisher Scientific).

Griess assay

Griess assay was performed as described (Gordon et al. 2011). Concentration of secreted nitric oxide was measured (representing reactive nitrogen species (RNS)) as nitrite levels in cell culture media using Griess reagent (Sigma-Aldrich) and sodium nitrite standard curve, prepared using a stock solution of 200 µM. The assay was performed in a 96 well-plate and absorbance was measured at 550 nm using SpectraMax spectrophotometer (Molecular Devices Corporation). The results were expressed as µM concentration of nitrite secreted.

Trans-epithelial electrical resistance (TEER)

TEER is the potential difference across the epithelium, which is a measure of the tightness of the cell-cell contacts within the epithelium. This is measured using a pair of electrodes (Srinivasan et al. 2015). NHBE cells were plated on 10.5mm trans-well inserts in a 12 well plate and allowed to grow. Cell confluence was monitored by TEER measurements with the Epithelial Voltohmmeter 2 (EVOM2, WPI, Sarasota, FL). The value obtained is an indication of the integrity of the epithelial cell monolayers. Once TEER value reached a steady state, treatments outlined in Table 5.2c were added to the apical surface of the cells and TEER measurements were performed every 12 hours for 5 days. The mean of four measurements per insert was calculated. The electrical resistance of inserts without cells was subtracted from all samples, and the resistance values obtained was multiplied with the surface area of the inserts for measuring the TEER values ($\Omega.cm^2$).

Statistical analysis

Data analysis was performed using GraphPad Prism 8.0 software (La Jolla, CA, USA). Raw data were analyzed with either Student's t-test or using one-way ANOVA, and Tukey's posttest was performed to compare all treatment groups. A p-value of < 0.05 was considered statistically significant. *$p < 0.05$, **$p < 0.01$, ***$p < 0.001$, ****$p < 0.0001$. * indicates different from control. Samples for all assays were derived from the same experiment and were processed in parallel.

Acknowledgements

We would like to thank Tracey Stewart at Iowa State University's Roy J. Carver High Resolution Microscopy Facility for assistance with transmission electron microscopy. We would like to thank Dr. Kevin Tracey (Feinstein Institutes for Medical Research, Northwell Health, NY) for providing us with the anti-HMGB1 neutralization antibody and Dr. Y.S. Prakash (Mayo Clinic, Rochester, MN) and Dr. K. L. Bailey (UNMC, Omaha, NE) for providing us with normal human bronchial epithelial cells when needed. We would also like to thank the department of biomedical sciences and Dr. M. Cho at Iowa State University for providing us with access to necessary equipment.

Potential Conflicts of Interest

The terms of this arrangement have been reviewed and approved by Iowa State University per its conflict-of-interest policies. All other authors have declared no potential conflicts of interest.

Funding

C.C. laboratory is funded through startup grant through Iowa State University, a pilot grant (5 U54 OH007548) from CDC-NIOSH (Centers for Disease Control and Prevention-The National

Institute for Occupational Safety and Health) and a seed grant though CVM (College of Veterinary Medicine) at Iowa State University.

References

Aghapour, M., Remels, A.H.V., Pouwels, S.D., Bruder, D., Hiemstra, P.S., Cloonan, S.M., Heijink, I.H., 2019. Mitochondria: at the crossroads of regulating lung epithelial cell function in chronic obstructive pulmonary disease. American Journal of Physiology-Lung Cellular and Molecular Physiology 318, L149–L164. https://doi.org/10.1152/ajplung.00329.2019

Agrawal, A., Mabalirajan, U., 2015. Rejuvenating cellular respiration for optimizing respiratory function: targeting mitochondria. American Journal of Physiology-Lung Cellular and Molecular Physiology 310, L103–L113. https://doi.org/10.1152/ajplung.00320.2015

An, J., Jr, H., Aj, N., Jd, D., J, K., Mj, D., Gm, T., B, K., Ab, S., R, G., Sc, G., Y, T., Dj, R., T, K., Ja, P., 2020. MyD88 regulates a prolonged adaptation response to environmental dust exposure-induced lung disease. Respir Res 21, 97–97. https://doi.org/10.1186/s12931-020-01362-8

Baik, A.H., Jain, I.H., 2020. Turning the Oxygen Dial: Balancing the Highs and Lows. Trends in Cell Biology 30, 516–536. https://doi.org/10.1016/j.tcb.2020.04.005

Bailey, K.L., Poole, J.A., Mathisen, T.L., Wyatt, T.A., Von Essen, S.G., Romberger, D.J., 2008. Toll-like receptor 2 is upregulated by hog confinement dust in an IL-6-dependent manner in the airway epithelium. American Journal of Physiology-Lung Cellular and Molecular Physiology 294, L1049–L1054. https://doi.org/10.1152/ajplung.00526.2007

Bhat, S.M., Massey, N., Karriker, L.A., Singh, B., Charavaryamath, C., 2019. Ethyl pyruvate reduces organic dust-induced airway inflammation by targeting HMGB1-RAGE signaling. Respiratory Research 20, 27. https://doi.org/10.1186/s12931-019-0992-3

Brookes, P.S., Yoon, Y., Robotham, J.L., Anders, M.W., Sheu, S.-S., 2004. Calcium, ATP, and ROS: a mitochondrial love-hate triangle. American Journal of Physiology-Cell Physiology 287, C817–C833. https://doi.org/10.1152/ajpcell.00139.2004

Cai, J., Yang, J., Jones, DeanP., 1998. Mitochondrial control of apoptosis: the role of cytochrome c. Biochimica et Biophysica Acta (BBA) - Bioenergetics 1366, 139–149. https://doi.org/10.1016/S0005-2728(98)00109-1

Cantaert, T., Baeten, D., Tak, P.P., van Baarsen, L.G., 2010. Type I IFN and TNFα cross-regulation in immune-mediated inflammatory disease: basic concepts and clinical relevance. Arthritis Research & Therapy 12, 219. https://doi.org/10.1186/ar3150

Chang, K., Marran, K., Valentine, A., Hannon, G.J., 2012. RNAi in Cultured Mammalian Cells Using Synthetic siRNAs. Cold Spring Harb Protoc 2012, pdb.prot071076. https://doi.org/10.1101/pdb.prot071076

Charavaryamath, C., Singh, B., 2006. Pulmonary effects of exposure to pig barn air. J Occup Med Toxicol 1, 10. https://doi.org/10.1186/1745-6673-1-10

CHAUNG, W.W., WU, R., JI, Y., DONG, W., WANG, P., 2012. Mitochondrial transcription factor A is a proinflammatory mediator in hemorrhagic shock. Int J Mol Med 30, 199–203. https://doi.org/10.3892/ijmm.2012.959

Chen, H., Detmer, S.A., Ewald, A.J., Griffin, E.E., Fraser, S.E., Chan, D.C., 2003. Mitofusins Mfn1 and Mfn2 coordinately regulate mitochondrial fusion and are essential for embryonic development. J Cell Biol 160, 189–200. https://doi.org/10.1083/jcb.200211046

Chen, Q., Sun, L., Chen, Z.J., 2016. Regulation and function of the cGAS–STING pathway of cytosolic DNA sensing. Nature Immunology 17, 1142–1149. https://doi.org/10.1038/ni.3558

Cloonan, S.M., Choi, A.M., 2012. Mitochondria: commanders of innate immunity and disease? Current Opinion in Immunology, Innate immunity / Antigen processing 24, 32–40. https://doi.org/10.1016/j.coi.2011.11.001

Cloonan, S.M., Choi, A.M.K., 2016. Mitochondria in lung disease. J Clin Invest 126, 809–820. https://doi.org/10.1172/JCI81113

Cloonan, S.M., Kim, K., Esteves, P., Trian, T., Barnes, P.J., 2020. Mitochondrial dysfunction in lung ageing and disease. European Respiratory Review 29. https://doi.org/10.1183/16000617.0165-2020

Ding, W.-X., Yin, X.-M., 2012. Mitophagy: mechanisms, pathophysiological roles, and analysis. Biol Chem 393, 547–564. https://doi.org/10.1515/hsz-2012-0119

Dranka, B.P., Benavides, G.A., Diers, A.R., Giordano, S., Zelickson, B.R., Reily, C., Zou, L., Chatham, J.C., Hill, B.G., Zhang, J., Landar, A., Darley-Usmar, V.M., 2011. Assessing bioenergetic function in response to oxidative stress by metabolic profiling. Free Radical Biology and Medicine 51, 1621–1635. https://doi.org/10.1016/j.freeradbiomed.2011.08.005

Eisner, V., Picard, M., Hajnóczky, G., 2018. Mitochondrial dynamics in adaptive and maladaptive cellular stress responses. Nature Cell Biology 20, 755–765. https://doi.org/10.1038/s41556-018-0133-0

Fetterman, J.L., Sammy, M.J., Ballinger, S.W., 2017. Mitochondrial Toxicity of Tobacco Smoke and Air Pollution. Toxicology 391, 18–33. https://doi.org/10.1016/j.tox.2017.08.002

Finkel, T., Menazza, S., Holmström, K.M., Parks, R.J., Liu, Julia, Sun, J., Liu, Jie, Pan, X., Murphy, E., 2015. The Ins and Outs of Mitochondrial Calcium. Circ Res 116, 1810–1819. https://doi.org/10.1161/CIRCRESAHA.116.305484

García, N., Chávez, E., 2007. Mitochondrial DNA fragments released through the permeability transition pore correspond to specific gene size. Life Sciences 81, 1160–1166. https://doi.org/10.1016/j.lfs.2007.08.019

Gordon, R., Hogan, C.E., Neal, M.L., Anantharam, V., Kanthasamy, A.G., Kanthasamy, A., 2011. A simple magnetic separation method for high-yield isolation of pure primary microglia. J. Neurosci. Methods 194, 287–296. https://doi.org/10.1016/j.jneumeth.2010.11.001

Hajnóczky, G., Saotome, M., Csordás, G., Weaver, D., Yi, M., 2007. Calcium Signalling and Mitochondrial Motility, in: Mitochondrial Biology: New Perspectives. John Wiley & Sons, Ltd, pp. 105–121. https://doi.org/10.1002/9780470725207.ch8

Handschin, C., Spiegelman, B.M., 2006. Peroxisome Proliferator-Activated Receptor γ Coactivator 1 Coactivators, Energy Homeostasis, and Metabolism. Endocrine Reviews 27, 728–735. https://doi.org/10.1210/er.2006-0037

Huang, C.-Y., Chiang, S.-F., Chen, W.T.-L., Ke, T.-W., Chen, T.-W., You, Y.-S., Lin, C.-Y., Chao, K.S.C., Huang, C.-Y., 2018. HMGB1 promotes ERK-mediated mitochondrial Drp1 phosphorylation for chemoresistance through RAGE in colorectal cancer. Cell Death & Disease 9, 1–15. https://doi.org/10.1038/s41419-018-1019-6

Jain, I.H., Zazzeron, L., Goli, R., Alexa, K., Schatzman-Bone, S., Dhillon, H., Goldberger, O., Peng, J., Shalem, O., Sanjana, N.E., Zhang, F., Goessling, W., Zapol, W.M., Mootha, V.K., 2016. Hypoxia as a therapy for mitochondrial disease. Science 352, 54–61. https://doi.org/10.1126/science.aad9642

Julian, M.W., Shao, G., Vangundy, Z.C., Papenfuss, T.L., Crouser, E.D., 2013. Mitochondrial transcription factor A, an endogenous danger signal, promotes TNFα release via RAGE- and TLR9-responsive plasmacytoid dendritic cells. PLoS ONE 8, e72354. https://doi.org/10.1371/journal.pone.0072354

Kelly, K.J., Poole, J.A., 2019. Pollutants in the workplace: Effect on occupational asthma. Journal of Allergy and Clinical Immunology 143, 2014–2015. https://doi.org/10.1016/j.jaci.2019.04.013

Kim, J.-Y., Cho, J.-J., Ha, J., Park, J.-H., 2002. The Carboxy Terminal C-Tail of BNip3 Is Crucial in Induction of Mitochondrial Permeability Transition in Isolated Mitochondria. Archives of Biochemistry and Biophysics 398, 147–152. https://doi.org/10.1006/abbi.2001.2673

Koopman, W.J.H., Visch, H.-J., Verkaart, S., van den Heuvel, L.W.P.J., Smeitink, J.A.M., Willems, P.H.G.M., 2005. Mitochondrial network complexity and pathological decrease in complex I activity are tightly correlated in isolated human complex I deficiency. American Journal of Physiology-Cell Physiology 289, C881–C890. https://doi.org/10.1152/ajpcell.00104.2005

Landes, T., Emorine, L.J., Courilleau, D., Rojo, M., Belenguer, P., Arnauné-Pelloquin, L., 2010. The BH3-only Bnip3 binds to the dynamin Opa1 to promote mitochondrial fragmentation and apoptosis by distinct mechanisms. EMBO reports 11, 459–465. https://doi.org/10.1038/embor.2010.50

Latchoumycandane, C., Anantharam, V., Kitazawa, M., Yang, Y., Kanthasamy, A., Kanthasamy, A.G., 2005. Protein kinase Cdelta is a key downstream mediator of manganese-induced apoptosis in dopaminergic neuronal cells. J. Pharmacol. Exp. Ther. 313, 46–55. https://doi.org/10.1124/jpet.104.078469

Lee, H.-C., Wei, Y.-H., 2005. Mitochondrial biogenesis and mitochondrial DNA maintenance of mammalian cells under oxidative stress. The International Journal of Biochemistry & Cell Biology 37, 822–834. https://doi.org/10.1016/j.biocel.2004.09.010

Lee, Y., Jeong, S.-Y., Karbowski, M., Smith, C.L., Youle, R.J., 2004. Roles of the Mammalian Mitochondrial Fission and Fusion Mediators Fis1, Drp1, and Opa1 in Apoptosis. MBoC 15, 5001–5011. https://doi.org/10.1091/mbc.e04-04-0294

Liesa, M., Palacín, M., Zorzano, A., 2009. Mitochondrial Dynamics in Mammalian Health and Disease. Physiological Reviews 89, 799–845. https://doi.org/10.1152/physrev.00030.2008

Liu, J., Fang, H., Chi, Z., Wu, Z., Wei, D., Mo, D., Niu, K., Balajee, A.S., Hei, T.K., Nie, L., Zhao, Y., 2015. XPD localizes in mitochondria and protects the mitochondrial genome from oxidative DNA damage. Nucleic Acids Res 43, 5476–5488. https://doi.org/10.1093/nar/gkv472

Livak, K.J., Schmittgen, T.D., 2001. Analysis of Relative Gene Expression Data Using Real-Time Quantitative PCR and the 2−ΔΔCT Method. Methods 25, 402–408. https://doi.org/10.1006/meth.2001.1262

MacVicar, T., Langer, T., 2016. OPA1 processing in cell death and disease – the long and short of it. J Cell Sci 129, 2297–2306. https://doi.org/10.1242/jcs.159186

Mahadev Bhat, S., Shrestha, D., Massey, N., Karriker, L.A., Kanthasamy, A.G., Charavaryamath, C., 2021. Organic dust exposure induces stress response and mitochondrial dysfunction in monocytic cells. Histochem Cell Biol. https://doi.org/10.1007/s00418-021-01978-x

Massey, N., Puttachary, S., Bhat, S.M., Kanthasamy, A.G., Charavaryamath, C., 2019. HMGB1-RAGE Signaling Plays a Role in Organic Dust-Induced Microglial Activation and Neuroinflammation. Toxicol Sci 169, 579–592. https://doi.org/10.1093/toxsci/kfz071

Massey, N., Shrestha, D., Bhat, S.M., Kondru, N., Charli, A., Karriker, L.A., Kanthasamy, A.G., Charavaryamath, C., 2021. Organic dust-induced mitochondrial dysfunction could be targeted via cGAS-STING or cytoplasmic NOX-2 inhibition using microglial cells and brain slice culture models. Cell Tissue Res. https://doi.org/10.1007/s00441-021-03422-x

May, S., Romberger, D.J., Poole, J.A., 2012. Respiratory Health Effects of Large Animal Farming Environments. J Toxicol Environ Health B Crit Rev 15, 524–541. https://doi.org/10.1080/10937404.2012.744288

Nakahira, K., Haspel, J.A., Rathinam, V.A.K., Lee, S.-J., Dolinay, T., Lam, H.C., Englert, J.A., Rabinovitch, M., Cernadas, M., Kim, H.P., Fitzgerald, K.A., Ryter, S.W., Choi, A.M.K., 2011. Autophagy proteins regulate innate immune responses by inhibiting the release of mitochondrial DNA mediated by the NALP3 inflammasome. Nature Immunology 12, 222–230. https://doi.org/10.1038/ni.1980

Nath Neerukonda, S., Mahadev-Bhat, S., Aylward, B., Johnson, C., Charavaryamath, C., Arsenault, R.J., 2018. Kinome analyses of inflammatory responses to swine barn dust extract in human bronchial epithelial and monocyte cell lines. Innate Immun 24, 366–381. https://doi.org/10.1177/1753425918792070

Ney, P.A., 2015. Mitochondrial autophagy: Origins, significance, and role of BNIP3 and NIX. Biochimica et Biophysica Acta (BBA) - Molecular Cell Research, Mitophagy 1853, 2775–2783. https://doi.org/10.1016/j.bbamcr.2015.02.022

Nordgren, T.M., Charavaryamath, C., 2018. Agriculture Occupational Exposures and Factors Affecting Health Effects. Curr Allergy Asthma Rep 18, 65. https://doi.org/10.1007/s11882-018-0820-8

Ott, M., Robertson, J.D., Gogvadze, V., Zhivotovsky, B., Orrenius, S., 2002. Cytochrome c release from mitochondria proceeds by a two-step process. PNAS 99, 1259–1263. https://doi.org/10.1073/pnas.241655498

Palmer, C.S., Osellame, L.D., Stojanovski, D., Ryan, M.T., 2011. The regulation of mitochondrial morphology: Intricate mechanisms and dynamic machinery. Cellular Signalling 23, 1534–1545. https://doi.org/10.1016/j.cellsig.2011.05.021

Parekh, A.B., 2003. Mitochondrial Regulation of Intracellular Ca2+ Signaling: More Than Just Simple Ca2+ Buffers. Physiology 18, 252–256. https://doi.org/10.1152/nips.01458.2003

Piantadosi, C.A., Suliman, H.B., 2017. Mitochondrial Dysfunction in Lung Pathogenesis. Annual Review of Physiology 79, 495–515. https://doi.org/10.1146/annurev-physiol-022516-034322

Ploumi, C., Daskalaki, I., Tavernarakis, N., 2017. Mitochondrial biogenesis and clearance: a balancing act. The FEBS Journal 284, 183–195. https://doi.org/10.1111/febs.13820

Poole, J.A., Barnes, C.S., Demain, J.G., Bernstein, J.A., Padukudru, M.A., Sheehan, W.J., Fogelbach, G.G., Wedner, J., Codina, R., Levetin, E., Cohn, J.R., Kagen, S., Portnoy, J.M., Nel, A.E., 2019. Impact of weather and climate change with indoor and outdoor air quality in asthma: A Work Group Report of the AAAAI Environmental Exposure and Respiratory Health Committee. Journal of Allergy and Clinical Immunology 143, 1702–1710. https://doi.org/10.1016/j.jaci.2019.02.018

Poole, J.A., Burrell, A.M., Wyatt, T.A., Kielian, T.L., Romberger, D.J., 2010. NOD2 Negatively Regulates Organic Dust-Induced Inflammation in Monocytes/Macrophages. Journal of Allergy and Clinical Immunology, Program and Abstracts of Papers to be Presented During Scientific Sessions 125, AB118. https://doi.org/10.1016/j.jaci.2009.12.467

Poole, J.A., Romberger, D.J., 2012. Immunological and Inflammatory Responses to Organic Dust in Agriculture. Curr Opin Allergy Clin Immunol 12, 126–132. https://doi.org/10.1097/ACI.0b013e3283511d0e

Poole, J.A., Wyatt, T.A., Essen, S.G.V., Hervert, J., Parks, C., Mathisen, T., Romberger, D.J., 2007. Repeat organic dust exposure–induced monocyte inflammation is associated with protein kinase C activity. Journal of Allergy and Clinical Immunology 120, 366–373. https://doi.org/10.1016/j.jaci.2007.04.033

Poole, J.A., Wyatt, T.A., Kielian, T., Oldenburg, P., Gleason, A.M., Bauer, A., Golden, G., West, W.W., Sisson, J.H., Romberger, D.J., 2011. Toll-like receptor 2 regulates organic dust-induced airway inflammation. Am. J. Respir. Cell Mol. Biol. 45, 711–719. https://doi.org/10.1165/rcmb.2010-0427OC

Pouwels, S.D., Heijink, I.H., ten Hacken, N.H., Vandenabeele, P., Krysko, D.V., Nawijn, M.C., van Oosterhout, A.J., 2014. DAMPs activating innate and adaptive immune responses in COPD. Mucosal Immunology 7, 215–226. https://doi.org/10.1038/mi.2013.77

Prakash, Y.S., Pabelick, C.M., Sieck, G.C., 2017. Mitochondrial Dysfunction in Airway Disease. CHEST 152, 618–626. https://doi.org/10.1016/j.chest.2017.03.020

Qi, L., Sun, X., Li, F.-E., Zhu, B.-S., Braun, F.K., Liu, Z.-Q., Tang, J.-L., Wu, C., Xu, F., Wang, H.-H., Velasquez, L.A., Zhao, K., Lei, F.-R., Zhang, J.-G., Shen, Y.-T., Zou, J.-X., Meng, H.-M., An, G.-L., Yang, L., Zhang, X.-D., 2015. HMGB1 Promotes Mitochondrial Dysfunction–Triggered Striatal Neurodegeneration via Autophagy and Apoptosis Activation. PLoS One 10. https://doi.org/10.1371/journal.pone.0142901

Qin, S., Wang, H., Yuan, R., Li, H., Ochani, M., Ochani, K., Rosas-Ballina, M., Czura, C.J., Huston, J.M., Miller, E., Lin, X., Sherry, B., Kumar, A., LaRosa, G., Newman, W., Tracey, K.J., Yang, H., 2006. Role of HMGB1 in apoptosis-mediated sepsis lethality. J Exp Med 203, 1637–1642. https://doi.org/10.1084/jem.20052203

Quinsay, M.N., Lee, Y., Rikka, S., Sayen, M.R., Molkentin, J.D., Gottlieb, R.A., Gustafsson, Å.B., 2010. Bnip3 mediates permeabilization of mitochondria and release of cytochrome c via a novel mechanism. Journal of Molecular and Cellular Cardiology 48, 1146–1156. https://doi.org/10.1016/j.yjmcc.2009.12.004

Ranieri, M., Brajkovic, S., Riboldi, G., Ronchi, D., Rizzo, F., Bresolin, N., Corti, S., Comi, G.P., 2013. Mitochondrial Fusion Proteins and Human Diseases [WWW Document]. Neurology Research International. https://doi.org/10.1155/2013/293893

Rizzuto, R., Bernardi, P., Pozzan, T., 2000. Mitochondria as all-round players of the calcium game. The Journal of Physiology 529, 37–47. https://doi.org/10.1111/j.1469-7793.2000.00037.x

Romberger, D.J., Bodlak, V., Von Essen, S.G., Mathisen, T., Wyatt, T.A., 2002. Hog barn dust extract stimulates IL-8 and IL-6 release in human bronchial epithelial cells via PKC activation. Journal of Applied Physiology 93, 289–296. https://doi.org/10.1152/japplphysiol.00815.2001

Rubartelli, A., Lotze, M.T., 2007. Inside, outside, upside down: damage-associated molecular-pattern molecules (DAMPs) and redox. Trends in Immunology 28, 429–436. https://doi.org/10.1016/j.it.2007.08.004

Schumacker, P.T., Gillespie, M.N., Nakahira, K., Choi, A.M.K., Crouser, E.D., Piantadosi, C.A., Bhattacharya, J., 2014. Mitochondria in lung biology and pathology: more than just a powerhouse. American Journal of Physiology-Lung Cellular and Molecular Physiology 306, L962–L974. https://doi.org/10.1152/ajplung.00073.2014

Seo, J., Ottesen, E.W., Singh, R.N., 2014. Antisense Methods to Modulate Pre-mRNA Splicing, in: Hertel, K.J. (Ed.), Spliceosomal Pre-MRNA Splicing: Methods and Protocols, Methods in Molecular Biology. Humana Press, Totowa, NJ, pp. 271–283. https://doi.org/10.1007/978-1-62703-980-2_20

Sethi, R.S., Schneberger, D., Charavaryamath, C., Singh, B., 2017. Pulmonary innate inflammatory responses to agricultural occupational contaminants. Cell Tissue Res. 367, 627–642. https://doi.org/10.1007/s00441-017-2573-4

Shrestha, D., Bhat, S.M., Massey, N., Santana Maldonado, C., Rumbeiha, W.K., Charavaryamath, C., 2021. Pre-exposure to hydrogen sulfide modulates the innate inflammatory response to organic dust. Cell Tissue Res. https://doi.org/10.1007/s00441-020-03333-3

Song, Z., Ghochani, M., McCaffery, J.M., Frey, T.G., Chan, D.C., 2009. Mitofusins and OPA1 Mediate Sequential Steps in Mitochondrial Membrane Fusion. MBoC 20, 3525–3532. https://doi.org/10.1091/mbc.e09-03-0252

Srinivasan, B., Kolli, A.R., Esch, M.B., Abaci, H.E., Shuler, M.L., Hickman, J.J., 2015. TEER measurement techniques for in vitro barrier model systems. J Lab Autom 20, 107–126. https://doi.org/10.1177/2211068214561025

Tang, D., Kang, R., Livesey, K.M., Kroemer, G., Billiar, T.R., Van Houten, B., Zeh, H.J., Lotze, M.T., 2011. High-Mobility Group Box 1 Is Essential for Mitochondrial Quality Control. Cell Metabolism 13, 701–711. https://doi.org/10.1016/j.cmet.2011.04.008

Tilokani, L., Nagashima, S., Paupe, V., Prudent, J., 2018. Mitochondrial dynamics: overview of molecular mechanisms. Essays Biochem 62, 341–360. https://doi.org/10.1042/EBC20170104

Trian, T., Benard, G., Begueret, H., Rossignol, R., Girodet, P.-O., Ghosh, D., Ousova, O., Vernejoux, J.-M., Marthan, R., Tunon-de-Lara, J.-M., Berger, P., 2007. Bronchial smooth muscle remodeling involves calcium-dependent enhanced mitochondrial biogenesis in asthma. Journal of Experimental Medicine 204, 3173–3181. https://doi.org/10.1084/jem.20070956

Ugrinova, I., Pasheva, E., 2017. HMGB1 Protein: A Therapeutic Target Inside and Outside the Cell. Adv Protein Chem Struct Biol 107, 37–76. https://doi.org/10.1016/bs.apcsb.2016.10.001

Warren, K.J., Dickinson, J.D., Nelson, A.J., Wyatt, T.A., Romberger, D.J., Poole, J.A., 2019. Ovalbumin-sensitized mice have altered airway inflammation to agriculture organic dust. Respiratory Research 20, 51. https://doi.org/10.1186/s12931-019-1015-0

West, A.P., Khoury-Hanold, W., Staron, M., Tal, M.C., Pineda, C.M., Lang, S.M., Bestwick, M., Duguay, B.A., Raimundo, N., MacDuff, D.A., Kaech, S.M., Smiley, J.R., Means, R.E., Iwasaki, A., Shadel, G.S., 2015. Mitochondrial DNA stress primes the antiviral innate immune response. Nature 520, 553–557. https://doi.org/10.1038/nature14156

Westrate, L.M., Drocco, J.A., Martin, K.R., Hlavacek, W.S., MacKeigan, J.P., 2014. Mitochondrial Morphological Features Are Associated with Fission and Fusion Events. PLOS ONE 9, e95265. https://doi.org/10.1371/journal.pone.0095265

Whitsett, J.A., Alenghat, T., 2015. Respiratory epithelial cells orchestrate pulmonary innate immunity. Nature Immunology 16, 27–35. https://doi.org/10.1038/ni.3045

Wu, Z., Puigserver, P., Andersson, U., Zhang, C., Adelmant, G., Mootha, V., Troy, A., Cinti, S., Lowell, B., Scarpulla, R.C., Spiegelman, B.M., 1999. Mechanisms Controlling Mitochondrial Biogenesis and Respiration through the Thermogenic Coactivator PGC-1. Cell 98, 115–124. https://doi.org/10.1016/S0092-8674(00)80611-X

Wunschel, J., Poole, J.A., 2016. Occupational agriculture organic dust exposure and its relationship to asthma and airway inflammation in adults. J Asthma 53, 471–477. https://doi.org/10.3109/02770903.2015.1116089

Yang, H., Wang, H., Chavan, S.S., Andersson, U., 2015. High Mobility Group Box Protein 1 (HMGB1): The Prototypical Endogenous Danger Molecule. Mol. Med. 21 Suppl 1, S6–S12. https://doi.org/10.2119/molmed.2015.00087

Ye, C., Choi, J.-G., Abraham, S., Wu, H., Diaz, D., Terreros, D., Shankar, P., Manjunath, N., 2012. Human macrophage and dendritic cell-specific silencing of high-mobility group protein B1 ameliorates sepsis in a humanized mouse model. PNAS 109, 21052–21057. https://doi.org/10.1073/pnas.1216195109

Zhang, Q., Raoof, M., Chen, Y., Sumi, Y., Sursal, T., Junger, W., Brohi, K., Itagaki, K., Hauser, C.J., 2010. Circulating mitochondrial DAMPs cause inflammatory responses to injury. Nature 464, 104–107. https://doi.org/10.1038/nature08780

Zhou, H., Wang, Y., Wang, W., Jia, J., Li, Y., Wang, Q., Wu, Y., Tang, J., 2009. Generation of Monoclonal Antibodies against Highly Conserved Antigens. PLOS ONE 4, e6087. https://doi.org/10.1371/journal.pone.0006087

Zorov, D.B., Juhaszova, M., Sollott, S.J., 2014. Mitochondrial Reactive Oxygen Species (ROS) and ROS-Induced ROS Release. Physiol Rev 94, 909–950. https://doi.org/10.1152/physrev.00026.2013

Zou, C., Wang, Y., Shen, Z., 2005. 2-NBDG as a fluorescent indicator for direct glucose uptake measurement. Journal of Biochemical and Biophysical Methods 64, 207–215. https://doi.org/10.1016/j.jbbm.2005.08.001

Appendix A. Supplementary figures

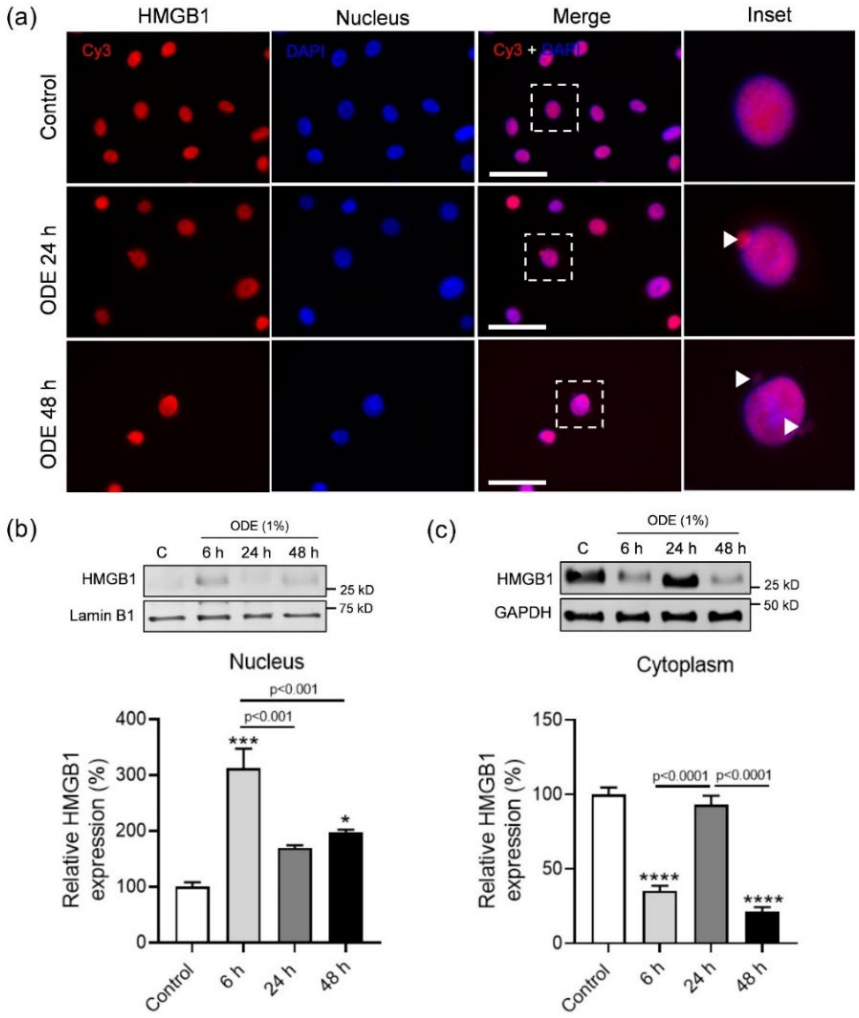

Figure 5.11 ODE exposure induces nuclear blebbing in NHBE cells
NHBE cells treated with medium (control) or ODE (1%) for 6, 24 and 48 h were stained with anti-HMGB1 antibody (Cy3) and nuclei counterstain (DAPI). Compared to controls, ODE treated cells showed nucleocytoplasmic translocation of HMGB1and nuclear blebbing 24 hours post-treatment. (a; arrows heads and box; Scale bar = 100 μm). Immunoblotting of nuclear and cytoplasmic fractions of treated cells was performed to measure expression of HMGB1. Compared to controls, cells showed an increase in HMGB1 expression in the nuclear fraction at 6 and 48 h (b). HMGB1 expression significantly increased in the cytoplasm at 24 h post-treatment (c). Samples for all

assays were derived from the same experiment and were processed in parallel. All protein bands were normalized over β-actin (37 kD) and percentage intensity relative to control was analyzed. Data was analyzed using one-way ANOVA with Tukey's multiple comparison test (*p < 0.05, **p < 0.01, ***p < 0.001, ****p < 0.0001) and represented as mean ± SEM with n = 3/treatment (* indicates significant difference from control).

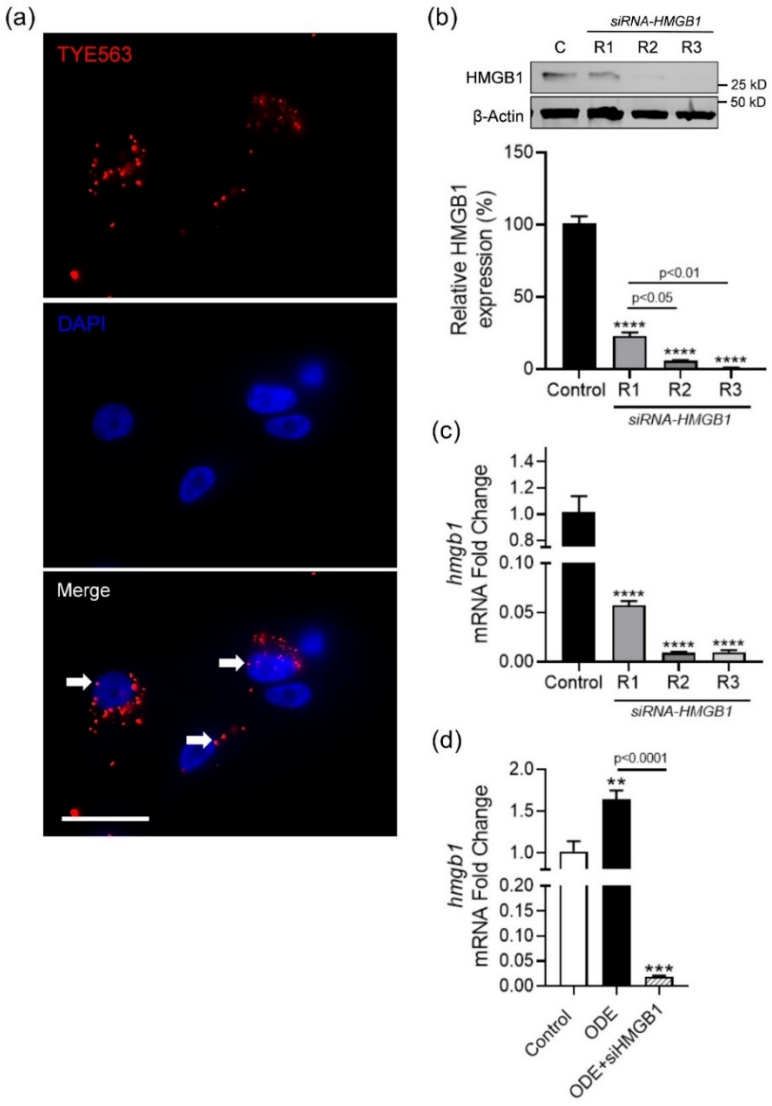

Figure 5.12 Confirmation of siRNA mediated knockdown on HMGB1
NHBE cells were treated with DsiRNAs for TYE 563 (transfection control, Cy3) or HMGB1 (R1, R2, R3) and a scrambled siRNA (negative control). 24 h post-transfection, the cells showed successful transfection of TYE 563 into the cells (a, arrows; Scale bar = 100 μm). HMGB1 knockdown was confirmed by immunoblotting (b) and qPCR (c). Significant decrease in HMGB1 protein and mRNA expression was seen on transfection with siRNA.R1 (10 nmol), siRNA.R2 (10 nmol) and siRNA.R3 (10 nmol). Changes in HMGB1 protein expression in NHBE cells with or without siRNA mediated HMGB1 knockdown and treated with ODE (1%) for 24 h was assessed (d). Samples for all assays were derived from the same experiment and were processed in parallel. All the protein bands were normalized over β-actin (37 kD) and percentage intensity relative to

control was analyzed. Data was analyzed using one-way ANOVA with Tukey's multiple comparison test (*p < 0.05, **p < 0.01, ***p < 0.001, ****p < 0.0001) and represented as mean ± SEM with n = 3/treatment (* indicates significant difference from control).

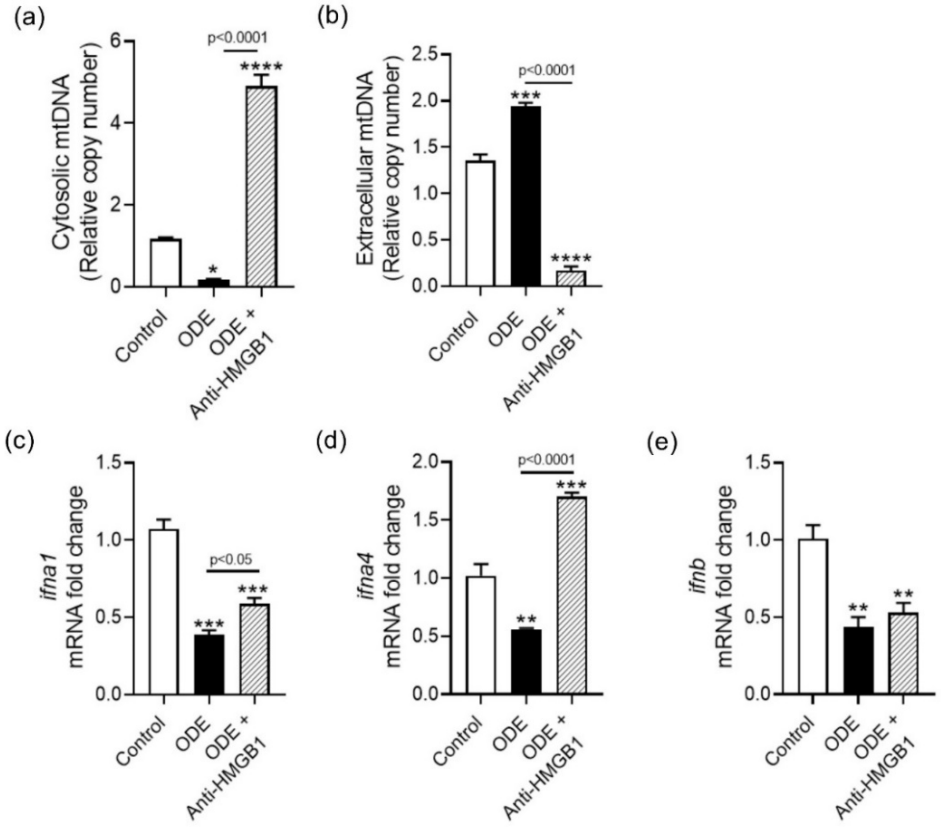

Figure 5.13 HMGB1 neutralization decreases extracellular secretion of mtDNA
Mitochondrial DNA (mtDNA) leakage into the cytosol (a) and extracellularly (b) in NHBE cells treated with medium or ODE (1%) followed by medium or HMGB1 neutralization antibody (10 µg/mL) for 8 h per day for 5 days was analyzed via qPCR. mRNA fold change of gene targets of mtDNA release, *ifna1* (c), *ifna4* (d), and *ifnb* (e), were measured by qPCR. For all the assays, samples were derived from the same experiment and were processed in parallel. Data was analyzed using one-way ANOVA with Tukey's multiple comparison test (*p < 0.05, **p < 0.01, ***p < 0.001, ****p < 0.0001) and represented as mean ± SEM with n = 3/treatment (* indicates significant difference from control).

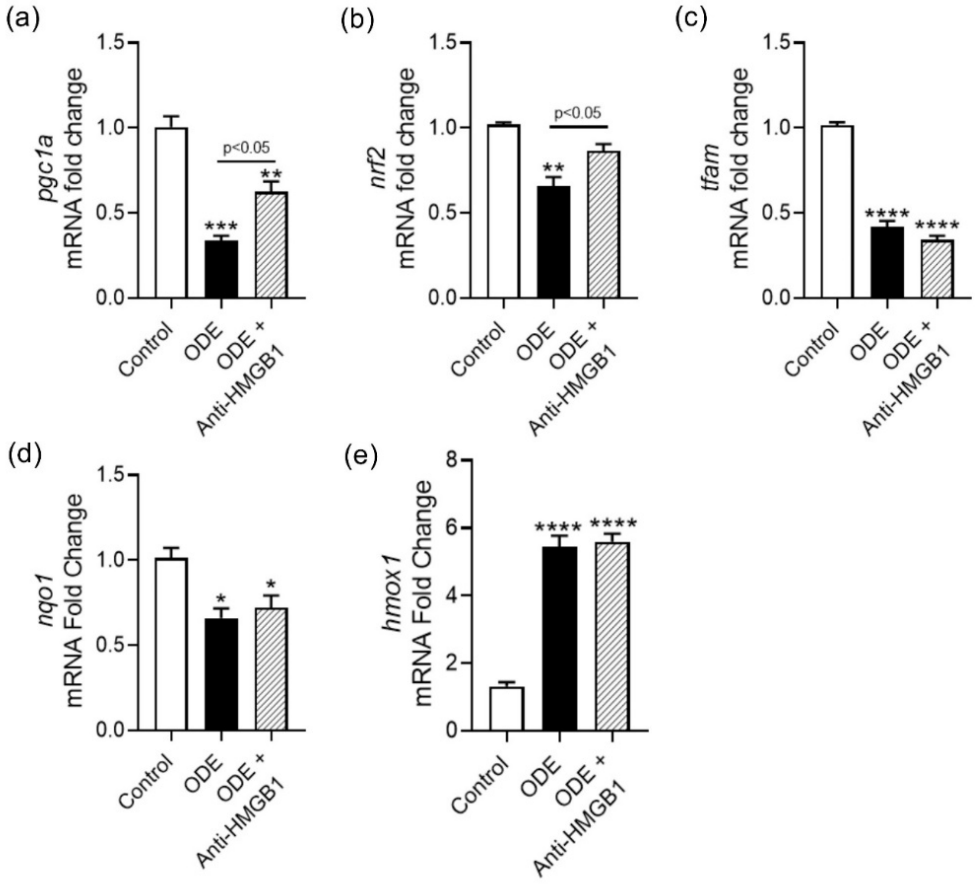

Figure 5.14 HMGB1 neutralization promotes mitochondrial biogenesis
Markers of mitochondrial biogenesis in NHBE cells treated with medium or ODE (1%) followed by medium or HMGB1 neutralization antibody (10 µg/mL) for 8 h per day for 5 days was measured. mRNA expression of *pgc1a* (a), *nrf2* (b) and *tfam* (c) were measured by qPCR. mRNA fold change of gene targets downstream of NRF2, *hmox1* (d), and *nqo1* (e), were measured by qPCR. For all the assays, samples were derived from the same experiment and were processed in parallel. Data was analyzed using one-way ANOVA with Tukey's multiple comparison test (*$p < 0.05$, **$p < 0.01$, ***$p < 0.001$, ****$p < 0.0001$) and represented as mean ± SEM with n = 3/treatment (* indicates significant difference from control).

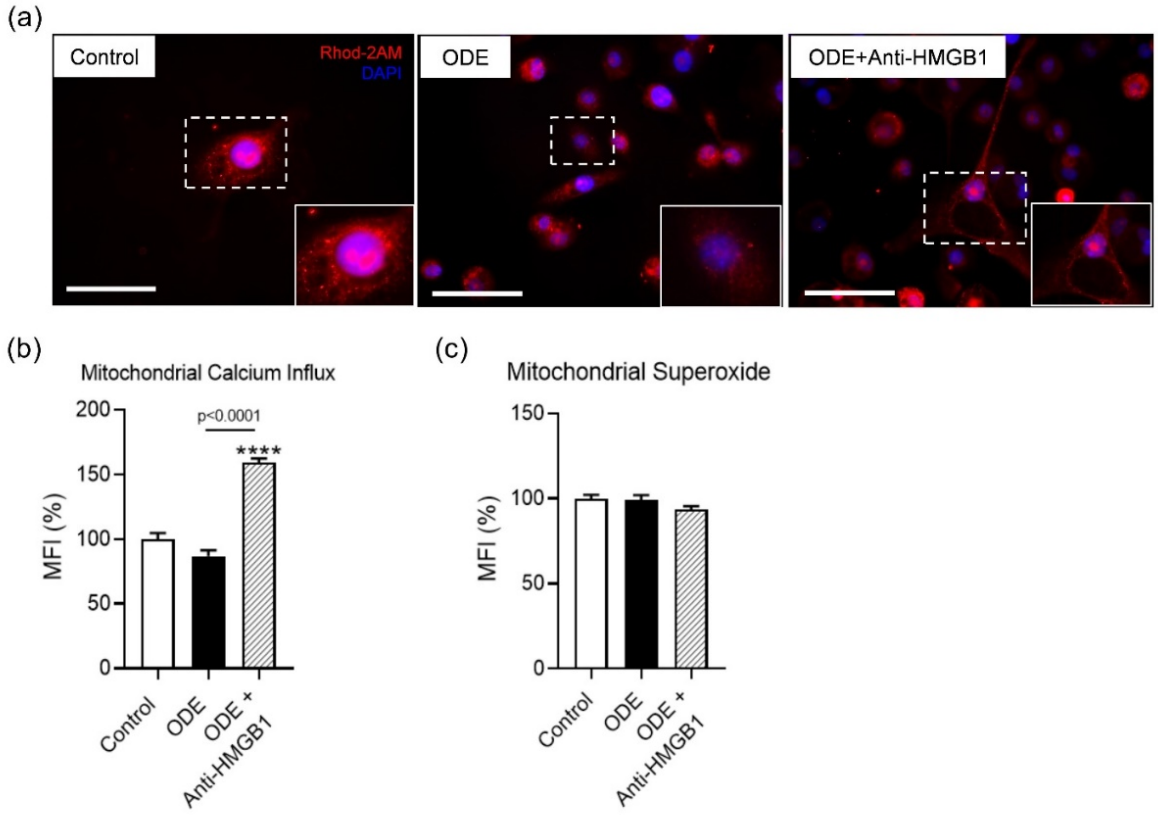

Figure 5.15 HMGB1 neutralization increases mitochondrial calcium influx
Intra-mitochondrial calcium levels in mitochondria isolated from NHBE cells treated with medium or ODE (1%) followed by medium or HMGB1 neutralization antibody (10 µg/mL) for 8 h per day for 5 days was visualized (a; Scale bar = 100 µm) and quantified by Rhod-2AM staining (b). Using Mito-SOX staining, the levels of superoxide anions (SOX) within the mitochondria was quantified (c). Samples for all assays were derived from the same experiment and were processed in parallel. Data was analyzed using one-way ANOVA with Tukey's multiple comparison test (*$p < 0.05$, **$p < 0.01$, ***$p < 0.001$, ****$p < 0.0001$) and represented as mean ± SEM with n = 6/treatment (* indicates significant difference from control).

Appendix B. Supplementary tables

Table 5.4 Control and HMGB1 DsiRNA sequences

Gene	Duplex name		Sequence (5'→3')
HMGB1	Ri.HMGB1.13.1 (R1)	Sense	CUGAUAAAAGGUUUUGUCAAACATT
		Antisense	CCGACUAUUUUCCAAAACAGUUUGUAA
	Ri.HMGB1.13.2 (R2)	Sense	GCAAAAUGUCAUCAUAUGCAUUUTT
		Antisense	UCCGUUUUACAGUAGUAUACGUAAAAA
	Ri.HMGB1.13.3 (R3)	Sense	CCAUUGGUGAUGUUGCGAAGAAACT
		Antisense	CAGGUAACCACUACAACGCUUCUUUGA
Negative Control	DsiRNA (NC)	Sense	CGUUAAUCGCGUAUAAUACGCGUAT
		Antisense	AUACGCGUAUUAUACGCGAUUAACGAC

Table 5.5 Primer sequences

Gene symbol	Primer Sequence (5'→3')	
mtdna	Forward	TGAGGCCAAATATCATTCTGAGGGGC
	Reverse	TTTCATCATGCGGAGATGTTGGATGG
mtnd1	Forward	GGCTATATACAACTACGCAAAGGC
	Reverse	GGTAGATGTGGCGGGTTTTAGG
16s	Forward	CCGCAAGGGAAAGATGAAAGAC
	Reverse	TCGTTTGGTTTCGGGGTTTC
hmgb1	Forward	GCGAAGAAACTGGGAGAGATGTG
	Reverse	GCATCAGGCTTTCCTTTAGCTCG
nos2	Forward	GCTCTACACCTCCAATGTGACC
	Reverse	CTGCCGAGATTTGAGCCTCATG
ifna	Forward	AGAAGGCTCCAGCCATCTCTGT
	Reverse	TGCTGGTAGAGTTCGGTGCAGA
ifna4	Forward	GTTCCAGAAGGCTCAAGCCATC
	Reverse	TAGGAGGCTCTGTTCCCAAGCA
ifnb	Forward	CTTGGATTCCTACAAAGAAGCAGC
	Reverse	TCCTCCTTCTGGAACTGCTGCA

Table 5.5 (continued)

Gene symbol	Primer Sequence (5'→3')	
tfam	Forward	GTGGTTTTCATCTGTCTTGGCAAG
	Reverse	TTCCCTCCAACGCTGGGCAATT
pgc1a	Forward	CCAAAGGATGCGCTCTCGTTCA
	Reverse	CGGTGTCTGTAGTGGCTTGACT
nrf2	Forward	CACATCCAGTCAGAAACCAGTGG
	Reverse	GGAATGTCTGCGCCAAAAGCTG
gstp1	Forward	TGGAAGGAGGAGGTGGTTACCA
	Reverse	GGTAAAGGGTGAGGTCTCCATC
hmox1	Forward	CCAGGCAGAGAATGCTGAGTTC
	Reverse	AAGACTGGGCTCTCCTTGTTGC
nqo1	Forward	CCTGCCATTCTGAAAGGCTGGT
	Reverse	GTGGTGATGGAAAGCACTGCCT
hif1a	Forward	TATGAGCCAGAAGAACTTTTAGGC
	Reverse	CACCTCTTTTGGCAAGCATCCTG
vhl	Forward	GACACACGATGGGCTTCTGGTT
	Reverse	ACAACCTGGAGGCATCGCTCTT
slc2a6	Forward	TCACCAAGTCCTTCCTGCCAGT
	Reverse	CACAGCAGCCTGTGAACACCAG
eno1	Forward	AGTCAACCAGATTGGCTCCGTG
	Reverse	CACAACCAGGTCAGCGATGAAG
foxj1	Forward	ACTCGTATGCCACGCTCATCTG
	Reverse	GAGACAGGTTGTGGCGGATTGA
cfap157	Forward	CAGCAGGAACTGGCTAATGAGC
	Reverse	ACGTCACTGTCCTCTTCATCGC
cld2	Forward	GTGACAGCAGTTGGCTTCTCCA
	Reverse	GGAGATTGCACTGGATGTCACC
ocld	Forward	ATGGCAAAGTGAATGACAAGCGG
	Reverse	CTGTAACGAGGCTGCCTGAAGT

Table 5.6 Array gene list

Assay ID	Gene Symbol(s)	Gene Name(s)
Hs99999901_s1	18s rRNA	-
Hs01060284_m1	ATP12A	ATPase H+/K+ transporting non-gastric alpha2 subunit
Hs00167575_m1	ATP4A	ATPase H+/K+ transporting alpha subunit
Hs01026288_m1	ATP4B	ATPase H+/K+ transporting beta subunit
Hs00900735_m1	ATP5A1	ATP synthase, H+ transporting, mitochondrial F1 complex, alpha subunit 1, cardiac muscle
Hs00969569_m1	ATP5B	ATP synthase, H+ transporting, mitochondrial F1 complex, beta polypeptide
Hs01101219_g1	ATP5C1	ATP synthase, H+ transporting, mitochondrial F1 complex, gamma polypeptide 1
Hs01076982_g1	ATP5F1	ATP synthase, H+ transporting, mitochondrial Fo complex subunit B1
Hs00829069_s1	ATP5G1	ATP synthase, H+ transporting, mitochondrial Fo complex subunit C1 (subunit 9)
Hs01086654_g1	ATP5G2	ATP synthase, H+ transporting, mitochondrial Fo complex subunit C2 (subunit 9)
Hs00266085_m1	ATP5G3	ATP synthase, H+ transporting, mitochondrial Fo complex subunit C3 (subunit 9)
Hs01046892_gH	ATP5H	ATP synthase, H+ transporting, mitochondrial Fo complex subunit D
Hs00273015_m1	ATP5I	ATP synthase, H+ transporting, mitochondrial Fo complex subunit E
Hs01081389_g1	ATP5J	ATP synthase, H+ transporting, mitochondrial Fo complex subunit F6
Hs04194830_s1	ATP5J2	ATP synthase, H+ transporting, mitochondrial Fo complex subunit F2
Hs00538946_g1	ATP5L	ATP synthase, H+ transporting, mitochondrial Fo complex subunit G
Hs00426889_m1	ATP5O	ATP synthase, H+ transporting, mitochondrial F1 complex, O subunit
Hs00429389_m1	ATP6V0A2	ATPase H+ transporting V0 subunit a2
Hs01084784_m1	ATP6V0D2	ATPase H+ transporting V0 subunit d2
Hs00375969_m1	ATP6V1C2	ATPase H+ transporting V1 subunit C2
Hs00369807_m1	ATP6V1E2	ATPase H+ transporting V1 subunit E2
Hs00373169_m1	ATP6V1G3	ATPase H+ transporting V1 subunit G3
Hs01018008_g1	BCS1L	BCS1 homolog, ubiquinol-cytochrome c reductase complex chaperone
Hs00971639_m1	COX4I1	cytochrome c oxidase subunit 4I1
Hs00261747_m1	COX4I2	cytochrome c oxidase subunit 4I2
Hs00362067_m1	COX5A	cytochrome c oxidase subunit 5A
Hs00426948_m1	COX5B	cytochrome c oxidase subunit 5B
Hs01924685_g1	COX6A1	cytochrome c oxidase subunit 6A1
Hs00193226_g1	COX6A2	cytochrome c oxidase subunit 6A2
Hs00266375_m1	COX6B1	cytochrome c oxidase subunit 6B1
Hs00376070_m1	COX6B2	cytochrome c oxidase subunit 6B2
Hs00269977_m1	COX6C	cytochrome c oxidase subunit 6C
Hs01652418_m1	COX7A2	cytochrome c oxidase subunit 7A2
Hs00190880_m1	COX7A2L	cytochrome c oxidase subunit 7A2 like

Table 5.6 (continued)

Assay ID	Gene Symbol(s)	Gene Name(s)
Hs00371307_m1	COX7B	cytochrome c oxidase subunit 7B
Hs00187909_m1	COX8A	cytochrome c oxidase subunit 8A
Hs00418377_m1	COX8C	cytochrome c oxidase subunit 8C
Hs00357717_m1	CYC1	cytochrome c1
Hs00383379_m1	LHPP	phospholysine phosphohistidine inorganic pyrophosphate phosphatase
Hs00244980_m1	NDUFA1	NADH:ubiquinone oxidoreductase subunit A1
Hs00190004_m1	NDUFA10	NADH:ubiquinone oxidoreductase subunit A10
Hs00418300_m1	NDUFA11	NADH:ubiquinone oxidoreductase subunit A11
Hs04187282_g1	NDUFA2	NADH:ubiquinone oxidoreductase subunit A2
Hs01547166_g1	NDUFA3	NADH:ubiquinone oxidoreductase subunit A3
Hs00800172_s1	NDUFA4	NDUFA4, mitochondrial complex associated
Hs01634019_g1	NDUFA5	NADH:ubiquinone oxidoreductase subunit A5
Hs00899690_m1	NDUFA6	NADH:ubiquinone oxidoreductase subunit A6
Hs01561430_m1	NDUFA7	NADH:ubiquinone oxidoreductase subunit A7
Hs00204417_m1	NDUFA8	NADH:ubiquinone oxidoreductase subunit A8
Hs00192290_m1	NDUFAB1	NADH:ubiquinone oxidoreductase subunit AB1
Hs00605903_m1	NDUFB10	NADH:ubiquinone oxidoreductase subunit B10
Hs00190006_m1	NDUFB2	NADH:ubiquinone oxidoreductase subunit B2
Hs00427185_m1	NDUFB3	NADH:ubiquinone oxidoreductase subunit B3
Hs00853558_g1	NDUFB4	NADH:ubiquinone oxidoreductase subunit B4
Hs00159582_m1	NDUFB5	NADH:ubiquinone oxidoreductase subunit B5
Hs00159583_m1	NDUFB6	NADH:ubiquinone oxidoreductase subunit B6
Hs00188142_m1	NDUFB7	NADH:ubiquinone oxidoreductase subunit B7
Hs00922355_g1	NDUFB8	NADH:ubiquinone oxidoreductase subunit B8
Hs00601381_mH	NDUFB9	NADH:ubiquinone oxidoreductase subunit B9
Hs00159587_m1	NDUFC1	NADH:ubiquinone oxidoreductase subunit C1
Hs01072843_m1	NDUFC2	NADH:ubiquinone oxidoreductase subunit C2
Hs00192297_m1	NDUFS1	NADH:ubiquinone oxidoreductase core subunit S1
Hs00190020_m1	NDUFS2	NADH:ubiquinone oxidoreductase core subunit S2
Hs01549083_m1	NDUFS3	NADH:ubiquinone oxidoreductase core subunit S3
Hs00942568_m1	NDUFS4	NADH:ubiquinone oxidoreductase subunit S4
Hs02578754_g1	NDUFS5	NADH:ubiquinone oxidoreductase subunit S5
Hs00190035_m1	NDUFS6	NADH:ubiquinone oxidoreductase subunit S6
Hs00257018_m1	NDUFS7	NADH:ubiquinone oxidoreductase core subunit S7
Hs00159597_m1	NDUFS8	NADH:ubiquinone oxidoreductase core subunit S8
Hs00957930_m1	NDUFV1	NADH:ubiquinone oxidoreductase core subunit V1
Hs00221478_m1	NDUFV2	NADH:ubiquinone oxidoreductase core subunit V2
Hs00221479_m1	NDUFV3	NADH:ubiquinone oxidoreductase subunit V3
Hs00192329_m1	OXA1L	OXA1L, mitochondrial inner membrane protein
Hs00535680_g1	PPA1	pyrophosphatase (inorganic) 1
Hs00602575_m1	PPA2	pyrophosphatase (inorganic) 2

Table 5.6 (continued)

Assay ID	Gene Symbol(s)	Gene Name(s)
Hs00417200_m1	SDHA	succinate dehydrogenase complex flavoprotein subunit A
Hs01042482_m1	SDHB	succinate dehydrogenase complex iron sulfur subunit B
Hs01698067_s1	SDHC	succinate dehydrogenase complex subunit C
Hs01098144_g1	SDHD	succinate dehydrogenase complex subunit D
Hs00199138_m1	UQCR11	ubiquinol-cytochrome c reductase, complex III subunit XI
Hs00163415_m1	UQCRC1	ubiquinol-cytochrome c reductase core protein I
Hs00996395_m1	UQCRC2	ubiquinol-cytochrome c reductase core protein II
Hs04194251_g1	UQCRFS1	ubiquinol-cytochrome c reductase, Rieske iron-sulfur polypeptide 1
Hs03045181_g1	UQCRH	ubiquinol-cytochrome c reductase hinge protein
Hs00416927_g1	UQCRQ	ubiquinol-cytochrome c reductase complex III subunit VII
Hs99999905_m1	GAPDH	glyceraldehyde-3-phosphate dehydrogenase
Hs99999909_m1	HPRT1	hypoxanthine phosphoribosyltransferase 1
Hs99999908_m1	GUSB	glucuronidase beta
Hs99999903_m1	ACTB	actin beta
Hs99999907_m1	B2M	beta-2-microglobulin
Hs00609297_m1	HMBS	hydroxymethylbilane synthase
Hs00183533_m1	IPO8	importin 8
Hs99999906_m1	PGK1	phosphoglycerate kinase 1
Hs99999902_m1	RPLP0	ribosomal protein lateral stalk subunit P0
Hs99999910_m1	TBP	TATA-box binding protein
Hs99999911_m1	TFRC	transferrin receptor
Hs99999901_s1	18S	Eukaryotic 18S rRNA
Hs00824723_m1	UBC	ubiquitin C

Table 5.7 Characteristics of primary antibodies

Epitope	Species/Clone	Dilution	Catalog #	Supplier
β-Actin	Mouse Monoclonal	1:10,000	ab6276	AbCam[a]
LaminB1	Rabbit Polyclonal	1:1000	ab16048	AbCam[a]
GAPDH	Rabbit Polyclonal	1:2500	ab9485	AbCam[a]
HMGB1	Rabbit Polyclonal	1:5000	ab79823	AbCam[a]
MFN1	Mouse Monoclonal	1:1000	sc-166644	Santa Cruz[b]
MFN2	Mouse Monoclonal	1:1000	sc-100560	Santa Cruz[b]
OPA1	Mouse Monoclonal	1:1000	sc-393296	Santa Cruz[b]
DRP1	Mouse Monoclonal	1:1000	sc-271583	Santa Cruz[b]
Parkin	Mouse Monoclonal	1:1000	sc-32282	Santa Cruz[b]
PINK1	Mouse Monoclonal	1:1000	sc-517353	Santa Cruz[b]
BNIP3	Mouse Monoclonal	1:1000	sc-56167	Santa Cruz[b]
Cytochrome C	Mouse Monoclonal	1:1000	sc-13156	Santa Cruz[b]
PGC1α	Mouse Monoclonal	1:1000	sc-518025	Santa Cruz[b]
NRF2	Mouse Monoclonal	1:1000	sc-365949	Santa Cruz[b]
TFAM	Mouse Monoclonal	1:1000	sc-376672	Santa Cruz[b]
HIF1α	Mouse Monoclonal	1:1000	sc-13515	Santa Cruz[b]
TLR9	Mouse Monoclonal	1:1000	sc-47723	Santa Cruz[b]
cGAS	Mouse Monoclonal	1:1000	sc-515777	Santa Cruz[b]
IFI16	Mouse Monoclonal	1:1000	sc-8023	Santa Cruz[b]
IRF3	Mouse Monoclonal	1:1000	sc-33641	Santa Cruz[b]

[a]Cambridge, United Kingdom
[b]Dallas, Texas, USA

Table 5.8 Characteristics of secondary antibodies

Expression system	Conjugate	Species/Clone	Dilution	Catalog #	Supplier
Donkey/IgG	Alexa Fluor® 680	Rabbit Polyclonal	1:10,000	A10043	Invitrogen[c]
Rabbit/IgG	Alexa Fluor® 680	Mouse Polyclonal	1:10,000	A27031	Invitrogen[c]
Donkey/IgG	IRDye® 800CW	Rabbit Polyclonal	1:10,000	926-32213	LI-COR[d]

[c]Thermofisher Scientific, USA
[d]Nebraska, USA

CHAPTER 6. CHAPTER 6. ROLE OF AIRWAY CLUB CELL SPECIFIC HMGB1 KNOCKOUT IN ORGANIC DUST INDUCED LUNG INFLAMMATION *IN VIVO*

Sanjana Mahadev Bhat [1,2], Nyzil Massey [1], Nawau Yar [3], Locke A. Karriker [4], Chong Wang [4], Chandrashekhar Charavaryamath [1*]

[1] Department of Biomedical Sciences, 2008 Vet Med Building, Iowa State University, Ames, IA, USA. [2] Immunobiology Interdepartmental Graduate Program, Iowa State University, Ames, IA, USA. [3] Biological Science Program, University of California, Santa Barbra, CA. [4] Department of Veterinary Diagnostic and Production Animal Medicine, Iowa State University, Ames, IA, USA.

[*]To whom correspondence should be addressed: Chandrashekhar Charavaryamath, BVSc, MVSc, PhD., Assistant Professor, Department of Biomedical Sciences, Iowa State University, Ames, IA 50011. Telephone: (515) 294-7710; Fax: (515) 294-2315; Email: chandru@iastate.edu

Keywords: OD, HMGB1, club cell, airway inflammation, mitochondrial dysfunction

Modified from a manuscript in preparation.

Author Contributions

S.M. Bhat participated in the design of experiments, performed the experiments, analyzed the data, and wrote the manuscript. N. Massey performed organic dust extraction and histology scoring. N. Yar assisted with the assays including western blot and leukocyte differential count. L. Karriker collected the organic dust samples and edited the manuscript. C. Wang helped with the statistical analysis of the data, interpretation, and graphical representation. C. Charavaryamath conceptualized the study, participated in the design of the experiments, performed dust extraction, participated in the interpretation of data, and edited the manuscript. All authors have read and approved the final manuscript.

Abbreviations

OD: Organic Dust; ODE: Organic Dust Extract; LPS: Lipopolysaccharide; CAFOs: Concentrated Animal Feed Operations; HMGB1: High Mobility Group Box 1; RAGE: Receptor For Advanced Glycation End Products; MAMPs: Microbial Associated Molecular Patterns; DAMPs: Damage Associated Molecular Patters; PRRs: Pathogen Recognition Receptors; COPD:

Chronic Obstructive Pulmonary Disease; CCSP: Club Cell Secretory Protein; AHR: Airway Hyperresponsiveness; EMT: Epithelial Mesenchymal Transition; ROS: Reactive Oxygen Species; iNOS: Inducible Nitric Oxide Synthase; TLR: Toll-like receptor; NOD2: Nucleotide-binding Oligomerization Domain-containing 2; IL: Interleukin; IFN: Interferons; TNF: Tumor Necrosis Factor; TFAM: mitochondrial Transcription Factor A; PGC1α: Peroxisome Proliferator-Activated Receptor Gamma Coactivator 1-alpha; NRF2: Nuclear Factor Erythroid 2-related factor 2; HIF1α: Hypoxia-Inducible Factor 1-alpha; ENO1: enolase 1; SLC2A6: Solute Carrier Family 2 Member 6; FOXJ1: Forkhead box protein J1; mtND1: mitochondrial NADH dehydrogenase 1; BALF: Bronchoalveolar Lavage Fluid; FITC: Fluorescein isothiocyanate; PKC: Protein Kinase C

Abstract

Agriculture animal production workers experience significant respiratory disease symptoms due to exposure to organic dust (OD). The role of secreted HMGB1 as a damage associated molecular pattern is well documented. However, the intracellular function of HMGB1 during airway inflammation has been poorly understood. We have previously shown that agricultural organic dust extract (ODE), with abundant microbial component diversity, promotes the secretion of HMGB1 during airway inflammation. The focus of this study was to determine the impact of conditional HMGB1 deficiency in ODE exposed airways, as opposed to elucidating the effects of secreted HMGB1 in airway inflammation. Following ODE exposure, mice with club cell-specific HMGB1 deletion showed an increase in airway inflammation. The lack of HMGB1 in the airways also increased the goblet cell numbers and tissue permeability, with significant histopathological changes. On the other hand, HMGB1 deficiency resulted in decreased production and release of certain DAMPs, particularly those released during mitochondrial dysfunction. Together, our results indicate that the increased inflammation in the airways of HMGB1 deficient mice could be due to club-cell specific role of HMGB1 in lung homeostasis.

Introduction

Occupational organic dust (OD) exposure in concentrated animal feed operations (CAFOs) has long been shown to be detrimental to the health of workers and is central to the development of chronic inflammatory airway diseases, including asthma, chronic bronchitis, and chronic obstructive pulmonary disease (COPD) reported in workers (Charavaryamath and Singh 2006; Poole and Romberger 2012). The composition of OD is complex and includes a variety of microbial associated molecular patterns (MAMPs). Hence exposure to OD could result in the activation of wide range of immune cells through pattern recognition receptors (PRRs), such as toll like receptors (TLRs) and nucleotide oligomerization domains (NODs) (Charavaryamath et al. 2008; Bailey et al. 2008; Poole et al. 2010; Schneberger et al. 2016). Interaction of MAMPs with PRRs leads to increased neutrophil influx, inflammatory cytokine release, airway hyper-responsiveness, and loss of lung function over time (Dosman et al. 2006a; Senthilselvan et al. 2007).

Several studies conducted using mouse models of intranasal administration of organic dust extract (ODE) have demonstrated inflammatory responses with acute and repetitive exposure (Poole et al. 2008; Poole et al. 2009; Shrestha et al. 2021). The results from animal studies have recapitulated many inflammatory features observed with human exposure to organic dust and gases in animal production units (Dosman et al. 2006a; Senthilselvan et al. 2007). The studies demonstrated an increased neutrophil, macrophage, and lymphocyte influx, airway hyper-responsiveness (AHR), and release of pro-inflammatory cytokines, including tumor necrosis factor (TNF)-α, interleukin (IL)-6, and neutrophil chemoattractant (CXCL1 and CXCL2), which resemble the human exposure response (Charavaryamath et al. 2005; Poole et al. 2009; Robbe et al. 2014b; Robbe et al. 2014a). In previous studies, it has been shown that ODE activates various

innate immune signaling pathways, such as protein kinase c (PKC) family, and MyD88 (Romberger et al. 2002; Nath Neerukonda et al. 2018; An et al. 2020).

Among the inflammatory mediators, damage associated molecular patters (DAMPs) are emerging as important players in orchestrating a sustained inflammatory response (Rubartelli and Lotze 2007; Li et al. 2013; Pouwels et al. 2014). Among the DAMPs, nuclear alarmin high mobility group box 1 (HMGB1) protein is gaining attention and we have demonstrated how HMGB1 could be targeted to reduce ODE mediated airway inflammation (Bhat et al. 2019; Jiang et al. 2020). HMGB1 is a highly conserved nuclear protein with a key role in the maintenance of chromatin structure and promotes target-specific transcriptional protein binding during homeostasis. HMGB1 has been shown to act as an extracellular signaling molecule which on binding to its receptors, receptor for advanced glycation end products (RAGE) and TLR 2 and 4, triggers pleiotropic effects, such as cell proliferation, differentiation, cell death, inflammation, and immunity (Andersson and Tracey 2011; Yang et al. 2015; Ugrinova and Pasheva 2017a; Ding et al. 2017). While the role of HMGB1 in the cytoplasm and extra-cellular milieu in accentuating inflammation is evident, another set of recent data have shown its role in wound healing underscoring the importance of dual roles played by HMGB1 and other alarmins (Ojo et al. 2015; Bertheloot and Latz 2017).

A global knockout of HMGB1 was observed to be fatal indicating the indispensable nature of this nuclear protein (Yanai et al. 2013). Interestingly, researchers explored the cell-specific role of HMGB1 in the digestive tract and found that HMGB1 has a role in intestinal epithelial cells in regulating tissue injury in inflammatory bowel disease (IBD) and other complex inflammatory disorders (Yamasaki et al. 2009; Vitali et al. 2011; Magna and Pisetsky 2014; Chen et al. 2020). Targeted deletion of HMGB1 in the intestinal epithelium led to the mitigation of the extent and

severity of inflammation-associated cellular injury by controlling the switch between the pro-autophagic and pro-apoptotic functions (Zhu et al. 2015). To our knowledge, we have not come across any targeted deletion of HMGB1 in the lung epithelial cells. A few studies have investigated the role of HMGB1 in cigarette smoke-induced lung inflammation and COPD where elevated levels of HMGB1 were found in the bronchoalveolar lavage (BAL) fluid of patients (Ferhani et al. 2010; Hou et al. 2011; Kanazawa et al. 2012; Ding et al. 2017). However, whether the release of HMGB1 is a direct consequence of smoking or related to the underlying inflammatory process is yet to be investigated. Furthermore, HMGB1 antagonism using anti-HMGB1 antibody or ethyl pyruvate ameliorated the lung damage in a murine pneumonia model and LPS-induced acute lung injury (Wang et al. 2020). This reflects the fact that the majority of HMGB1 research has focused on its extracellular functions rather than its intracellular/cytosolic functions during inflammation, despite it being found in the cell cytosol under these conditions.

The indication that HMGB1 levels were altered in various lung injury models led us to study the intracellular role of this protein using a murine model of intra-nasal exposure to ODE. The lung club cells abundant in the lung bronchioles, play a significant role in the repair and regeneration of the lung and are involved in the disease process (Jones-Freeman and Starkey 2020). Further, HMGB1 from $CC10^{+}$ (Club Cell Secretory Protein, CCSP) club cells drive type 2 immune response in mouse models of respiratory syncytial virus infection (Chen et al. 2018). Therefore, to elucidate the intracellular (normal nuclear) role of HMGB1 in an ODE-induced lung inflammation model, we chose to delete HMGB1 in a club cell-specific manner. To investigate this, we developed and used a club cell-specific HMGB1 knockout murine model and hypothesized that HMGB1 signaling may play a crucial role in the regulation of airway inflammation in response to ODE. Our findings demonstrate that, with ODE exposure of club cell-specific HMGB1 KO mice,

there is increased histopathological features of airway inflammation along with increased mucus production and tissue permeability. We further identified that the lack of HMGB1 in club cells was protective through reduced cellular influx and reactive species generation. These dichotomous results suggest that intracellular HMGB1 has dual functions in ODE-induced airway inflammation.

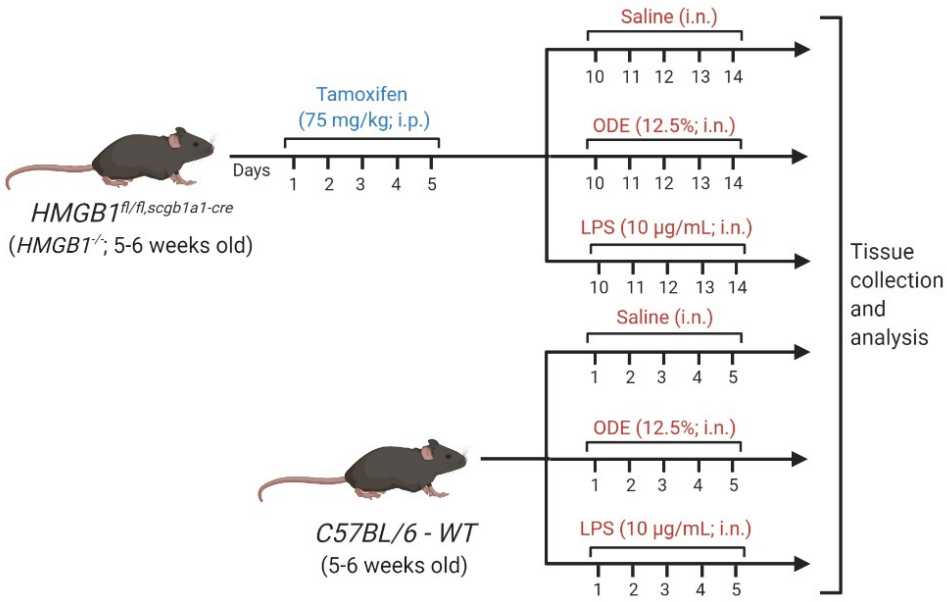

Figure 6.1 Experimental protocol
Club cell specific HMGB1 knockout (*HMGB1*$^{-/-}$) mice were adminitered tamoxifen (TAM; 75 mg/kg) intraperitoneally (i.p.) for 5 consecutive days. After a 5 days wait period, the mice were intranasally (i.n.) challenged with saline or 12.5% of organic dust extract (ODE) or 1 µg/mL of lipopolysaccharide (LPS). Age matched C56BL/6 (wild type, WT) mice were intranasally (i.n.) challenged with saline or 12.5% of organic dust extract (ODE) or 1 µg/mL of lipopolysaccharide (LPS).

Results

Generation of lung club-cell specific HMGB1 KO mice

Mice globally deficient in HMGB1 have been shown to die within 24 hours of birth, (Calogero et al. 1999) and hence we generated a lung club cell-specific HMGB1 knockout model to test the role of HMGB1 in physiologic disease models. We crossed the cre and floxed mice to create mice lacking HMGB1 in club cells (*Scgb1a1-cre HMGB*$^{fl/fl}$) of the lungs. In CreER^{TM}/LoxP studies, recombination of the floxed reporter allele is dependent on the dose of tamoxifen (TAM)

and occurs only in cells that express Cre (Figure 6.10a) (Hayashi and McMahon 2002). Adult (5–6 week old) *Scgb1a1-cre, HMGB$^{fl/fl}$* mice were injected with 75 mg/kg dose of TAM for 5 consecutive days, intraperitoneally (i.p.) (represented as *HMGB1$^{-/-}$*). One pup from each litter was given sham injections and used as controls to assess for leaky inducible cre recombinase (represented as *HMGB1$^{fl/fl}$*). The animals were quarantined for 5-7 days to allow the cre recombinase to take effect, after which the lungs were harvested (Figure 6.1). We confirmed HMGB1 knockout in club cells by confocal microscopy where the club cells were identified by immunofluorescence staining for Scgb1a1 (Secretoglobin 1a1, also known as CC10 or CCSP), location, and morphology, and the tissues were counter stained with anti-HMGB1 antibody (Figure 6.2a). As expected, recombination occurred in club cells (CCSP) throughout the bronchioles and lacked nuclear HMGB1, with no significant changes in the overall gross or microscopic anatomy of the lungs when compared to wild-type (WT) animals (Figure 6.2a and Figure 6.10c). Overall, all the animals (*HMGB1$^{-/-}$* and *HMGB1$^{fl/fl}$*) appeared healthy and showed no abnormalities. The knockout was further confirmed by qPCR, were fold change of HMGB1, and the target exons (exon 2 and exon 3) were measured (Figure 6.10a and 6.10b). We observed a significant decrease in the fold change of all targets in *HMGB1$^{-/-}$* mice when compared to WT and *HMGB1$^{fl/fl}$* mice.

Club-cell specific HMGB1 knockdown does not alter lung HMGB1 levels following exposure to ODE

HMGB1 levels in the lungs, serum and bronchoalveolar lavage fluid (BALF) were measured in *HMGB1$^{-/-}$* mice treated with saline, LPS (1 µg/mL; positive control) and ODE (12.5%) intranasally for 5 consecutive days (Figure 6.1, and Table 6.1). Exposure to LPS and ODE significantly increased HMGB1 protein expression and mRNA fold change in the lungs of WT mice, while in *HMGB1$^{-/-}$* mice the levels were significantly low in control, as well as on LPS and ODE exposure, further confirming HMGB1 knockout (Figure 6.2b, 6.2c and 6.2d).

Immunoblotting using cell-free BALF and blood serum samples was performed to quantify the levels of HMGB1 released into the airways and blood, respectively, wherein decreased levels of HMGB1 in *HMGB1*$^{-/-}$ mice was observed compared to WT mice (Figure 6.2e and 6.2f). Coomassie brilliant blue (CBB) staining was performed on the SDS gels of BALF and serum samples and were used as representation of protein loading controls (Figure 6.2g and 6.2h).

ODE mediated cellular influx into airways was decreased in HMGB1$^{-/-}$ mice

There was a significant increase in total cell influx following intranasal exposure to ODE for 5 days compared to control in both WT and *HMGB1*$^{-/-}$ mice (Figure 6.3a). Neutrophil influx, a characteristic feature of ODE-induced airway inflammation was increased in both ODE-exposed WT and *HMGB1*$^{-/-}$ mice (Figure 6.3c). In addition, alveolar macrophages were also elevated in both ODE exposed WT and *HMGB1*$^{-/-}$ mice compared to control (Figure 6.3b). Total airway cellular influx, neutrophils numbers and macrophages numbers were significantly decreased in ODE exposed *HMGB1*$^{-/-}$ mice when compared to ODE exposed WT mice. *HMGB1*$^{-/-}$ mice exposed to saline showed a significant increase in total cellular influx compared to WT mice exposed to saline. mRNA fold change of *tlr2* and *tlr4* increased significantly in *HMGB1*$^{-/-}$ mice upon exposure to both saline and ODE when compared to WT mice (Figure 6.3d and 6.3e). In addition, an increase in the mRNA fold change of selected proinflammatory cytokines, *il1b and tnfa*, was observed in ODE exposed WT and *HMGB1*$^{-/-}$ mice compared to WT exposed to saline (Figure 6.3f and 6.3g). Expression of *il10* was significantly decreased in ODE exposed *HMGB1*$^{-/-}$ mice when compared to the ones exposed to saline (Figure 6.3h). On the other hand, expression of *tgfb* in ODE exposed *HMGB1*$^{-/-}$ mice was significantly higher than saline exposed WT and *HMGB1*$^{-/-}$ mice, with no significant change in ODE exposed WT mice (Figure 6.3i).

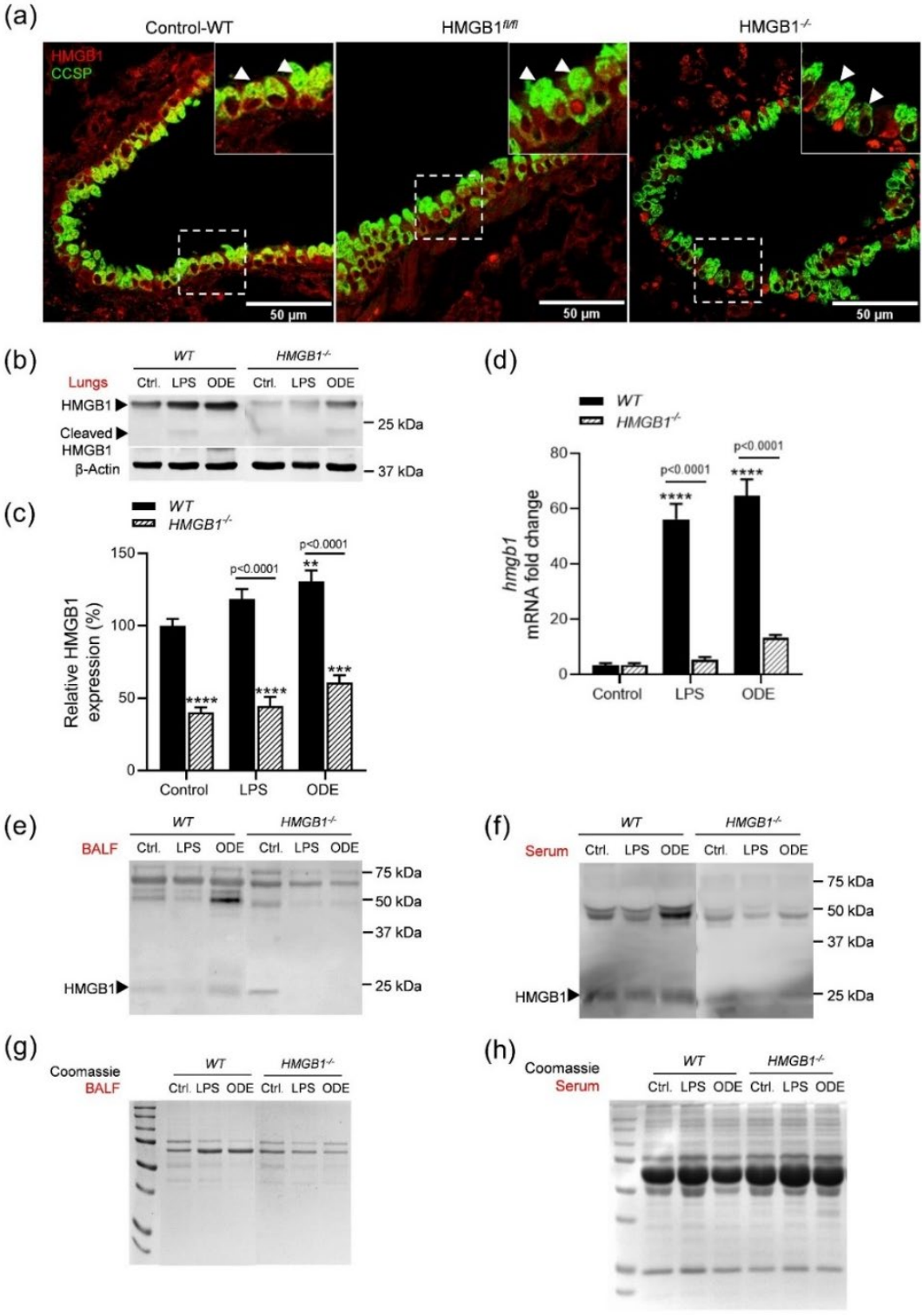

Figure 6.2 Intranasal ODE exposure increases HMGB1 expression in the airways
Confocal microscopic images of bronchioles from the lungs of untreated *wild-type (control, C57BL/6)*, *HMGB1*$^{fl/fl,\ scgb1a1\text{-}Cre}$ without TAM (*HMGB1*$^{fl/fl}$) and *HMGB1*$^{fl/fl,\ scgb1a1\text{-}Cre}$ with TAM (*HMGB1*$^{-/-}$) mice stained for HMGB1 (red), and club cells (CCSP; green) (originial magnification, x400). Arrow heads indicate club cells (a). Immunoblot (b & c) and mRNA fold change (d) of

HMGB1 expression in the lungs from control and HMGB1$^{-/-}$ mice after 5 days of saline, LPS (1 μg/mL) or ODE (12.5%) exposure. Immunoblot of HMGB1 expression in the bronchalveolar lavage (BALF) (e) and serum (f) from control and *HMGB1*$^{-/-}$ mice after 5 days of saline, LPS (1 μg/mL) or ODE (12.5%) exposure. Coomassie blue staining for loading control in the BALF (g) and serum (h) from control and *HMGB1*$^{-/-}$ mice after 5 days of saline, LPS or ODE exposure. All the protein bands were normalized over β-actin (37 kD) and percentage intensity relative to control was analyzed. Data was analyzed using one-way ANOVA with Tukey's multiple comparison test (*$p < 0.05$, **$p < 0.01$, ***$p < 0.001$, ****$p < 0.0001$) and represented as mean ± SEM with n = 4-6 mice/group (*indicates significant difference from control).

The lung wet-to-dry weight ratio was measured 24 hours after the final intranasal administration of saline or ODE (Figure 6.3j). Compared to saline exposed WT and *HMGB1*$^{-/-}$ mice, there was a significant increase in the ratio in ODE exposed mice indicative of increased ODE-mediated edema, with no effect of conditional HMGB1 knockout. To investigate whether the lack of HMGB1 has any impact on the expression of one of its major target receptors, RAGE, immunoblotting was performed to measure the expression (Figure 6.3k). Following ODE exposure, RAGE expression significantly increased in *HMGB1*$^{-/-}$ mice compared to WT.

Goblet cell metaplasia is observed in airways of *HMGB1*$^{-/-}$ mice

Lung tissue sections were stained with periodic acid Schiff (PAS) to detect goblet cells (Figure 6.6a). The number of goblet (PAS+) cells were manually counted and normalized to the length of the basement membrane (Figure 6.6b). We observe a significant increase in the number of goblet cells in ODE exposed WT and *HMGB1*$^{-/-}$ animals compared to saline exposed WT animals. We also documented an increase in the number of goblet cells in *HMGB1*$^{-/-}$ mice exposed to saline. To corroborate this, mRNA fold change of *muc5ac* was measured by qRT-PCR (Figure 6.6c). In WT mice, ODE exposure significantly increased the fold change in the expression of *muc5ac* gene. In *HMGB1*$^{-/-}$ mice, saline and ODE exposure significantly increased the fold change in the expression of *muc5ac* gene when compared to saline exposed WT mice. Further, *muc5ac* gene expression was significantly increased in the ODE exposed *HMGB1*$^{-/-}$ mice when compared to ODE exposed WT and saline exposed *HMGB1*$^{-/-}$ mice. In addition, expression of forkhead box

protein J1 (FoxJ1), the transcription factor involved in ciliogenesis and a marker for motile cilia, was measured in the lungs post-exposure (Figure 6.6d). A decrease in FoxJ1 expression was observed in *HMGB1*$^{-/-}$ mice exposed to saline and ODE as well as in WT mice exposed to ODE.

Lack of HMGB1 exacerbates loss of tight junction integrity in *HMGB1*$^{-/-}$ mice

24 h after the final exposure, airway tissue permeability was measured by intranasal instillation of FITC-Dextran (10 mg/ kg of body weight) for 1 hour. Compared to saline exposed WT mice, ODE exposed WT mice showed an increase in the fluorescence intensity (FI) in the blood serum. Saline-exposed *HMGB1*$^{-/-}$ mice had significantly higher FI values when compared to saline-exposed WT mice. On the other hand, the FI values were significantly decreased in *HMGB1*$^{-/-}$ mice exposed to ODE when compared to ODE exposed WT mice, respectively (Figure 6.7a). To corroborate this, the expression of tight and adherens junction markers was measured. Fold change of claudins, *cldn1* and *cldn5* significantly increased in ODE exposed WT mice when compared to WT saline group, with no significant increase in *cldn18*. There was an increase in fold change of *cldn1*, *cldn5,* and *cldn18* in *HMGB1*$^{-/-}$ mice exposed to both saline and ODE compared to saline exposed WT mice (Figure 6.7b, 6.7c, and 6.7d). An increase in the expression of cadherins, *ecad,* and *ncad* mRNA in *HMGB1*$^{-/-}$ mice exposed to both saline and ODE was observed compared to saline exposed WT mice. Expression of *ecad* increased significantly in ODE exposed *HMGB1*$^{-/-}$ mice when compared to saline exposed animals (Figure 6.7e). However, expression of *ncad* decreased significantly in ODE exposed *HMGB1*$^{-/-}$ mice when compared to saline exposed animals (Figure 6.7f). On the other hand, protein expression of zonula occludens-1 (ZO-1) and occludin was significantly decreased in *HMGB1*$^{-/-}$ mice exposed to both saline and ODE compared to saline exposed WT mice (Figure 6.7g and 6.7h). ZO-1 protein levels were also decreased in WT mice exposed to ODE (Figure 6.7.h).

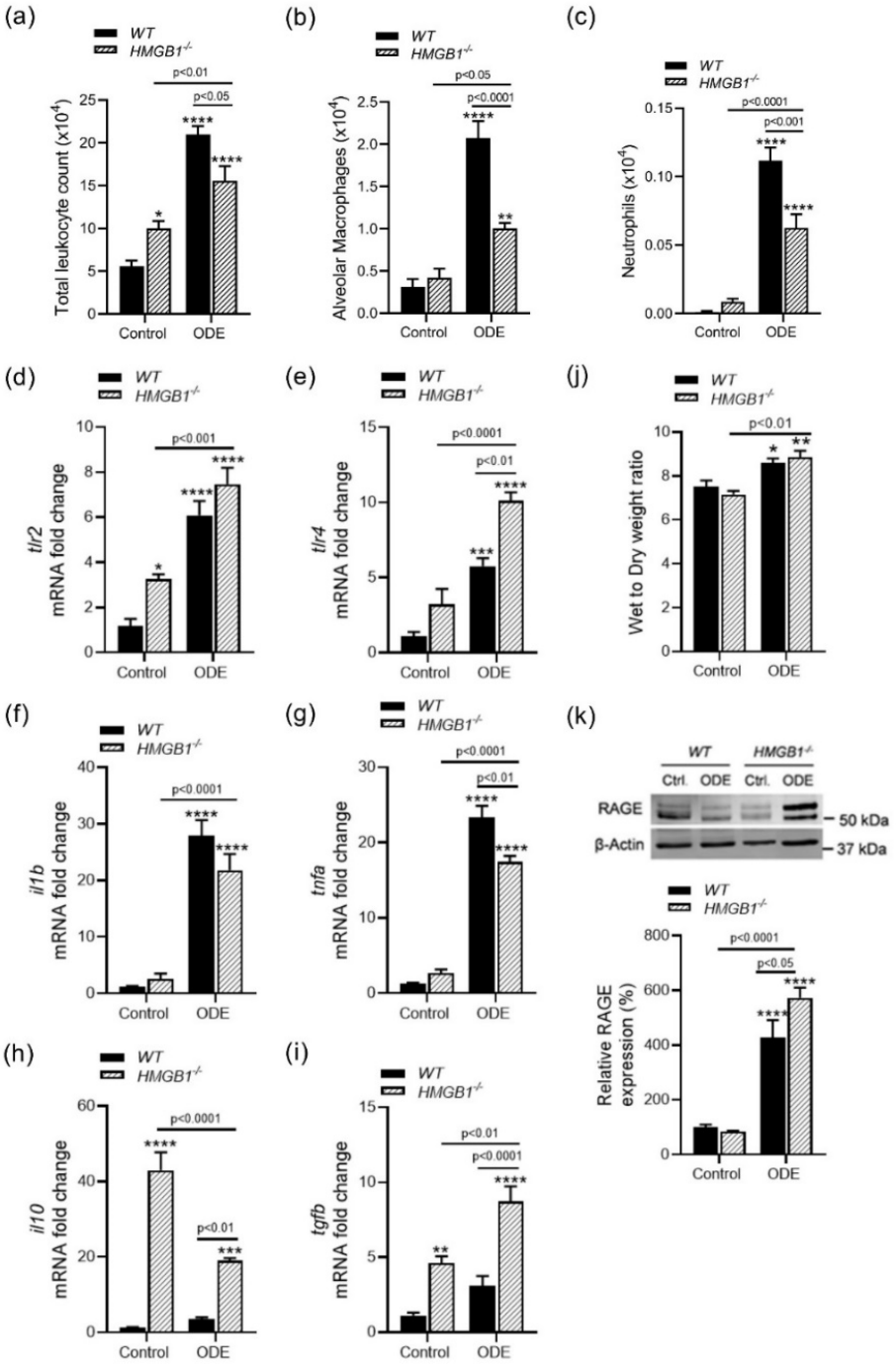

Figure 6.3 Loss of HMGB1 decreases cellular influx into the airways in ODE mediated airway inflammation

Bronchoalveolar lavage fluid (BALF) cells obtained from lungs of control and *HMGB1*$^{-/-}$ mice after 5 days of saline or ODE (12.5%) exposure, stained with Shandon Kwik Diff staining solution. Total leukocyte count (a) and differential cell count of alveolar macrophages (b) and neutrophils (c) in BALF. mRNA fold change of *tlr2* (d), *tlr4* (e), *il1b* (f), *tnfa* (g), *il10* (h), and *tgfb* (i) expression in the lungs from control and *HMGB1*$^{-/-}$ mice after 5 days of saline or ODE exposure. Lung wet to dry weight ratios in control and *HMGB1*$^{-/-}$ mice after 5 days of saline or ODE exposure (j). Immunoblot of RAGE protein expression in the lungs from control and *HMGB1*$^{-/-}$ mice after 5

days of saline or ODE (12.5%) exposure (k). All the protein bands were normalized over β-actin (37 kD) and percentage intensity relative to control was analyzed. Data was analyzed using one-way ANOVA with Tukey's multiple comparison test (*p < 0.05, **p < 0.01, ***p < 0.001, ****p < 0.0001) and represented as mean ± SEM with n = 4-8 mice/group (*indicates significant difference from control).

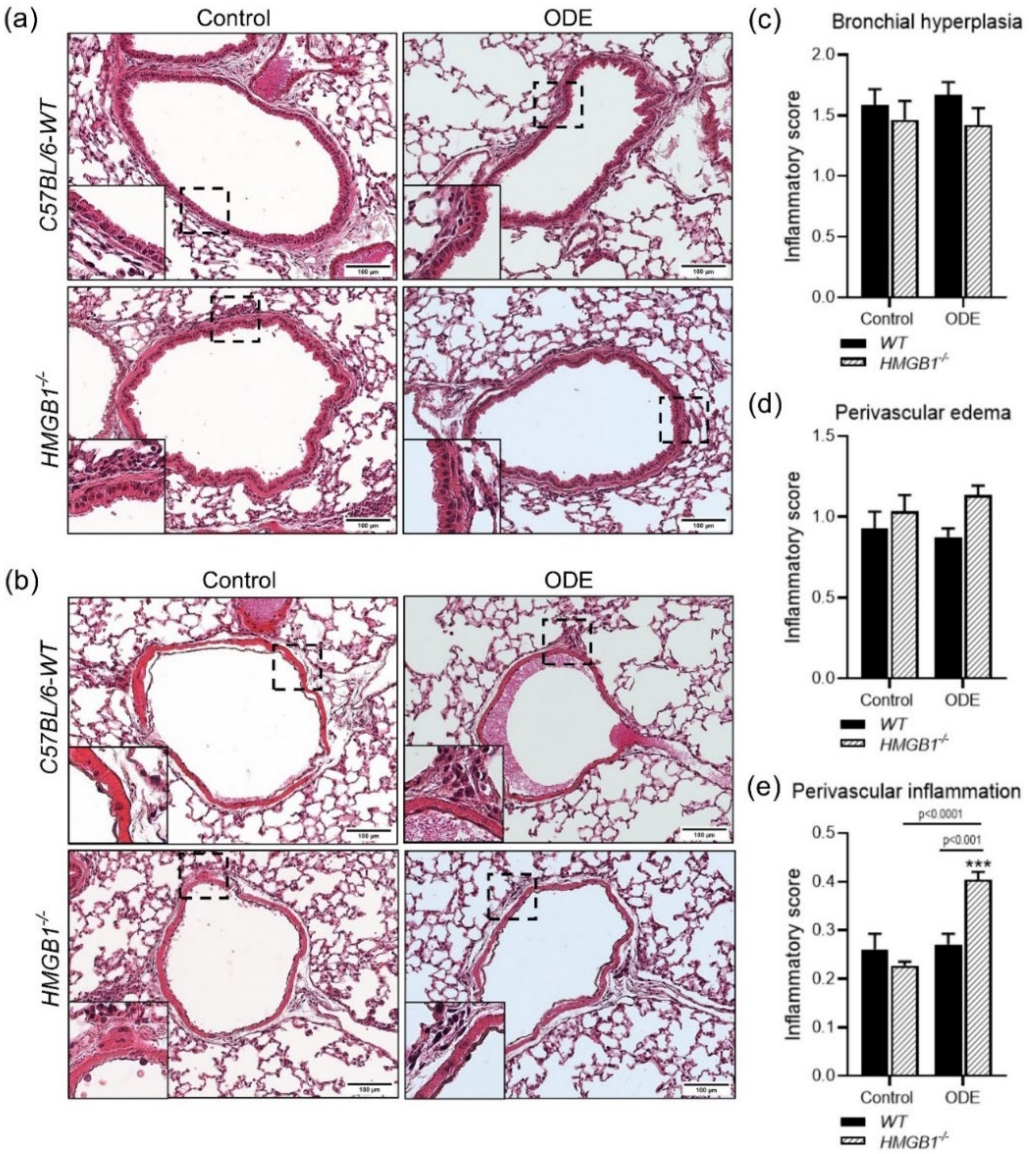

Figure 6.4 Lack of HMGB1 exacerbates ODE mediated perivascular inflammation
Formalin fixed lung tissue sections from control and *HMGB1*$^{-/-}$ mice after 5 days of exposure to saline or ODE (12.5%) were stained with heamtoxylin and eosin (H&E). Representative images of H&E stained bronchioles (a) and blood vessels (c) were obtained. Insets: images were shown with higher magnification images (original magnification, x200). Semiquantitative histopathology scoring of bronchial hyperplasia (b), perivascular edema (d), and perivascuar inflammation is presented (e). Data was analyzed using one-way ANOVA with Tukey's multiple comparison test (*p < 0.05, **p < 0.01, ***p < 0.001, ****p < 0.0001) and represented as mean ± SEM with n = 3-5 fields/ mice and 8 mice/group (*indicates significant difference from control).

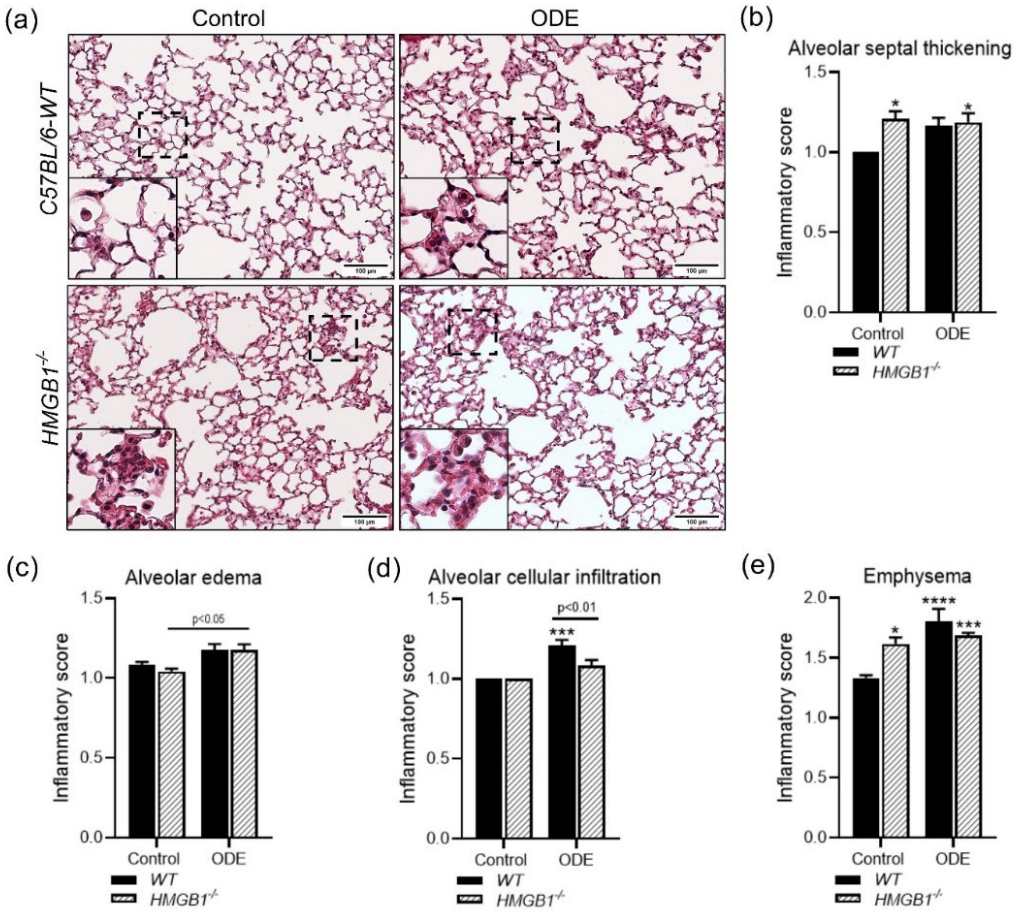

Figure 6.5 ODE exposure induces alveolar septal thickening and emphysema
Formalin fixed lung tissues obtained from control and *HMGB1*$^{-/-}$ mice after 5 days of saline or ODE (12.5%) exposure were stained with hematoxylin and eosin (H&E). Images of H&E stained alveoli were obtained. Insets: images were shown with higher magnification images (original magnification, x200) (a). Semiquantitative histology scoring of alveolar septal thickening (b), alveolar edema (c), cellular infiltration (d) and emphysema (e). Data was analyzed using one-way ANOVA with Tukey's multiple comparison test (*$p < 0.05$, **$p < 0.01$, ***$p < 0.001$, ****$p < 0.0001$) and represented as mean ± SEM with n = 3-5 fields/ mice and 8 mice/group (*indicates significant difference from control).

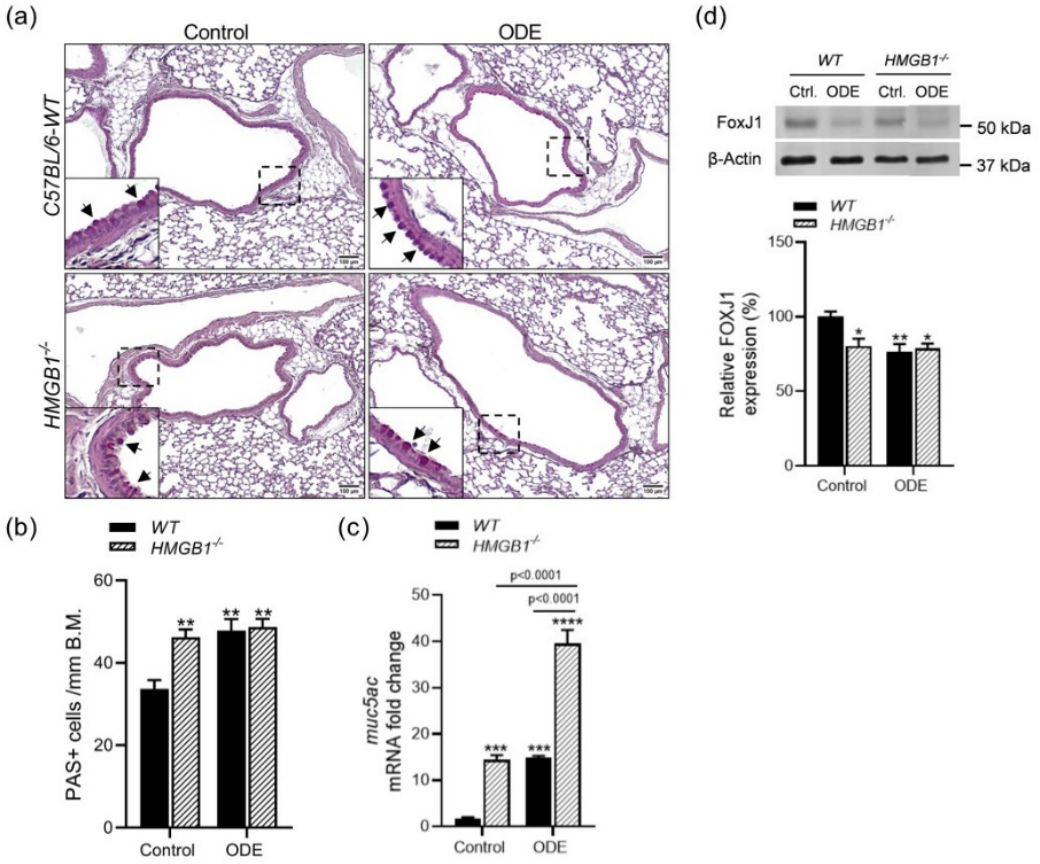

Figure 6.6 HMGB1 deficient mice have increased airway periodic acid schiff (PAS) staining Formalin fixed lung tissues obtained from control and *HMGB1*$^{-/-}$ mice after 5 days of saline or ODE (12.5%) exposure were stained with periodic acid schiff (PAS) for detection of goblet cells. Insets: images were shown with higher magnification images. Arrows indicate PAS-positive cells. (a). Quantification of the number of PAS-positive cells goblet cells per mm of basement membrane (BM) (b). mRNA fold change of *muc5ac* expression in the lungs from control and *HMGB1*$^{-/-}$ mice after 5 days of saline or ODE (12.5%) exposure (c). Immunoblot of FoxJ1 protein expression in the lungs from control and *HMGB1*$^{-/-}$ mice after 5 days of saline or ODE (12.5%) exposure (d). All the protein bands were normalized over β-actin (37 kD) and percentage intensity relative to control was analyzed. Data was analyzed using one-way ANOVA with Tukey's multiple comparison test (*$p < 0.05$, **$p < 0.01$, ***$p < 0.001$, ****$p < 0.0001$) and represented as mean ± SEM with n = 2-4 fields/ mice and 8 mice/group (*indicates significant difference from control).

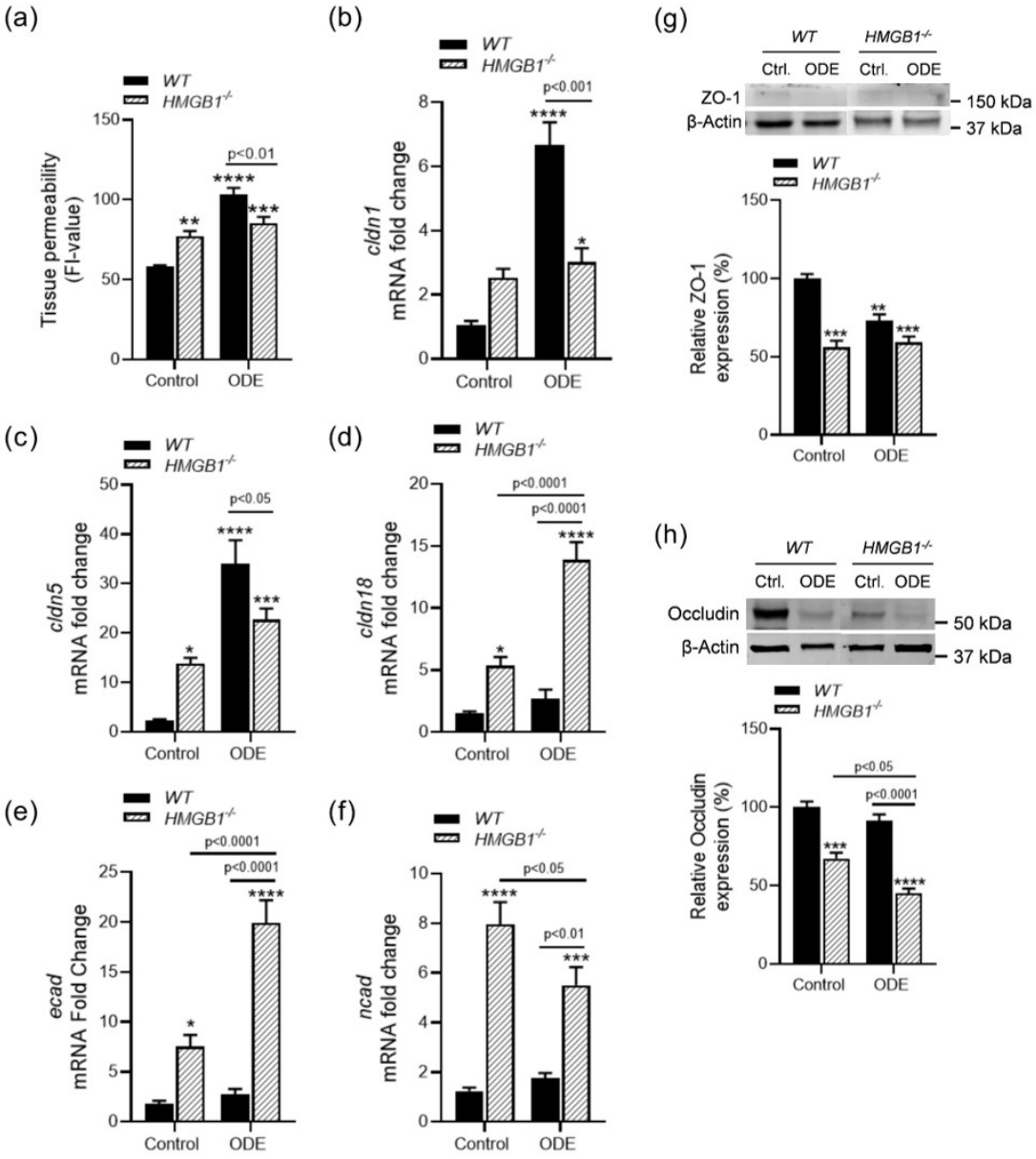

Figure 6.7 ODE exposure decreases airway epithelium junction integrity
Lung permeability assay using 10 mg/kg b.w. of FITC-Dextran via intranasal (i.n.) administration in control and *HMGB1*$^{-/-}$ mice after 5 days of saline or ODE (12.5%) exposure (a). mRNA fold change of *cldn1* (b), *cldn5* (c), *cldn18* (d), *ecad* (e), and *ncad* (f) expression in the lungs from control and *HMGB1*$^{-/-}$ mice after 5 days of saline or ODE exposure. Immunoblot of ZO-1 (g) and Occludin (h) protein expression in the lungs from control and *HMGB1*$^{-/-}$ mice after 5 days of saline or ODE (12.5%) exposure (k). All the protein bands were normalized over β-actin (37 kD) and percentage intensity relative to control was analyzed. Data was analyzed using one-way ANOVA with Tukey's multiple comparison test (*$p < 0.05$, **$p < 0.01$, ***$p < 0.001$, ****$p < 0.0001$) and represented as mean ± SEM with n = 4-6 mice/group (*indicates significant difference from control).

mtDNA levels release into airways is decreased in *HMGB1*$^{-/-}$ mice

Our previous studies have shown induction of mitochondrial dysfunction and release of mitochondrial DNA (mtDNA) into the extracellular spaces following ODE-induced cellular stress. In order to quantify the amount of secreted mtDNA in the airways and blood stream, cell-free BALF and serum samples were processed (Figure 6.8a and 6.8b). Levels of mtDNA were significantly increased in ODE exposed WT and *HMGB1*$^{-/-}$ mice compared to saline exposed WT mice in both BALF and serum. When compared to WT mice exposed to ODE, the levels of mtDNA in BALF was significantly decreased in *HMGB1*$^{-/-}$ mice exposed to ODE. However, this decrease was not statistically significant in the serum samples. In addition, the expression of other DAMPs associated with mitochondrial damage and dysfunction was measured in the lungs post-exposure. Fold change of *nos2* gene, encoding for inducible nitric oxide synthase (iNOS), significantly increased with ODE exposure in both WT and *HMGB1*$^{-/-}$ mice compared to saline exposed WT mice (Figure 6.8c). Between the ODE exposed mice, the expression of *nos2* was significantly decreased in *HMGB1*$^{-/-}$ mice compared to WT mice. The expression of GP91Phox protein, a subunit of NADPH oxidase, was measured to assess superoxide production (Figure 6.8d). The expression of GP91Phox was increased in ODE exposed WT mice, while the levels were significantly decreased in ODE exposed *HMGB1*$^{-/-}$ mice comparable to saline exposed WT mice. In addition, saline exposed *HMGB1*$^{-/-}$ mice showed significantly reduced expression of GP91Phox compared to all groups. The expression of mitochondria specific proteins cytochrome c and TFAM were measured as well. There was a significant increase in cytochrome c in *HMGB1*$^{-/-}$ animals exposed to saline compared to WT, while the levels in ODE exposed mice remained comparable to saline exposed WT mice (Figure 6.8e). Expression of TFAM on the other hand were significantly decreased in *HMGB1*$^{-/-}$ mice exposed to saline or ODE (Figure 6.8f). On the other hand, TFAM levels were significantly increased in ODE-exposed WT mice.

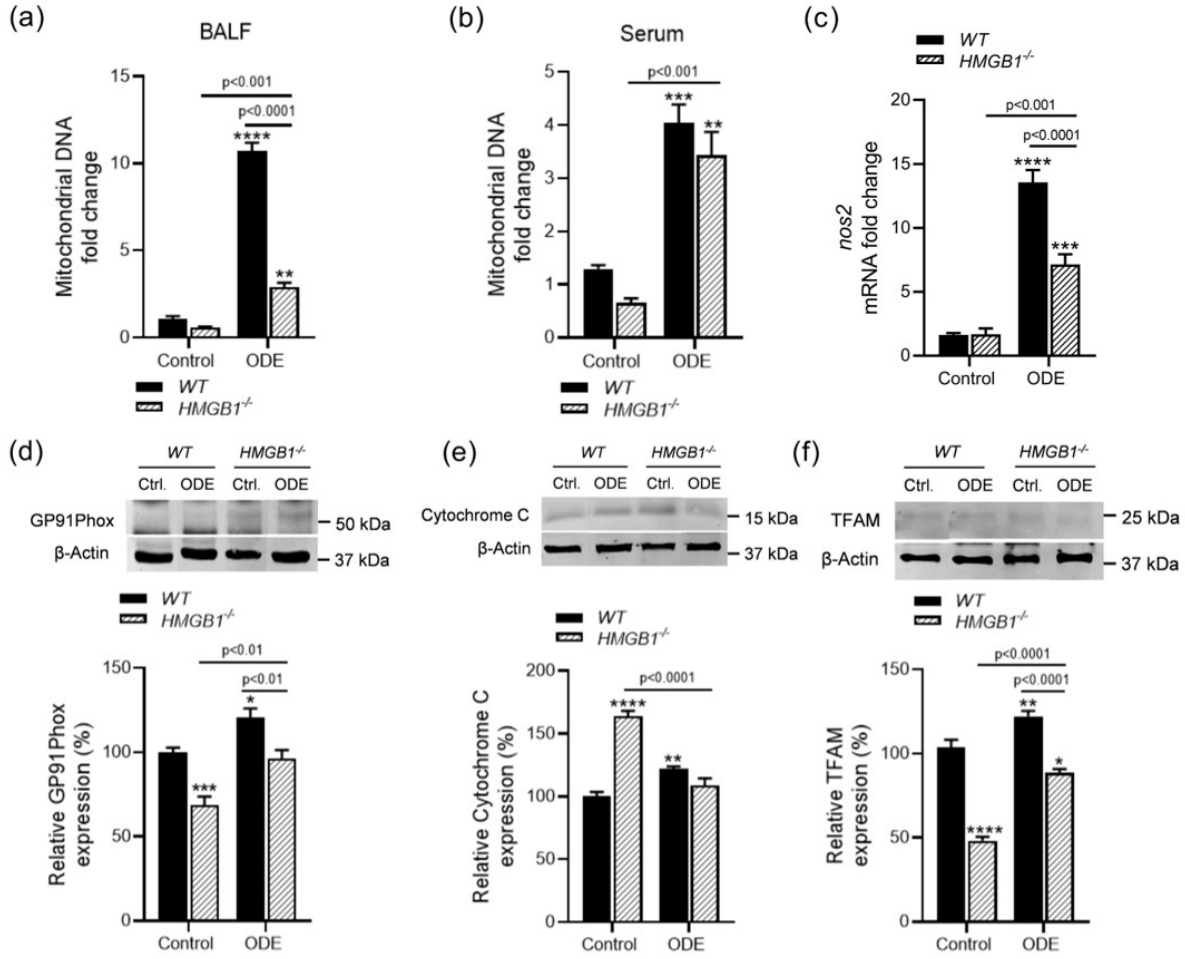

Figure 6.8 ODE exposure induces mitochondrial DNA release into BALF
Measurement of mitochondrial DNA (mtDNA) released into the airway spaces, collected in BALF (a), and blood serum (b) of control and *HMGB1*$^{-/-}$ mice after 5 days of saline or ODE (12.5%) exposure. mRNA fold change of *nos2* expression in the lungs from control and *HMGB1*$^{-/-}$ mice after 5 days of saline or ODE exposure (c). Immunoblot of GP91Phox (d), Cytochrome C (e), and TFAM (f) protein expression in the lungs from control and *HMGB1*$^{-/-}$ mice after 5 days of saline or ODE (12.5%) exposure. All the protein bands were normalized over β-actin (37 kD) and percentage intensity relative to control was analyzed. Data was analyzed using one-way ANOVA with Tukey's multiple comparison test (*$p < 0.05$, **$p < 0.01$, ***$p < 0.001$, ****$p < 0.0001$) and represented as mean ± SEM with n = 4-6 mice/group (*indicates significant difference from control).

Glucose uptake and hypoxia is increased in *HMGB1*$^{-/-}$ mice

Expression of markers associated with mitochondrial biogenesis were measured in the lungs of mice. Fold change of key marker that initiates mitochondrial biogenesis, peroxisome proliferator-activated receptor gamma coactivator 1-alpha (*pcg1a*), was found to increase in ODE

exposed WT and *HMGB1*$^{-/-}$ mice compared to WT mice exposed to saline (Figure 6.9a). The downstream target of PGC1α, nuclear factor erythroid 2-related factor 2 (NRF2) protein expression was measured. NRF2 protein expression was significantly decreased in ODE exposed WT and *HMGB1*$^{-/-}$ mice compared to saline exposed WT mice (Figure 6.9b). Additionally, NRF2 levels were also significantly decreased in saline exposed *HMGB1*$^{-/-}$ mice compared to WT. Protein expression of sirtuin 1 (SIRT1), the upstream regulator of PGC1a, was measured to assess the probability of mitochondrial biogenesis occurring in the lungs (Figure 6.9c). SIRT1 expression was significantly decreased in ODE exposed WT and *HMGB1*$^{-/-}$ mice compared to WT saline group. A similar decrease was observed in saline exposed *HMGB1*$^{-/-}$ mice but was significantly higher when compared to ODE exposed *HMGB1*$^{-/-}$ mice. Oxygen sensing and adaptations, a consequence of mitochondrial dysfunction, were evaluated in the lungs of the mice. *HMGB1*$^{-/-}$ mice exposed to ODE showed a significant increase in mRNA fold change of (*hif1a*), while the levels were minimally higher in ODE exposed WT mice and saline exposed *HMGB1*$^{-/-}$ mice when compared to WT saline group (Figure 6.9d). Fold change expression of genes involved in glucose uptake and glycolysis, solute carrier family 2 member 6 (*slc2a6*) and enolase 1 (*eno1*), was measured in the lungs. ODE exposed WT and *HMGB1*$^{-/-}$ mice showed a significant increase in *eno1* expression compared to saline groups (Figure 6.9e). On the other hand, *HMGB1*$^{-/-}$ mice exposed to saline and ODE had increased *slc2a6* expression, with no significant increase in ODE exposed WT mice (Figure 6.9f). Between the *HMGB1*$^{-/-}$ mice, *slc2a6* expression decreased in ODE exposed mice compared to saline exposed mice.

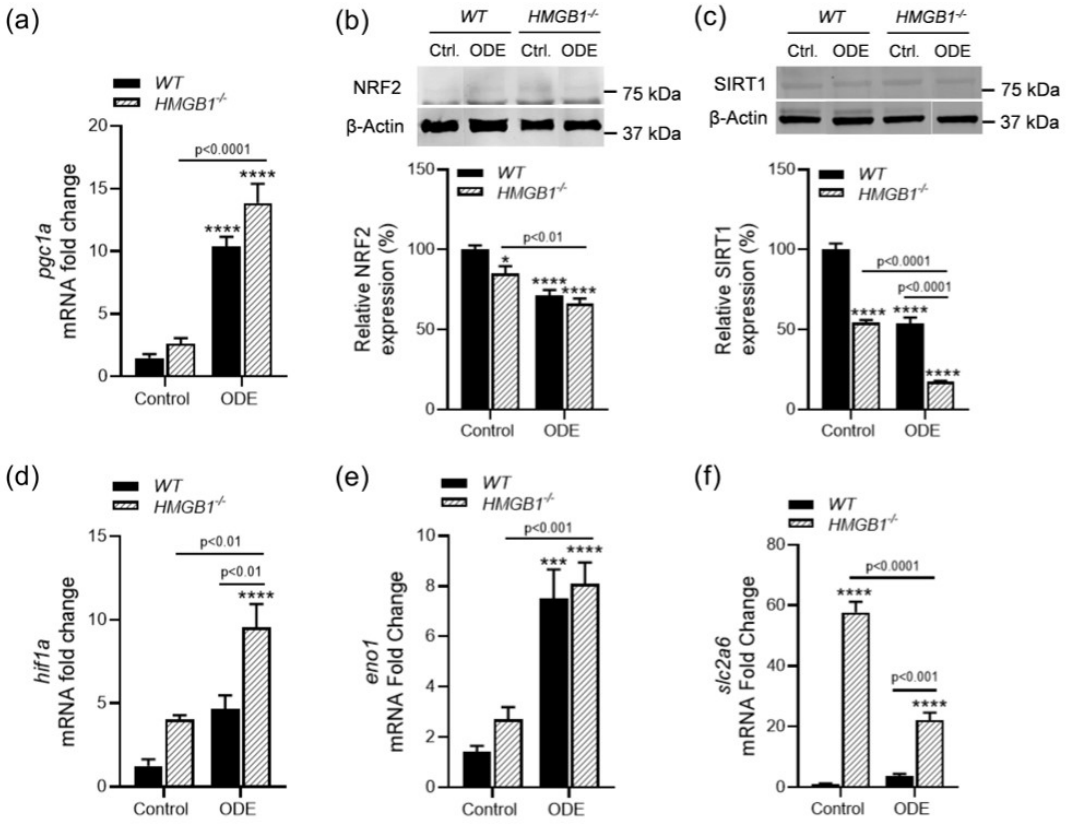

Figure 6.9 Lack of HMGB1 promotes increased glucose uptake in ODE exposed airways
mRNA fold change of *pgc1a* expression in the lungs from control and *HMGB1*$^{-/-}$ mice after 5 days of saline or ODE (12.5%) exposure (c). Immunoblot of NRF2 (d), and SIRT1 (f) protein expression in the lungs from control and *HMGB1*$^{-/-}$ mice after 5 days of saline or ODE (12.5%) exposure. mRNA fold change of *hif1a* (d), *eno1* (e), and *slc2a6* (f) expression in the lungs from control and *HMGB1*$^{-/-}$ mice after 5 days of saline or ODE (12.5%) exposure. All the protein bands were normalized over β-actin (37 kD) and percentage intensity relative to control was analyzed. Data was analyzed using one-way ANOVA with Tukey's multiple comparison test (*$p < 0.05$, **$p < 0.01$, ***$p < 0.001$, ****$p < 0.0001$) and represented as mean ± SEM with n = 4-6 mice/group (* indicates significant difference from control).

Discussion

Overall, we mechanistically describe the role of HMGB1 in regulating OD-induced lung inflammation in a cell-specific manner. Repeated exposure to OD is known to change innate immune responses in the airways, thus resulting in chronic respiratory disease and airway obstruction (Sundblad et al. 2009). Targeting host defense response to MAMPs present in OD and/or common downstream proteins is one strategy to reduce lung inflammatory diseases.

Previous studies have reported that intranasal challenge with ODE activates TLR2, TLR4, and TLR9 and signals via MyD88 in mouse lungs (Charavaryamath et al. 2008; Bailey et al. 2008; Schneberger et al. 2016; An et al. 2020). To address the role of DAMPs, we chose to focus on a prototype DAMP molecule known as HMGB1. Previously using *in vitro* models, we have demonstrated that ethyl pyruvate mediated blockage of secreted HMGB1 and siRNA mediated knockdown of HMGB1 downregulates ODE-induced reactive oxygen species (ROS) generation and augments IL-10 production to promote anti-inflammatory effects (Bhat et al. 2019; Massey et al. 2019). Other studies have also shown a reduction in cytokine storm and amelioration of CLP-induced sepsis lethality on siRNA-mediated knockdown of HMGB1 in murine macrophages and dendritic cells (Ye et al. 2012). Studies have correlated the presence of high levels of HMGB1 in blood and lungs to respiratory dysfunction and COPD development (Ferhani et al. 2010; Kanazawa et al. 2012). Also, COPD mediated airway inflammation usually involves increased inflammatory mediators such as CXCL-8, an HMGB1 ligand and an essential mediator of neutrophil recruitment (Pouwels et al. 2014; Barnes 2017). To identify the impact of HMGB1 on ODE-mediated airway inflammation *in vivo,* we employed a club cell-specific HMGB1 knockout murine model. Here we show that in contrast to previous work, HMGB1 acts as a double-edged sword wherein lack of intracellular HMGB1 in club cells amplifies the ODE-exposure induced airway pathology despite the decrease in cellular influx and release of DAMPs in *HMGB1*$^{-/-}$ mice.

Murine models of intranasal exposure to ODE recapitulate many features of airway inflammatory disease observed in exposed agricultural workers (Charavaryamath et al. 2005; Poole et al. 2009). Despite over two decades of research in understanding the OD-induced airway inflammatory disease pathophysiology, the precise role of intracellular HMGB1 in OD-exposure-induced lung inflammation remains mostly unknown. Since global knockdown of HMGB1 gene

is fatal, we generated mice conditionally deficient in HMGB1 in the club cells. The use of these mice as the *in vivo* model of ODE-induced lung inflammation allowed us to examine both the importance of nuclear HMGB1 and club cells in host response to ODE exposure. A hallmark of OD exposure is the increased influx of neutrophils and macrophages (Sundblad et al. 2009). Consistent with previous studies, we document an increase in total leukocyte influx into the airways, in addition to an increase in the fold change of *tlr2*, *tlr4*, *il1b* and *tnfa* genes on exposure to ODE in WT animals (Poole et al. 2009; Sundblad et al. 2009; Poole and Romberger 2012). In ODE exposed HMGB1$^{-/-}$ mice, although we observe a significant decrease in cellular influx into the airways, an increase in pro-inflammatory mediators listed is observed, with a few of them showing a considerable increase even without ODE exposure. Collectively the overall response due to a mixture of inflammatory markers and cellular influx could be determining the extent of lung pathology potentiated following ODE exposure in both types of mice.

Histopathological analysis of the lungs from WT and *HMGB1*$^{-/-}$ mice showed significant changes in the tissues both with and without ODE exposure. ODE exposed *HMGB1*$^{-/-}$ mice showed perivascular inflammation, alveolar septal thickening, alveolar edema and emphysema. *HMGB1*$^{-/-}$ mice showed increased emphysema and septal thickening with saline exposure alone. As observed in earlier studies, airway mucin (Muc5ac) expression and goblet cell numbers were increased in ODE exposed WT mice, but interestingly *HMGB1*$^{-/-}$ mice showed an increase in both goblet cell numbers and muc5ac gene expression with or without exposure to ODE (Dickinson et al. 2018). Lung club cells can self-renew and give rise to ciliated cells following lung injury (Hiemstra and Bourdin 2014; Barnes 2015). On ODE exposure, a decrease in the expression of FoxJ1 is observed in WT mice but *HMGB1*$^{-/-}$ mice had decreased expression of FoxJ1 with and without ODE exposure as well. It is possible that the lack of HMGB1 in club cells is promoting goblet cell

metaplasia and loss of cilia in the airways thus impacting the mucociliary clearance. However, further studies using lineage tracing may be necessary to mechanistically validate our current observation.

Increased epithelial permeability is a hallmark of mucosal inflammation. Epithelial junctional complexes can be disrupted directly by inhaled substances that penetrate the mucus layer or indirectly by cytokines and other inflammatory mediators (Grainge and Davies 2013). Our observation of ODE exposure induced increase in the airway epithelial permeability is in line with the aforementioned studies. On the other hand, in *HMGB1*$^{-/-}$ mice the permeability was decreased compared to WT mice exposed to ODE but remained significantly higher compared to WT mice exposed to saline. Interestingly, mRNA fold change of tight junction markers (claudin 1, claudin 5 and claudin 18) are increased across all the strains of animals compared to control. In addition to claudins, epithelial barrier function is also maintained by the occludin proteins, which are anchored to the cytoskeleton by ZO-1 thus forming a complex (Georas and Rezaee 2014). Occludin and ZO-1 proteins form the intact intercellular barrier at tight junctions, and differences in their expression account for differences in the barrier function and paracellular permeability among epithelia (Ye et al. 2003; Ohtake et al. 2003; Raleigh et al. 2011). Our study showed a decrease in the expression of both occludin and ZO-1 proteins on exposure to ODE and the decrease is exacerbated by the lack of HMGB1 in the club cells. This change in the pattern of expression of key markers of epithelial barrier integrity paralleled by the changes in tissue permeability suggests a decreased synthesis occurring at the translational level due to ODE-induced cellular stress and/ or lack of intracellular HMGB1. Lack of HMGB1 also significantly altered the fold change of *ecad* and *ncad* genes, where we document a significant increase in the *ecad* expression on exposure to ODE. E-cad and N-cad are key regulators of epithelial

mesenchymal transition (EMT) which is characterized by the loss of E-cad and enhanced expression of N-cad (Nieto 2011). Emerging data suggest that EMT likely contributes to airway remodeling and has been shown to occur on exposure to house dust mite (HDM) and in asthma in concert with the production of TGF-β1 (Hackett et al. 2009; Heijink et al. 2010).

HMGB1 is essential as a nucleosome protein and is critical for mitochondrial quality control (Tang et al. 2011). Our current findings expand on our earlier report of how the loss of intracellular HMGB1 leads to increased protection against mitochondrial dysfunction in human bronchial epithelial cells (unpublished data). Consistent with previous studies, there is an increase in mitochondrial DNA (mtDNA) release with ODE exposure (unpublished data). This increase is seen in both cell-free BAL fluid and serum samples. However, ODE induced a significant increase in mtDNA levels in the BAL fluid of *HMGB1*$^{-/-}$ mice but not in the serum, suggesting an impact of club cell-specific loss of HMGB1 in *HMGB1*$^{-/-}$ mice. Our results are in agreement with the previous work showing the release of mtDNA from dysfunctional mitochondria in response to stress and/or infection (Nakahira et al. 2011).

TFAM is an endogenous DAMP, required for the maintenance of mtDNA and is known to enhance the release of TNFα (Hallberg and Larsson 2011; Julian et al. 2013). We documented an increase in the expression of TFAM in WT mice exposed to ODE. Among the *HMGB1*$^{-/-}$ mice, baseline (saline exposed) expression of TFAM was significantly lower than WT. Following ODE exposure, TFAM levels in *HMGB1*$^{-/-}$ mice were increased when compared to *HMGB1*$^{-/-}$ mice exposed to saline. However, the expression of TFAM in ODE exposed *HMGB1*$^{-/-}$ mice was significantly lower than ODE exposed WT mice. These results underscore the importance of loss of HMGB1 in club cells of the airways. Interestingly, a significant increase in cytochrome c levels was observed in saline exposed HMGB1$^{-/-}$ mice, which decreased on exposure to ODE.

Club cells are known to contain a large number of mitochondria due to their high level of metabolic activity (Hiemstra and Bourdin 2014). In saline exposed *HMGB1*$^{-/-}$ mice, the increase in cytochrome c could be a mechanism to compensate for the cellular stress induced by the lack of HMGB1. Another key component associated with inflammation and mitochondrial dysfunction is the generation of reactive species (Cloonan et al. 2020). Consistent with previous studies, *nos2* expression was significantly upregulated in WT mice exposed to ODE. In ODE exposed *HMGB1*$^{-/-}$ mice, levels of *nos2* remained significantly higher than controls. However, the expression of *nos2* reduced when compared to WT mice. A similar pattern of expression was observed with GP91Phox, a subunit of NADPH oxidases which is involved in the generation of superoxide anions (O_2^-) (Banerjee and Henderson 2012). GP91Phox expression is significantly decreased in saline exposed *HMGB1*$^{-/-}$ mice and increased in ODE exposed WT mice. Although we document an increase in ODE exposed *HMGB1*$^{-/-}$ mice compared to that of saline, the levels remain comparable to WT control. Studies have shown that with a targeted deletion of the GP91Phox subunit, superoxide overproduction is markedly reduced indicating an essential role in the production of superoxide (Liu et al. 2006a; Banerjee and Henderson 2012). The increase in the expression of GP91Phox observed in ODE exposed WT mice could be resulting in uncontrolled production of ROS, implicated in tissue destruction and various disease states. Collectively, these data suggest a role for HMGB1 in exacerbating mitochondrial dysfunction induced following inflammation in response to ODE.

Mitochondrial biogenesis is thought to arise during conditions of high energy demand or cellular stress (Wu et al. 1999; Ploumi et al. 2017). Loss of mitochondrial biogenesis in the airways has previously been observed in COPD (Aghapour et al. 2019). In previous studies with normal human bronchial cells, ODE exposure induced mitochondrial biogenesis in cells lacking HMGB1

(unpublished data). In the present study, we measured an increase in *pgc1a* fold change in both WT and *HMGB1*$^{-/-}$ mice exposed to ODE. The expression of NRF2 was also measured which, regulated by PGC1α, promotes the expression of TFAM and induces mitochondrial biogenesis (Austin and St-Pierre 2012). The decreased expression of both NRF2 and TFAM in *HMGB1*$^{-/-}$ mice is evidence of a possible lack of mitochondrial biogenesis. NRF2 also has a key regulatory role in handling the cellular resistance to oxidants (Ma 2013). The decreased expression of NRF2 observed could be substantially increasing the susceptibility of mice to a broad range of disease conditions associated with oxidative pathology. To further corroborate the lack of biogenesis occurring, we measured the expression of SIRT1 which is involved in the deacetylation of PGC1α (Austin and St-Pierre 2012; Mendes et al. 2017) in turn promoting mitochondrial biogenesis and quality control. The decreased SIRT1 expression is indicative of the lack of biogenesis occurring in the airways. However, further studies focusing particularly on club cells lacking HMGB1 will provide us a better understanding on mitochondrial dysfunction and its correlation with HMGB1.

In a previous study, lack of HMGB1 in normal human bronchial epithelial cells developed a hypoxia response on exposure to ODE (unpublished data). Consistent with this, *HMGB1*$^{-/-}$ mice on exposure to ODE also show an increase in fold change of HIF1α, indicative of hypoxia. As shown in earlier studies, intermittent hypoxia in the absence of HMGB1 could be imparting a therapeutic effect on the mitochondria and thus having a positive regulatory effect (unpublished data). One of the physiological adaptations to hypoxia in an organism is increased glycogen metabolism (Jain et al. 2016; Baik and Jain 2020). To identify the impact on glucose uptake and glycolysis in these mice, expression of *slc2a6* and *eno1*, genes involved in glucose uptake and glycolysis, was measured. On ODE exposure, both WT and *HMGB1*$^{-/-}$ mice showed a significant increase in *eno1* fold change, however, only *HMGB1*$^{-/-}$ mice with and without ODE exposure

showed an increase in *slc2a6*. This indicates that in *HMGB1*$^{-/-}$ mice the glycolytic ability is enhanced and is consistent with our previous findings in normal human bronchial epithelial cells (unpublished data).

Collectively, HMGB1 is an important effector molecule that plays a significant role in many pathologies with an underlying inflammatory cascade. Extracellular HMGB1 is proinflammatory, whereas intracellular HMGB1 is known to be anti-inflammatory (Lotze and Tracey 2005; Yang et al. 2015). However, the observed disease phenotype was likely regulated in the epithelial cell, independent of inflammatory cells. In the present study, we found that HMGB1 deficient mouse airways developed heightened histopathology. Taken together, HMGB1 appears to be a critical regulator of various inflammatory mechanisms in airway epithelial cells exposed to complex, agriculture organic dust. This current study demonstrated the use of a novel murine model to determine the importance of HMGB1 in the airways, without any significant baseline impact on the histology or mortality of the animals. Future studies will focus on the determination of the signaling mechanisms of HMGB1 to link its relevance to the histopathological changes observed and exploit it for potential preventative and therapeutic strategies.

Materials and Methods

Ethics statement

All animal work and procedures performed were approved by the Institutional Animal Care and Use Committee (IACUC) and Institutional Biosafety Committee (IBC) of the Iowa State University. Animals were bred under the protocol IACUC 19-016, IACUC 20-107 and IBC 19-141. Research experiments with the animals were performed under the protocol IACUC 19-226 and IBC 19-178. NIH guidelines were followed for the care and handling of mice in this study.

Table 6.1 Reagents stock and working concentrations

Treatment	Stock concentration	Working concentration
Organic Dust Extract (ODE)	100% in HBSS	12.5% in PBS
Lipopolysaccharide (LPS)	1.8 mg/mL	1 µg/mL in PBS
Tamoxifen (TAM)	20 mg/mL	75 mg/kg
Sodium Pentobarbital	390 mg/mL	100 mg/kg
FITC-Dextran	50 mg/mL	10 mg/kg

Organic dust extract preparation

Organic dust samples (OD) were collected and an aqueous extract was prepared as previously described (Romberger et al. 2002; Bhat et al. 2019). Settled dust from the surfaces of swine housing facilities were collected and 1 g of the dust was mixed with sterile Hank's Balanced Salt Solution (10 mL; Gibco). The solution was incubated for one hour with stirring at room temperature and centrifuged twice for 20 min at 1365 x g. The supernatant obtained was filter sterilized (0.22 µm filter), to remove larger coarse article and microbes. The filtered ODE solution was aliquoted and stored at -20°C until use in the experiments. The concentration of filter-sterilized organic dust extract (ODE) samples was considered 100% and a dilution of 12.5% (v/v) before use in experiments. The 12.5% concentration used has been previously shown to elicit lung inflammation in mice (Poole et al. 2009).

Endotoxin estimation

The levels of endotoxin in the ODE samples were quantified using the Pierce Chromogenic Endotoxin Quant Kit (Thermofisher Scientific). The ODE samples were diluted in a ratio of 1:50 in endotoxin-free water. The diluted samples (50 µL) along with reconstituted amebocyte lysate reagent, were added into an endotoxin-free 96-well plate in a sample to lysate ratio of 1:1, in triplicates. The standard was reconstituted as per the manufacturer's recommendation and added to the plate in a sample to lysate ratio of 1:1. The microplate was incubated at 37°C for 12 to 35

minutes based on the range of standards used. Following incubation, 100 µL of chromogenic substrate was added and the plate was incubated at 37°C for 6 minutes. 50 µL of stop solution (25% acetic acid) was added and absorbance was read at 405 nm using spectrophotometer reader (SpectraMax M2 Gemini Microplate Reader, Molecular Devices, San Jose, CA). The average of blank wells was deducted from the standards and sample absorbance values. A linear standard graph was plotted with R>98% and sample concentrations were extrapolated from the equation of the slope using the OD values. All calculations were done in excel.

Table 6.2 Endotoxin concentrations in ODE samples used in our experiments

Sample No.	Endotoxin (EU/mL)
8	6.315 ± 0.2
9	5.20 ± 0.1
10	10.67 ± 0.3
11	8.052 ± 0.1

Animal models

Hmgb1$^{fl/fl}$ mice of C57BL/6 genetic background were originally generated by Dr. Eugene B. Chang's laboratory (University of Chicago, IL) (Zhu et al. 2015). Dr. Chang's groups has previously generated intestinal epithelial cell-specific HMGB1 KO mice (Zhu et al. 2015).

We procured several breeding pairs of *Hmgb1*$^{fl/fl}$ mice from Dr. Chang's group. *Scgb1a1-creER*^{TM} mice of C57BL/6 genetic background, expressing club cell-specific tamoxifen-inducible cre recombinase, were obtained from The Jackson Laboratory (Ann Arbor, MI) and crossed with *Hmgb1*$^{fl/fl}$ mice to generated *Hmgb1*$^{fl/fl\ Scgb1a1\text{-}cre}$ mice (Rawlins et al. 2009). The first generation (F1) of litters were utilized for all experiments. For all experiments, 6–8-week-old animals of both sexes were used in equal proportions. Age and sex-matched C57BL/6 (wild type) mice, obtained from The Jackson Laboratory, were used as controls. The animals were distributed into groups where all groups had roughly equal numbers of the sexes and equal average weights.

Tamoxifen Administration and animal treatments

A 20 mg/mL tamoxifen (TAM; Sigma Aldrich) solution was prepared in corn oil (Sigma Aldrich). *Hmgb1*$^{fl/fl\ Scgb1a1\text{-}cre}$ adults (~5-6 weeks old) were injected intraperitoneally with 75 mg/kg body weight TAM every day up to five times (represented as *Hmgb1*$^{-/-}$). Following the final injection, the mice were quarantined for 24 h before returning them to the normal animal room. A 5 day wait period was followed between the final injection and treatment. One animal per litter were given sham injections with vehicle (corn oil) which were used as negative control (represented as *Hmgb1*$^{fl/fl}$). Throughout the course of the injections and post-injection, the animals were closely monitored for any adverse reactions.

A total of 24 *Hmgb1*$^{fl/fl\ Scgb1a1\text{-}cre}$ and 24 C57BL/6 mice (7-10 weeks old) were divided into three groups per mice strain (outlined in Figure 6.1 and Table 6.4). Mice were lightly anesthetized by isoflurane (2-3%) inhalation, following which saline, LPS (1 µg/mL) or ODE (12.5%) were instilled intranasally (50 µL/mice). The treatments were performed every 24 h for 5 consecutive days. Approximately 24 h following the final treatment the mice were euthanized by intraperitoneal administration of sodium pentobarbital (100 mg/kg b.w.) as per the American Veterinary Medical Association (AVMA) Guidelines for Euthanasia of Animals. The use of sodium pentobarbital was done under the approval and license of the department of drug enforcement agency (DEA) and Iowa Board of Pharmacy.

FITC-Dextran permeability assay

Changes in epithelial permeability after administration of treatments were measured by FITC-Dextran leakage from the airways into the blood. 24 h after the final treatment administration, 50 mL of FITC-Dextran (10 mg/kg b.w., 24 µL per nostril; Sigma) dissolved in sterile PBS was administered via i.n. route into the airways. After instillation, the mouse was set vertically for 2 min until it breathed steadily. The mice were sacrificed one hour later, and blood

was collected by cardiac puncture. Finally, the blood was treated with 10 mL of EDTA (60 mg/ml) and centrifuged at 7000 rpm for 10 min. Approximately 500 µl of plasma was harvested from each mouse. The fluorescence intensity (FI value) of the plasma (~200 µL) was determined at an excitation/emission wavelength of 485/528 nm using a spectrophotometer plate reader (SpectraMax M2 Gemini Molecular Device Microplate Reader) (Chen et al. 2014).

Lung wet-to-dry weight ratio

After the final treatment administration and mice were euthanized. The diaphragmatic lobe of the right lung was excised separately and rapidly weighed to obtain the "wet" weight. Samples were oven-dried (65°C) for 48 h to determine the stable dry lung weight. The ratio of the wet-to-dry (W/D) lung weight was calculated to assess lung tissue edema (Chen et al. 2014).

Bronchoalveolar lavage and cytospins

Post animal euthanasia, the trachea was exposed and cannulated with a 23-gauge needle just below the larynx. Bronchoalveolar lavage fluid (BALF) was collected from the lungs by instilling 1 mL cold PBS with 0.1 mM EDTA and recovered by aspiration a total of three times. The BALF from each mouse was pooled and was centrifuged at 800 x g to collect cells (Sun et al. 2017). The supernatant from the first milliliter of cell-free BALF was recovered and frozen at -80°C for other assays. Cells from the BALF were resuspended, and total cell numbers were determined by using a hemacytometer. First, cytospins were prepared by the Iowa State University clinical pathology laboratory (College of Veterinary Medicine) and stained with Shandon Kwik Diff Staining (Thermofisher Scientific) to enumerate differential leukocyte count. A total of 500 cells were counted and individual leukocyte populations were identified. Using the total leukocyte count, the absolute count of each cell population was calculated.

Tissue collection

After whole lung lavage, lungs were harvested from each treatment group. The right lung was tied off at the primary bronchus, removed, flash-frozen in liquid nitrogen, and stored in -80°C. The left lung was slowly inflated with ~200-300 μL of 4% paraformaldehyde (PFA; Sigma, St. Louis, MO). To obtain uniform lung inflation during fixation, the lungs were fixed at a 25 cm height water pressure. The lungs were stored in 4% PFA for 24 h, followed by 70% ethanol. The fixed lungs were embedded in paraffin and sectioned into 5-micron slices by the Iowa State University histopathology laboratory (College of Veterinary Medicine).

Histology, mucus staining and histopathology analysis

Hematoxylin and eosin (H&E) staining was performed according to standard protocol (Fischer et al. 2008). Each slide was entirely reviewed at scanning magnifications (×2, ×10, and ×20 objectives; Nikon Eclipse TE2000-U microscope; SPOT Advanced imaging software, Michigan, USA). The histopathological scores were determined by an experienced researcher blinded to the treatment conditions. The scoring system utilized a standardized set of photos representing the spectrum of inflammatory changes for each parameter in the bronchioles, blood vessels, and alveolar septa. (outlined in Table 6.3).

For mucus staining, Richard-Allan Scientific Chromaview – Advanced Testing Periodic Acid-Schiff (PAS) kit (Thermofisher Scientific) was used as per the manufacturer's instructions. PAS-positive cells lining the surface epithelium were counted in between 6 and 9 airways. The numbers were normalized to the length of the basement membrane, which was determined using ImageJ (NIH Image) (Shi et al. 2002). Images were obtained using Nikon Eclipse TE2000-U microscope and SPOT Advanced imaging software (Michigan, USA).

Table 6.3 Histology scoring criteria

Score	Bronchial hyperplasia / club cells per 100 µm	Perivascular edema	Septa	Alveolar edema	Emphysema	Cellular infiltration (alveolar / perivascular)
0	<5	Up to 50 µm	<10 µm	1-100 µm	50-200 µm	1-10 total neutrophil
1	5-15/100	50-100 µm	10-15 µm	101-200 µm	300-400 µm	10-20 total neutrophil
2	15-25/100	100-150 µm	15-20 µm	201-300 µm	400-500 µm	30-50
3	>25	>150 µm	>20 µm	>301 µm	>500	>50

Immunofluorescence staining and imaging

Immunohistochemistry was performed according to a standard protocol. Lung sections were subjected to antigen retrieval by immersion in pre-heated citrate buffer (10 mM citric acid, 0.05% Tween 20, and pH 6) to 90°C for 20 min prior to staining. Sections were then washed in PBS a few times to remove antigen retrieval reagents, blocked with PBS containing 10% donkey serum and 0.02% Triton-X100 for 1 h at room temperature. Afterward, primary antibodies diluted in PBS containing 2.5% donkey serum, 0.25% sodium azide, and 0.1% Triton X-100 were added to the sections for 16-18 h incubation at 4°C. Sections were rinsed with PBS and incubated with either dye-conjugated or biotinylated secondary antibody at room temperature for 1 h. After washing with PBS, incubated with biotinylated secondary antibodies, sections were treated with dye-streptavidin for 45 min and then thoroughly rinsed in PBS. Sections were then treated with a nuclear-stain, 4′,6-diamidino-2- phenylindole (DAPI) and cover-slipped. Negative control was the section without primary antibody staining. The list of antibodies used in the study are shown in Table 6.6 and 6.7. Confocal microscopic images were captured using a Leica TCS SP5 X Laser-Scanning Confocal instrument (Exton, PA) and analyzed using ImageJ software (National Institutes of Health).

mtDNA isolation and detection

To determine mitochondrial DNA (mtDNA) levels in blood plasma and BALF, mtDNA was isolated using the Genomic DNA Purification kit (ThermoFisher Scientific) as per the

manufacturer's instructions. The purity and concentration of the isolated DNA was measured using NanoVue Plus Spectrophotometer (GE Healthcare). Due to low concentrations, the mtDNA was first amplified using long-range PCR and the primers used are listed in Table 6.5. PCR reactions were performed at 95°C for 1 min followed by 35 cycles at 94°C for 30 s, 56°C for 30 s, 72°C for 1 min and a final elongation for 5 min. The concentration of amplified mtDNA obtained was adjusted to ensure equal amounts of template mtDNA from each sample was used for qPCR reaction.

qRT-PCR was performed using 500 ng of template DNA in a 10 µL reaction volume using SYBR master mix and 1 µM of primers specific for mitochondrial ND1 and housekeeping gene 16S rRNA. The primers for mitochondrial ND1, listed in Table 6.5, were synthesized at Iowa State University's DNA Facility. The qRT-PCR reactions were run in a QuantiStudio-3™ (Thermofisher Scientific) detection system and the data was analyzed using $2^{-\Delta\Delta CT}$ method (Livak and Schmittgen 2001).

qRT-PCR

Total RNA was isolated from the lung homogenate using TRIzol extraction methods (Seo et al. 2014) and RNA concentration was measured using NanoVue Plus spectrophotometer (GE Healthcare, UK). 1 µg of RNA was used to synthesize cDNA using the High-Capacity cDNA Reverse Transcription Kit (ThermoFisher Scientific) following the manufacturer's protocol.

RT-qPCR was performed using 500 ng of template DNA in a 10 µL reaction volume using SYBR master mix and 1 µM of primers for the target of interest. The housekeeping gene 18S rRNA (ThermoFisher Scientific) was used in all qPCR reactions. No-template controls and dissociation curves were run for all reactions to exclude cross-contamination. The primers for genes of interest listed in Table 6.5 were synthesized at Iowa State University's DNA Facility. The

qRT-PCR reactions were run in a QuantiStudio-3™ (Thermofisher Scientific) detection system and the data was analyzed using $2^{-\Delta\Delta CT}$ method (Livak and Schmittgen 2001).

Immunoblot analysis

The lungs were lysed using RIPA buffer with 1X HALT protease inhibitor and EDTA (Thermofisher Scientific). concentration was measured using the Bradford protein assay kit (BioRad). Equal amounts of protein (20 µg/sample), along with a molecular weight marker (Bio-Rad), were run on 10–12% sodium dodecyl sulfate/polyacrylamide gel electrophoresis (SDS-PAGE) as previously described (Bhat et al. 2019). Proteins were transferred onto a nitrocellulose membrane and nonspecific binding sites were blocked with Intercept® blocking buffer (LI-COR, Lincoln, NE). The membranes were then incubated with different primary antibodies and dilutions listed in Table 6.6. Next, membranes were incubated with one of the following secondary antibodies: Alexa Fluor 680 goat anti-mouse, Alexa Fluor 680 donkey anti-rabbit, or IRDye 800CW donkey anti-rabbit (1:10,000; LI-COR). To confirm equal protein loading, blots were probed with relevant housekeeping proteins listed in Table 6.6. Western blot images were captured using Odyssey® CLx IR imaging system (LI-COR Biotechnology) and analysis was performed using ImageJ software (National Institutes of Health).

Statistics

Data analysis was performed using GraphPad Prism 8.0 software (La Jolla, CA, USA). Raw data were analyzed with either Student's t-test or using one-way ANOVA, and Tukey's posttest was performed to compare all treatment groups. A p-value of < 0.05 was considered statistically significant. *$p < 0.05$, **$p < 0.01$, ***$p < 0.001$, ****$p < 0.0001$. * indicates different from control. For all the assays, samples were derived from the same experiment and were processed in parallel in order to minimize variation.

Acknowledgments

We thank Dr. Eugene B. Chang for providing us with HMGB-floxed mice. We also thank Dr. Kathleen Mullin, Dr. Steven Wilson, and Dr. Giuseppe Dell'Anna of the Iowa State University Laboratory Animal Resource (LAR) for assistance with the planning and development of conditional HMGB1-KO breeding colony. We thank Virginia Montgomery at Iowa State University Veterinary Pathology and Histology Laboratory for assistance with lung-tissue processing, and sectioning, and Margaret Carter at Iowa State University High Resolution Microscopy Facility for assisting us in confocal microscopy imaging. In addition, we thank Dr. Anumantha Kanthasamy, Dr. Michael Cho and the Iowa State University's Department of Biomedical Sciences for access to instruments and equipment.

Potential Conflicts of Interest

The terms of this arrangement have been reviewed and approved by Iowa State University per its conflict-of-interest policies. All other authors have declared no potential conflicts of interest.

Funding

C.C. laboratory is funded through a startup grant and College of Veterinary Medicine (CVM) seed grant through Iowa State University.

References

Aghapour M, Remels AHV, Pouwels SD, Bruder D, Hiemstra PS, Cloonan SM, Heijink IH (2019) Mitochondria: at the crossroads of regulating lung epithelial cell function in chronic obstructive pulmonary disease. American Journal of Physiology-Lung Cellular and Molecular Physiology 318(1):L149–L164. https://doi.org/10.1152/ajplung.00329.2019

An J, Jr H, Aj N, Jd D, J K, Mj D, Gm T, B K, Ab S, R G, Sc G, Y T, Dj R, T K, Ja P (2020) MyD88 regulates a prolonged adaptation response to environmental dust exposure-induced lung disease. Respir Res 21(1):97–97. https://doi.org/10.1186/s12931-020-01362-8

Andersson U, Tracey KJ (2011) HMGB1 Is a Therapeutic Target for Sterile Inflammation and Infection. Annu Rev Immunol 29:139–162. https://doi.org/10.1146/annurev-immunol-030409-101323

Austin S, St-Pierre J (2012) PGC1α and mitochondrial metabolism – emerging concepts and relevance in ageing and neurodegenerative disorders. J Cell Sci 125(21):4963–4971. https://doi.org/10.1242/jcs.113662

Baik AH, Jain IH (2020) Turning the Oxygen Dial: Balancing the Highs and Lows. Trends in Cell Biology 30(7):516–536. https://doi.org/10.1016/j.tcb.2020.04.005

Bailey KL, Poole JA, Mathisen TL, Wyatt TA, Von Essen SG, Romberger DJ (2008) Toll-like receptor 2 is upregulated by hog confinement dust in an IL-6-dependent manner in the airway epithelium. American Journal of Physiology-Lung Cellular and Molecular Physiology 294(6):L1049–L1054. https://doi.org/10.1152/ajplung.00526.2007

Banerjee ER, Henderson WR (2012) Defining the molecular role of gp91phox in the immune manifestation of acute allergic asthma using a preclinical murine model. Clinical and Molecular Allergy 10(1):2. https://doi.org/10.1186/1476-7961-10-2

Barnes PJ (2017) Cellular and molecular mechanisms of asthma and COPD. Clinical Science 131(13):1541–1558. https://doi.org/10.1042/CS20160487

Barnes PJ (2015) Club Cells, Their Secretory Protein, and COPD. CHEST 147(6):1447–1448. https://doi.org/10.1378/chest.14-3171

Bertheloot D, Latz E (2017) HMGB1, IL-1α, IL-33 and S100 proteins: dual-function alarmins. Cellular & Molecular Immunology 14(1):43–64. https://doi.org/10.1038/cmi.2016.34

Bhat SM, Massey N, Karriker LA, Singh B, Charavaryamath C (2019) Ethyl pyruvate reduces organic dust-induced airway inflammation by targeting HMGB1-RAGE signaling. Respiratory Research 20(1):27. https://doi.org/10.1186/s12931-019-0992-3

Calogero S, Grassi F, Aguzzi A, Voigtländer T, Ferrier P, Ferrari S, Bianchi ME (1999) The lack of chromosomal protein Hmg1 does not disrupt cell growth but causes lethal hypoglycaemia in newborn mice. Nature Genetics 22(3):276–280. https://doi.org/10.1038/10338

Charavaryamath C, Janardhan KS, Townsend HG, Willson P, Singh B (2005) Multiple exposures to swine barn air induce lung inflammation and airway hyper-responsiveness. Respir Res 6:50. https://doi.org/10.1186/1465-9921-6-50

Charavaryamath C, Juneau V, Suri SS, Janardhan KS, Townsend H, Singh B (2008) Role of Toll-like receptor 4 in lung inflammation following exposure to swine barn air. Exp Lung Res 34(1):19–35. https://doi.org/10.1080/01902140701807779

Charavaryamath C, Singh B (2006) Pulmonary effects of exposure to pig barn air. J Occup Med Toxicol 1:10. https://doi.org/10.1186/1745-6673-1-10

Chen H, Wu S, Lu R, Zhang Y, Zheng Y, Sun J (2014) Pulmonary Permeability Assessed by Fluorescent-Labeled Dextran Instilled Intranasally into Mice with LPS-Induced Acute Lung Injury. PLOS ONE 9(7):e101925. https://doi.org/10.1371/journal.pone.0101925

Chen L, Li J, Ye Z, Sun B, Wang L, Chen Y, Han J, Yu M, Wang Y, Zhou Q, Seidler U, Tian D, Xiao F (2020) Anti-High Mobility Group Box 1 Neutralizing-Antibody Ameliorates Dextran Sodium Sulfate Colitis in Mice. Front Immunol 11. https://doi.org/10.3389/fimmu.2020.585094

Chen S, Yu G, Xie J, Tang W, Gao L, Long X, Ren L, Xie X, Deng Y, Fu Z, Liu E (2018) High-mobility group box-1 protein from CC10+ club cells promotes type 2 response in the later stage of respiratory syncytial virus infection. American Journal of Physiology-Lung Cellular and Molecular Physiology 316(1):L280–L290. https://doi.org/10.1152/ajplung.00552.2017

Cloonan SM, Kim K, Esteves P, Trian T, Barnes PJ (2020) Mitochondrial dysfunction in lung ageing and disease. European Respiratory Review 29(157). https://doi.org/10.1183/16000617.0165-2020

Dickinson JD, Sweeter JM, Staab EB, Nelson AJ, Bailey KL, Warren KJ, Jaramillo AM, Dickey BF, Poole JA (2018) MyD88 controls airway epithelial Muc5ac expression during TLR activation conditions from agricultural organic dust exposure. American Journal of Physiology-Lung Cellular and Molecular Physiology 316(2):L334–L347. https://doi.org/10.1152/ajplung.00206.2018

Ding J, Cui X, Liu Q (2017) Emerging role of HMGB1 in lung diseases: friend or foe. J Cell Mol Med 21(6):1046–1057. https://doi.org/10.1111/jcmm.13048

Dosman JA, Fukushima Y, Senthilselvan A, Kirychuk SP, Lawson JA, Pahwa P, Cormier Y, Hurst T, Barber EM, Rhodes CS (2006) Respiratory response to endotoxin and dust predicts evidence of inflammatory response in volunteers in a swine barn. American Journal of Industrial Medicine 49(9):761–766. https://doi.org/10.1002/ajim.20339

Ferhani N, Letuve S, Kozhich A, Thibaudeau O, Grandsaigne M, Maret M, Dombret M-C, Sims GP, Kolbeck R, Coyle AJ, Aubier M, Pretolani M (2010) Expression of High-Mobility Group Box 1 and of Receptor for Advanced Glycation End Products in Chronic Obstructive Pulmonary Disease. Am J Respir Crit Care Med 181(9):917–927. https://doi.org/10.1164/rccm.200903-0340OC

Fischer AH, Jacobson KA, Rose J, Zeller R (2008) Hematoxylin and eosin staining of tissue and cell sections. CSH Protoc 2008:pdb.prot4986. https://doi.org/10.1101/pdb.prot4986

Georas SN, Rezaee F (2014) Epithelial barrier function: at the frontline of asthma immunology and allergic airway inflammation. J Allergy Clin Immunol 134(3):509–520. https://doi.org/10.1016/j.jaci.2014.05.049

Grainge CL, Davies DE (2013) Epithelial Injury and Repair in Airways Diseases. CHEST 144(6):1906–1912. https://doi.org/10.1378/chest.12-1944

Hackett T-L, Warner SM, Stefanowicz D, Shaheen F, Pechkovsky DV, Murray LA, Argentieri R, Kicic A, Stick SM, Bai TR, Knight DA (2009) Induction of Epithelial–Mesenchymal Transition in Primary Airway Epithelial Cells from Patients with Asthma by Transforming Growth Factor-β1. Am J Respir Crit Care Med 180(2):122–133. https://doi.org/10.1164/rccm.200811-1730OC

Hallberg BM, Larsson N-G (2011) TFAM forces mtDNA to make a U-turn. Nature Structural & Molecular Biology 18(11):1179–1181. https://doi.org/10.1038/nsmb.2167

Hayashi S, McMahon AP (2002) Efficient Recombination in Diverse Tissues by a Tamoxifen-Inducible Form of Cre: A Tool for Temporally Regulated Gene Activation/Inactivation in the Mouse. Developmental Biology 244(2):305–318. https://doi.org/10.1006/dbio.2002.0597

Heijink IH, Postma DS, Noordhoek JA, Broekema M, Kapus A (2010) House Dust Mite–Promoted Epithelial-to-Mesenchymal Transition in Human Bronchial Epithelium. Am J Respir Cell Mol Biol 42(1):69–79. https://doi.org/10.1165/rcmb.2008-0449OC

Hiemstra PS, Bourdin A (2014) Club cells, CC10 and self-control at the epithelial surface. European Respiratory Journal 44(4):831–832. https://doi.org/10.1183/09031936.00089214

Hou C, Zhao H, Liu L, Li W, Zhou X, Lv Y, Shen X, Liang Z, Cai S, Zou F (2011) High Mobility Group Protein B1 (HMGB1) in Asthma: Comparison of Patients with Chronic Obstructive Pulmonary Disease and Healthy Controls. Mol Med 17(7–8):807–815. https://doi.org/10.2119/molmed.2010.00173

Jain IH, Zazzeron L, Goli R, Alexa K, Schatzman-Bone S, Dhillon H, Goldberger O, Peng J, Shalem O, Sanjana NE, Zhang F, Goessling W, Zapol WM, Mootha VK (2016) Hypoxia as a therapy for mitochondrial disease. Science 352(6281):54–61. https://doi.org/10.1126/science.aad9642

Jiang L, Shao Y, Tian Y, Ouyang C, Wang X (2020) Nuclear Alarmin Cytokines in Inflammation. J Immunol Res 2020. https://doi.org/10.1155/2020/7206451

Jones-Freeman B, Starkey MR (2020) Bronchioalveolar stem cells in lung repair, regeneration and disease. The Journal of Pathology 252(3):219–226. https://doi.org/10.1002/path.5527

Julian MW, Shao G, Vangundy ZC, Papenfuss TL, Crouser ED (2013) Mitochondrial transcription factor A, an endogenous danger signal, promotes TNFα release via RAGE- and TLR9-responsive plasmacytoid dendritic cells. PLoS ONE 8(8):e72354. https://doi.org/10.1371/journal.pone.0072354

Kanazawa H, Tochino Y, Asai K, Ichimaru Y, Watanabe T, Hirata K (2012) Validity of HMGB1 measurement in epithelial lining fluid in patients with COPD. European Journal of Clinical Investigation 42(4):419–426. https://doi.org/10.1111/j.1365-2362.2011.02598.x

Li G, Tang D, Lotze MT (2013) Ménage à Trois in Stress: DAMPs, Redox and Autophagy. Semin Cancer Biol 23(5):380–390. https://doi.org/10.1016/j.semcancer.2013.08.002

Liu JQ, Zelko IN, Erbynn EM, Sham JSK, Folz RJ (2006) Hypoxic pulmonary hypertension: role of superoxide and NADPH oxidase (gp91phox). American Journal of Physiology-Lung Cellular and Molecular Physiology 290(1):L2–L10. https://doi.org/10.1152/ajplung.00135.2005

Livak KJ, Schmittgen TD (2001) Analysis of Relative Gene Expression Data Using Real-Time Quantitative PCR and the 2−ΔΔCT Method. Methods 25(4):402–408. https://doi.org/10.1006/meth.2001.1262

Lotze MT, Tracey KJ (2005) High-mobility group box 1 protein (HMGB1): nuclear weapon in the immune arsenal. Nature Reviews Immunology 5(4):331–342. https://doi.org/10.1038/nri1594

Ma Q (2013) Role of Nrf2 in Oxidative Stress and Toxicity. Annu Rev Pharmacol Toxicol 53:401–426. https://doi.org/10.1146/annurev-pharmtox-011112-140320

Magna M, Pisetsky DS (2014) The Role of HMGB1 in the Pathogenesis of Inflammatory and Autoimmune Diseases. Mol Med 20(1):138–146. https://doi.org/10.2119/molmed.2013.00164

Massey N, Puttachary S, Bhat SM, Kanthasamy AG, Charavaryamath C (2019) HMGB1-RAGE Signaling Plays a Role in Organic Dust-Induced Microglial Activation and Neuroinflammation. Toxicol Sci 169(2):579–592. https://doi.org/10.1093/toxsci/kfz071

Mendes KL, Lelis D de F, Santos SHS (2017) Nuclear sirtuins and inflammatory signaling pathways. Cytokine & Growth Factor Reviews 38:98–105. https://doi.org/10.1016/j.cytogfr.2017.11.001

Nakahira K, Haspel JA, Rathinam VAK, Lee S-J, Dolinay T, Lam HC, Englert JA, Rabinovitch M, Cernadas M, Kim HP, Fitzgerald KA, Ryter SW, Choi AMK (2011) Autophagy proteins regulate innate immune responses by inhibiting the release of mitochondrial DNA mediated by the NALP3 inflammasome. Nature Immunology 12(3):222–230. https://doi.org/10.1038/ni.1980

Nath Neerukonda S, Mahadev-Bhat S, Aylward B, Johnson C, Charavaryamath C, Arsenault RJ (2018) Kinome analyses of inflammatory responses to swine barn dust extract in human bronchial epithelial and monocyte cell lines. Innate Immun 24(6):366–381. https://doi.org/10.1177/1753425918792070

Nieto MA (2011) The Ins and Outs of the Epithelial to Mesenchymal Transition in Health and Disease. Annu Rev Cell Dev Biol 27(1):347–376. https://doi.org/10.1146/annurev-cellbio-092910-154036

Ohtake K, Maeno T, Ueda H, Ogihara M, Natsume H, Morimoto Y (2003) Poly-l-Arginine Enhances Paracellular Permeability via Serine/Threonine Phosphorylation of ZO-1 and Tyrosine Dephosphorylation of Occludin in Rabbit Nasal Epithelium. Pharm Res 20(11):1838–1845. https://doi.org/10.1023/B:PHAM.0000003383.86238.d1

Ojo OO, Ryu MH, Jha A, Unruh H, Halayko AJ (2015) High-mobility group box 1 promotes extracellular matrix synthesis and wound repair in human bronchial epithelial cells. American Journal of Physiology-Lung Cellular and Molecular Physiology 309(11):L1354–L1366. https://doi.org/10.1152/ajplung.00054.2015

Ploumi C, Daskalaki I, Tavernarakis N (2017) Mitochondrial biogenesis and clearance: a balancing act. The FEBS Journal 284(2):183–195. https://doi.org/10.1111/febs.13820

Poole JA, Alexis NE, Parks C, MacInnes AK, Gentry-Nielsen MJ, Fey PD, Larsson L, Allen-Gipson D, Essen SGV, Romberger DJ (2008) Repetitive organic dust exposure in vitro impairs macrophage differentiation and function. Journal of Allergy and Clinical Immunology 122(2):375-382.e4. https://doi.org/10.1016/j.jaci.2008.05.023

Poole JA, Burrell AM, Wyatt TA, Kielian TL, Romberger DJ (2010) NOD2 Negatively Regulates Organic Dust-Induced Inflammation in Monocytes/Macrophages. Journal of Allergy and Clinical Immunology 125(2, Supplement 1):AB118. https://doi.org/10.1016/j.jaci.2009.12.467

Poole JA, Romberger DJ (2012) Immunological and Inflammatory Responses to Organic Dust in Agriculture. Curr Opin Allergy Clin Immunol 12(2):126–132. https://doi.org/10.1097/ACI.0b013e3283511d0e

Poole JA, Wyatt TA, Oldenburg PJ, Elliott MK, West WW, Sisson JH, Von Essen SG, Romberger DJ (2009) Intranasal organic dust exposure-induced airway adaptation response marked by persistent lung inflammation and pathology in mice. American Journal of Physiology-Lung Cellular and Molecular Physiology 296(6):L1085–L1095. https://doi.org/10.1152/ajplung.90622.2008

Pouwels SD, Heijink IH, ten Hacken NH, Vandenabeele P, Krysko DV, Nawijn MC, van Oosterhout AJ (2014) DAMPs activating innate and adaptive immune responses in COPD. Mucosal Immunology 7(2):215–226. https://doi.org/10.1038/mi.2013.77

Raleigh DR, Boe DM, Yu D, Weber CR, Marchiando AM, Bradford EM, Wang Y, Wu L, Schneeberger EE, Shen L, Turner JR (2011) Occludin S408 phosphorylation regulates tight junction protein interactions and barrier function. Journal of Cell Biology 193(3):565–582. https://doi.org/10.1083/jcb.201010065

Rawlins EL, Okubo T, Xue Y, Brass DM, Auten RL, Hasegawa H, Wang F, Hogan BLM (2009) The Role of Scgb1a1+ Clara Cells in the Long-Term Maintenance and Repair of Lung Airway, but Not Alveolar, Epithelium. Cell Stem Cell 4(6):525–534. https://doi.org/10.1016/j.stem.2009.04.002

Robbe P, Draijer C, Borg TR, Luinge M, Timens W, Wouters IM, Melgert BN, Hylkema MN (2014a) Distinct macrophage phenotypes in allergic and nonallergic lung inflammation. American Journal of Physiology-Lung Cellular and Molecular Physiology 308(4):L358–L367. https://doi.org/10.1152/ajplung.00341.2014

Robbe P, Spierenburg E a. J, Draijer C, Brandsma CA, Telenga E, Oosterhout A van, Berge M van den, Luinge M, Melgert BN, Heederik D, Timens W, Wouters IM, Hylkema MN (2014b) Shifted T-cell polarisation after agricultural dust exposure in mice and men. Thorax 69(7):630–637. https://doi.org/10.1136/thoraxjnl-2013-204295

Romberger DJ, Bodlak V, Von Essen SG, Mathisen T, Wyatt TA (2002) Hog barn dust extract stimulates IL-8 and IL-6 release in human bronchial epithelial cells via PKC activation. Journal of Applied Physiology 93(1):289–296. https://doi.org/10.1152/japplphysiol.00815.2001

Rubartelli A, Lotze MT (2007) Inside, outside, upside down: damage-associated molecular-pattern molecules (DAMPs) and redox. Trends in Immunology 28(10):429–436. https://doi.org/10.1016/j.it.2007.08.004

Schneberger D, Aulakh G, Channabasappa S, Singh B (2016) Toll-like receptor 9 partially regulates lung inflammation induced following exposure to chicken barn air. Journal of Occupational Medicine and Toxicology 11(1):31. https://doi.org/10.1186/s12995-016-0121-x

Senthilselvan A, Chénard L, Ulmer K, Gibson-Burlinguette N, Leuschen C, Dosman JA (2007) Excess Respiratory Symptoms in Full-time Male and Female Workers in Large-Scale Swine Operations. CHEST 131(4):1197–1204. https://doi.org/10.1378/chest.06-2323

Seo J, Ottesen EW, Singh RN (2014) Antisense Methods to Modulate Pre-mRNA Splicing. In: Hertel KJ (ed) Spliceosomal Pre-mRNA Splicing: Methods and Protocols. Humana Press, Totowa, NJ, pp 271–283

Shi ZO-Q, Fischer MJ, Sanctis GTD, Schuyler MR, Tesfaigzi Y (2002) IFN-γ, But Not Fas, Mediates Reduction of Allergen-Induced Mucous Cell Metaplasia by Inducing Apoptosis. The Journal of Immunology 168(9):4764–4771. https://doi.org/10.4049/jimmunol.168.9.4764

Shrestha D, Bhat SM, Massey N, Santana Maldonado C, Rumbeiha WK, Charavaryamath C (2021) Pre-exposure to hydrogen sulfide modulates the innate inflammatory response to organic dust. Cell Tissue Res. https://doi.org/10.1007/s00441-020-03333-3

Sun F, Xiao G, Qu Z (2017) Murine Bronchoalveolar Lavage. Bio Protoc 7(10). https://doi.org/10.21769/BioProtoc.2287

Sundblad B-M, Scheele I von, Palmberg L, Olsson M, Larsson K (2009) Repeated exposure to organic material alters inflammatory and physiological airway responses. European Respiratory Journal 34(1):80–88. https://doi.org/10.1183/09031936.00105308

Tang D, Kang R, Livesey KM, Kroemer G, Billiar TR, Van Houten B, Zeh HJ, Lotze MT (2011) High-Mobility Group Box 1 Is Essential for Mitochondrial Quality Control. Cell Metabolism 13(6):701–711. https://doi.org/10.1016/j.cmet.2011.04.008

Ugrinova I, Pasheva E (2017) Chapter Two - HMGB1 Protein: A Therapeutic Target Inside and Outside the Cell. In: Donev R (ed) Advances in Protein Chemistry and Structural Biology. Academic Press, pp 37–76

Vitali R, Stronati L, Negroni A, Nardo GD, Pierdomenico M, Giudice E del, Rossi P, Cucchiara S (2011) Fecal HMGB1 Is a Novel Marker of Intestinal Mucosal Inflammation in Pediatric Inflammatory Bowel Disease. American Journal of Gastroenterology 106(11):2029–2040. https://doi.org/10.1038/ajg.2011.231

Wang J, Li R, Peng Z, Hu B, Rao X, Li J (2020) HMGB1 participates in LPS-induced acute lung injury by activating the AIM2 inflammasome in macrophages and inducing polarization of M1 macrophages via TLR2, TLR4, and RAGE/NF-κB signaling pathways Corrigendum in /10.3892/ijmm.2020.4530. International Journal of Molecular Medicine 45(1):61–80. https://doi.org/10.3892/ijmm.2019.4402

Wu Z, Puigserver P, Andersson U, Zhang C, Adelmant G, Mootha V, Troy A, Cinti S, Lowell B, Scarpulla RC, Spiegelman BM (1999) Mechanisms Controlling Mitochondrial Biogenesis and Respiration through the Thermogenic Coactivator PGC-1. Cell 98(1):115–124. https://doi.org/10.1016/S0092-8674(00)80611-X

Yamasaki H, Mitsuyama K, Masuda J, Kuwaki K, Takedatsu H, Sugiyama G, Yamada S, Sata M (2009) Roles of high-mobility group box 1 in murine experimental colitis. Mol Med Rep 2(1):23–27. https://doi.org/10.3892/mmr_00000056

Yanai H, Matsuda A, An J, Koshiba R, Nishio J, Negishi H, Ikushima H, Onoe T, Ohdan H, Yoshida N, Taniguchi T (2013) Conditional ablation of HMGB1 in mice reveals its protective function against endotoxemia and bacterial infection. PNAS 110(51):20699–20704. https://doi.org/10.1073/pnas.1320808110

Yang H, Wang H, Chavan SS, Andersson U (2015) High Mobility Group Box Protein 1 (HMGB1): The Prototypical Endogenous Danger Molecule. Mol Med 21 Suppl 1:S6–S12. https://doi.org/10.2119/molmed.2015.00087

Ye C, Choi J-G, Abraham S, Wu H, Diaz D, Terreros D, Shankar P, Manjunath N (2012) Human macrophage and dendritic cell-specific silencing of high-mobility group protein B1 ameliorates sepsis in a humanized mouse model. PNAS 109(51):21052–21057. https://doi.org/10.1073/pnas.1216195109

Ye L, Martin TA, Parr C, Harrison GM, Mansel RE, Jiang WG (2003) Biphasic effects of 17-β-estradiol on expression of occludin and transendothelial resistance and paracellular permeability in human vascular endothelial cells. Journal of Cellular Physiology 196(2):362–369. https://doi.org/10.1002/jcp.10315

Zhu X, Messer JS, Wang Y, Lin F, Cham CM, Chang J, Billiar TR, Lotze MT, Boone DL, Chang EB (2015) Cytosolic HMGB1 controls the cellular autophagy/apoptosis checkpoint during inflammation. J Clin Invest 125(3):1098–1110. https://doi.org/10.1172/JCI76344

Appendix A. Supplementary figure

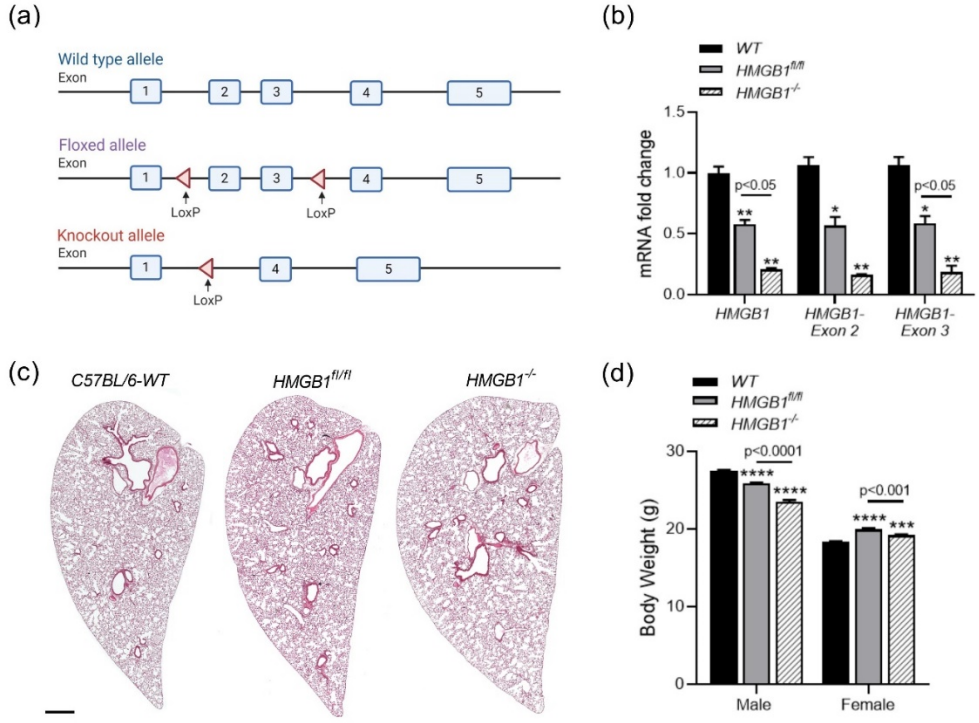

Figure 6.10 Generation and characterization of *HMGB1$^{fl/fl,\ scgb1a1\text{-}Cre}$* mice
HMGB1$^{fl/fl}$ mice were generated by flanking exons 2 and 3 of the gene with LoxP sites. Breeding *HMGB1$^{fl/fl}$* mice to mice expressing an inducible CRE-recombinase under the secretoglobin, family 1A, member 1 (uteroglobin) (Scgb1a1) gene promotor resulted in deletion of the HMGB1 start codon and a frame shift resulting in early termination of translation in lung club cells (a). mRNA fold change of *hmgb1* and target *hmgb1* exon sequence expression in untreated *wild-type (control, C57BL/6)*, *HMGB1$^{fl/fl,\ scgb1a1\text{-}Cre}$* without TAM (*HMGB1$^{fl/fl}$*) and *HMGB1$^{fl/fl,\ scgb1a1\text{-}Cre}$* with TAM (*HMGB1$^{-/-}$*) mice (b). Histological comparison of lungs from untreated *wild-type (control, C57BL/6)*, *HMGB1$^{fl/fl,\ scgb1a1\text{-}Cre}$* without TAM (*HMGB1$^{fl/fl}$*) and *HMGB1$^{fl/fl,\ scgb1a1\text{-}Cre}$* with TAM (*HMGB1$^{-/-}$*) mice (original magnification, x20) (c). Weight of age and sex-matched *wild-type (control, C57BL/6)*, *HMGB1$^{fl/fl,\ scgb1a1\text{-}Cre}$* without TAM (*HMGB1$^{fl/fl}$*) and *HMGB1$^{fl/fl,\ scgb1a1\text{-}Cre}$* with TAM (*HMGB1$^{-/-}$*) mice (d). For all the assays, samples were derived from the same experiment and were processed in parallel. Data was analyzed using one-way ANOVA with Tukey's multiple comparison test (*$p < 0.05$, **$p < 0.01$, ***$p < 0.001$, ****$p < 0.0001$) and represented as mean ± SEM with n = 4-8 mice/group (*indicates significant difference from control).

Appendix B. Supplementary tables

Table 6.4 Treatment and groups

Treatment	Administration	Exposure duration	Animal number (Male: Female)	Species
Saline			8 (6:2)	
LPS (1μg/mL)	i. n.		8 (5:3)	*C57BL/6*
ODE (12.5%)		Once every 24 hours for 5 consecutive days	8 (4:4)	
Saline			8 (4:4)	
LPS (1μg/mL)	i. n.		8 (5:3)	*HMGB1*$^{-/-}$
ODE (12.5%)			8 (4:4)	
KO controls	-	-	2 (1:1)	*HMGB1*$^{fl/fl}$

Table 6.5 Primer sequences

Gene symbol	Primer Sequence (5'→3')	
mtdna-s1	Forward	CCACCGCGGTCATACGATTA
	Reverse	GAGGTCACCCCAACCGAAAT
mtdna-s2	Forward	TGGGGTGACCTCGGAGAATA
	Reverse	TTGGTTAGTTTGCCGCGTTG
mtnd1	Forward	CTAGCAGAAACAAACCGGG
	Reverse	CCGGCTGCGTATTCTACGTT
16s	Forward	CCGCAAGGGAAAGATGAAAGAC
	Reverse	TCGTTTGGTTTCGGGGTTTC
hmgb1	Forward	CCAAGAAGTGCTCAGAGAGGTG
	Reverse	GTCCTTGAACTTCTTTTTGGTCTC
hmgb1-exon 2	Forward	CCCGGATGCTTCTGTCAACTT
	Reverse	TAGCAGACATGGTCTCCACCT
hmgb1-exon 3	Forward	GGTGGAGACCATGTCTGCTAA
	Reverse	CATAACGAGCCTTGTCAGCCT
tlr2	Forward	ACAGCAAGGTCTTCCTGGTTCC
	Reverse	GCTCCCTTACAGGCTGAGTTCT
tlr4	Forward	AGCTTCTCCAATTTTTCAGAACTTC
	Reverse	TGAGAGGTGGTGTAAGCCATGC
il1b	Forward	TGGACCTTCCAGGATGAGGACA
	Reverse	GTTCATCTCGGAGCCTGTAGTG

Table 6.5 (continued)

Gene symbol	Primer Sequence (5'→3')	
tnfa	**Forward**	**GGTGCCTATGTCTCAGCCTCTT**
	Reverse	GCCATAGAACTGATGAGAGGGAG
il10	Forward	CGGGAAGACAATAACTGCACCC
	Reverse	CGGTTAGCAGTATGTTGTCCAGC
tgfb	Forward	TGATACGCCTGAGTGGCTGTCT
	Reverse	CACAAGAGCAGTGAGCGCTGAA
muc5ac	Forward	CCACTTTCTCCTTCTCCACACC
	Reverse	GGTTGTCGATGCAGCCTTGCTT
cldn1	Forward	GGACTGTGGATGTCCTGCGTTT
	Reverse	GCCAATTACCATCAAGGCTCGG
cldn5	Forward	TGACTGCCTTCCTGGACCACAA
	Reverse	CATACACCTTGCACTGCATGTGC
cldn18	Forward	TGGTAGCATGGATGACTCTGCC
	Reverse	GCTGTGGACATCCAGAAGTTGG
ecad	Forward	GGTCATCAGTGTGCTCACCTCT
	Reverse	GCTGTTGTGCTCAAGCCTTCAC
ncad	Forward	CCTCCAGAGTTTACTGCCATGAC
	Reverse	CCACCACTGATTCTGTATGCCG
nos2	Forward	GAGACAGGGAAGTCTGAAGCAC
	Reverse	CCAGCAGTAGTTGCTCCTCTTC
pgcia	Forward	GAATCAAGCCACTACAGACACCG
	Reverse	CATCCCTCTTGAGCCTTTCGTG
hif1a	Forward	CCTGCACTGAATCAAGAGGTTGC
	Reverse	CCATCAGAAGGACTTGCTGGCT
eno1	Forward	TACCGCCACATTGCTGACTTGG
	Reverse	GCTTGTTGCCAGCATGAGAACC
scl2a6	Forward	GGCTCCTATCTGTGCTGATTGC
	Reverse	CCTTGGCACAAACTGGACGTAG

Table 6.6 Characteristics of primary antibodies

Epitope	Species/Clone	Dilution	Catalog #	Supplier
β-Actin	Mouse Monoclonal	1:10,000	ab6276	AbCam[a]
HMGB1	Rabbit Polyclonal	1:1000	ab79823	AbCam[a]
CCSP	Rabbit Polyclonal	1:500	WRAB-3950	Seven Hills Bioreagents[b]
RAGE	Rabbit Polyclonal	1:1000	ab3611	AbCam[a]
Foxj1	Mouse Monoclonal	1:1000	sc-53139	Santa Cruz[c]
Occludin	Mouse Monoclonal	1:1000	sc-271842	Santa Cruz[c]
ZO-1	Mouse Monoclonal	1:1000	sc-33725	Santa Cruz[c]
GP91Phox	Rabbit Polyclonal	1:1000	ab80508	AbCam[a]
Cytochrome C	Mouse Monoclonal	1:1000	sc-13156	Santa Cruz[c]
TFAM	Mouse Monoclonal	1:1000	sc-376672	Santa Cruz[c]
NRF2	Mouse Monoclonal	1:1000	sc-365949	Santa Cruz[c]
SIRT1	Mouse Monoclonal	1:1000	sc-74504	Santa Cruz[c]

[a]Cambridge, United Kingdom
[b]Ohio, USA
[c]Dallas, Texas, USA

Table 6.7 Characteristics of secondary antibodies

Expression system	Conjugate	Species/Clone	Dilution	Catalog #	Supplier
Donkey/IgG	Alexa Fluor® 680	Rabbit Polyclonal	1:10,000	A10043	Invitrogen[d]
Rabbit/IgG	Alexa Fluor® 680	Mouse Polyclonal	1:10,000	A27031	Invitrogen[d]
Donkey/IgG	IRDye® 800CW	Rabbit Polyclonal	1:10,000	926-32213	LI-COR[e]
Donkey/IgG	Cy3	Rabbit Polyclonal	1:400	711-165-152 (106486)	Jackson Immunoresearch[f]
Donkey/IgG	FITC	Rabbit Polyclonal	1:250	711-095-152 (106796)	Jackson Immunoresearch[e]

[d]Thermofisher Scientific, USA
[e]Nebraska, USA
[f]Pennsylvania, USA

CHAPTER 7. EFFECT OF NEUTRALIZATION OF SECRETED HMGB1 ON ORGANIC DUST INDUCED LUNG INFLAMMATION *IN VIVO*

Sanjana Mahadev Bhat [1,2], Nyzil Massey [1], Locke A. Karriker [3], Chong Wang [4], Chandrashekhar Charavaryamath [1*]

[1] Department of Biomedical Sciences, 2008 Vet Med Building, Iowa State University, Ames, IA, USA. [2] Immunobiology Interdepartmental Graduate Program, Iowa State University, Ames, IA, USA. [3] Department of Veterinary Diagnostic and Production Animal Medicine, 2203 Lloyd Veterinary Medical Center, Iowa State University, Ames, IA, USA

[*]To whom correspondence should be addressed: Chandrashekhar Charavaryamath, BVSc, MVSc, PhD., Assistant Professor, Department of Biomedical Sciences, Iowa State University, Ames, IA 50011. Telephone: (515) 294-7710; Fax: (515) 294-2315; Email: chandru@iastate.edu

Keywords: OD, HMGB1, antibody neutralization, airway inflammation

Modified from a manuscript in preparation.

Author Contributions

S.M. Bhat participated in the design of experiments, performed the experiments, analyzed the data, and wrote the manuscript. N. Massey performed organic dust extraction and histology scoring. L. Karriker collected the organic dust samples and edited the manuscript. C. Wang advised and assisted with statistics. C. Charavaryamath conceptualized the study, participated in the design of the experiments, performed dust extraction, participated in the interpretation of data, and edited the manuscript. All authors have read and approved the final manuscript.

Abbreviations

OD: Organic Dust; ODE: Organic Dust Extract; LPS: Lipopolysaccharide; CAFOs: Concentrated Animal Feed Operations; HMGB1: High Mobility Group Box 1; RAGE: Receptor For Advanced Glycation End Products; MAMPs: Microbial Associated Molecular Patterns; DAMPs: Damage Associated Molecular Patters; PRRs: Pathogen Recognition Receptors; COPD: Chronic Obstructive Pulmonary Disease; AHR: Airway Hyperresponsiveness; EMT: Epithelial Mesenchymal Transition; ROS: Reactive Oxygen Species; iNOS: Inducible Nitric Oxide

Synthase; TLR: Toll-like receptor; NOD2: Nucleotide-binding Oligomerization Domain-containing 2; IL: Interleukin; IFN: Interferons; TNF: Tumor Necrosis Factor; FOXJ1: Forkhead box protein J1; BALF: Bronchoalveolar Lavage Fluid; FITC: Fluorescein isothiocyanate; PKC: Protein Kinase C

Abstract

Exposure to organic dust (OD) in animal production environment is an occupational hazard that causes respiratory dysfunction in barn workers. Despite recent advances in understanding the innate inflammatory responses to organic dust exposure, a detailed understanding of how damage-associated molecular patterns (DAMPs) secreted from host cells exacerbate exposure-induced inflammation remains elusive. High mobility group box 1 (HMGB1) is a nuclear protein, and when secreted outside the cell, it acts as a proinflammatory DAMP. Our previous work has shown that OD-exposure of human airway epithelial cells induces nucleocytoplasmic translocation and secretion of HMGB1. However, the precise role of HMGB1 in OD-induced lung inflammation remains elusive. Therefore, we tested a hypothesis that neutralization of secreted HMGB1 will reduce ODE-exposure-induced lung inflammation. We administered saline or OD to mice through the intranasal route with or without anti-HMGB1 antibodies via intraperitoneal route daily for five days. Following euthanasia, blood, lavage fluid, and lung tissues were collected to quantify lung inflammation. The data was analyzed using student's t-test and one-way ANOVA and a $p \leq 0.05$ was considered significant. Here, we report that OD-exposure induces secretion of HMGB1 into the lungs of exposed mice. Intraperitoneal administration of anti-HMGB1 antibodies significantly decreased the tissue histopathology and pro-inflammatory mediators. These data demonstrate that specific inhibition of endogenous HMGB1 therapeutically reduces the OD exposure-induced airway inflammation.

Introduction

Occupation exposure to concentrated animal feeding operations (CAFOs) environment is associated with negative respiratory and other health effects (Sethi et al. 2017; Nordgren and Charavaryamath 2018). Exposed workers report a variety of respiratory symptoms including bronchitis, rhinitis, chronic cough and phlegm, occupational asthma, and organic dust toxic syndrome (Kirkhorn and Garry 2000; May et al. 2012). The incidences of respiratory and other health effects have been linked to occupational exposure to the complex environment in CAFOs where workers in these facilities are constantly exposed to a wide variety of contaminants such as organic dust, microbial components, and gases (ammonia, methane, hydrogen sulfide) (May et al. 2012; Nordgren and Charavaryamath 2018). Mechanistically, exposure to contaminants is known to induce secretion of proinflammatory mediators and induce lung inflammation. The organic dust (OD) found in the contaminants, is of mainly animal origin and is rich in a variety of microbial associated molecular patterns (MAMPs). Exposure to these MAMPs is known to induce activation of pattern recognition receptors (PRRs) such as toll like receptors (TLRs) leading to a host of downstream innate inflammatory responses in the airways and leading to loss of lung function (Charavaryamath et al. 2005; Poole and Romberger 2012; Hribar and Schultz). Studies using murine models intranasally exposed organic dust extract (ODE) have demonstrated increased influx of lymphocytes, airway hyper-responsiveness (AHR), and release of proinflammatory cytokines, including tumor necrosis factor (TNF)-α, interleukin (IL)-6, and neutrophil chemoattractants (CXCL1 and CXCL2) (Poole et al. 2008; Poole et al. 2009; Poole and Romberger 2012). Exposure to ODE has also been shown to activate downstream signaling molecules and transcription factors such as protein kinase c (PKC) family, MyD88 and NFκB (Romberger et al. 2002; Poole et al. 2009; Dickinson et al. 2018). In addition to PRR mediated-inflammatory response, damage associated molecular patterns (DAMPs) are beginning to emerge as factors that

exacerbate the inflammation (Pandolfi et al. 2016). However, the role of DAMPs in OD exposure-induced lung inflammation remains elusive.

High mobility group box 1 (HMGB1), is an essential nucleosome protein and an intracellular transcription factor. HMGB1 is a prototype DAMP molecule and has previously been identified as a late mediator of systemic inflammation (Andersson and Tracey 2011). Nuclear HMGB1 is secreted actively and passively from activated immune cells and necrotic cells, respectively (Lotze and Tracey 2005; Ugrinova and Pasheva 2017a). The release of HMGB1 begins approximately 8-12 hours after the release of early acting proinflammatory cytokines such as TNFα and IL-1β on exposure to various noxious materials (Wang et al. 1999). This delayed inflammatory reaction is mediated by the binding of HMGB1 to its receptors, receptor for advanced glycation end products (RAGE), TLR2, and TLR4. Now, a growing list of other receptors that could bind to HMGB1 has been identified (Yang et al. 2020). The secreted HMGB1 has cytokine like activity that stimulates the release of multiple proinflammatory cytokines, neutrophil, and smooth muscle cell chemotaxis, as well as increases epithelial cell permeability (Abraham et al. 2000; Degryse et al. 2001; Sappington et al. 2002). Elevated levels of HMGB1 have been found in the bronchoalveolar lavage (BAL) fluid, serum, and sputum of patients with chronic obstructive pulmonary disease (COPD) (Kanazawa et al. 2012). A murine model of chronic exposure to cigarette smoke (CS) had shown elevated levels of HMGB1 protein in the lungs indicating a role for HMGB1 in the pathogenesis of CS-induced lung inflammation (Bezerra et al. 2011). Systemic administration of HMGB1 is shown to be lethal and on the other hand, the use of anti-HMGB1 antibodies protects against the lethality induced by HMGB1 release (Wang et al. 1999; Abraham et al. 2000). Previously we have demonstrated that ODE exposure of bronchial epithelial cells leads to the release of nuclear HMGB1. The use of anti-HMGB1 neutralizing

antibody not only decreased the levels of secreted HMGB1 but significantly reduced the production of proinflammatory cytokine and NFκB activation. In addition, ethyl pyruvate (EP)-mediated blockage of nucleocytoplasmic translocation of HMGB1 downregulated the production of proinflammatory mediators (Bhat et al. 2019). Similarly, EP mediated blockade of HMGB1 release has also been shown to rescue animals from the lethal sequelae of systemic inflammation, even when the first dose is given 24 h after the induction of endotoxemia and colitis (Ulloa et al. 2002; Kim et al. 2008; Davé et al. 2009). These results indicate that nuclear HMGB1 when released into the cytoplasm and extra-cellular milieu could augment inflammatory process and strategies that target HMGB1 could abrogate inflammation.

The identification of a cytokine role for HMGB1 and its downstream action in airway inflammation renew the potential for specific cytokine inhibitors in the treatment of OD-mediated respiratory disorders in a significantly wider treatment window than the strategies currently available. Therefore, to identify the role of extracellular HMGB1 in the airways on repeated OD exposure, we administered anti-HMGB1 antibodies systemically and tested a hypothesis that neutralization of secreted HMGB1 will reduce ODE-exposure induced lung inflammation. Our findings demonstrate that neutralization of secreted HMGB1 significantly decreased the histopathological features of OD mediated airway inflammation along with decreased mucus production and tissue permeability. Furthermore, neutralization of HMGB1 also reduced cellular influx and reactive species generation, suggesting that HMGB1 specific antagonists may be effective in the clinical management of airway inflammation.

Results

Airway HMGB1 levels are decreased with systemic neutralization of secreted HMGB1

HMGB1 levels in the lungs, serum and bronchoalveolar lavage fluid (BALF) were measured in C57BL/6 mice treated with saline, or ODE (12.5%) intranasally followed by vehicle

or anti-HMGB1 neutralizing antibodies (10 µg/mice) administered intraperitoneally and for 5 consecutive days (Figure 7.1, and Table 7.2). Exposure to ODE significantly increased HMGB1 protein expression in the lungs, while in mice administered with anti-HMGB1 neutralizing antibodies, the levels were low in control, as well as on ODE exposure (Figure 7.2a). Coomassie brilliant blue (CBB) staining was performed on the SDS gels of BALF and serum samples and were used as a representation of protein loading controls (Figure 7.2d and 7.2e). HMGB1 neutralization decreased the levels of ODE-exposure induced HMGB1 levels in both BALF and serum with the decrease being higher in serum samples (Figure 7.2b and 7.2c).

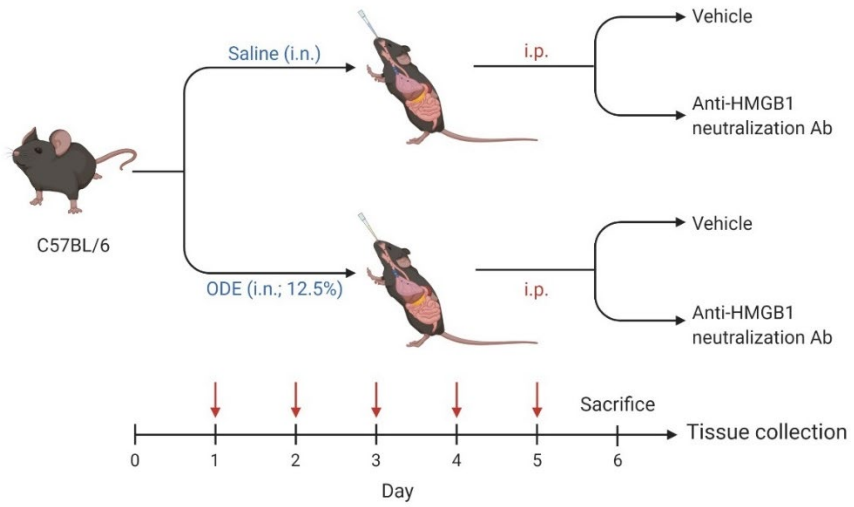

Figure 7.1 Experimental protocol
Age-matched C57BL/6 (wild type, WT) mice were intranasally (i.n.) challenged with saline or 12.5% of organic dust extract (ODE) for 5 days (day 1 through day 5). In parallel, the mice were administered with vehicle or anti-HMGB1 neutralization antibody (10 µg/mice) intraperitoneally (i.p.) for 5 days (day 1 through day 5).

To investigate whether the systemic neutralization of secreted HMGB1 has any impact on the expression of RAGE in the lungs, we performed immunoblotting to quantify the expression of RAGE (Figure 7.2f). Following ODE exposure, RAGE expression significantly increased in ODE exposed mice treated with vehicle. However, ODE exposed mice with anti-HMGB1 antibody treatment showed significantly decreased levels of RAGE and levels were similar to controls.

Following ODE exposure without HMGB1 neutralization, mRNA fold change of *tlr2* and *tlr4* increased significantly (Figure 7.2g and 7.2h) and upon HMGB1 neutralization, the expression of *tlr4* significantly decreased while the expression of *tlr2* remained high on ODE exposure.

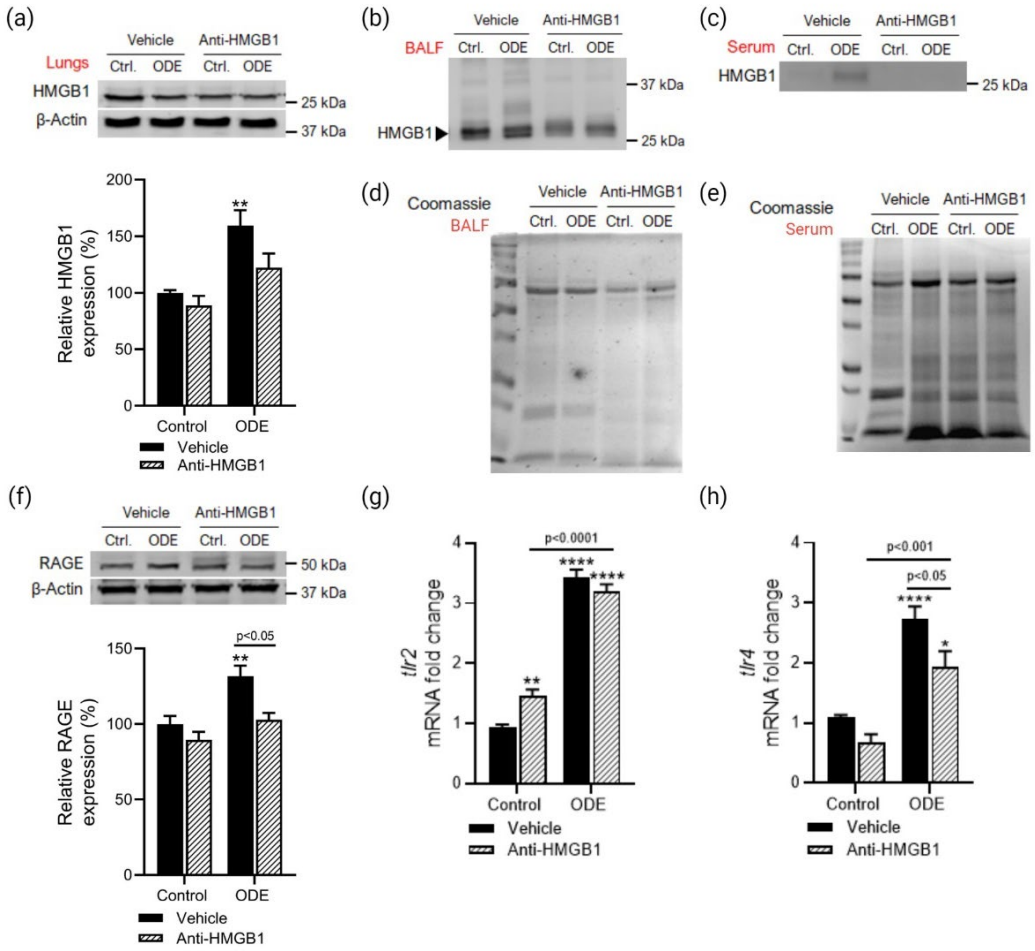

Figure 7.2 Systemic HMGB1 neutralization decreases HMGB1 expression in the airways and serum

Immunoblot of HMGB1 expression in the lungs from mice after 5 days of saline, or ODE (12.5%) exposure with either vehicle or anti-HMGB1 neutralizing antibody treatment (10 µg/mice) (a). Immunoblot of HMGB1 expression in the bronchoalveolar lavage (BALF) (b) and serum (c) from control and ODE exposed mice after 5 days with or without HMGB1 neutralization. Coomassie blue staining for loading control in the BALF (d) and serum (e) from mice after 5 days of saline or ODE exposure with or without HMGB1 neutralization. Immunoblot of RAGE protein expression in the lungs from control and ODE exposed mice after 5 days with or without HMGB1 neutralization (f). mRNA fold change of *tlr2* (g) and *tlr4* (h) expression in the lungs from control and ODE exposed mice after 5 days with or without HMGB1 neutralization. Data was analyzed using one-way ANOVA with Tukey's multiple comparison test (*$p < 0.05$, **$p < 0.01$, ***$p < 0.001$, ****$p < 0.0001$) and represented as mean ± SEM with n = 4-6 mice/group (*indicates significant difference from control).

ODE mediated cellular influx into airways was decreased on HMGB1 neutralization

Compared to vehicle treated controls, mice exposed to ODE (with vehicle treatment) showed significantly higher influx of total leukocytes, neutrophils, and macrophages into the airways (Figure 7.3a-c). Following treatment with anti-HMGB1 neutralizing antibodies, there was a significant decrease in total leukocytes, neutrophils, and macrophage numbers recruited into the airways (Figure 7.3a-c). Following neutralization, only airway neutrophil numbers remained higher when compared to controls treated with anti-HMGB1 antibodies (Figure 7.3c).

The lung wet-to-dry weight ratio was measured 24 hours after the final treatment (Figure 7.3d). Compared to saline exposed mice, there was a significant increase in the ratio in ODE exposed mice without neutralization indicative of increased ODE-mediated edema. The ratio was significantly decreased in ODE exposed mice with HMGB1 neutralization which was comparable to both saline groups. mRNA fold change of selected proinflammatory cytokines, *il1b, and tnfa*, was measured in the lungs from control and ODE exposed mice after 5 days with or without HMGB1 neutralization (Figure 7.3e and 7.3f). Both *il1b* and *tnfa* expression was significantly increased in ODE exposed mice. While *il1b* levels significantly decreased in ODE exposed animals with HMGB1 neutralization, *tnfa* levels in this group was similar to ODE exposed mice without neutralization. Saline-exposed mice with HMGB1 neutralization had increased *tnfa* expression. Expression of *il10* was significantly decreased in ODE exposed mice without neutralization when compared to the ones exposed to saline (Figure 7.3g). On HMGB1 neutralization *il10* expression was significantly increased on exposure to both saline and ODE. On the other hand, expression of *tgfb* in ODE exposed mice with and without neutralization was significantly higher than saline exposed WT mice (Figure 7.3h). The expression of GP91Phox protein, a subunit of NADPH oxidase, was measured to assess superoxide production (Figure 7.3i). The expression of GP91Phox was increased in ODE exposed mice without neutralization, while

the levels were lower in ODE exposed mice with HMGB1 neutralization. Fold change of *nos2* gene, encoding for inducible nitric oxide synthase (iNOS), significantly increased with ODE exposure in mice compared to saline exposed WT mice with and without HMGB1 neutralization (Figure 7.3j).

HMGB1 neutralization decreases ODE mediated lung histopathological changes

Formalin fixed lung sections were stained with hematoxylin and eosin (H&E) and histopathological changes were examined. The changes observed were scored by an experienced researcher blinded to the study and the scoring criteria are listed in Table 7.3. There was evidence of minimal increase in hyperplasia in the bronchioles of ODE-exposed mice compared to saline exposure, with no change on HMGB1 neutralization (Figure 7.4a and 7.4c). There was increased peribronchial cellular infiltration in ODE exposed mice without neutralization when compared to saline as well as the mice with HMGB1 neutralization (Figure 7.4d). A similar pattern was also seen in peribronchial edema, although not significant (Figure 7.4e). Vascular smooth muscle thickness was significantly increased in ODE exposed mice, which was significantly decreased on HMGB1 neutralization (Figure 7.4b and 7.4f). Increased perivascular cellular infiltration was observed in ODE exposed mice when compared to saline and HMGB1 neutralization did not affect the perivascular cellular infiltration (Figure 7.4g). Similar to peribronchial edema, perivascular edema was increased, although not significantly, in ODE exposed mice which was reduced minimally on HMGB1 neutralization (Figure 7.4h). In the distal airways, there was a minimal increase in emphysema and alveolar edema on ODE exposure which was not statistically significant (Figure 7.5a-7.5c). On the other hand, ODE exposure increased cellular infiltration into the alveoli and thickening of the alveolar septa (Figure 7.5d and 7.5e). With HMGB1 neutralization, ODE-mediated cellular infiltration and septal thickening was decreased. Albeit not

significant, saline exposed mice with HMGB1 neutralization showed an increase in cellular infiltration and septal thickening.

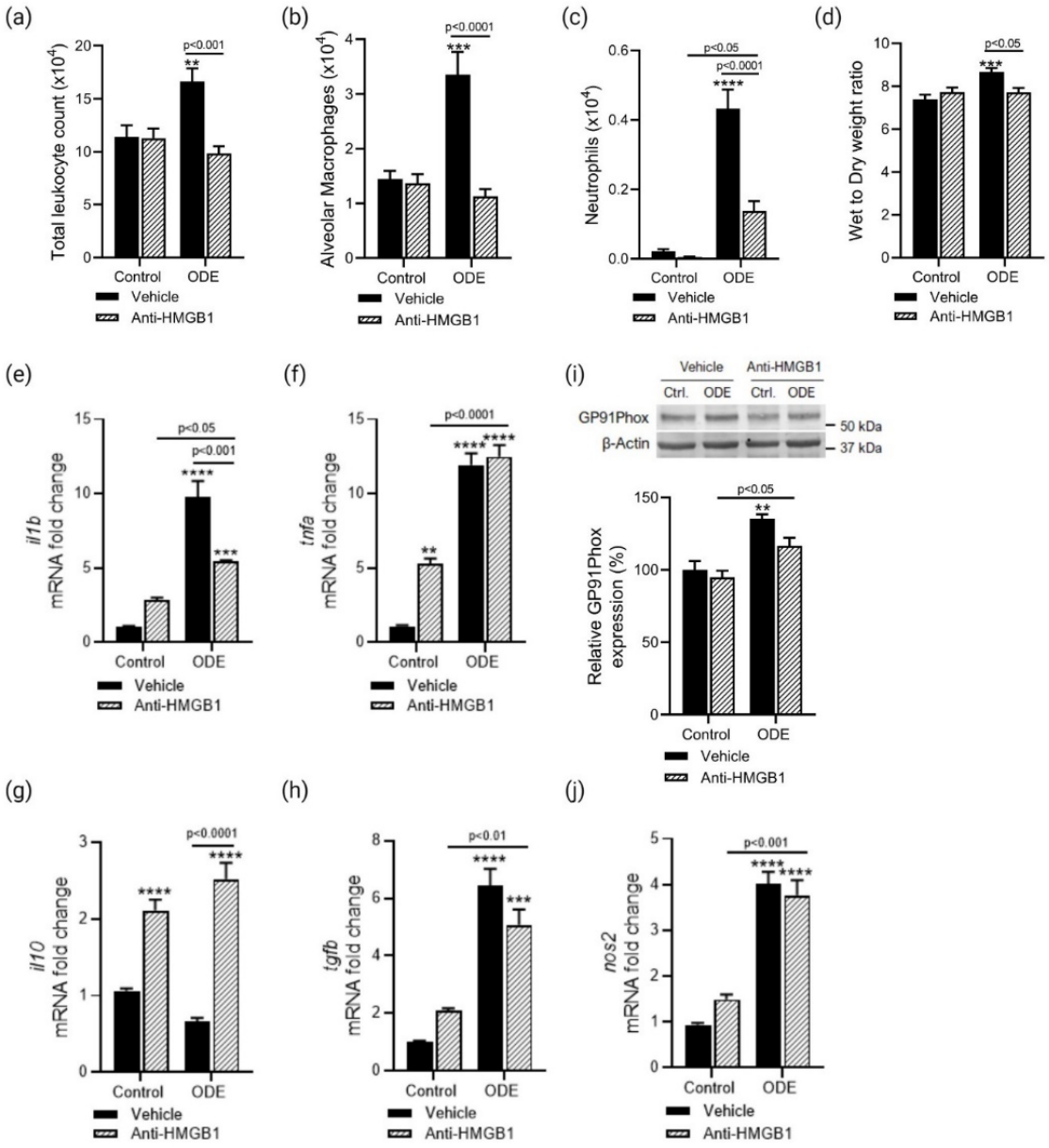

Figure 7.3 Systemic HMGB1 neutralization decreases cellular influx into the airways in ODE mediated airway inflammation

Bronchoalveolar lavage fluid (BALF) cells obtained from lungs from mice after 5 days of saline, or ODE (12.5%) exposure, and vehicle or anti-HMGB1 neutralizing antibody (10 μg/mice), stained with Shandon Kwik Diff staining solution. Total leukocyte count (a) and differential cell count of alveolar macrophages (b) and neutrophils (c) in BALF. Lung wet to dry weight ratios in control and ODE exposed mice after 5 days with or without HMGB1 neutralization (d). mRNA

fold change of *il1b* (e), *tnfa* (f), *il10* (g), *tgfb* (h) and *nos2* (j) expression in the lungs from control and ODE exposed mice after 5 days with or without HMGB1 neutralization. Immunoblot of GP91Phox protein expression in the lungs from control and ODE exposed mice after 5 days with or without HMGB1 neutralization (i). Data was analyzed using one-way ANOVA with Tukey's multiple comparison test (*$p < 0.05$, **$p < 0.01$, ***$p < 0.001$, ****$p < 0.0001$) and represented as mean ± SEM with n = 6-10 mice/group (*indicates significant difference from control).

ODE exposure induced goblet cell metaplasia is decreased with systemic HMGB1 neutralization

Lung tissue sections were stained with periodic acid Schiff (PAS) to detect goblet cells (Figure 7.6a). The number of goblet (PAS+) cells was manually counted and normalized to the length of the basement membrane (Figure 7.6b). A significant increase in the number of goblet cells was observed in ODE exposed mice with and without neutralization compared to saline. The number of PAS+ cells was significantly decreased in ODE exposed mice with HMGB1 neutralization when compared to the ones without neutralization. There was also an increase in the number of goblet cells in saline exposed mice with HMGB1 neutralization. To corroborate this, mRNA fold change of *muc5ac* was measured by qRT-PCR (Figure 7.6c). A similar pattern of expression was observed in muc5asc to that of PAS+ cells. In addition, expression of forkhead box protein J1 (FoxJ1), the transcription factor involved in ciliogenesis and a marker for motile cilia, was measured in the lungs post-exposure (Figure 7.6d). A decrease in FoxJ1 expression was observed in mice exposed to ODE with and without HMGB1 neutralization. On the other hand, FoxJ1 expression in saline exposed mice with neutralization was significantly increased when compared to the ones without neutralization.

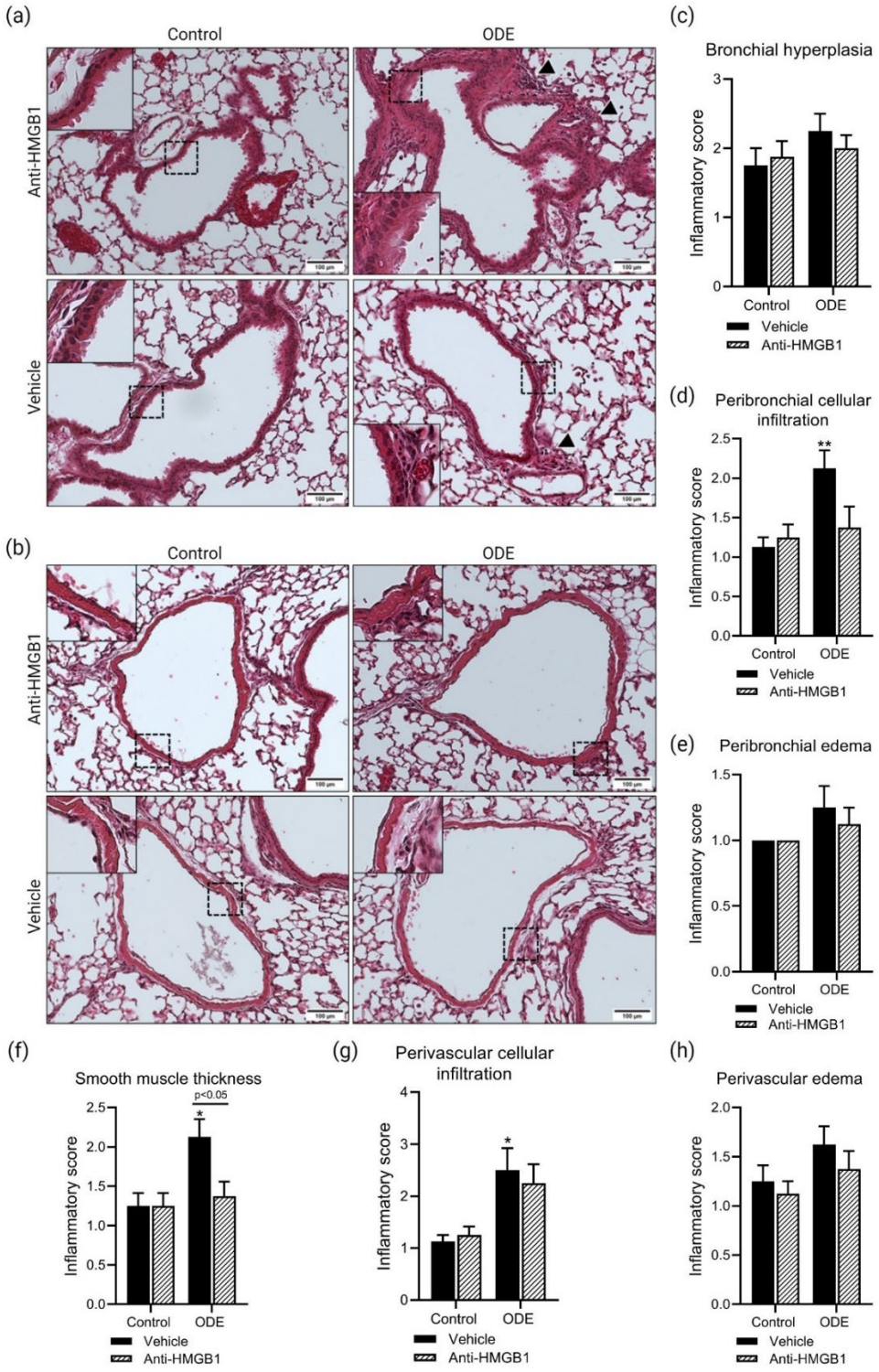

Figure 7.4 ODE exposure increases peribronchial edema and smooth muscle thickness
Formalin fixed lung tissue sections from mice after 5 days of saline, or ODE (12.5%) exposure, and vehicle or anti-HMGB1 neutralizing antibody (10 μg/mice) were stained with hematoxylin and eosin (H&E). Representative images of H&E stained bronchioles (a) and blood vessels (b) were obtained. Insets: images are shown with higher magnification (original magnification, x200).

Arrows indicate regions of inflammatory cell infiltrate (a). Semiquantitative histopathology scoring of bronchial hyperplasia (c), peribronchial cellular infiltration (d), peribronchial edema (e), smooth muscle thickness (f), perivascular cellular infiltration (g) and perivascular edema (h) was performed. Data was analyzed using one-way ANOVA with Tukey's multiple comparison test (*p < 0.05, **p < 0.01, ***p < 0.001, ****p < 0.0001) and represented as mean ± SEM with n = 3-5 fields/ mice and 4 mice/group (*indicates significant difference from control).

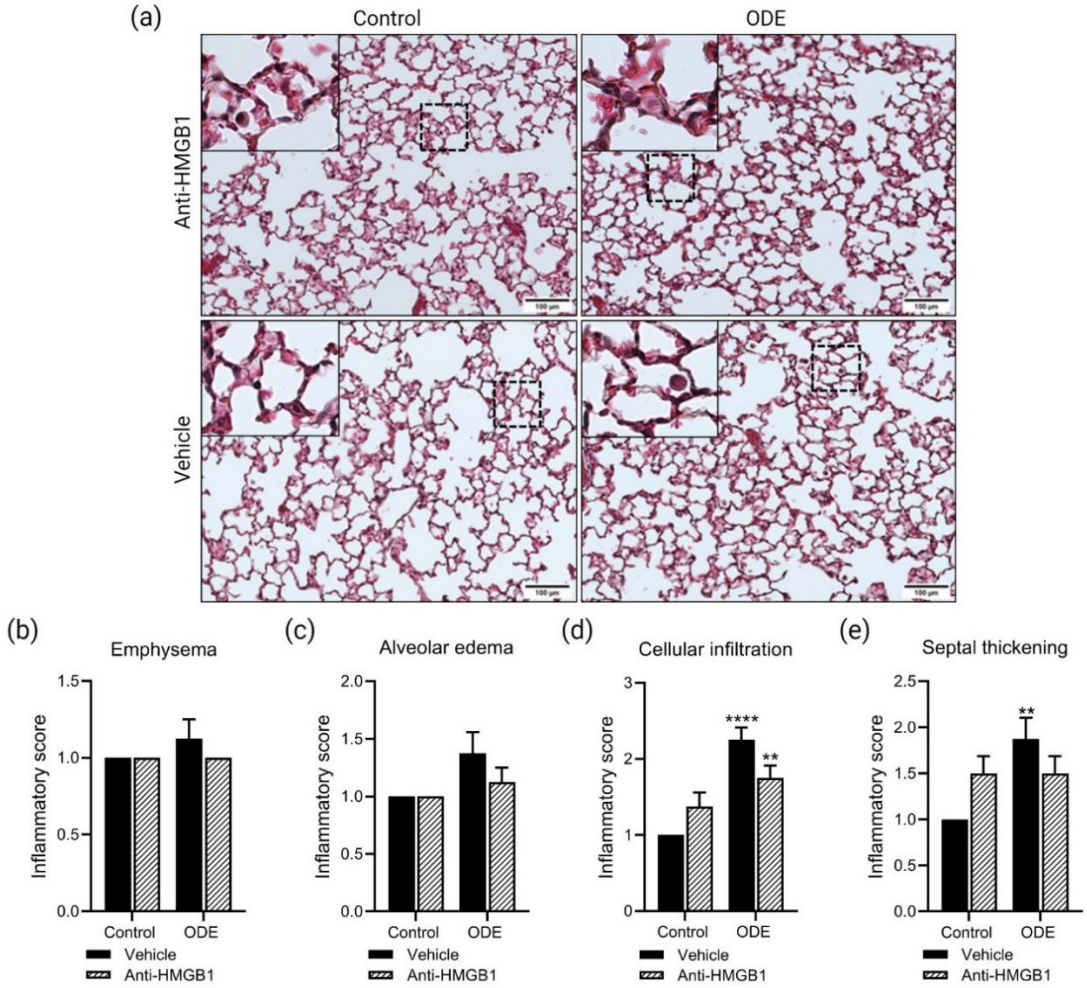

Figure 7.5 HMGB1 neutralization does now ameliorate ODE induced alveolar septal thickening

Formalin fixed lung tissues obtained from mice after 5 days of saline, or ODE (12.5%) exposure, and vehicle or anti-HMGB1 neutralizing antibody (10 µg/mice) were stained with hematoxylin and eosin (H&E). Images of H&E stained alveoli were obtained. Insets: images were shown with higher magnification images (original magnification, x200) (a). Semiquantitative histology scoring of emphysema (b), alveolar edema (c), cellular infiltration (d) and alveolar septal thickening (e) was performed. Data was analyzed using one-way ANOVA with Tukey's multiple comparison test (*p < 0.05, **p < 0.01, ***p < 0.001, ****p < 0.0001) and represented as mean ± SEM with n = 3-5 fields/ mice and 8 mice/group (*indicates significant difference from control).

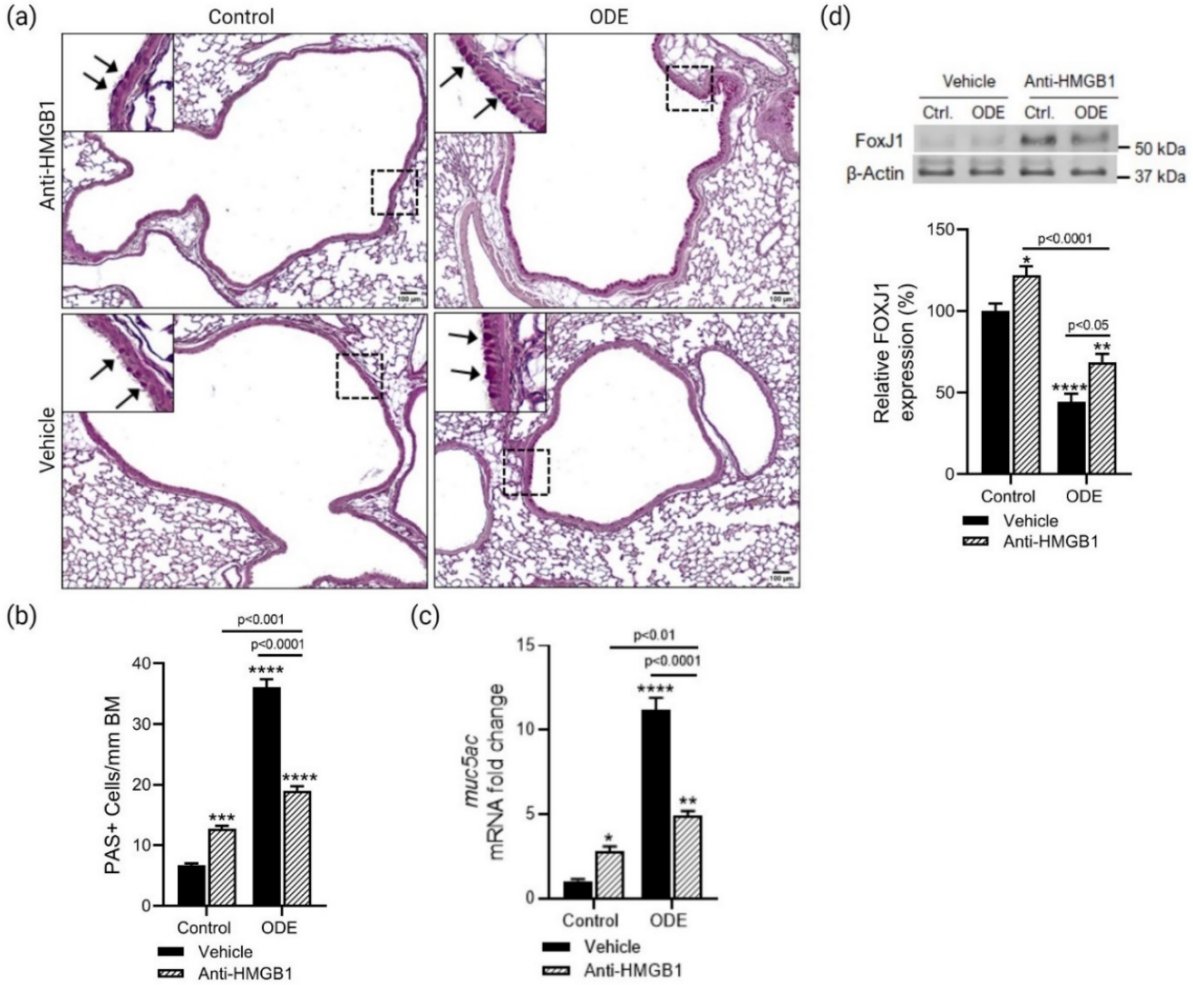

Figure 7.6 HMGB1 neutralization decreases airway periodic acid schiff (PAS) positive cells Formalin fixed lung tissues obtained from mice after 5 days of saline, or ODE (12.5%) exposure, and vehicle or anti-HMGB1 neutralizing antibody (10 µg/mice) were stained with periodic acid schiff (PAS) for detection of goblet cells. Insets: images were shown with higher magnification images. Arrows indicate PAS-positive cells. (a). Quantification of the number of PAS-positive cells goblet cells per mm of basement membrane (BM) (b). mRNA fold change of *muc5ac* expression in the lungs from control and ODE exposed mice after 5 days with or without HMGB1 neutralization (c). Immunoblot of FoxJ1 protein expression in the lungs from control and ODE exposed mice after 5 days with or without HMGB1 neutralization (d). Data was analyzed using one-way ANOVA with Tukey's multiple comparison test (*$p < 0.05$, **$p < 0.01$, ***$p < 0.001$, ****$p < 0.0001$) and represented as mean ± SEM with n = 2-4 fields/ mice and 8 mice/group (*indicates significant difference from control).

HMGB1 neutralization rescues ODE mediated loss of tight junction integrity

24 h after the final exposure, airway tissue permeability was measured by intranasal instillation of FITC-Dextran (10 mg/ kg of body weight) for 1 hour. Compared to saline exposed mice, ODE exposed mice without neutralization showed an increase in the fluorescence intensity (FI) in the blood serum. (Figure 7.7a). On HMGB1 neutralization, the FI value remained comparable to saline exposed mice. To corroborate this, the expression of tight and adherens junction markers was measured. Protein expression of zonula occludens-1 (ZO-1) and occludin was significantly increased in saline exposed mice with HMGB1 neutralization (Figure 7.7b and 7.7c). Occludin expression in mice exposed to ODE showed a minimal decrease. ZO-1 protein levels were significantly decreased in mice exposed to ODE, while on HMGB1 neutralization the levels were significantly increased (Figure 7.7d and 7.7e). Fold change of claudins, *cldn1* and *cldn5* significantly increased in saline and ODE exposed mice with HMGB1 neutralization when compared to the saline group, with a more prominent increase in the ODE group. Fold change of *cldn18* was significantly increased on ODE exposure compared to saline, while HMGB1 neutralization in saline and ODE mice showed a more prominent increase compared to ODE alone (Figure 7.7f). An increase in the expression of cadherins, *ecad,* and *ncad* mRNA in mice exposed to both saline and ODE with HMGB1 neutralization was observed compared to saline exposed mice. Expression of *ecad* increased significantly in ODE exposed mice without neutralization when compared to saline exposed mice (Figure 7.7g). However, expression of *ncad* in ODE exposed mice remained comparable to saline exposed animals (Figure 7.7h).

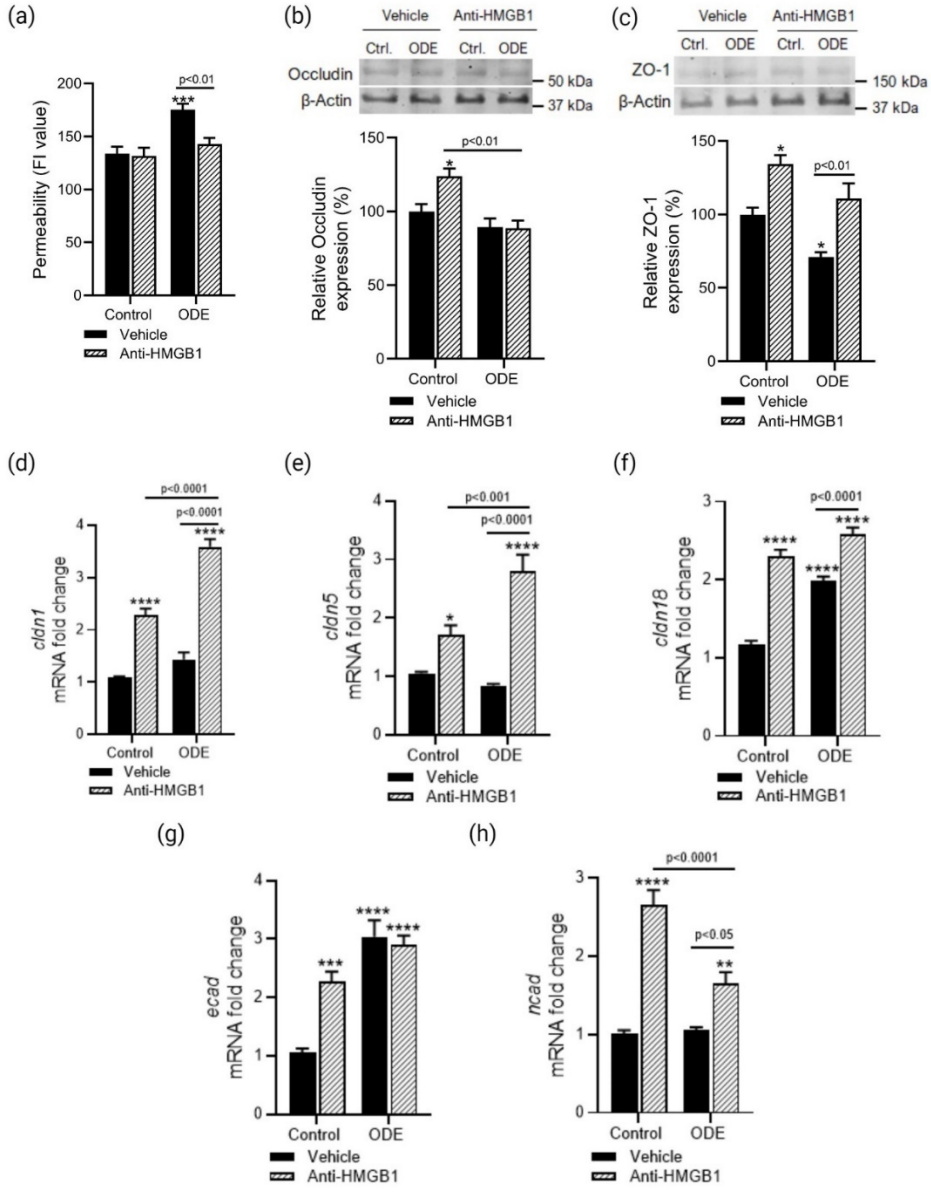

Figure 7.7 Systemic HMGB1 neutralization decreases ODE exposure-induced increase in airway epithelium permeability

Lung permeability assay using 10 mg/kg b.w. of FITC-Dextran via intranasal (i.n.) administration in mice after 5 days of saline, or ODE (12.5%) exposure, and vehicle or anti-HMGB1 neutralizing antibody (10 µg/mice) (a). Immunoblot of ZO-1 (b) and Occludin (c) protein expression in the lungs from control and ODE exposed mice after 5 days with or without HMGB1 neutralization. mRNA fold change of *cldn1* (d), *cldn5* (e), *cldn18* (f), *ecad* (g), and *ncad* (h) expression in the lungs from control and ODE exposed mice after 5 days with or without HMGB1 neutralization. Data was analyzed using one-way ANOVA with Tukey's multiple comparison test (*$p < 0.05$, **$p < 0.01$, ***$p < 0.001$, ****$p < 0.0001$) and represented as mean ± SEM with n = 4-6 mice/group (*indicates significant difference from control).

Discussion

In the present study, using a murine model of OD exposure induced lung inflammation, we report a role for HMGB1. Our results describe how systemic neutralization of HMGB1 curtails OD-induced lung inflammation through reductions in the expressions of secreted HMGB1, RAGE, TLR4, influx of inflammatory cells into airways, and other inflammatory mediators. Repeated exposure to OD is known to induce significant changes in innate immune responses through activation of PRRs and secretions of proinflammatory mediators (Poole et al. 2008; Sundblad et al. 2009). Targeting OD exposure-induced proinflammatory mediators is a potential strategy to reduce the manifestation of chronic airway diseases.

Murine models of intranasal ODE exposure recapitulate many features of airway inflammatory disease similar to that observed in exposed agricultural workers (Charavaryamath et al. 2005; Poole et al. 2009). Despite the several years of research conducted in understanding the OD-induced airway inflammatory disease pathophysiology, the role of extracellularly secreted HMGB1 in OD exposure-induced lung inflammation remains mostly unknown. Recently, we used a bronchial epithelial cell model of ODE exposure, where we demonstrate how targeting HMGB1 could abrogate ODE-induced inflammation (Bhat et al. 2019). To translate these results into a pre-clinical model and to test whether neutralization of extracellular HMGB1 would reduce ODE-induced inflammation, we chose to use a C57BL/6 mouse model. In our intranasal exposure model, mice were intraperitoneally treated with vehicle or anti-HMGB1 neutralizing antibodies. A hallmark of OD exposure is the increased influx of neutrophils and macrophages (Poole et al. 2008; Sundblad et al. 2009). Consistent with this, we document an increase in total leukocyte influx into the airways on exposure to ODE. This increase in total leukocytes was characterized by an increase in absolute neutrophil and macrophage numbers. Systemic HMGB1 neutralization significantly decreased the ODE-induced increase in total leukocytes, neutrophils, and macrophages in BALF

to indicate a prime role for extracellular HMGB1 in decreasing the leukocyte mediated inflammation. Our data showed that ODE exposure increases the expression of RAGE whereas systemic neutralization of HMGB1 decreases the expression of RAGE as well as expression of HMGB1 in the lung, BALF, and serum indicating that, systemic neutralization of HMGB1 would reduce inflammation by blocking the signaling via HMGB1-RAGE axis. Our observation of ODE-induced increases in the expression of *tlr2 and tlr4* are in line with our previous published work (Bhat et al. 2019). It is interesting to note that, systemic neutralization of HMGB1 reduced the ODE exposure induced increases in *tlr4* but not *tlr2* fold changes. Though our study does not explore the underlying mechanisms, it does raise interesting questions about the possibility of TLR2 mediated signaling even with HMGB1 neutralization.

ODE exposure increased the expression of *il1b* and *tnfa* and systemic neutralization of HMGB1 reduced the levels of *il1b* but not *tnfa* levels. It is interesting to note that HMGB1 neutralization did not decrease the expression of *tlr2*. Hence it remains to be determined whether ODE exposure induces TLR2 mediated signaling to increase the expression of TNFα. Poole et al., have shown that TLR2 regulates the OD exposure induced signaling, and the CAFO environment is rich in Gram-positive bacteria that are known to induce TLR2-mediated signaling (Poole et al. 2011; S et al. 2016).

Another key component associated with inflammation is the generation of reactive species (Ahmed 2011; Poole and Romberger 2012). Consistent with previous studies, *nos2* expression was significantly upregulated in ODE-exposed mice. On neutralization of HMGB1, levels of *nos2* remained significantly higher than controls. Expression of GP91Phox, a subunit of NADPH oxidases which is involved in the generation of superoxide anions (O_2^-) was measured as well (Banerjee and Henderson 2012). GP91Phox expression was significantly increased in ODE

exposed mice. Although we document a relatively small increase in GP91Phox expression with neutralization, the levels are not significantly higher. Studies have shown that a decrease in GP91Phox expression decreases superoxide overproduction (Liu et al. 2006a; Banerjee and Henderson 2012). The increase in the expression of GP91Phox observed in ODE exposed mice could be resulting in overproduction of ROS, implicated in tissue destruction and various disease states. Collectively, these data suggest a role for extracellular HMGB1 in exacerbating oxidative stress induced following ODE-mediated inflammation.

Histopathological analysis of the lungs from OD exposed mice showed significant changes in the tissues with and without HMGB1 neutralization. ODE exposed mice showed an increase in cellular infiltration, smooth muscle thickness, edema, alveolar septal thickening, and emphysema. On HMGB1 neutralization, these histopathological changes were decreased. As observed in earlier studies, airway mucin (Muc5ac) expression and goblet cell numbers were increased on ODE exposure (Dickinson et al. 2018). Interestingly on HMGB1 neutralization, the number of PAS-positive cells increased as well as *muc5ac* gene expression with or without exposure to ODE. Studies have shown that chronic exposure to OD leads to dysfunctional mucociliary clearance in workers (Wyatt et al. 2008). Consistent with this data, a decrease in the expression of FoxJ1 was observed in ODE exposed mice which increased on HMGB1 neutralization. In addition, the expression of FoxJ1 was significantly increased in saline exposed mice with HMGB1 neutralization as well. It is possible that the neutralization of secreted HMGB1 systemically could be maintaining the balance between goblet cell numbers and cilia in the airways thus impacting the mucociliary clearance. However, further studies may be necessary to mechanistically validate our current observation.

Increased epithelial permeability is a hallmark of airway inflammation (Grainge and Davies 2013; Georas and Rezaee 2014). Epithelial junctional complexes can be disrupted directly by inhaled noxious substances that are capable of penetrating the mucus layer or by the release of other inflammatory mediators (Grainge and Davies 2013). In line with this, we observed an increase in the airway epithelial permeability on exposure to ODE. Neutralization of HMGB1 maintained the integrity of epithelial permeability even on exposure to ODE. Interestingly, mRNA fold change of tight junction markers (claudin 1, claudin 5, and claudin 18) are increased in animals administered with neutralization antibody compared to control. Animals exposed to ODE alone showed a significant increase in claudin 18, which is indicative of upregulation of alveolar type II cell-mediated repair response (Kotton 2018). In addition to claudins, epithelial barrier function is also maintained by the occludin proteins anchored to the cytoskeleton by ZO-1 (Georas and Rezaee 2014). Occludin and ZO-1 proteins form intact intercellular barriers at tight junctions, and differences in their expression account for the change in barrier function and paracellular permeability in the epithelium (Ye et al. 2003; Ohtake et al. 2003; Raleigh et al. 2011). Our study showed a decrease in the expression of both occludin and ZO-1 proteins on exposure to ODE. On HMGB1 neutralization, the expression of both markers was increased with or without ODE exposure. This pattern of expression of key markers of epithelial barrier integrity paralleled by the changes in tissue permeability suggests that secreted HMGB1 has a negative impact on the integrity of the epithelium. Neutralization of HMGB1 also significantly increased the fold change of *ecad* and *ncad* genes with or without ODE, with a significant increase in the *ecad* expression on exposure to ODE. E-cad and N-cad are key regulators of epithelial mesenchymal transition (EMT) which is characterized by the loss of E-cad and enhanced expression of N-cad which contributes to airway remodeling (Nieto 2011).

Collectively, it appears that HMGB1 contributes to the development of tissue changes in OD-mediated airway inflammation. The kinetics of HMGB1 release enables the development of therapy against the effects of this cytokine to be delayed by as much as 24 h after exposure to a noxious stimulus. To date, no other pathogenic mediators of OD-mediated airway inflammation have been specifically targeted this late in the course of exposure to rescue animals from airway pathology. In the present study, we found that antibody-mediated neutralization of secreted HMGB1 assists in downregulating the development of OD-mediated histopathology. Taken together, extracellular HMGB1 is a critical mediator of various inflammatory mechanisms in airway epithelial cells exposed to organic dust. It will be important to delineate the connection between the neutralization of HMGB1 and immune-regulatory mechanisms because these two systems occupy a critical final common pathway to tissue injury and airway diseases which will be the focus of our future studies. Based on this it should be possible to design clinical studies of OD mediated airway inflammation in workers who have elevated HMGB1 levels to assess the effects of HMGB1 antagonists.

Materials and Methods

Ethics statement

All animal work and procedures performed were approved by the Institutional Animal Care and Use Committee (IACUC) and Institutional Biosafety Committee (IBC) of the Iowa State University. Research with the animals were done under the protocol IACUC 19-296 and IBC 19-188. NIH guidelines were followed for the care and handling of mice in this study.

Organic dust extract (ODE) preparation

Organic dust (OD) samples were collected and an aqueous extract was prepared as previously described (Romberger et al. 2002; Bhat et al. 2019). Briefly, the dust settled on the surfaces of swine housing facilities was collected and 1 g was mixed into sterile Hank's Balanced

Salt Solution (10 mL; Gibco). The solution was incubated for one hour at room temperature and centrifuged for 20 min at 1365 x g. The final supernatant obtained was filter-sterilized (0.22 μm), to remove larger coarse particles and microbes. Stock ODE (100%) samples were aliquoted and frozen at stored at -20°C until use in experiments. The stock was diluted in sterile phosphate buffer saline (PBS) to a final concentration of 12.5% (v/v). The 12.5% concentration used has been previously shown to elicit lung inflammation in mice (Poole et al. 2009).

Endotoxin estimation

The levels of endotoxin in the ODE samples were quantified using the Pierce Chromogenic Endotoxin Quant Kit (Thermofisher Scientific) according to the manufacturer's instructions. The ODE samples were diluted in a ratio of 1:50 in endotoxin-free water. The diluted samples (50 μL) along with reconstituted amebocyte lysate reagent, were added into an endotoxin-free 96-well plate in a sample to lysate ratio of 1:1, in triplicates. The standard was reconstituted and added to the plate in a sample to lysate ratio of 1:1. The plate was incubated at 37°C for 12 to 35 minutes based on the range of standards used. Following incubation, 100 μL of chromogenic substrate was added and the plate was incubated at 37°C for 6 minutes. 50 μL of stop solution (25% acetic acid) was added and absorbance was read at 405 nm using a spectrophotometer reader (SpectraMax M2 Gemini Microplate Reader, Molecular Devices, San Jose, CA). The average of blank wells was deducted from the standards and sample absorbance values. A linear standard graph was plotted, and sample concentrations (undiluted) were extrapolated from the equation of the slope using the OD values (Table 7.1).

Table 7.1 Endotoxin concentrations in ODE samples used in our experiments

Sample No.	Endotoxin (EU/mL)
8	6.315 ± 0.2
9	5.20 ± 0.1
10	10.67 ± 0.3
11	8.052 ± 0.1

Animals model and treatment

Age and sex-matched C57BL/6 mice (6-8 week old) were purchased from The Jackson Laboratory (Ann Arbor, MI), allowed to acclimatize for three days before randomly assigning to different treatment groups. Mice in all groups were lightly anesthetized by isoflurane (2-3%) inhalation, following which saline (PBS), or ODE (12.5%) were intranasally (i.n.; 50 µL/mice) instilled. We then assigned mice into 3 major groups for the second treatment: (i) sham (mice without any treatment); (ii) control IgG (10 µg/mice; data not shown); (iii) 10 µg anti-HMGB1 antibody (10 µg/mice). The antibody was administered by intraperitoneal (i.p.) injection every 24 hours for 5 days (Figure 7.1 and Table 7.2). Approximately 24 h following the final treatment the mice were euthanized by intraperitoneal administration of sodium pentobarbital (100 mg/kg b.w.) as per the American Veterinary Medical Association (AVMA) Guidelines for Euthanasia of Animals. The use of sodium pentobarbital was performed under the approval and licenses from the department of drug enforcement agency (DEA) and Iowa Board of Pharmacy. The controlled drugs were maintained in the approved safe-lock box with an inventory of the amounts used.

Table 7.2 Stock and working concentrations of the reagents

Treatment	Stock concentration	Working concentration
Organic Dust Extract (ODE)	100% in HBSS	12.5% in PBS
Anti-HMGB1 neutralizing antibody	1.8 mg/mL	0.5 mg/kg
Sodium Pentobarbital	390 mg/mL	100 mg/kg
FITC-Dextran	50 mg/mL	10 mg/kg

FITC-Dextran permeability assay

Permeability alterations after treatment administration were measured by FITC-Dextran leakage from the airways into the bloodstream. 50 µL of FITC-Dextran (10 mg/kg b.w., 24 µL per nostril; Sigma) dissolved in sterile PBS was introduced intranasally into the airways 24 h after the final treatment administration. After instillation, the mouse was set vertically for 2 min until it breathed steadily. The mice were sacrificed one hour later, and blood was collected by cardiac puncture. Finally, the blood was treated with 10 mL of EDTA (60 mg/mL) and centrifuged at 7000 rpm for 10 min. The fluorescence intensity (FI value) of the plasma (~200 µL) was determined at an excitation/emission wavelength of 485/528 nm using SpectraMax M2 Gemini Microplate Reader (Molecular Devices, San Jose, CA)(Chen et al. 2014).

Lung wet-to-dry weight ratio

After the final treatment administration and mice were euthanized. The diaphragmatic lobe of the right lung was excised separately and rapidly weighed to obtain the "wet" weight. Samples were oven-dried (65°C) for 48 h to determine the stable dry weight. The ratio of the wet-to-dry (W/D) weight was calculated to assess lung tissue edema (Chen et al. 2014).

Bronchoalveolar lavage and cytospins

Post animal euthanasia, the trachea was exposed and cannulated with a 23-gauge needle just below the larynx. Bronchoalveolar lavage fluid (BALF) was collected from the lungs by instilling 1 ml cold PBS with 0.1 mM EDTA and recovered by aspiration. This was done a total of three times and the BALF from each mouse was pooled and was centrifuged at 800 x g for 10 min to collect cells (Sun et al. 2017). The supernatant from the first milliliter of cell-free BALF was recovered and frozen at -80°C for other assays. Cells from the BALF were resuspended, and total cell numbers were determined by using a hemacytometer. Differential cell counts were determined on cytospins prepared by the Iowa State University clinical pathology laboratory

(College of Veterinary Medicine) and stained with Shandon Kwik Diff Staining (Thermofisher Scientific). Differential cell counts were determined by manual counting of 500 cells per slide per mouse.

Tissue collection

After whole lung lavage, lungs were harvested from each treatment group. The right lung was tied off at the primary bronchus, excised, flash-frozen in liquid nitrogen, and stored in -80° C. The left lung was slowly inflated with ~200-300 µL of 4% paraformaldehyde (PFA; Sigma, St. Louis, MO). To obtain uniform lung inflation during fixation, the lungs were fixed at a 25 cm height. The inflated lungs were submerged in 4% PFA for 24 h, followed by 70% ethanol. The fixed lungs were embedded in paraffin and sectioned into 5-micron slices by the Iowa State University histopathology laboratory (College of Veterinary Medicine).

Histology, mucus staining, and histopathology analysis

Hematoxylin and eosin (H&E) staining was performed according to standard protocol (Fischer et al. 2008). Each slide was entirely reviewed at scanning magnifications (×2, ×10, and ×20 objectives; Nikon Eclipse TE2000-U microscope; SPOT Advanced imaging software, Michigan, USA). The histopathological scores were determined by an experienced researcher blinded to the treatment conditions. The scoring system utilized a standardized set of photos representing the spectrum of inflammatory changes for each parameter in the bronchioles, blood vessels, and alveolar septa (outlined in Table 7.3).

For mucus staining, Richard-Allan Scientific Chromaview – Advanced Testing Periodic Acid-Schiff (PAS) kit (Thermofisher Scientific) was used as per the manufacturer's instructions. PAS-positive cells lining the surface epithelium were counted in 6 to 8 airways per mouse. The numbers were normalized to the length of the basement membrane, which was determined using

ImageJ (National Institutes of Health) (Shi et al. 2002). Images were obtained using Nikon Eclipse TE2000-U microscope and SPOT Advanced imaging software (Michigan, USA).

Table 7.3 Histology scoring criteria

Score	Peribronchiolar edema	Bronchial hyperplasia / club cells per 100 µm	Smooth muscle	Perivascular edema	Septa	Alveolar edema	Emphysema	Cellular infiltration
1	nil	<5	<5 µm	Up to 50 µm	<10 µm	1-100 µm	50-200 µm	1-10 total neutrophil
2	1-100 µm	5-15/100	5-20 µm	50-100 µm	10-15 µm	101-200 µm	300-400 µm	10-20 total neutrophil
3	100-200 µm	15-25/100	25-100 µm	100-150 µm	15-20 µm	201-300 µm	400-500 µm	30-50
4	>200 µm	>25	>100 µm	>150 µm	>20 µm	>301 µm	>500	>50

qRT-PCR

Total RNA was isolated from the lung homogenate using TRIzol extraction methods (Seo et al. 2014) and RNA concentration was measured using NanoVue Plus spectrophotometer (GE Healthcare, UK). 1µg of RNA was used to synthesize cDNA using the High-Capacity cDNA Reverse Transcription Kit (ThermoFisher Scientific) according to the manufacturer's instructions.

RT-qPCR was performed using 500 ng of template DNA in a 10 µL reaction volume using SYBR green master mix and 1 µM of primers for target of interest. The housekeeping gene 18S rRNA (ThermoFisher Scientific) was used in all qPCR reactions. No-template controls and dissociation curves were run for all reactions to exclude cross-contamination. The primers for genes of interest listed in Table 7.4 were synthesized at Iowa State University's DNA Facility. The qRT-PCR reactions were run in a QuantiStudio-3™ (Thermofisher Scientific) detection system and the data was analyzed using $2^{-\Delta\Delta CT}$ method (Livak and Schmittgen 2001).

Immunoblot analysis

The lungs were lysed using RIPA buffer with 1X HALT protease inhibitor and EDTA (Thermofisher Scientific). Protein concentration was measured using the Bradford protein assay kit (BioRad). Equal amounts of protein (20 µg/sample), along with a molecular weight marker (Bio-Rad), were run on 10–12% sodium dodecyl sulfate/polyacrylamide gel electrophoresis (SDS-

PAGE) as previously described (Bhat et al. 2019). Proteins were transferred onto a nitrocellulose membrane and nonspecific binding sites were blocked with Intercept® blocking buffer (LI-COR, Lincoln, NE). The membranes were then incubated with different primary antibodies and dilutions listed in Table 7.5. Next, membranes were incubated with one of the following secondary antibodies: Alexa Fluor 680 goat anti-mouse, Alexa Fluor 680 donkey anti-rabbit, or IRDye 800CW donkey anti-rabbit (1:10,000; LI-COR). To confirm equal protein loading, blots were probed with relevant housekeeping proteins listed in Table 7.5. Western blot images were captured using Odyssey® CLx IR imaging system (LI-COR Biotechnology) and analysis was performed using ImageJ software (National Institutes of Health).

Statistics

Data analysis was performed using GraphPad Prism 8.0 software (La Jolla, CA, USA). Raw data were analyzed with either Student's t-test or using one-way ANOVA, and Tukey's posttest was performed to compare all treatment groups. A p-value of < 0.05 was considered statistically significant. *$p < 0.05$, **$p < 0.01$, ***$p < 0.001$, ****$p < 0.0001$. * indicates different from control. For all the assays, samples were derived from the same experiment and were processed in parallel to minimize variation.

Acknowledgments

We would like to thank Dr. Kevin Tracey (Feinstein Institutes for Medical Research, Northwell Health, NY) for providing us with the anti-HMGB1 neutralization antibody. We thank Virginia Montgomery at Iowa State University Veterinary Pathology and Histology Laboratory for assistance with lung-tissue processing, and sectioning. In addition, we thank Dr. Anumantha Kanthasamy, Dr. Michael Cho and the Iowa State University Department of Biomedical Sciences for access to instruments and equipment.

Potential Conflicts of Interest

The terms of this arrangement have been reviewed and approved by Iowa State University per its conflict-of-interest policies. All other authors have declared no potential conflicts of interest.

Funding

C.C. laboratory is funded through a startup grant through Iowa State University and a seed grant awarded by the college of veterinary medicine (CVM) at Iowa State University.

References

Abraham E, Arcaroli J, Carmody A, Wang H, Tracey KJ (2000) Cutting Edge: HMG-1 as a Mediator of Acute Lung Inflammation. The Journal of Immunology 165(6):2950–2954. https://doi.org/10.4049/jimmunol.165.6.2950

Ahmed AU (2011) An overview of inflammation: mechanism and consequences. Front Biol 6(4):274. https://doi.org/10.1007/s11515-011-1123-9

Andersson U, Tracey KJ (2011) HMGB1 Is a Therapeutic Target for Sterile Inflammation and Infection. Annu Rev Immunol 29:139–162. https://doi.org/10.1146/annurev-immunol-030409-101323

Banerjee ER, Henderson WR (2012) Defining the molecular role of gp91phox in the immune manifestation of acute allergic asthma using a preclinical murine model. Clinical and Molecular Allergy 10(1):2. https://doi.org/10.1186/1476-7961-10-2

Bezerra FS, Valença SS, Pires KMP, Lanzetti M, Pimenta WA, Schmidt AC, Porto LC, Zin WA (2011) Long-term exposure to cigarette smoke impairs lung function and increases HMGB-1 expression in mice. Respiratory Physiology & Neurobiology 177(2):120–126. https://doi.org/10.1016/j.resp.2011.03.023

Bhat SM, Massey N, Karriker LA, Singh B, Charavaryamath C (2019) Ethyl pyruvate reduces organic dust-induced airway inflammation by targeting HMGB1-RAGE signaling. Respiratory Research 20(1):27. https://doi.org/10.1186/s12931-019-0992-3

Charavaryamath C, Janardhan KS, Townsend HG, Willson P, Singh B (2005) Multiple exposures to swine barn air induce lung inflammation and airway hyper-responsiveness. Respir Res 6:50. https://doi.org/10.1186/1465-9921-6-50

Chen H, Wu S, Lu R, Zhang Y, Zheng Y, Sun J (2014) Pulmonary Permeability Assessed by Fluorescent-Labeled Dextran Instilled Intranasally into Mice with LPS-Induced Acute Lung Injury. PLOS ONE 9(7):e101925. https://doi.org/10.1371/journal.pone.0101925

Davé SH, Tilstra JS, Matsuoka K, Li F, DeMarco RA, Beer-Stolz D, Sepulveda AR, Fink MP, Lotze MT, Plevy SE (2009) Ethyl pyruvate decreases HMGB1 release and ameliorates murine colitis. Journal of Leukocyte Biology 86(3):633–643. https://doi.org/10.1189/jlb.1008662

Degryse B, Bonaldi T, Scaffidi P, Müller S, Resnati M, Sanvito F, Arrigoni G, Bianchi ME (2001) The High Mobility Group (Hmg) Boxes of the Nuclear Protein Hmg1 Induce Chemotaxis and Cytoskeleton Reorganization in Rat Smooth Muscle Cells. Journal of Cell Biology 152(6):1197–1206. https://doi.org/10.1083/jcb.152.6.1197

Dickinson JD, Sweeter JM, Staab EB, Nelson AJ, Bailey KL, Warren KJ, Jaramillo AM, Dickey BF, Poole JA (2018) MyD88 controls airway epithelial Muc5ac expression during TLR activation conditions from agricultural organic dust exposure. American Journal of Physiology-Lung Cellular and Molecular Physiology 316(2):L334–L347. https://doi.org/10.1152/ajplung.00206.2018

Fischer AH, Jacobson KA, Rose J, Zeller R (2008) Hematoxylin and eosin staining of tissue and cell sections. CSH Protoc 2008:pdb.prot4986. https://doi.org/10.1101/pdb.prot4986

Georas SN, Rezaee F (2014) Epithelial barrier function: at the frontline of asthma immunology and allergic airway inflammation. J Allergy Clin Immunol 134(3):509–520. https://doi.org/10.1016/j.jaci.2014.05.049

Grainge CL, Davies DE (2013) Epithelial Injury and Repair in Airways Diseases. CHEST 144(6):1906–1912. https://doi.org/10.1378/chest.12-1944

Hribar C, Schultz M Understanding Concentrated Animal Feeding Operations and Their Impact on Communities. :30

Kanazawa H, Tochino Y, Asai K, Ichimaru Y, Watanabe T, Hirata K (2012) Validity of HMGB1 measurement in epithelial lining fluid in patients with COPD. European Journal of Clinical Investigation 42(4):419–426. https://doi.org/10.1111/j.1365-2362.2011.02598.x

Kim HS, Cho IH, Kim JE, Shin YJ, Jeon J-H, Kim Y, Yang YM, Lee K-H, Lee JW, Lee W-J, Ye S-K, Chung M-H (2008) Ethyl pyruvate has an anti-inflammatory effect by inhibiting ROS-dependent STAT signaling in activated microglia. Free Radic Biol Med 45(7):950–963. https://doi.org/10.1016/j.freeradbiomed.2008.06.009

Kirkhorn SR, Garry VF (2000) Agricultural lung diseases. Environ Health Perspect 108(Suppl 4):705–712

Kotton DN (2018) Claudin-18: unexpected regulator of lung alveolar epithelial cell proliferation. J Clin Invest 128(3):903–905. https://doi.org/10.1172/JCI99799

Liu JQ, Zelko IN, Erbynn EM, Sham JSK, Folz RJ (2006) Hypoxic pulmonary hypertension: role of superoxide and NADPH oxidase (gp91phox). American Journal of Physiology-Lung Cellular and Molecular Physiology 290(1):L2–L10. https://doi.org/10.1152/ajplung.00135.2005

Livak KJ, Schmittgen TD (2001) Analysis of Relative Gene Expression Data Using Real-Time Quantitative PCR and the 2−ΔΔCT Method. Methods 25(4):402–408. https://doi.org/10.1006/meth.2001.1262

Lotze MT, Tracey KJ (2005) High-mobility group box 1 protein (HMGB1): nuclear weapon in the immune arsenal. Nature Reviews Immunology 5(4):331–342. https://doi.org/10.1038/nri1594

May S, Romberger DJ, Poole JA (2012) Respiratory Health Effects of Large Animal Farming Environments. J Toxicol Environ Health B Crit Rev 15(8):524–541. https://doi.org/10.1080/10937404.2012.744288

Nieto MA (2011) The Ins and Outs of the Epithelial to Mesenchymal Transition in Health and Disease. Annu Rev Cell Dev Biol 27(1):347–376. https://doi.org/10.1146/annurev-cellbio-092910-154036

Nordgren TM, Charavaryamath C (2018) Agriculture Occupational Exposures and Factors Affecting Health Effects. Curr Allergy Asthma Rep 18(12):65. https://doi.org/10.1007/s11882-018-0820-8

Ohtake K, Maeno T, Ueda H, Ogihara M, Natsume H, Morimoto Y (2003) Poly-l-Arginine Enhances Paracellular Permeability via Serine/Threonine Phosphorylation of ZO-1 and Tyrosine Dephosphorylation of Occludin in Rabbit Nasal Epithelium. Pharm Res 20(11):1838–1845. https://doi.org/10.1023/B:PHAM.0000003383.86238.d1

Pandolfi F, Altamura S, Frosali S, Conti P (2016) Key Role of DAMP in Inflammation, Cancer, and Tissue Repair. Clinical Therapeutics 38(5):1017–1028. https://doi.org/10.1016/j.clinthera.2016.02.028

Poole JA, Alexis NE, Parks C, MacInnes AK, Gentry-Nielsen MJ, Fey PD, Larsson L, Allen-Gipson D, Essen SGV, Romberger DJ (2008) Repetitive organic dust exposure in vitro impairs macrophage differentiation and function. Journal of Allergy and Clinical Immunology 122(2):375-382.e4. https://doi.org/10.1016/j.jaci.2008.05.023

Poole JA, Romberger DJ (2012) Immunological and Inflammatory Responses to Organic Dust in Agriculture. Curr Opin Allergy Clin Immunol 12(2):126–132. https://doi.org/10.1097/ACI.0b013e3283511d0e

Poole JA, Wyatt TA, Kielian T, Oldenburg P, Gleason AM, Bauer A, Golden G, West WW, Sisson JH, Romberger DJ (2011) Toll-like receptor 2 regulates organic dust-induced airway inflammation. Am J Respir Cell Mol Biol 45(4):711–719. https://doi.org/10.1165/rcmb.2010-0427OC

Poole JA, Wyatt TA, Oldenburg PJ, Elliott MK, West WW, Sisson JH, Von Essen SG, Romberger DJ (2009) Intranasal organic dust exposure-induced airway adaptation response marked by persistent lung inflammation and pathology in mice. American Journal of Physiology-Lung Cellular and Molecular Physiology 296(6):L1085–L1095. https://doi.org/10.1152/ajplung.90622.2008

Raleigh DR, Boe DM, Yu D, Weber CR, Marchiando AM, Bradford EM, Wang Y, Wu L, Schneeberger EE, Shen L, Turner JR (2011) Occludin S408 phosphorylation regulates tight junction protein interactions and barrier function. Journal of Cell Biology 193(3):565–582. https://doi.org/10.1083/jcb.201010065

Romberger DJ, Bodlak V, Von Essen SG, Mathisen T, Wyatt TA (2002) Hog barn dust extract stimulates IL-8 and IL-6 release in human bronchial epithelial cells via PKC activation. Journal of Applied Physiology 93(1):289–296. https://doi.org/10.1152/japplphysiol.00815.2001

S A, La W, L DA, Br F, Ej D, J A, K S, Cl W-L, Jr MP, Bs P, Da S, Iv Y (2016) Novel Innate Immune Genes Regulating the Macrophage Response to Gram Positive Bacteria. Genetics 204(1):327–336. https://doi.org/10.1534/genetics.115.185314

Sappington PL, Yang R, Yang H, Tracey KJ, Delude RL, Fink MP (2002) HMGB1 B box increases the permeability of Caco-2 enterocytic monolayers and impairs intestinal barrier function in mice. Gastroenterology 123(3):790–802. https://doi.org/10.1053/gast.2002.35391

Seo J, Ottesen EW, Singh RN (2014) Antisense Methods to Modulate Pre-mRNA Splicing. In: Hertel KJ (ed) Spliceosomal Pre-mRNA Splicing: Methods and Protocols. Humana Press, Totowa, NJ, pp 271–283

Sethi RS, Schneberger D, Charavaryamath C, Singh B (2017) Pulmonary innate inflammatory responses to agricultural occupational contaminants. Cell Tissue Res 367(3):627–642. https://doi.org/10.1007/s00441-017-2573-4

Shi ZO-Q, Fischer MJ, Sanctis GTD, Schuyler MR, Tesfaigzi Y (2002) IFN-γ, But Not Fas, Mediates Reduction of Allergen-Induced Mucous Cell Metaplasia by Inducing Apoptosis. The Journal of Immunology 168(9):4764–4771. https://doi.org/10.4049/jimmunol.168.9.4764

Sun F, Xiao G, Qu Z (2017) Murine Bronchoalveolar Lavage. Bio Protoc 7(10). https://doi.org/10.21769/BioProtoc.2287

Sundblad B-M, Scheele I von, Palmberg L, Olsson M, Larsson K (2009) Repeated exposure to organic material alters inflammatory and physiological airway responses. European Respiratory Journal 34(1):80–88. https://doi.org/10.1183/09031936.00105308

Ugrinova I, Pasheva E (2017) Chapter Two - HMGB1 Protein: A Therapeutic Target Inside and Outside the Cell. In: Donev R (ed) Advances in Protein Chemistry and Structural Biology. Academic Press, pp 37–76

Ulloa L, Ochani M, Yang H, Tanovic M, Halperin D, Yang R, Czura CJ, Fink MP, Tracey KJ (2002) Ethyl pyruvate prevents lethality in mice with established lethal sepsis and systemic inflammation. PNAS 99(19):12351–12356. https://doi.org/10.1073/pnas.192222999

Wang H, Bloom O, Zhang M, Vishnubhakat JM, Ombrellino M, Che J, Frazier A, Yang H, Ivanova S, Borovikova L, Manogue KR, Faist E, Abraham E, Andersson J, Andersson U, Molina PE, Abumrad NN, Sama A, Tracey KJ (1999) HMG-1 as a Late Mediator of Endotoxin Lethality in Mice. Science 285(5425):248–251. https://doi.org/10.1126/science.285.5425.248

Wang J, Li R, Peng Z, Hu B, Rao X, Li J (2020) HMGB1 participates in LPS-induced acute lung injury by activating the AIM2 inflammasome in macrophages and inducing polarization of M1 macrophages via TLR2, TLR4, and RAGE/NF-κB signaling pathways Corrigendum in /10.3892/ijmm.2020.4530. International Journal of Molecular Medicine 45(1):61–80. https://doi.org/10.3892/ijmm.2019.4402

Wyatt TA, Sisson JH, Essen SGV, Poole JA, Romberger DJ (2008) Exposure to hog barn dust alters airway epithelial ciliary beating. European Respiratory Journal 31(6):1249–1255. https://doi.org/10.1183/09031936.00015007

Yang H, Wang H, Andersson U (2020) Targeting Inflammation Driven by HMGB1. Front Immunol 11. https://doi.org/10.3389/fimmu.2020.00484

Ye L, Martin TA, Parr C, Harrison GM, Mansel RE, Jiang WG (2003) Biphasic effects of 17-β-estradiol on expression of occludin and transendothelial resistance and paracellular permeability in human vascular endothelial cells. Journal of Cellular Physiology 196(2):362–369. https://doi.org/10.1002/jcp.10315

Appendix. Supplementary tables

Table 7.4 Primer sequences

Gene symbol	Primer Sequence (5'→3')	
tlr2	Forward	ACAGCAAGGTCTTCCTGGTTCC
	Reverse	GCTCCCTTACAGGCTGAGTTCT
tlr4	Forward	AGCTTCTCCAATTTTTCAGAACTTC
	Reverse	TGAGAGGTGGTGTAAGCCATGC
il1b	Forward	TGGACCTTCCAGGATGAGGACA
	Reverse	GTTCATCTCGGAGCCTGTAGTG
tnfa	Forward	GGTGCCTATGTCTCAGCCTCTT
	Reverse	GCCATAGAACTGATGAGAGGGAG
il10	Forward	CGGGAAGACAATAACTGCACCC
	Reverse	CGGTTAGCAGTATGTTGTCCAGC
tgfb	Forward	TGATACGCCTGAGTGGCTGTCT
	Reverse	CACAAGAGCAGTGAGCGCTGAA
muc5ac	Forward	CCACTTTCTCCTTCTCCACACC
	Reverse	GGTTGTCGATGCAGCCTTGCTT
cldn1	Forward	GGACTGTGGATGTCCTGCGTTT
	Reverse	GCCAATTACCATCAAGGCTCGG
cldn5	Forward	TGACTGCCTTCCTGGACCACAA
	Reverse	CATACACCTTGCACTGCATGTGC
cldn18	Forward	TGGTAGCATGGATGACTCTGCC
	Reverse	GCTGTGGACATCCAGAAGTTGG
ecad	Forward	GGTCATCAGTGTGCTCACCTCT
	Reverse	GCTGTTGTGCTCAAGCCTTCAC
ncad	Forward	CCTCCAGAGTTTACTGCCATGAC
	Reverse	CCACCACTGATTCTGTATGCCG
nos2	Forward	GAGACAGGGAAGTCTGAAGCAC
	Reverse	CCAGCAGTAGTTGCTCCTCTTC

Table 7.5 Characteristics of primary antibodies

Epitope	Species/Clone	Dilution	Catalog #	Supplier
β-Actin	Mouse Monoclonal	1:10,000	ab6276	AbCam[a]
HMGB1	Rabbit Polyclonal	1:1000	ab79823	AbCam[a]
RAGE	Rabbit Polyclonal	1:1000	ab3611	AbCam[a]
Foxj1	Mouse Monoclonal	1:1000	sc-53139	Santa Cruz[b]
Occludin	Mouse Monoclonal	1:1000	sc-271842	Santa Cruz[b]
ZO-1	Mouse Monoclonal	1:1000	sc-33725	Santa Cruz[b]
GP91Phox	Rabbit Polyclonal	1:1000	ab80508	AbCam[a]

[a]Cambridge, United Kingdom

[b]Dallas, Texas, USA

Table 7.6 Characteristics of secondary antibodies

Expression system	Conjugate	Species/Clone	Dilution	Catalog #	Supplier
Donkey/IgG	Alexa Fluor® 680	Rabbit Polyclonal	1:10,000	A10043	Invitrogen[c]
Rabbit/IgG	Alexa Fluor® 680	Mouse Polyclonal	1:10,000	A27031	Invitrogen[c]
Donkey/IgG	IRDye® 800CW	Rabbit Polyclonal	1:10,000	926-32213	LI-COR[d]

[c]Thermofisher Scientific, USA

[d]Nebraska, USA

CHAPTER 8. GENERAL CONCLUSION

Summary

Agriculture environmental exposure to organic dust has been linked to increased morbidity in exposed individuals (Von Essen and Donham 1999). Individuals exposed to OD are at an increased risk of developing significant respiratory diseases, such as chronic obstructive pulmonary diseases (COPD) and bronchitis (Von Essen and Romberger 2003; Charavaryamath and Singh 2006). Studies employing single and repeated exposure models via intranasal inhalation of OD have shown reproducible and activated inflammatory airway responses (Poole et al. 2008; Sundblad et al. 2009) recapitulating features of human exposure to work environment rich in OD. Although OD-mediated acute inflammatory responses have been well characterized over the years, little is known regarding the inflammatory mechanisms underlying the OD exposure-induced respiratory disease pathogenesis.

Studies have examined the role of various pattern recognition receptors (PRRs), most notably toll like receptor (TLR) family, in propagating innate responses to OD exposure. These receptors can detect a broad range of microbial components, which are also found in OD. In all cases, TLRs signal through the same pathway by recruiting the MyD88 protein, which initiates a signaling cascade leading to induction of several immune-related pathways such as p38 and NFκB (nuclear factor kappa B) (Charavaryamath et al. 2008; Bailey et al. 2008; Poole et al. 2011; Schneberger et al. 2016). Studies have identified additional families of innate immune receptors, such as NOD-like receptors that mimic some of the binding range of TLRs, signaling to the NFκB and mitogen-activated protein (MAP) kinase pathways (Poole et al. 2010).

The primary focus of the research presented in this dissertation was to investigate the role of HMGB1, a ubiquitous signaling molecule, in the lung in response to OD. Because the role of a

DAMP in inflammation is largely a function of its cellular expression, we first documented the expression and kinetics of HMGB1 in intact lungs of rats exposed to OD and human bronchial epithelial cells. Having established the protein expression, we proceeded to examine cytokine and cellular changes on exposure to ODE in normal and in models where HMGB1 expression was either decreased or inhibited.

HMGB1 and OD exposure

Current literature describes the role and kinetics of HMGB1 in various disease states and have labeled the HMGB1 protein as a late mediator of sterile inflammation (Wang et al. 1999; Andersson and Tracey 2011). Despite significant progress in understanding the structure, mechanism of release, and receptors, the intracellular signaling pathways downstream of HMGB1 remain relatively poorly defined. In chapter 3 we have identified the role HMGB1 plays in the induction of inflammation, particularly on OD exposure. Using *in vitro* OD exposure models with or without blocking HMGB1 translocation and secretion, we identified that HMGB1 potentiates a majority of the late inflammatory cascades and cytokine production. Using *in vivo* models, we identified how HMGB1 plays a significant role in regulating OD-mediated tissue pathology and loss of epithelial junction integrity. Neutralization of extracellular HMGB1 decreased the cellular influx into the airways, which is a characteristic pathological feature of OD exposure. With the use of our *in vitro* and *in vivo* models we highlighted the difference in impact and function of intracellular versus extracellular HMGB1 on OD exposure. This work gives us the opportunity to consider HMGB1 as a possible therapeutic target for intervention in treating OD-mediated airway inflammation.

Mitochondrial dysfunction in OD mediated inflammation

Mitochondria (mt) are the essential cellular organelles and are emerging as a possible therapeutic target in many inflammatory diseases. Mitochondrial biology has seen a surge in

popularity in the past 5 years, however, it is only recently that we are beginning to understand how this organelle regulates cellular homeostasis and contributes to disease processes in the lung (Aghapour et al. 2019; Cloonan et al. 2020). Previous studies have shown a link between mitochondrial dynamics and innate immune signaling (Cloonan and Choi 2012). Based on the evidence, we examined whether OD-exposure would induce mitochondrial damage and dysfunction. We have described how exposure to OD significantly changed mitochondrial dynamics, structural integrity, and function. We identified that OD exposure increases the release of mtDAMPs such as mtDNA due to the loss of mitochondrial membrane integrity, and decrease in mitochondrial bioenergetics. Our observation of OD exposure induced mitochondrial dysfunction was consistent with that identified in various respiratory disorders such as COPD, and cigarette smoke exposure (Prakash et al. 2017).

HMGB1 and mitochondria

Recent studies have suggested an essential role for HMGB1 in autophagic surveillance with important effects on mitochondrial quality control (Tang et al. 2011). Building on our observation that OD exposure induces mitochondrial dysfunction, we hypothesized that HMGB1 plays a crucial role in promoting OD-mediated mitochondrial dysfunction. In chapter 5, OD-mediated dysregulation of mitochondrial respiration was rescued using HMGB1 neutralizing antibody or knockdown of intracellular HMGB1 in primary human bronchial epithelial cells. In addition to this, we also observed a decrease in the release of mtDAMPs and increased metabolism. This phenomenon was observed in our *in vivo* models as well, wherein the lack of intracellular HMGB1 increased the expression of markers associated with OXPHOS and glycolytic activity, as well as decreased the production of reactive species.

Thus, in this dissertation, we have identified prospective targets for the development of targeted therapies to mitigate OD-mediated airway inflammation. The identification of HMGB1

provides us with a wider window for intervention against OD-mediated airway inflammation and pathogenesis. However, we believe that additional mechanistic data may be required to understand the distinctive functions and pathways associated with OD-mediated airway inflammation, HMGB1, and mitochondria. Therefore, while we are enthusiastic about our discoveries, we exercise caution in recommending these two as therapeutic targets.

Strengths and limitations

The primary strength of this dissertation is its cohesive progression of data. Each chapter is built on a stand-alone hypothesis driven work and provides essential mechanistic data for the following chapter. For example, Chapter 3 introduces the implications of OD mediated HMGB1 secretion which is presented again in chapters 5 through 7. In another example, Chapter 4 describes the OD mediated changes in mitochondrial structure and dynamics, which we expand upon further in chapter 5 by focusing on the impact on metabolism and respiration, and its correlation with HMGB1, thus helping us in understanding the physiological function and application of HMGB1 as a potential therapeutic target. Aside from the coordinating themes throughout the dissertation, additional strength was the use of both mouse models as well as human cell culture models to augment and substantiate the findings.

The major limitations of this research can be summarized as a partial lack of functional assays in our experiments. For example, the question of whether neutralizing HMGB1 would rescue OD exposure induced loss of lung function could have been answered if we had used invasive or non-invasive lung function assays in our murine models. Further, in addition to the mitochondrial respiration/metabolism markers, the use of assays to measure airway epithelial cilia beat frequency (CBF) would have been valuable. These additional assays would have added value to the translational potential of our findings to human exposure induced lung diseases.

Future directions

To elucidate the importance of HMGB1 in the pathogenesis of OD-mediated airway diseases and to plan for future therapeutic intervention, there are several basic questions to resolve. However, future research is required to address fundamental questions regarding HMGB1 on OD exposure, such as, what is the quantitative relationship between the extracellular HMGB1 from necrotic cells versus active secretion from immunocompetent cells, and other putative HMGB1 sources? Are there other HMGB1 receptors in addition to the ones currently known? What factors contribute towards the post-translational modifications (PTMs) of HMGB1 and whether these PTMs could be targeted. To what extent are other signaling molecules needed for the proinflammatory role of HMGB1? Will HMGB1 be validated as a clinical target to modulate acute or chronic airway inflammation, or will it be too dangerous to interfere with a molecule that is so central for the interplay between necrotic cell death with subsequent inflammation and repair responses? These are indeed very exciting questions that need to be addressed and elucidated in the near future. Therefore, targeted pharmacological interventions against HMGB1 using its antibodies, inhibitors, or antagonists, would become novel therapeutic approaches for OD-mediated lung diseases.

References

Aghapour M, Remels AHV, Pouwels SD, Bruder D, Hiemstra PS, Cloonan SM, Heijink IH (2019) Mitochondria: at the crossroads of regulating lung epithelial cell function in chronic obstructive pulmonary disease. American Journal of Physiology-Lung Cellular and Molecular Physiology 318(1):L149–L164. https://doi.org/10.1152/ajplung.00329.2019

Andersson U, Tracey KJ (2011) HMGB1 Is a Therapeutic Target for Sterile Inflammation and Infection. Annu Rev Immunol 29:139–162. https://doi.org/10.1146/annurev-immunol-030409-101323

Bailey KL, Poole JA, Mathisen TL, Wyatt TA, Von Essen SG, Romberger DJ (2008) Toll-like receptor 2 is upregulated by hog confinement dust in an IL-6-dependent manner in the airway epithelium. American Journal of Physiology-Lung Cellular and Molecular Physiology 294(6):L1049–L1054. https://doi.org/10.1152/ajplung.00526.2007

Charavaryamath C, Juneau V, Suri SS, Janardhan KS, Townsend H, Singh B (2008) Role of Toll-like receptor 4 in lung inflammation following exposure to swine barn air. Exp Lung Res 34(1):19–35. https://doi.org/10.1080/01902140701807779

Charavaryamath C, Singh B (2006) Pulmonary effects of exposure to pig barn air. J Occup Med Toxicol 1:10. https://doi.org/10.1186/1745-6673-1-10

Cloonan SM, Choi AM (2012) Mitochondria: commanders of innate immunity and disease? Current Opinion in Immunology 24(1):32–40. https://doi.org/10.1016/j.coi.2011.11.001

Cloonan SM, Kim K, Esteves P, Trian T, Barnes PJ (2020) Mitochondrial dysfunction in lung ageing and disease. European Respiratory Review 29(157). https://doi.org/10.1183/16000617.0165-2020

Poole JA, Alexis NE, Parks C, MacInnes AK, Gentry-Nielsen MJ, Fey PD, Larsson L, Allen-Gipson D, Essen SGV, Romberger DJ (2008) Repetitive organic dust exposure in vitro impairs macrophage differentiation and function. Journal of Allergy and Clinical Immunology 122(2):375-382.e4. https://doi.org/10.1016/j.jaci.2008.05.023

Poole JA, Burrell AM, Wyatt TA, Kielian TL, Romberger DJ (2010) NOD2 Negatively Regulates Organic Dust-Induced Inflammation in Monocytes/Macrophages. Journal of Allergy and Clinical Immunology 125(2, Supplement 1):AB118. https://doi.org/10.1016/j.jaci.2009.12.467

Poole JA, Wyatt TA, Kielian T, Oldenburg P, Gleason AM, Bauer A, Golden G, West WW, Sisson JH, Romberger DJ (2011) Toll-like receptor 2 regulates organic dust-induced airway inflammation. Am J Respir Cell Mol Biol 45(4):711–719. https://doi.org/10.1165/rcmb.2010-0427OC

Prakash YS, Pabelick CM, Sieck GC (2017) Mitochondrial Dysfunction in Airway Disease. CHEST 152(3):618–626. https://doi.org/10.1016/j.chest.2017.03.020

Schneberger D, Aulakh G, Channabasappa S, Singh B (2016) Toll-like receptor 9 partially regulates lung inflammation induced following exposure to chicken barn air. Journal of Occupational Medicine and Toxicology 11(1):31. https://doi.org/10.1186/s12995-016-0121-x

Sundblad B-M, Scheele I von, Palmberg L, Olsson M, Larsson K (2009) Repeated exposure to organic material alters inflammatory and physiological airway responses. European Respiratory Journal 34(1):80–88. https://doi.org/10.1183/09031936.00105308

Tang D, Kang R, Livesey KM, Kroemer G, Billiar TR, Van Houten B, Zeh HJ, Lotze MT (2011) High-Mobility Group Box 1 Is Essential for Mitochondrial Quality Control. Cell Metabolism 13(6):701–711. https://doi.org/10.1016/j.cmet.2011.04.008

Von Essen S, Donham K (1999) Illness and injury in animal confinement workers. Occup Med 14(2):337–350

Von Essen S, Romberger D (2003) The respiratory inflammatory response to the swine confinement building environment: the adaptation to respiratory exposures in the chronically exposed worker. J Agric Saf Health 9(3):185–196. https://doi.org/10.13031/2013.13684

Wang H, Bloom O, Zhang M, Vishnubhakat JM, Ombrellino M, Che J, Frazier A, Yang H, Ivanova S, Borovikova L, Manogue KR, Faist E, Abraham E, Andersson J, Andersson U, Molina PE, Abumrad NN, Sama A, Tracey KJ (1999) HMG-1 as a Late Mediator of Endotoxin Lethality in Mice. Science 285(5425):248–251. https://doi.org/10.1126/science.285.5425.248